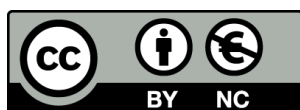# SMALL-MOLECULE MIMICS OF RIESKE OXYGENASES. APPLICATION TO SELECTIVE ALIPHATIC C-H HYDROXYLATION AND OLEFINS SYN-DIHYDROXYLATION

Margarida Borrell Recasens

Universitat de Girona

DOCTORAL THESIS

SMALL-MOLECULE MIMICS OF RIESKE OXYGENASES. APPLICATION TO SELECTIVE ALIPHATIC C-H HYDROXYLATION AND OLEFIN *SYN*-DIHYDROXYLATION

MARGARIDA BORRELL RECASENS

2021

Doctoral programme in Chemistry

Supervised by Dr. Miquel Costas Salgueiro
Tutor: Dr. Miquel Costas Salgueiro

Presented in partial fulfilment of the requirements for a doctoral degree from the Universitat de Girona.

Universitat
de Girona

Dr. Miquel Costas Salgueiro from Universitat de Girona.

DECLARE:

That the thesis entitled "Small Molecule Mimics of Rieske Oxygenases. Application to Selective Aliphatic C-H Hydroxylation and Olefin *Syn*-dihydroxylation", presented by Margarida Borrell Recasens to obtain a doctoral degree, has been completed under my supervision and meets the requirements to opt for an International Doctorate.

For all intents and purposes, I hereby sign this document.

Dr. Miquel Costas Salgueiro

Girona, 13th July 2021

Tamdiu discendum est quamdiu nescias; si proverbio credimus, 'quamdiu vivis'

Et cal apendre mentre duri la teva ignorància; si creiem en el proverbi, mentre duri la teva vida.

Sèneca, Epístoles 76, 3

FULL LIST OF PUBLICATIONS

This thesis is based on a compendium of the following publications:

Chapter III

"Mechanistically Driven Development of an Iron Catalyst for Selective *Syn*-Dihydroxylation of Alkenes with Aqueous Hydrogen Peroxide". **Margarida Borrell**, Miquel Costas. *J. Am. Chem. Soc.* **2017**, 139, 36, 12821-12829. (Impact factor: 14.720, position 13/177 in chemistry, 1St quartile).

Chapter IV

"Greening Oxidation Catalysis: Iron Catalyzed Alkene *Syn*-Dihydroxylation with Aqueous Hydrogen Peroxide in Green Solvents". **Margarida Borrell**, Miquel Costas. *ACS Sustainable Chem. Eng.* **2018**, 6, 7, 8410-8416. (Impact factor: 6.97, position 25/177 in chemistry, 1St quartile).

Chapter V

"Characterized *cis*-Fe^V(O)(OH) intermediate mimics enzymatic oxidations in the gas phase". **Margarida Borrell**,[#] Erik Andris,[#] Rafael Navrátil, Jana Roithová, Miquel Costas. *Nat. Commun.* **2019,** 10, 901. (Impact factor: 12.121, position 6/71 multidisciplinary sciences, 1St quartile) ([#]equal contribution).

Chapter VI

"Site-selective and product chemoselective aliphatic C-H bond hydroxylation of polyhydroxylated substrates". **Margarida Borrell**, Sergio Gil-Caballero, Massimo Bietti, Miquel Costas. *ACS Catal.* **2020**, 10, 8, 4702-4709. (Impact factor: 12.160, position 12/159 in physical chemistry, 1St quartile).

All these publications have been published in journals that belong to the first quartile according to JCR.

Publications not included in this thesis:

"Oxidation of alkane and alkene moieties with biologically inspired nonheme iron catalysts and hydrogen peroxide: from free radicals to stereoselective transformations". Giorgio Olivo, Olaf Cussó, Margarida Borrell, Miquel Costas. *J. Biol. Inorg. Chem*. **2017**, *22*, 425-452.

"Biomimetic Oxidation in Organic Synthesis". Laia Vicens, Margarida Borrell, Miquel Costas. *Science of Synthesis Reference Library: Catalytic Oxidations in Organic Synthesis. Thieme*, **2017**, 113-190.

"Spectroscopic and DFT Characterization of a Highly Reactive Nonheme Fe^V–Oxo Intermediate" Ruixi Fan; Joan Serrano-Plana, Williamson Oloo, Apparao Draksharapu, Estefania Delgado-Pinar, Anna Company, Vlad Martin-Diaconescu, Margarida Borrell, Julio Lloret-Fillol, Elisa García-España, Yisong Guo, Emile Bominaar, Larry Que, Miquel Costas, Eckard Münck. *J. Am. Chem. Soc*. **2018,** 140, 11, 3916-3928.

"Nickel-Catalyzed Decarbonylative Amination of Carboxylic Acid Esters". Christian A. Malapit[#], Margarida Borrell[#], Michael W. Milbauer, Conor E. Brigham, Melanie S. Sanford. *J. Am. Chem. Soc.* **2020**, 142, 13, 5918-5923. (# equal contribution)

''Aromatic C−H Hydroxylation Reactions with Hydrogen Peroxide Catalyzed by Bulky Manganese Complexes''. Eduard Masferrer-Rius, Margarida Borrell, Martin Lutz, Miquel Costas, Robertus J. M. Klein Gebbink. *Adv. Synth. Catal.* **2021**, 363,1-14.

LIST OF ABBREVIATIONS

^{13}C-NMR	Carbon nuclear magnetic resonance
^{1}H-NMR	Proton nuclear magnetic resonance
2-eha	2-Ethylhexanoic acid
Å	Ångström
A/K	Alcohol/ketone ratio
Abs	Absorbance
AcOH	Acetic acid
AE	Atom Economy
Anh	Anhydrous
Ar	Argon
Asp	Aspartic acid
BpdLx	Bispidine derivatives
Bpka	3-(dipyridin-2-yl-methyl)-1,5,7-trimethyl-2,4-dioxo-3-azabicyclo[3.3.3]nonane-7-carboxylic acid
Bqcn	*N,N'*-dimethyl-*N,N'*-bis(2-methyl-8-quinolyl)-cyclohexane-1,2-diamine
Bqpn	*N,N'*-dimethyl-*N,N'*-bis(2-methylquinolin-8-yl)-1,2-diphenylethane-1,2-diamine
BZDO	Benzoate1,2-dioxygenase
Cat	Catalyst
CF$_3$SO$_3$, OTf	Trifluoromethanesulfonate anion
Conv	Conversion
Cyt P450	Cytochrome P450
d	Doublet
DFT	Density functional theory

DMF	Dimethyl formamide
DMM	Dimethyl methoxide
e⁻	Electron
ED	Electron defiicent
EDG	Electron donating group
Equiv.	Equivalent
Et_2O	Diethyl ether
EtOAc	Ethyl acetate
EWG	Electron withdrawing group
FT-IR	Fourier transform infrared spectroscopy
GC	Gas chromatography
GS-MS	Gas chromatography-mass spectrometry
h	Hours
H_2O_2	Hydrogen peroxide
HAT	Hydrogen atom transfer
HFIP	1,1,1,3,3,3-Hexafluoro-2-propanol
IR	Infrared spectroscopy
IRPD	Infrared photodissociation
KIE	Kinetic isotope effect
KshAB	3-ketosteroid 9α-hydroxylase
M	Metal
m/z	Mass to charge ratio
Mcp	*N,N'*-dimethyl-*N,N'*-bis(2-pyridylmethyl)-cyclohexane-1,2-diamine
Mcpp	*N,N'*-dimethyl-*N,N'*-bis{[(*R*)-4,5-pinenepyridin-2-yl]-methyl}-cyclohexane-1,2-diamine)
Me	Methyl
MeCN	Acetonitrile

Men	*N,N'*-dimethyl-*N,N'*-bis(2-pyridylmethyl)ethane-1,2-diamine
MeOH	Methanol
MHz	Megahertz
min	Minutes
mL	Milliliter
mM	Millimolar
MW	Molecular weight
n-BuLi	n-Butyllithium
NADH	Nicotinamide adenine dinucleotide
NDO	Naphtalenen-1,2-dioxigenase
OAc	Acetate group
ºC	Celsius degrees
Ox	Oxidant
PC	Propylene carbonate
PCC	Pyridinium chlorochromate
pdp	*N,N'*-bis(2-pyridylmethyl)-2,2'-bipyrrolidine
Ph	Phenyl
Ph-dpah	*N*-(di-(2-pyridin-2-yl)methyl)benzamide.
ppm	Parts per million
Py	Pyridine
Pytacn	1-(2'-pyridylmethyl)-4,7-dimethyl-1,4,7-triazacyclononane.
q	Quadruplet
QTOF	Quadrupole time-of-flight
r.t.	Room temperatura
s	Singlet
sept	Septuplet
Solv	Solvent

t	Triplet
*t*Bu	*Tert*-butyl group
TFE	2,2,2-Trifluoroethanol
THF	Tetrahydrofuran
TN	Turnover number
tips	*Tris*(isopropyl)silyl
tpa	*Tris*(2-pyridylmethyl)amine
w/w	Weight/weight
δ	Chemical Shift
λ	Wavenumber
ν	Frequency

ACKNOWLEDGMENTS

GRAPHICAL ABSTRACT

Summary. (p. 9)
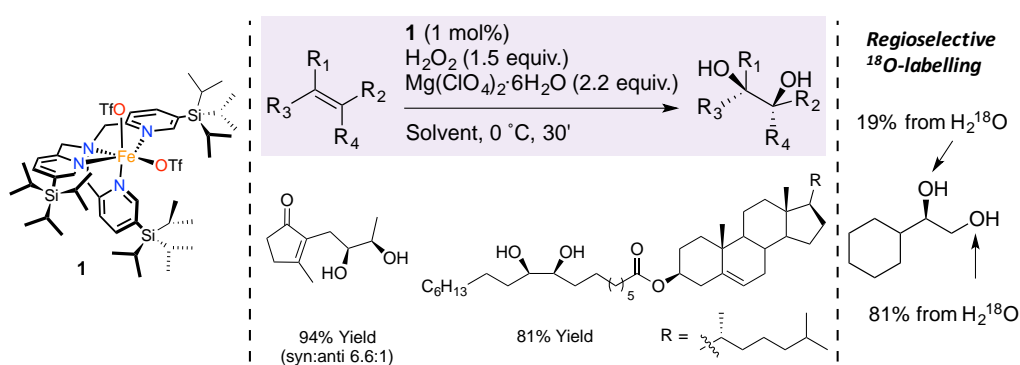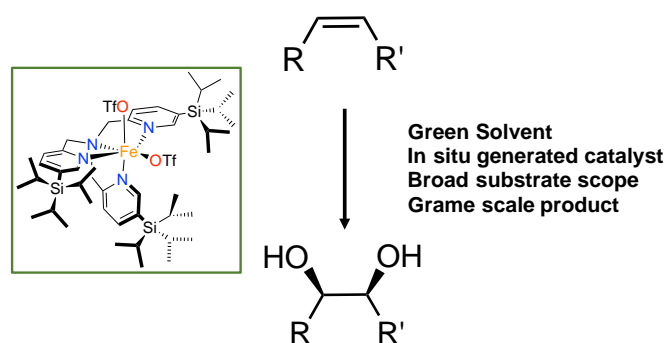
Chapter V. Characterized *cis*-Fe^V(O)(OH) Intermediate Mimics Enzymatic Oxidations in the Gas Phase. (p. 67)

Chapter VI. Site-selective and product chemoselective aliphatic C-H bond hydroxylation of polyhydroxylated substrates. (p. 79)
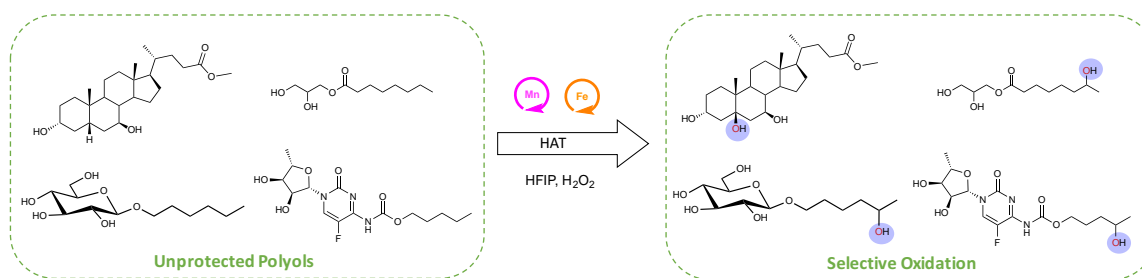
Chapter VII. Results and Discussion (p. 89)

Chapter VIII. Conclusions and Perspectives (p. 131)

Chapter IX. Experimental section (p. 135)

TABLE OF CONTENTS

LIST OF FIGURES

2

LIST OF TABLES

LIST OF SCHEMES

Supplementary Data Information

The material listed below can be found in the attached CD:

- Pdf file of the PhD dissertation
- Pdf file of the Digital Annex containing additional NMR, GC and GC-MS.
- CIF files for crystal structure of **[Fe(OTf)$_2$(^{5tips3}tpa)]$^{2+}$** and **P14b** oxidation product Chapter VI.

SUMMARY

Oxidations are an important kind of reactions which are traditionally performed using stoichiometric oxidants that generate a large amount of waste.

Syn-dihydroxylation of alkenes is a paradigmatic example because it is a cornerstone reaction in organic synthesis that still relies in the use of heavy metal oxides, specially Os and Ru based oxides in catalytic amounts, but also $KMnO_4$, in stoichiometric amounts. Acetonitrile and halogenated solvents are widely used solvents in these reactions because of their robust nature against oxidants. However, metal catalyzed oxidations in green solvents are basically unknown. Rieske oxygenases are nonheme iron enzymes that catalyzes the olefin cis-dihydroxylation among other reactions. Is well know that the $Fe^V(O)(OH)$ species play a key role as intermediates in arene dihydroxylation catalyzed by Rieske oxygenases. However, the inability to accumulate these intermediates in solution has thus far prevented their spectroscopic and chemical characterization.

In this thesis, we were able to synthetizes an iron catalyst bearing a sterically encumbered tetradentate ligand. The steric demand of the ligand was envisioned as a key element to support a high catalytic activity by preventing bimolecular decomposition paths, and facilitating product release. This catalyst provides good to excellent yields of *syn*-diol products (up to 97% isolated yield) of a broad range of olefins.

Also, these excellent yields can be also obtained using the same mild conditions but in a mixture of polycarbonate and ethyl acetate, solvents that are recognized as particularly suitable from the perspective of sustainability.

In this part of the thesis we address the problem of the characterization of highly reactive $Fe^V(O)(OH)$ species using gas-phase ion spectroscopy. Using this method, we could confirm that $[Fe^V(O)(OH)(^{5tips3}tpa)]^{2+}$ hydroxylates C-H bonds in a rebound mechanism and performs the *syn*-dihydroxylation of alkenes and arenes.

Other paradigmatic case, is the functionalization of non-activated aliphatic C-H bonds because it transforms an inert aliphatic C-H group into alcohol and carbonyls moieties, which are some of the most versatile functional groups in organic synthesis. However, the inert nature of the aliphatic C-H bond and the multitude of C-H bonds present in the vast majority of organic molecules convert this reaction in a big challenge for synthetic chemistry.

With this problem in mind, we have developed a manganese catalyzed chemoselective C-H oxidation with hydrogen peroxide using a fluorinated alcohol solvent. These solvents induce a reversal of polarity in C-H bonds adjacent to hydroxyl groups, protecting the a priori oxidation sensitive hydroxyl moieties, favouring instead site selective and product chemoselective C-H oxidation at remote positions.

RESUM

Les reaccions d'oxidació tradicionalment es realitzen utilitzant oxidants estequiomètrics que generen una gran quantitat de residus.

La *sin*-dihidroxilació d'alquens n'és un exemple paradigmàtic perquè és una reacció que es pot considerar pedra angular en síntesi orgànica, i actualment encara es porta a terme amb oxidants basats en metalls pesats, especialment òxids d'Os i Ru en quantitats catalítiques, però també $KMnO_4$, en quantitats estequiomètriques. L'acetonitril i els dissolvents halogenats són dissolvents àmpliament utilitzats en aquestes reaccions per la seva naturalesa robusta en vers les oxidacions. No obstant això, les oxidacions catalitzades per metalls en dissolvents menys tòxics són bàsicament desconegudes. Les oxigenases de Rieske, són enzims de ferro no hemo que catalitzen la *sin*-dihidroxilació d'olefines entre altres reaccions. És ben sabut que les espècies de $Fe^V(O)(OH)$ tenen un paper clau com a intermediaris en la di hidroxilació d'arens catalitzada per les oxigenases de Rieske. No obstant això, la incapacitat per acumular aquests intermedis en solució a impedit, fins ara, la seva caracterització espectroscòpica i química. En aquesta tesi, vam ser capaços de sintetitzar un catalitzador de ferro amb un lligand tetradentat estèticament impedit. La demanda estèrica del lligand es va concebre com un element clau per donar suport a una alta activitat catalítica evitant camins de descomposició bimoleculars i facilitant l'alliberament del producte, proporcionant rendiments entre bons i excel·lents del producte *sin*-diol (fins a un 97% de rendiment aïllat) per una àmplia gamma d'olefines. A més, aquests excel·lents rendiments es van obtenir utilitzant les mateixes condicions suaus, però en una barreja de policarbonat i acetat d'etil, dissolvents que es reconeixen especialment adequats des de la perspectiva de sostenibilitat. En aquesta tesi també abordem el problema de la caracterització d'espècies de $Fe^V(O)(OH)$ altament reactives, mitjançant espectroscòpia iònica en fase gasosa. Mitjançant aquest mètode, es confirma que $[Fe^V(O)(OH)(^{5tips3}tpa)]^{2+}$ hidroxila enllaços C-H via el mecanisme de rebot i realitza la *sin*-dihidroxilació d'alquens i arenes. Un altre cas paradigmàtic és la funcionalització d'enllaços C-H alifàtics, pel fet de transformar enllaços inerts C-H en grups d'alcohols i carbonils, que són alguns dels grups més versàtils i funcionals en síntesi orgànica. No obstant això, la naturalesa inert de l'enllaç C-H alifàtic i la multitud d'enllaços C-H presents a la molècula, fan d'aquesta una de les reaccions més difícils en l'actualitat. Amb aquest problema en ment, vam poder desenvolupar una oxidació C-H quimioselectiva catalitzada per manganès, peròxid d'hidrogen com a oxidant i alcohol fluorat com a dissolvent. Aquests dissolvents causen un revers de la polaritat en els C-H adjacents, que indueixen un efecte de protecció contra la sobreoxidació de l'hidroxil, sensible a l'oxidació, afavorint l'oxidació C-H selectiva en posicions remotes.

RESUMEN

Las reacciones de oxidación tradicionalmente se realizan utilizando oxidantes estequiométricos los cuales generan una gran cantidad de residuos.

La *sin*-dihidroxilación de alquenos es un ejemplo paradigmático porque es una reacción que se considera una piedra angular en síntesis orgánica, y actualmente todavía se realiza con oxidantes basados en metales pesados, especialmente óxidos de Os y Ru en cantidades catalíticas, pero también KMnO4, en cantidades estequiometrias. El acetonitrilo y los disolventes halogenados son disolventes ampliamente utilizados en estas reacciones por su naturaleza robusta frente a las oxidaciones. Sin embargo, las oxidaciones catalizadas por metales en disolventes menos tóxicos son básicamente desconocidas. Las Oxigenasas de Rieske, son enzimas de hierro no hemo que catalizan la *sin*-dihidroxilación de olefinas entre otras reacciones. Es bien sabido que las especies de $Fe^V(O)(OH)$ tienen un papel clave como intermediarios en la di hidroxilación de arenos catalizada por las Oxigenasas de Rieske. Sin embargo, la incapacidad para acumular estos intermedios en solución ha impedido, hasta ahora, su caracterización espectroscópica y química. En esta tesis, fuimos capaces de sintetizar un catalizador de hierro con un ligando tetradentado estéticamente impedido. La demanda estérica del ligando se concibió como un elemento clave para apoyar una alta actividad catalítica evitando caminos de descomposición bimoleculares y facilitando la liberación del producto, proporcionando rendimientos entre buenos y excelentes del producto *sin*-diol (hasta un 97 % de rendimiento aislado) para una amplia gama de olefinas. Además, estos excelentes rendimientos se obtuvieron también utilizando las mismas condiciones suaves, pero en una mezcla de policarbonato y acetato de etilo, disolventes que se reconocen especialmente adecuados desde la perspectiva de sostenibilidad. En esta tesis también abordamos el problema de la caracterización de especies de $Fe^V(O)(OH)$ altamente reactivas, mediante espectroscopia iónica en fase gaseosa. Mediante este método, se confirma que $[Fe^V(O)(OH)(^{5tips3}tpa)]^{2+}$ hidroxila enlaces C-H vía el mecanismo de rebote y realiza la sin-dihidroxilación de alquenos y arenas. Otro caso paradigmático es la funcionalización de enlaces C-H alifáticos, por el hecho de transformar enlaces inertes C-H en alcoholes y carbonilos, que son algunos de los grupos más versátiles y funcionales en síntesis orgánica. Sin embargo, la naturaleza inerte del enlace C-H alifático y la multitud de enlaces C-H presentes en la molécula, hacen de estas reacciones uno de los retos más difíciles de la química sintética en la actualidad. Con este problema en mente, pudimos desarrollar una oxidación C-H quimioselectiva catalizada por manganeso, peróxido de hidrógeno como oxidante en un alcohol fluorado como disolvente. Estos disolventes inducen un reverso de polaridad sobre los enlaces C-H adyacentes al grupo hidroxilo, cosa que se traslada en un efecto de protección contra la sobreoxidación del grupo hidroxilo, comúnmente sensible a la oxidación, favoreciendo la oxidación C-H selectiva en posiciones remotas.

Chapter I.

General Introduction

The development of sustainable oxidation methods targeting alkane and alkene moieties is a subject of current importance because this class of reactions is widely used in bulk and fine chemistry, and current methodologies are far from satisfactory in terms of environmental impact. Contemporary methodologies for this class of transformations are mainly based on heavy metal oxides and toxic organic oxidants exhibiting poor atom economy and therefore produce large amounts of toxic waste.[1]

Selectivity is also a major issue in hydrocarbon oxidation reactions because the rather inert nature of these substrates requires the use of forcing reaction conditions and highly reactive oxidants, which translate into side reactions and substantial amounts of side products. Particularly critical is the oxidation of alkane moieties, for which limited competent oxidizing reagents exist, and for which the presence of multiple C-H bonds within a molecule makes site selectivity a great challenge.[2] In the case of *syn*-dihydroxylation reactions, they are commonly performed with high valent metal oxides such as OsO_4, RuO_4^- and MnO_4^-. The toxicity, the cost and the large amount of waste of these reactions motivate the development of new, more sustainable catalytic methodologies.[3]

 The development of sustainable oxidation methodologies ideally needs to target the use of oxidants that produce no waste, catalysts based on non-toxic metals, mild reaction conditions, and no explosive or toxic volatile solvents. The use of catalysts based on first row transition metals that are highly abundant and exhibit a minor environmental impact constitute promising alternatives. Particularly interesting are methods employing hydrogen peroxide as oxidant since the only byproduct is water.[4]

The use of iron and manganese based catalysts constitutes an interesting option, given the availability and limited cost and toxicity of these metals. Taking inspiration from iron dependent enzymes, iron and manganese coordination complexes are been actively explored as catalysts for alkane and alkene oxidation, employing peroxides as oxidizing agents.[5] Few examples have been discovered that provide products in synthetically valuable yields and there is mounting evidence that manipulation of the catalyst architecture may lead to more efficient catalysts, and may also serve to manipulate their selectivity at chemo, regio and stereoselective level.[6-7] Development of this class of catalysts will provide novel oxidation methods of high value in synthesis.

I.1. Oxidations in nature

Nature performs challenging C=C and C-H oxidations with iron enzymes in a very selective manner. These reactions proceed with high levels of regio, chemo- and stereoselectivity, while operating under mild conditions and producing minimum waste.[8] In contrast, these *oxidations* still represent a major challenge for contemporary synthetic chemistry.

Rieske dioxygenases are one of the most versatile family of non-heme iron metalloenzymes.[9] These are bacterial enzymes which catalyze a wide variety of reactions such as aliphatic C-H hydroxylation, arene and olefin *syn*-dihydroxylation, desaturations, sulfoxidations and O- and N-dealkylation.[10] Among them, particularly interesting are aliphatic C-H hydroxylation, and arene/olefin *syn*-dihydroxylation; aliphatic C-H hydroxylation takes place chemo- and site-electively at unactivated aliphatic C-H bond in the presence of *a priori* oxidation sensitive functional groups, and a number of C-H bonds, some of which are weaker and *a priori* more reactive, present in the substrate (Scheme I.1).
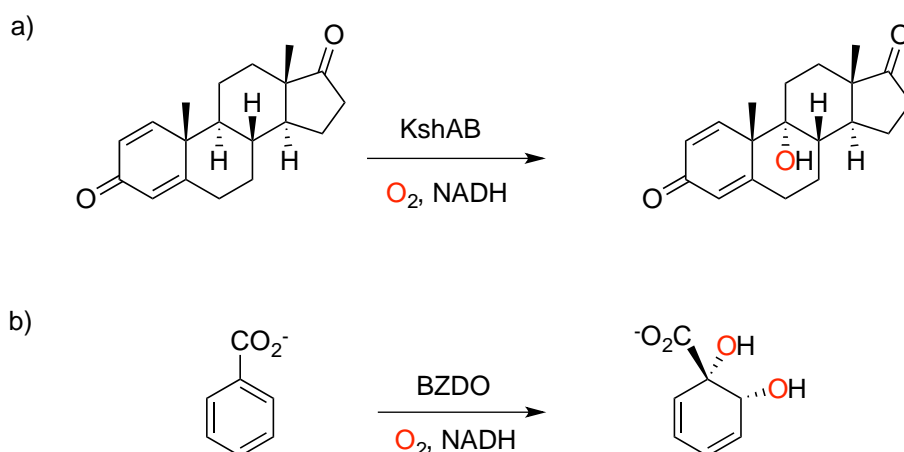
Scheme I.1. Examples of selective oxidations of the family of Rieske dioxygenases. a) Site selective C-H hydroxylation of a steroidal substrate.[11] b) *syn*-dihydroxylation of arenes by benzoate 1,2-dioxygenase.[12]

On the other hand, arene *syn*-dihydroxylation is a reaction exclusive to this class of enzymes, unattainable with traditional organic reagents, while olefin *syn*-dihydroxylation is a cornerstone transformation in organic synthesis currently performed with stoichiometric or catalytic amounts of high valent metal oxides, being osmium[13] and ruthenium[14] the most common choices.

This class of enzymes is also particularly interesting from a structural and mechanistic perspective. One of the best studied enzymes of Rieske dioxygenase family is Naphtalene 1,2-dioxygenase (NDO), characterized in 1998 from *Pseudomonas putida*.[15] The crystallographic structure of NDO can be divided in two components; the oxygenase and the reductase component. The active site of this enzyme is the oxygenase component and contains and iron center coordinated to three protein residues, two histidine and a bidentate aspartate or glutamate,[16] leaving two *cis* sites available that can coordinate a molecule of water, oxygen or the substrate. The reductase component contains a Fe_2-S_2 cluster, responsible to transfer the electrons. (Figure I.1)
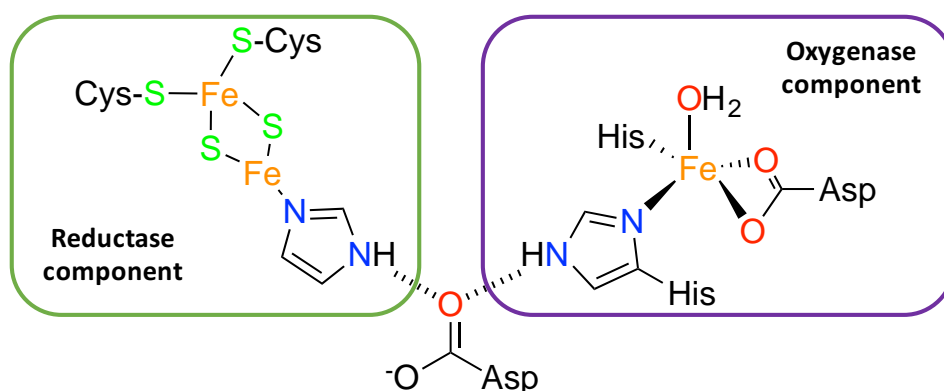
Figure I.1. Structure of NDO from *Pseudomonas putida.*

The proposed mechanism of this enzyme starts with the iron(II) form. The arrival of the substrate to the enzyme active site induces conformational changes that triggers reaction of the ferrous center with O_2 followed by electron transfer from the reductase component to generate a ferric hydroperoxide (Fe^{III}-OOH). Then the O-O bond cleavage is proposed to take place and a Fe^V=O is formed. This species is presumably the responsible for the oxidation (Scheme I.2). Labelling experiments using $H_2^{18}O$ have shown an incorporation between 3-10% of labelled oxygen to the *syn*-diol product in peroxide-shunt reactions (H_2O_2 as oxidant),[17] making a strong argument that the oxidizing specie is an iron-oxo intermediate, capable of exchanging the oxo moiety with water. It is important to notice that the well-studied enzyme Cytochrome P450 operates via an iron(IV)-oxo porphyrin radical cation.[18-20] Thus, Rieske dioxygenase enzymes are the only family of enzymes for which Fe^V=O intermediates are postulated.[16] Direct observation for these species has not been achieved so far.
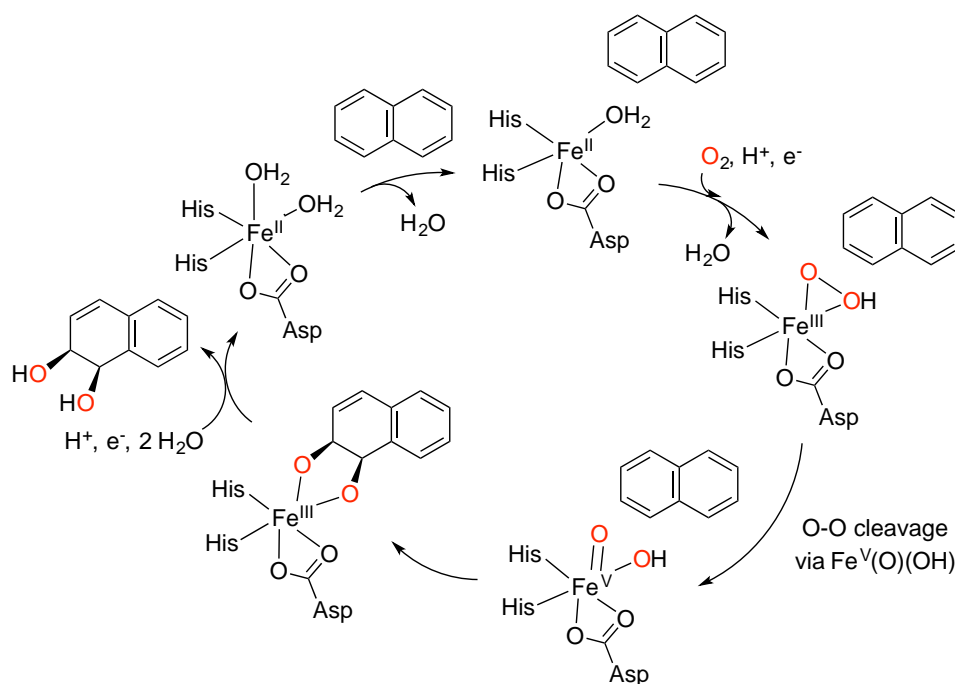
Scheme I.2. Proposed catalytic mechanism for *syn*-dihydroxylation catalayzed by Rieske dioxygenase.

These enzymes are a source of inspiration for the development of novel catalysts and oxidation methods, since reactions occur in a catalytic manner and take place under mild conditions, with non-toxic metals that can activate O_2 in a very efficient and selective manner.[21] Moreover, these enzymes contain iron in the active center, what makes them even more interesting, as this is a very abundant, non-toxic element, and can adopt different oxidation and spin states, which confer its compounds with a very rich chemistry.

I.2. Functional models of Rieske oxygenases as oxidation catalysts

The first example of the *syn*-dihydroxylation of olefins with a functional model of Rieske dioxygenases was reported in 1999 by Que and coworkers.[22] It was shown that the non-heme iron catalyst $[Fe^{II}(^{6\text{-}Me_3}tpa)(CH_3CN)_2](ClO_4)_2$ (Figure I.2) in combination with H_2O_2 (10 equiv. with respect to catalyst) catalyzes the *syn*-dihydroxylation of different olefins (1000 equiv. with respect to catalyst) delivering up to 5.2 turnover numbers (TN) of the corresponding diol. This catalyst contains an Fe^{II} center ligated to a N-donor tetradentate ligand that leaves two *cis* labile sites, occupied by acetonitrile solvent molecules. In this work, Que demonstrated that the presence of the two-labile *cis*-coordination sites was key for the catalyst being able to perform a *syn*-dihydroxylation of alkenes when reacted with H_2O_2.

Later on, Que and co-workers also reported the first example of *syn*-dihydroxylation of an aromatic double bond with a synthetic catalyst, [Fe^{II}(tpa)(CH$_3$CN)$_2$](OTf)$_2$ (Scheme I.3) and H$_2$O$_2$, effectively mimicking Naphthalene dioxygenase. Using analogous experimental conditions to the oxidation of non-aromatic olefins. When naphthalene was used as substrate, four products were obtained; *cis*-1,2-dihydro-1,2-naphthalenediol ,1-naphthol, 2-naphthol and 1,4-naphthoquinone. Among them, the diol (*cis*-1,2-dihydro-1,2-naphthalenediol) was the major product, in up to 3 TN (Scheme I. 3).[23]
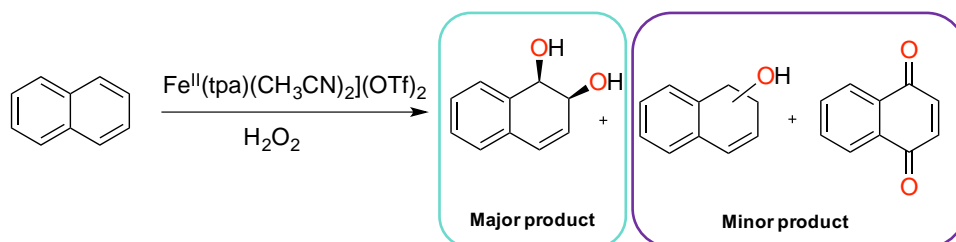
Scheme I.3. Naphthalene oxidation by [Fe^{II}(tpa)(CH$_3$CN$_2$)](OTf)$_2$.

The discovery that non-heme iron complexes catalyze *syn*-dihydroxylation of arenes and alkenes with H$_2$O$_2$ raised the interest of the synthetic bioinorganic and organic synthesis community to create small molecule iron catalysts for this transformation.[3]

I.3. *Syn*-dihydroxylation

After the pioneering works of Que and co-workers, a number of catalysts have been developed (representative examples depicted in Figure I.2). These include complexes that reproduce the coordination center of the active site of the enzyme ([Fe(Cl)(Bpka)]), and also complexes with polydentate ligands that incorporate nitrogen and oxygen donors (for example [Fe(PrL$_1$)](OTf)$_2$), but the most commonly developed catalysts are based in tetradentate N-rich ligands.

Que and Chen, where the first who described the *syn*-dihydroxylation of olefins using a large excess of substrate (1000 equiv. and 10 equiv. of H$_2$O$_2$), which prevented the potential synthetic utility of the catalysts. Nevertheless, they demonstrated that reactions exhibited selectivity properties that may eventually find utility in synthesis, provided substrate limiting conditions could be found.[22] Critical problems found in reaction performed under substrate limiting conditions include catalyst deactivation, limited chemoselectivity, competitive epoxidation, overoxidation and modest yields.

[Fe(BpdL₁)(CH₃CN)₂]²⁺   **[Fe(Cl)(Bpka)]**   **[Fe(OTf)₂(PrL₁)]**   **[Fe(OTf)₂(ph-dpah)₂]**

(S,S')-[Fe(⁶ᴹᵉ²pbp)(CH₃CN)₂]²⁺   **[Fe(OTf)₂(ᴹᵉ,⁴ˣ,⁶ʸpytacn)]**   **[Fe(OTf)₂(ᴹᵉ,ᴴpytacn)]**   **(S,S')-[Fe(OTf)₂(⁶ᴹᵉ²bqcn)]**
X,Y= Me or H

[Fe(⁵ᴹᵉ²men)(CH₃CN)₂]²⁺   **[Fe(tpa)(CH₃CN)₂]²⁺**   **[Fe(⁶ᴹᵉ³tpa)(CH₃CN)₂]²⁺**   **[Fe(⁵ᴹᵉ³tpa)(CH₃CN)₂]²⁺**
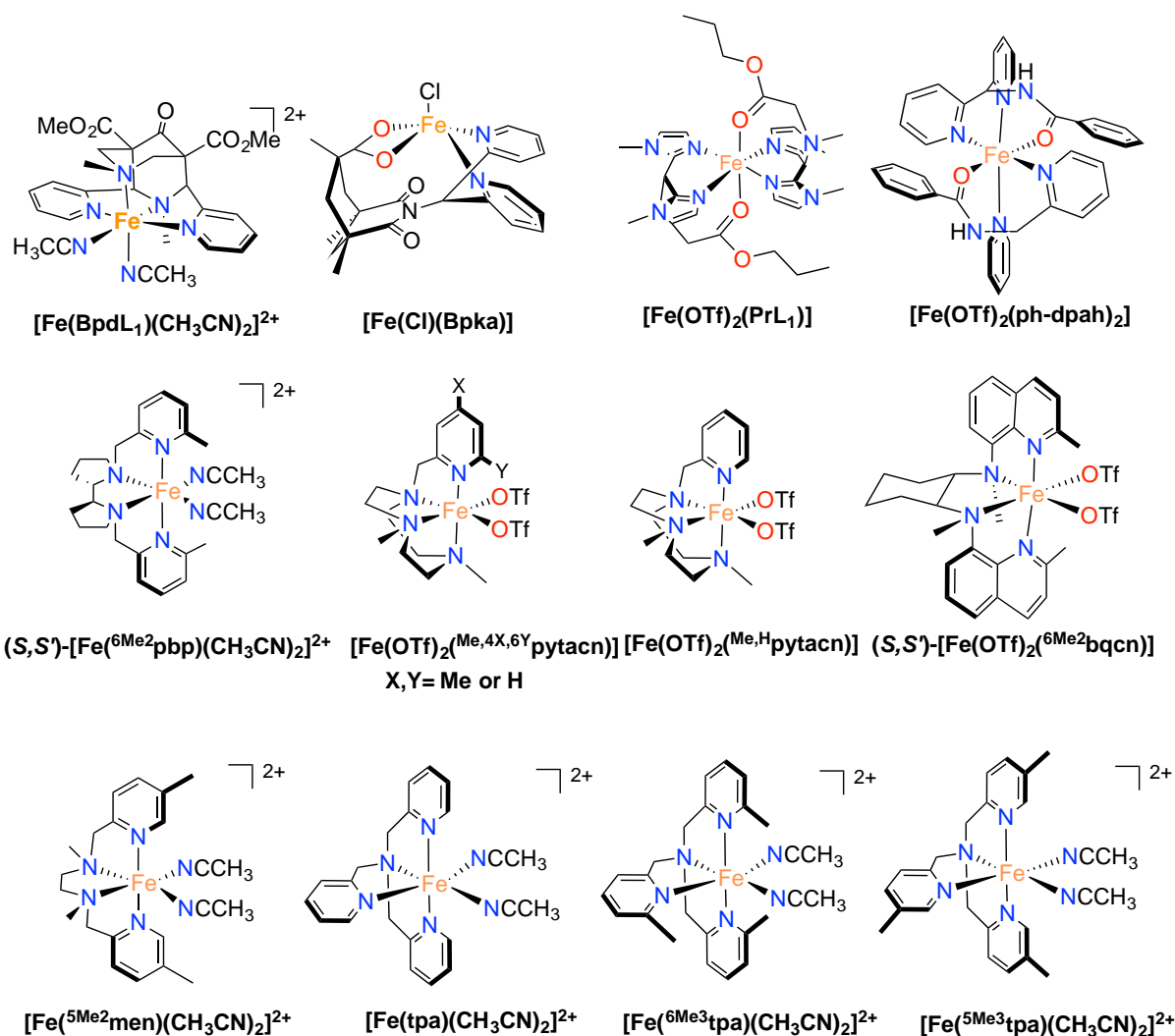
Figure I.2. Representative examples of iron complexes competent for the *syn*-dihydroxylation reaction.[24-33]

I.3.1. *Syn*-dihydroxylation in preparative conditions

Most of the catalysts work with excess of substrate as in the first works by Que and co-workers. Until Que described the use of ([Fe⁵ᴹᵉ³tpa)(CH₃CN)₂]²⁺ in combination with H_2O_2 as oxidant.[29] This system is limited to aliphatic olefins, and exhibits poor mass balances and moderate yields. Also, limited to aliphatic olefins is the system [Fe(OTf)₂(ᴹᵉ,ᴹᵉPytacn)] in combination with H_2O_2, reported by Prat *et al.*[34] This system displays moderate yields and chemoselectivity towards the diol and poor mass balance. On 2010, Che and co-workers described a catalyst ([Fe^{III}(Cl)₂(LN₄Me₂)]⁺) that also works under substrate-limiting conditions;[35] this system uses Oxone as oxidant and provides good yields and chemoselectivities, the substrate scope was limited to electron-deficient (ED) olefins. Later on, Che described the use of a catalyst [Fe(OTf)₂(bqcn)] that achieved good yields and high enantioselectivity in the dihydroxylation of electron deficient olefins.[26] More recently the same

group reported the catalyst [Fe(OTf)$_2$(bqpn)] that performs the enantioselective *syn*-dihydroxylation of trisubstituted electron-deficient alkenes in up to 98% yields and 99.9% ee (Figure I.3).[36]

[Fe(OTf)$_2$(Me,MePytacn)]
H$_2$O$_2$ as oxidant
Limited to aliphatic olefins
Moderate yields and selectivity
Poor mass balance

[Fe(^{5Me3}tpa)(CH$_3$CN)$_2$]$^{2+}$
R= H
R=Me

[Fe(Cl)$_2$(LN$_4$Me$_2$)]$^+$
Oxone as oxidant
Good yields and
selectivities limited
to ED olefins

(*S,S*)-[Fe(OTf)2(bqcn)]
H$_2$O$_2$ as oxidant
Good yields limited to
ED olefins
High enantioselectivity

cis-α-[Fe(OTf)$_2$(2-Me$_2$-bqpn)]
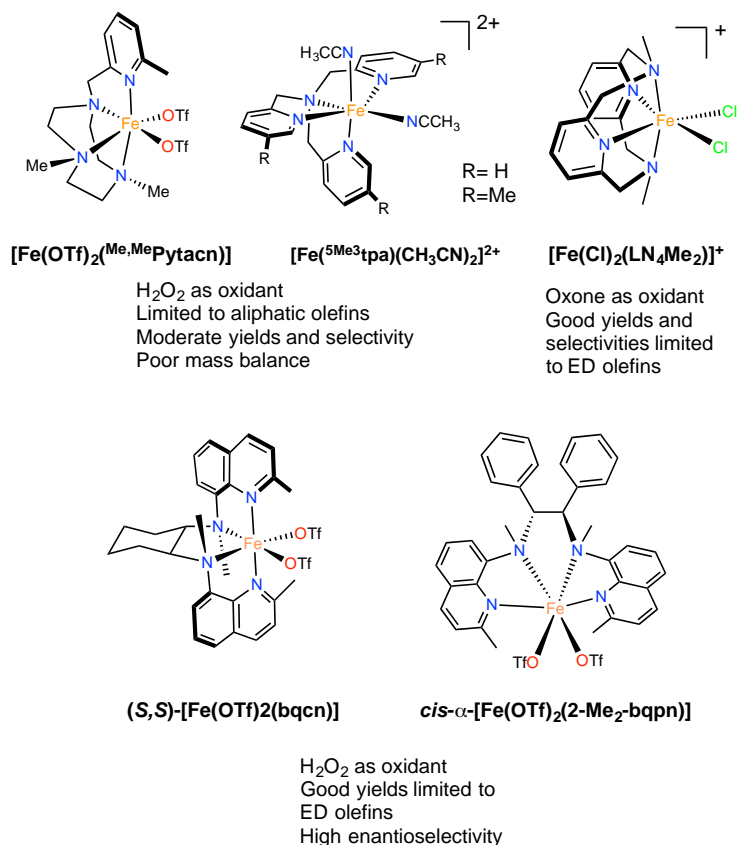
Figure I.3. Iron catalyst that work under substrate-limiting conditions.

I.3.2. Reaction mechanisms

Mechanistic studies have shown that non-heme iron catalysts can be grouped in two different classes (Class A and Class B) according to the mechanism in which they operate (Scheme I.4).[37] Their reactivity in front of different olefins suggests that Class A catalysts operate via electrophilic oxidants (electron rich olefins react preferentially over electron poor olefins), while Class B catalysts generate nucleophilic oxidants (electron poor olefins react preferentially over electron rich olefins).

Isotopic labeling experiments have demonstrated that for Class A catalysts, the two oxygen atoms incorporated into a *cis*-diol come from different origins: one from water and other from the oxidant. For this reason, the pathway operating in this class of catalysts is also known as water assisted mechanism. In contrast, for Class B catalysts both oxygen atoms incorporated into a *cis*-diol come from the same molecule of hydrogen peroxide.

As neither dioxygen nor water are involved in the formation of the diol, this pathway is also known as non-water assisted mechanism.[37] The difference between Class A and Class B is also related to the spin state of the ferric hydroperoxide (Fe^{III}-OOH) intermediate generated when the catalysts reacts with H_2O_2. Class A catalysts generate low-spin Fe^{III}-OOH intermediates, as happens with [Fe(OTf)$_2$(tpa)] that contains a strong field tpa ligand. In the other hand, Class B catalysts generate high-spin Fe^{III}-OOH intermediates. In this case, [Fe(OTf)$_2$($^{6\text{-Me3}}$tpa)], containing a weak field ligand, is a prototypical example of this type of catalysts.
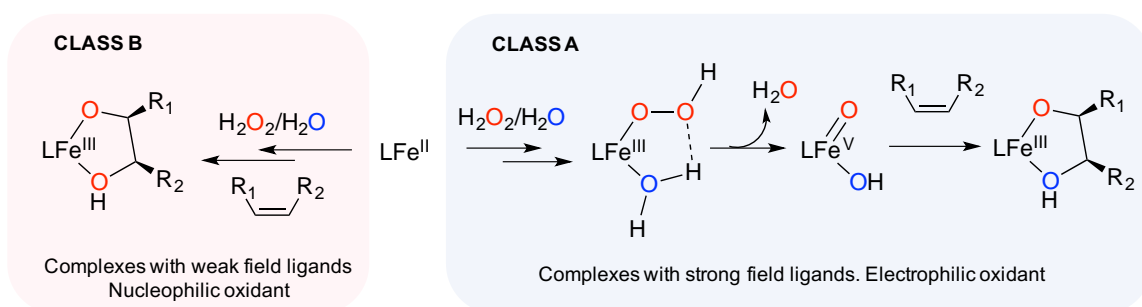
Scheme I.4. Summary of the two types of catalysts described (Class A in blue and Class B in red).

The mechanism for Class A and Class B starts from the initial ferrous complex, that in acetonitrile solvent contains two acetonitrile ligands in the labile positions. After oxidation with 0.5 equiv. of H_2O_2, a Fe^{III}-OH intermediate is formed, which reacts with a molecule of H_2O_2 to generate a metastable Fe^{III}-OOH intermediate. In this point, the two mechanisms start to differ.

For Class A catalysts, the Fe^{III}-OOH adopts a low spin state. It is proposed that the O-O bond is cleaved in a heterolytic manner forming a Fe^{V}(O)(OH) species and releasing a water molecule. In this high-valent species, one of the oxygen atoms come from the H_2O_2 and the other from a water molecule. This species is then responsible for the two oxygens delivery to an olefin via a formal [3+2] addition.

Other mechanisms can be postulated, but discarded after experimental evidences. First, the two oxygen atoms could be transferred directly from the Fe^{III}OOH, but this is not consistent with the labelling experiments that shown a single ^{18}O incorporation in the diol product. Secondly, the O-O bond cleavage could occur in a homolytic manner. If this occurs, hydroxyl radical species would be formed, which is not compatible with the stereospecificity observed in the reactions.

From these studies, it can be concluded that an electrophilic Fe^{V} species is the responsible of the oxidation of hydrocarbons. However, this intermediate has not been well characterized until the present thesis. This is because this intermediate is very reactive, even at low temperature, and it cannot be accumulated in solution, which avoid its isolation. However, direct evidences in favor of these species has gained, mainly by means of mass spectrometry.[38-39]

On an opposite manner, for Class B catalysts, the Fe^{III}-OOH adopts a high spin species. In this case, the O-O bond is not activated towards cleavage, and therefore the direct transfer of the two oxygen atoms is presumably produced from the Fe^{III}-OOH species. It is postulated that an isomerization of this species towards a side-on $Fe^{III}(\eta^2$-OOH) intermediate activates this compound towards reaction with the olefin.[40] In this case, both oxygen atoms come from the same molecule of hydrogen peroxide.

Differences between this mechanism and the one proposed for Class A catalyst are best evidenced in the origin of the oxygen atoms in the diol product: in the Class A mechanism one of the oxygens comes from a water molecule and the other from the oxidant whereas in Class B mechanism both oxygens atoms come from the same molecule of hydrogen peroxide.

These mechanisms proposed are based on experimental data such as spectroscopic characterization of the ferric intermediates as well as isotopic labelling experiments, and have been validated by DFT calculations.[41] Most remarkably, it is proposed that the spin state of the catalyst is a determinant factor for the mechanisms of peroxide activation and C=C oxidation.

A second proposal mechanism has been put forward which considers that the complexes may operate through a Fe^{II}/Fe^{IV} cycle. In this scenario, the Fe^{II} reacts with the H_2O_2 molecule and forms the Fe^{IV}-oxo reactive species. O-O activation in this mechanism does not require a water molecule, and results in the insertion of the two oxygen atoms of a single H_2O_2 molecule in the olefin. Isotopic labelling experiments are consistent with this mechanism, which has been also validated by DFT methods. This proposal mechanism is strongly related to the type of the ligand. Specifically, weak-field ligands favor this mechanism.[24-25]

I.4. C-H oxidation

The functionalization of non-activated aliphatic C-H bonds is a very challenging reaction due to the poorly reactive nature of the C-H bonds.[2] Along with their inert character, the multitude of aliphatic C-H bonds and other functional groups present in a molecule makes site-selective functionalization a difficult problem. However, this reaction is very attractive because it converts a simple C-H bond into a C-O bond, which can be subsequently converted into a myriad of diverse products.

I.4.1. Iron catalyzed C-H oxidations via enzyme-like mechanisms

In a series of landmark studies, Que and co-workers showed that mononuclear iron complexes $[Fe(tpa)(CH_3CN)_2]^{2+}$ and $[Fe(men)(CH_3CN)_2]^{2+}$ react with H_2O_2 to form an oxidizing species that is very reactive and at the same time highly selective when reacting with hydrocarbons.[42] Different experimental evidences allowed the proposal of a mechanism for this reaction (Scheme I.5). First, the high A/K ratio observed in the oxidation of cyclohexane (5-11) is in accordance with the presence of a metal-based oxidant, which generates short-live radicals. This is not consistent in with the presence of hydroxyl radicals since long-live radicals would be then generated, and as a consequence a A/K around 1 would be obtained (Scheme I.5, a). A conclusive evidence that long-live radicals are not involved in the mechanism is found in the oxidation of *cis*-1,2-dimethylcyclohexane, since the reaction occurs in stereoretentive manner (Scheme I.5, b). Finally, isotopic labelling experiments performed with both catalyst demonstrates that the O-atom found in the product comes from H_2O_2 and H_2O, but not from atmospheric O_2 (Scheme I.5, c). Moreover, the incorporation of ^{18}O to the product when ^{18}O-labelled water was added suggested that the oxygen atoms of the metal-based oxidant can exchange with the water in the media. This behavior is typical of M=O moieties, which suggested the presence of a high-valent iron-oxo species as the responsible for the oxidation reaction. A drawback of these systems is that they operate in conditions of large excess of oxidant, and cannot be used for organic synthesis.

[Fe(tpa)(CH$_3$CN)$_2$]$^{2+}$ [Fe(men)(CH$_3$CN)$_2$]$^{2+}$

a)

[Fe(tpa(CH$_3$CN)$_2$]$^{2+}$	A/K= 5
[Fe(men)(CH$_3$CN)$_2$]$^{2+}$	A/K= 11

b)

[Fe(tpa(CH$_3$CN)$_2$]$^{2+}$	cis:trans= >99:1
[Fe(men)(CH$_3$CN)$_2$]$^{2+}$	cis:trans= 98:2

c)

[Fe(tpa(CH$_3$CN)$_2$]$^{2+}$	^{18}O= 70%
[Fe(men)(CH$_3$CN)$_2$]$^{2+}$	^{18}O= 84%

[Fe(tpa(CH$_3$CN)$_2$]$^{2+}$	^{18}O= 27%
[Fe(men)(CH$_3$CN)$_2$]$^{2+}$	^{18}O= 18%
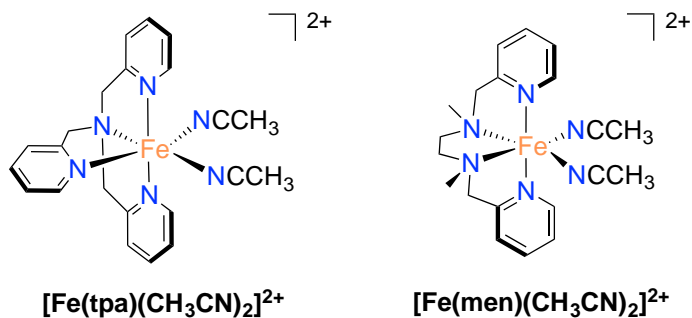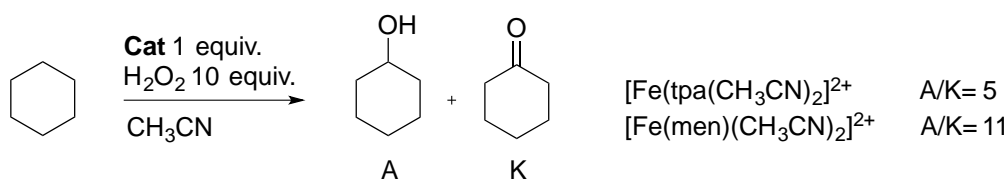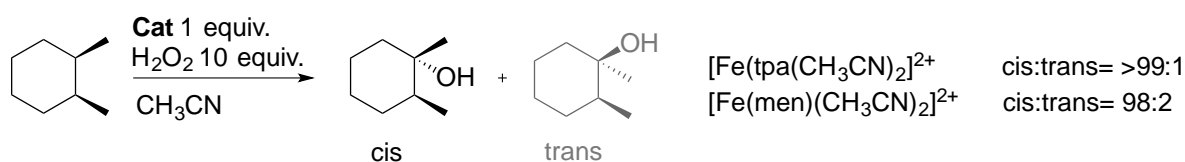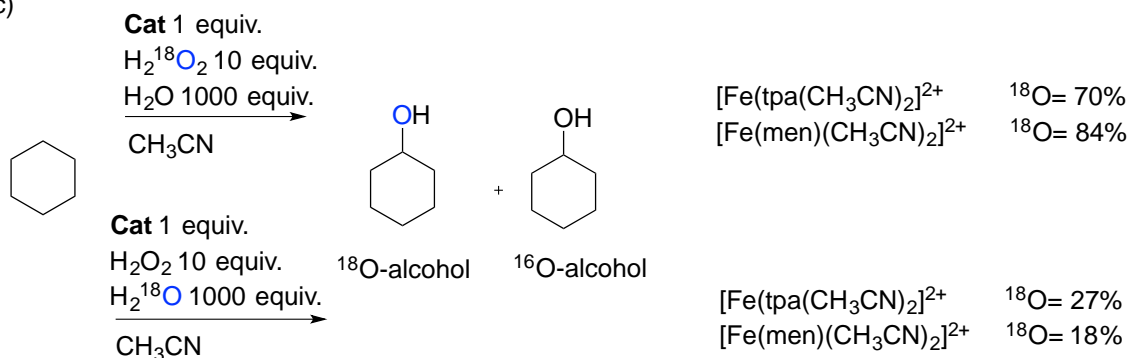
Scheme I.5. a) and b) mechanistic probes of the oxidation of cyclohexane and *cis*-1,2-dimethylcyclohexane with [Fe(tpa)(CH$_3$CN)$_2$]$^{2+}$ and [Fe(men)(CH$_3$CN)$_2$]$^{2+}$. d) labelling experiment of cyclohexane with both catalyst.

I.4.2. Selective C-H oxidation in preparative conditions.

Pioneering work of White, showed that a non-heme iron catalyst [Fe(pdp)(CH$_3$CN)$_2$]$^{2+}$ in combination with acetic acid, catalyzes the oxidation of aliphatic C-H bonds using H$_2$O$_2$ delivering product yields suitable for synthesis.[43-45]. Later on, some other iron catalysts have proved to be competent as synthetic tools (Scheme I.6).[46-47]

(S,S)-[Fe(OTf)₂(pdp)]

(S,S)-[Fe(OTf)$_2$(pdp)] Λ-[Fe(OTf)$_2$(mcpp)]   [Fe(OTf)$_2$(^{Me,Me}pytacn)]

cat	Conv. (%)	Yield A (%)	Yield K (%)
(S,S)-[Fe(OTf)$_2$(pdp)]	66	22	22
Λ-[Fe(OTf)$_2$(mcpp)]	78	36	7
[Fe(OTf)$_2$(^{Me,Me}pytacn]	72	15	33
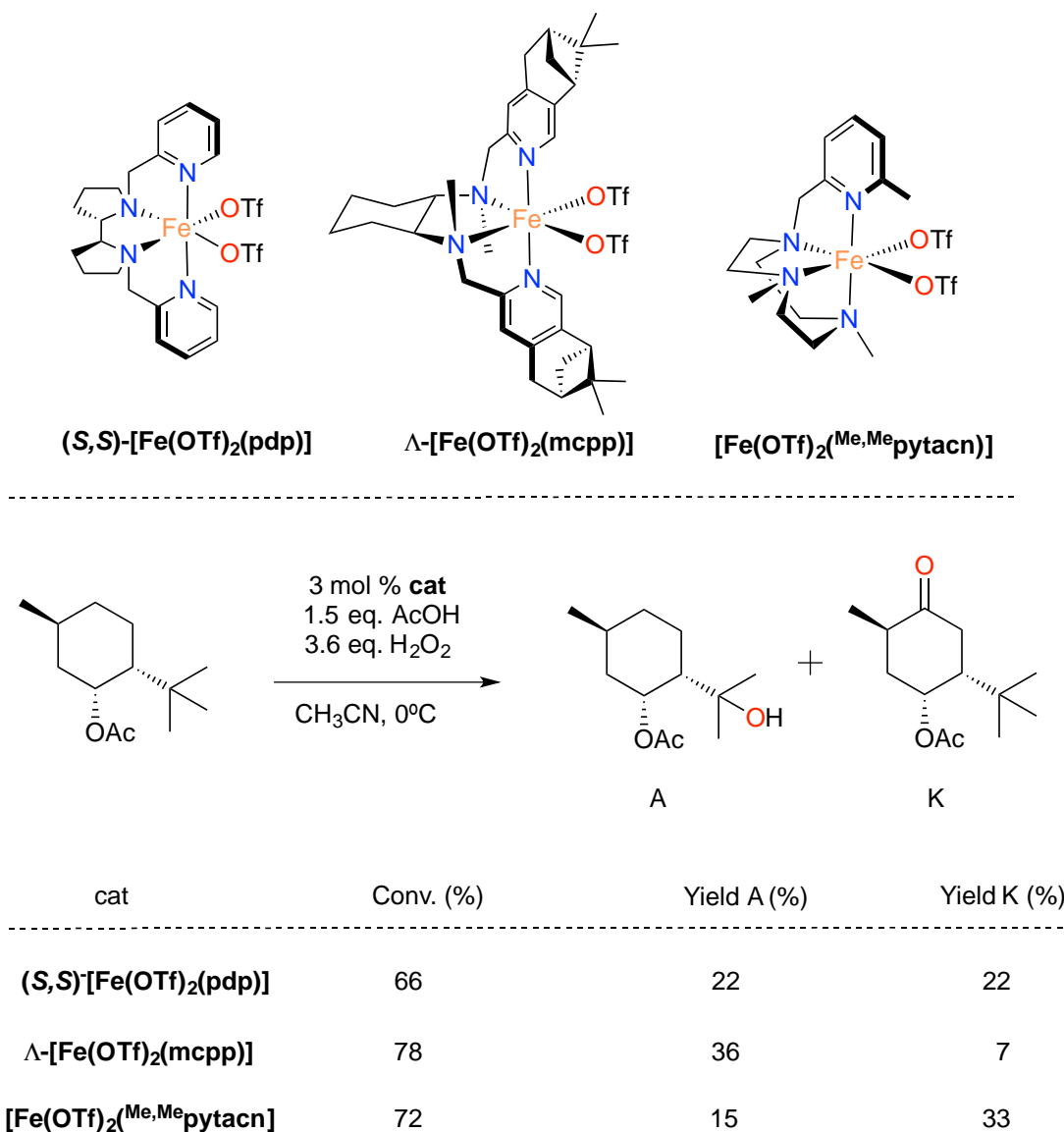
Scheme I.6. Some relevant examples of iron complexes suitable for C-H activation working at substrate-limiting conditions.[46]

White and co-workers also showed that these reactions proceed in a selective manner, and identified selectivity parameters that permit the prediction of the site-selectivity of the C-H oxidation: electronic, steric, directed and stereoelectronics (Scheme I.7).[43-44, 48]
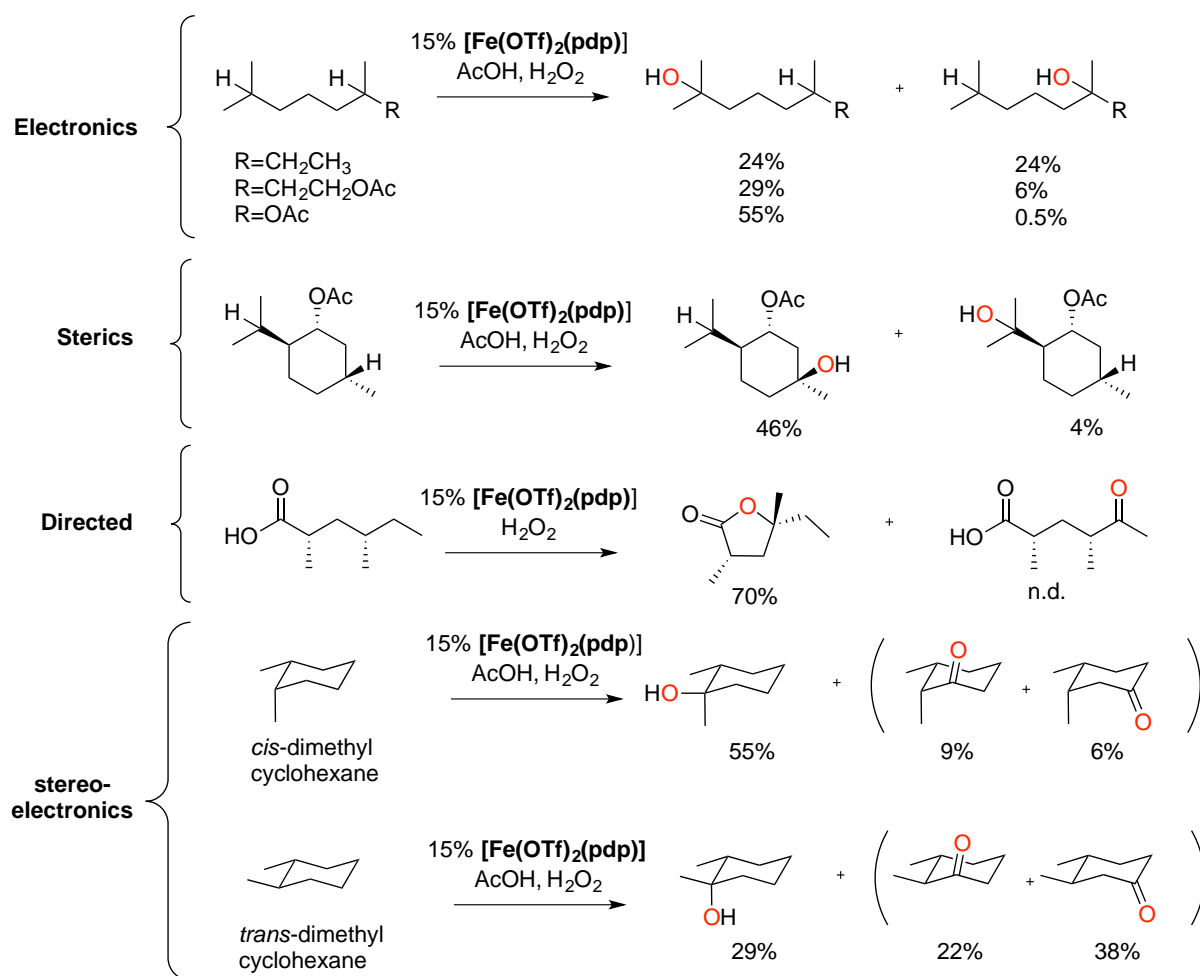
Scheme I.7. Electronic, steric, directed and stereoelectronic.

I.4.3. Selective C-H oxidations at remote sites

The oxidation of nitrogen-containing molecules such as amines o amides has attracted interest in the recent years because these moieties are highly present in natural products, drugs and bioactive molecules.[49-51]

White and co-workers showed that the protonation of amines using Lewis or Brønsted acids driven the amine group very strong EWG, which deactivates the α-C-H and direct the oxidation towards a remote C(sp3)-H bond (Scheme I.8).[52]
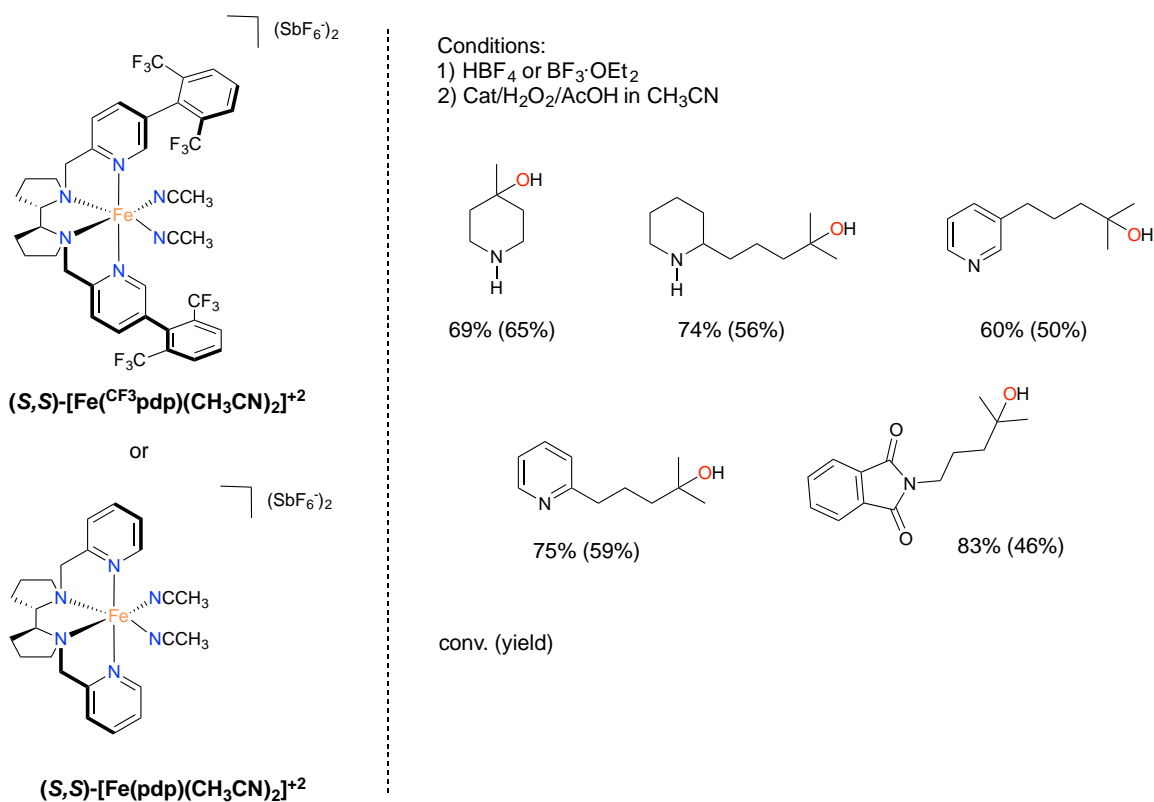
Scheme I.8. Remote oxidation of amine with protonation.

In a similar manner, her group also reported that the protection of amides using MeOTf deactivates the α-C-H bond and allows the oxidation of the most remote position (Scheme I.9, a).[53] Selective oxidation of amides can be accomplished with Mn catalysts. Electronic and stereoelectronic effects can be used to direct oxidation towards the proximal or remote oxidation of C-H bonds (Scheme I.9, b).[54]
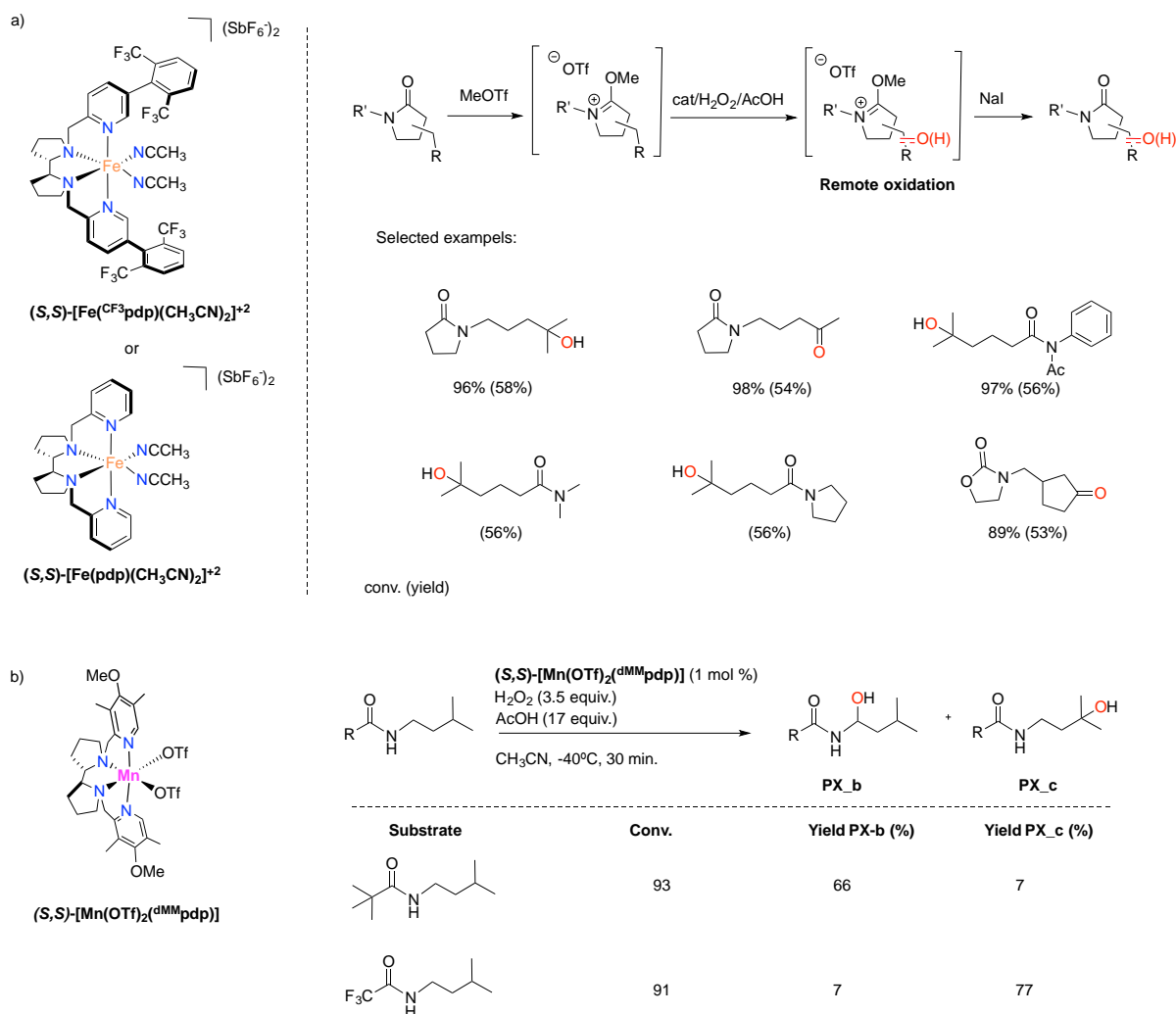
Scheme I.9. Remote oxidation of amides.

In a parallel manner, other strategy based on medium effects was studied by our group to govern the chemo- and site-selectivity in C-H oxidation reactions. [55] It consists in the use of fluorinated alcohol solvents, which are very powerful hydrogen donors and strongly interact with the hydroxyl or carbonyl group via hydrogen bonding. This interaction causes a polarity reversal that strongly deactivates the proximal C-H bonds towards oxidation, as well as protects the functional group towards oxidation, which directs the oxidation towards remote positions. This impact of fluorinated solvent was studied in the oxidation of amines, amides and alcohols (Scheme I. 10).
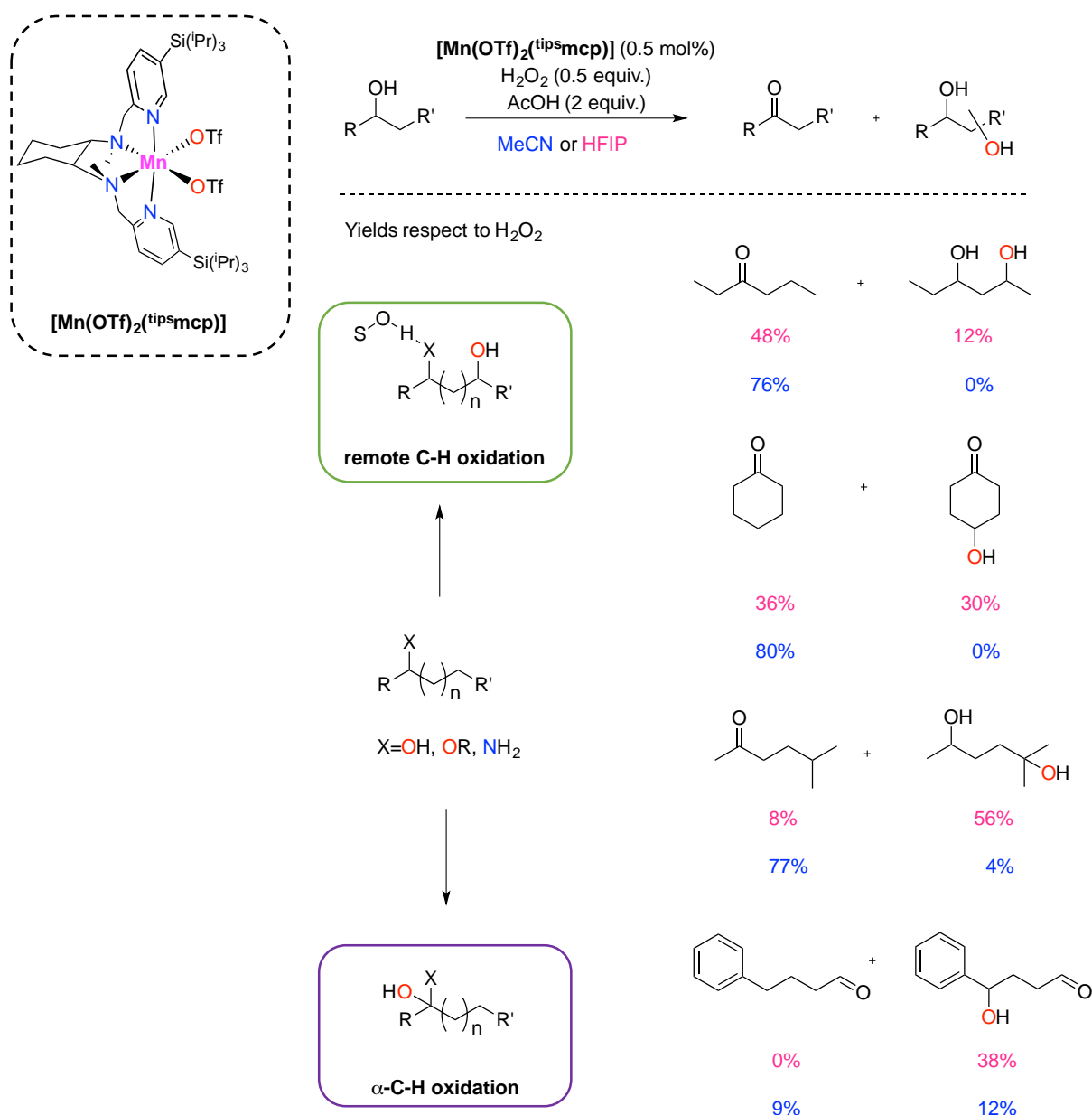
Scheme I.10. Impact of the solvent on the remote oxidation of alcohols.

I.4.4. The role of carboxylic acids in iron catalyzed C-H oxidation

 As it can be seen in the previous examples of C-H oxidation, most of them used a carboxylic acid as additive, the positive effect of acetic acid in the oxidation activity of these catalysts was disclosed by Jacobsen *and co-workers*.[56] They demonstrated that the use of AcOH improves systematically the yields in the epoxidation of aliphatic olefins. Later on, Que and co-worker provided a mechanistic frame to understand the role of the carboxylic acid, proposing that it assists the activation of the O-O bond of H_2O_2 and generates a $Fe^V(O)(OAc)$ oxidant. This mechanism was named *carboxylic acid-assisted* and it is proposed that is the one operating in the iron-catalyzed aliphatic C-H oxidation (Scheme I.11).[57]

The mechanism starts with the Fe^{II} precatalyst that undergoes initial oxidation to Fe^{III}-OOH with 1.5 equivalents of H_2O_2. After that, the heterolytic cleavage of the O-O bond assisted by the carboxylic acid leads to the formation of a $Fe^V=O$ species. These species engage in a hydrogen atom transfer (HAT) with a C-H bond of the substrate, generating a carbon centered radical intermediate on the substrate, which finally undergoes a rebound with the hydroxyl ligand from the Fe^{IV}-OH leading to the hydroxylated product.[58]
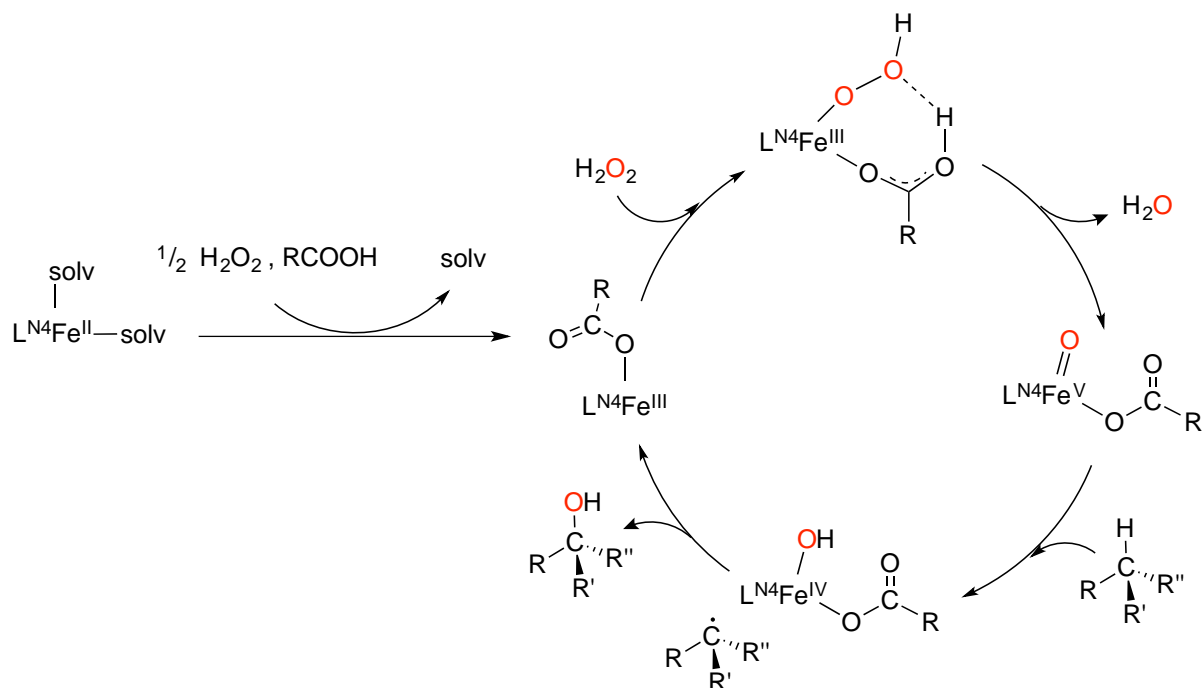
Scheme I.11. C-H oxidation carboxylic acid-assisted mechanism.

I.4.5. Catalytic oxidations with manganese complexes

The same mechanism is proposed to be operative with analogous manganese complexes, that have also used in oxidation reactions with H_2O_2. These reactions are also interesting since Mn is a first-row transition metal and like iron, it presents a low cost and low toxicity. Stack [59-60] and Bryliakov[61] first showed that the use of Mn complexes related to Que's and White's iron catalysts are also good catalysts for the same type of oxidation reactions commonly performed with the latter iron catalysts (Scheme I.12).

Moreover, the same selectivity patterns are observed with the two metals. For all these similarities in properties and performance in oxidation chemistry, it is suggested that similar mechanisms may be operative.[62]
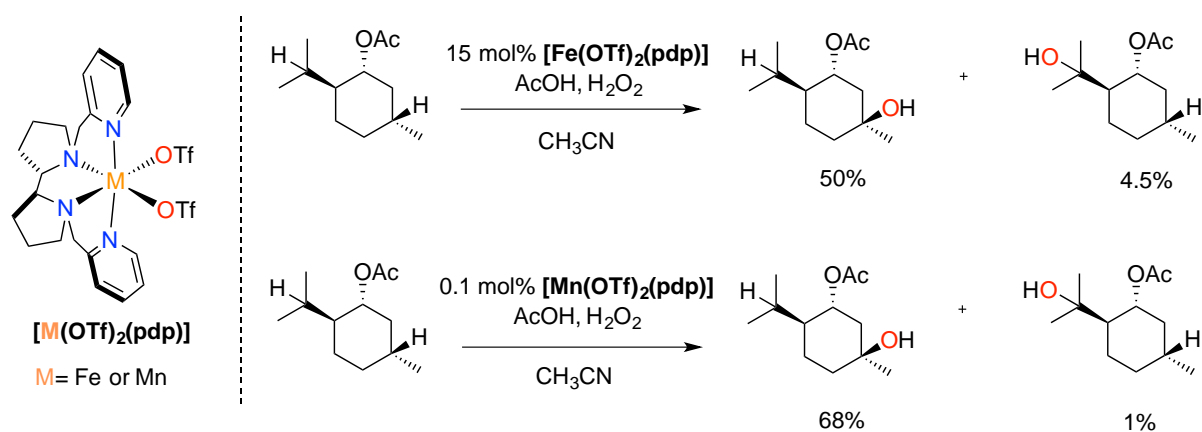
Scheme I.12. Selected example of selective oxidation with iron[43] and manganese[63] catalyst.

I.5. References

(1)   Beller, M., The Current Status and Future Trends in Oxidation Chemistry. *Adv. Synth. Catal.* **2004,** *346* (2-3), 107-108.

(2)   Newhouse, T.; Baran, P. S., If C-H Bonds Could Talk: Selective C-H Bond Oxidation. *Angew. Chem. Int. Ed.* **2011,** *50* (15), 3362-3374.

(3)   Achard, T.; Bellemin-Laponnaz, S., Recent Advances on Catalytic Osmium-Free Olefin syn-Dihydroxylation. *Eur. J. Org. Chem.* **2021***, 2021* (6), 877-896.

(4)   Noyori, R.; Aoki, M.; Sato, K., Green oxidation with aqueous hydrogen peroxide. *Chem. Commun.* **2003,** (16), 1977-1986.

(5)   Olivo, G.; Cusso, O.; Costas, M., Biologically Inspired C-H and C=C Oxidations with Hydrogen Peroxide Catalyzed by Iron Coordination Complexes. *Chem. Asian J.* **2016,** *11* (22), 3148-3158.

(6)   Borrell, M.; Gil-Caballero, S.; Bietti, M.; Costas, M., Site-Selective and Product Chemoselective Aliphatic C–H Bond Hydroxylation of Polyhydroxylated Substrates. *ACS Catal.* **2020,** *10* (8), 4702-4709.

(7)   Sun, W.; Sun, Q., Bioinspired Manganese and Iron Complexes for Enantioselective Oxidation Reactions: Ligand Design, Catalytic Activity, and Beyond. *Acc. Chem. Res.* **2019,** *52* (8), 2370-2381.

(8)   Costas, M.; Mehn, M. P.; Jensen, M. P.; Que, L., Dioxygen Activation at Mononuclear Nonheme Iron Active Sites: Enzymes, Models, and Intermediates. *Chem. Rev.* **2004,** *104* (2), 939-986.

(9)   Barry, S. M.; Challis, G. L., Mechanism and Catalytic Diversity of Rieske Non-Heme Iron-Dependent Oxygenases. *ACS Catal.* **2013,** *3* (10), 2362-2370.

(10)   Resnick, S. M.; Gibson, D. T., Regio- and stereospecific oxidation of fluorene, dibenzofuran, and dibenzothiophene by naphthalene dioxygenase from Pseudomonas sp. strain NCIB 9816-4. *Appl. Environ. Microbiol.* **1996,** *62* (11), 4073.

(11)   Moccia, J.; D'Angelo, I.; Strynadka, N.; Eltis, L., Characterization of 3-Ketosteroid 9 - Hydroxylase, a Rieske Oxygenase in the Cholesterol Degradation Pathway of Mycobacterium tuberculosis. *J. Biol. Chem.* **2009,** *284*, 9937-46.

(12)   Rivard, B. S.; Rogers, M. S.; Marell, D. J.; Neibergall, M. B.; Chakrabarty, S.; Cramer, C. J.; Lipscomb, J. D., Rate-Determining Attack on Substrate Precedes Rieske Cluster Oxidation during Cis-Dihydroxylation by Benzoate Dioxygenase. *Biochemistry* **2015,** *54* (30), 4652-4664.

(13)   Zaitsev, A. B.; Adolfsson, H., Recent developments in asymmetric dihydroxylations. *Synthesis* **2006,** (11), 1725-1756.

(14)   Shing, T. K. M.; Tam, E. K. W.; Tai, V. W. F.; Chung, I. H. F.; Jiang, Q., Ruthenium-catalyzed cis-dihydroxylation of alkenes: Scope and limitations. *Chem. Eur. J.* **1996,** *2* (1), 50-57.

(15)   Kauppi, B.; Lee, K.; Carredano, E.; Parales, R. E.; Gibson, D. T.; Eklund, H.; Ramaswamy, S., Structure of an aromatic-ring-hydroxylating dioxygenase - naphthalene 1,2-dioxygenase. *Structure* **1998,** *6* (5), 571-586.

(16)   Koehntop, K. D.; Emerson, J. P.; Que, L., The 2-His-1-carboxylate facial triad: a versatile platform for dioxygen activation by mononuclear non-heme iron(II) enzymes. *J. Biol. Inorg. Chem.* **2005,** *10* (2), 87-93.

(17)   Wolfe, M. D.; Lipscomb, J. D., Hydrogen Peroxide-coupled cis-Diol Formation Catalyzed by Naphthalene 1,2-Dioxygenase. *J. Biol. Chem.* **2003,** *278* (2), 829-835.

(18)   Groves, J. T., High-valent iron in chemical and biological oxidations. *J. Inorg. Biochem.* **2006,** *100* (4), 434-447.

(19)   Rittle, J.; Green, M. T., Cytochrome P450 Compound I: Capture, Characterization, and C-H Bond Activation Kinetics. *Science* **2010,** *330* (6006), 933.

(20)   Meunier, B.; de Visser, S. P.; Shaik, S., Mechanism of Oxidation Reactions Catalyzed by Cytochrome P450 Enzymes. *Chem. Rev.* **2004,** *104* (9), 3947-3980.

(21)   Que, L.; Tolman, W. B., Biologically inspired oxidation catalysis. *Nature* **2008,** *455*, 8.

(22)   Chen, K.; Que Jr., L., cis-Dihydroxylation of Olefins by a Non-Heme Iron Catalyst: A Functional Model for Rieske Dioxygenases. *Angew. Chem. Int. Ed.* **1999,** *38* (15), 2227-2229.

(23)   Feng, Y.; Ke, C.-y.; Xue, G.; Que Jr., L., Bio-inspired arene cis-dihydroxylation by a non-haem iron catalyst modeling the action of naphthalene dioxygenase *Chem. Commun.* **2009,** (1), 50-52.

(24)   Bukowski, M. R.; Comba, P.; Lienke, A.; Limberg, C.; Lopez de Laorden, C.; Mas-Ballesté, R.; Merz, M.; Que Jr., L., Catalytic Epoxidation and 1,2-Dihydroxylation of Olefins with Bispidine–Iron(II)/H2O2 Systems. *Angew. Chem. Int. Ed.* **2006,** *45* (21), 3446-3449.

(25)   Oldenburg, P. D.; Feng, Y.; Pryjomska-Ray, I.; Ness, D.; Que Jr., L., Olefin Cis-Dihydroxylation with Bio-Inspired Iron Catalysts. Evidence for an FeII/FeIV Catalytic Cycle. *J. Am. Chem. Soc.* **2010,** *132* (50), 17713-17723.

(26)   Zang, C.; Liu, Y.; Xu, Z.-J.; Tse, C.-W.; Guan, X.; Wei, J.; Huang, J.-S.; Che, C.-M., Highly Enantioselective Iron-Catalyzed cis-Dihydroxylation of Alkenes with Hydrogen Peroxide Oxidant via an FeIII-OOH Reactive Intermediate. *Angew. Chem. Int. Ed.* **2016,** *55* (35), 10253-10257.

(27) Oldenburg, P. D.; Shteinman, A. A.; Que, L., Jr., Iron-Catalyzed Olefin cis-Dihydroxylation Using a Bio-Inspired N,N,O-Ligand. *J. Am. Chem. Soc.* **2005,** *127* (45), 15672-15673.

(28) Prat, I.; Font, D.; Company, A.; Junge, K.; Ribas, X.; Beller, M.; Costas, M., Fe(PyTACN)-Catalyzed cis-Dihydroxylation of Olefins with Hydrogen Peroxide. *Adv. Synth. Catal.* **2013,** *355* (5), 947-956.

(29) Ryu, J. Y.; Kim, J.; Costas, M.; Chen, K.; Nam, W.; Que Jr., L., High Conversion of Olefins to cis-Diols by Non-heme Iron Catalysts and H2O2. *Chem. Commun.* **2002,** *12*, 1288-1289.

(30) Suzuki, K.; Oldenburg, P. D.; Que, L., Iron-Catalyzed Asymmetric Olefin cis-Dihydroxylation with 97 % Enantiomeric Excess. *Angew. Chem. Int. Ed.* **2008,** *47* (10), 1887-1889.

(31) Bruijnincx, P. C. A.; Buurmans, I. L. C.; Gosiewska, S.; Moelands, M. A. H.; Lutz, M.; Spek, A. L.; van Koten, G.; Klein Gebbink, R. J. M., Iron(II) Complexes with Bio-Inspired N,N,O Ligands as Oxidation Catalysts: Olefin Epoxidation and cis-Dihydroxylation. *Chem. Eur. J.* **2008,** *14* (4), 1228-1237.

(32) Company, A.; Feng, Y.; Güell, M.; Ribas, X.; Luis, J. M.; Que Jr., L.; Costas, M., Olefin-Dependent Discrimination between Two Nonheme HO-FeV=O Tautomeric Species in Catalytic H2O2 Epoxidations. *Chem. Eur. J.* **2009,** *15* (14), 3359-3362.

(33) Bautz, J.; Comba, P.; Lopez de Laorden, C.; Menzel, M.; Rajaraman, G., Biomimetic High-Valent Non-Heme Iron Oxidants for the cis-Dihydroxylation and Epoxidation of Olefins. *Angew. Chem. Int. Ed.* **2007,** *46* (42), 8067-8070.

(34) Prat, I.; Company, A.; Corona, T.; Parella, T.; Ribas, X.; Costas, M., Assessing the Impact of Electronic and Steric Tuning of the Ligand in the Spin State and Catalytic Oxidation Ability of the Fe. *Inorg. Chem.* **2013,** *52*, 9229−9244-9229−9244.

(35) Chow, T. W.-S.; Wong, E. L.-M.; Guo, Z.; Liu, Y.; Huang, J.-S.; Che, C.-M., cis-Dihydroxylation of Alkenes with Oxone Catalyzed by Iron Complexes of a Macrocyclic Tetraaza Ligand and Reaction Mechanism by ESI-MS Spectrometry and DFT Calculations. *J. Am. Chem. Soc.* **2010,** *132* (38), 13229-13239.

(36) Wei, J.; Wu, L.; Wang, H.-X.; Zhang, X.; Tse, C.-W.; Zhou, C.-Y.; Huang, J.-S.; Che, C.-M., Iron-Catalyzed Highly Enantioselective cis-Dihydroxylation of Trisubstituted Alkenes with Aqueous H2O2. *Angew. Chem. Int. Ed.* **2020,** *59* (38), 16561-16571.

(37) Fujita, M.; Costas, M.; Que Jr., L., Iron Catalyzed Olefin Cis-Dihydroxylation by H2O2: Electrophilic versus Nucleophilic Mechanisms. *J. Am. Chem. Soc.* **2003,** *125* (33), 9912-9913.

(38)   Prat, I.; Mathieson, J. S. J. S.; Güell, M.; Ribas, X.; Luis, J. M. J. M.; Cronin, L.; Costas, M., Observation of Fe(V)=O using variable-temperature mass spectrometry and its enzyme-like C–H and C=C oxidation reactions. *Nat. Chem.* **2011,** *3* (10), 788-793.

(39)   Xu, S.; Veach, J. J.; Oloo, W. N.; Peters, K. C.; Wang, J.; Perry, R. H.; Que, L., Detection of a transient FeV(O)(OH) species involved in olefin oxidation by a bio-inspired non-haem iron catalyst. *Chem. Commun.* **2018,** *54* (63), 8701-8704.

(40)   Iyer, S. R.; Javadi, M. M.; Feng, Y.; Hyun, M. Y.; Oloo, W. N.; Kim, C.; Que, L., Jr., A chameleon catalyst for nonheme iron-promoted olefin oxidation. *Chem. Commun.* **2014,** *50* (89), 13777-80.

(41)   Chen, K.; Costas, M.; Que, J. L., Spin state tuning of non-heme iron-catalyzed hydrocarbon oxidations: participation of FeIII-OOH and FeV[double bond, length as m-dash]O intermediates. *J. Chem. Soc. Dalton Trans.* **2002,** (5), 672-679.

(42)   Chen, K.; Que, L., Stereospecific Alkane Hydroxylation by Non-Heme Iron Catalysts: Mechanistic Evidence for an FeVO Active Species. *J. Am. Chem. Soc.* **2001,** *123* (26), 6327-6337.

(43)   Chen, M. S.; White, M. C., A predictably selective aliphatic C-H oxidation reaction for complex molecule synthesis. *Science* **2007,** *318* (5851), 783-7.

(44)   Chen, M. S.; White, M. C., Combined Effects on Selectivity in Fe-Catalyzed Methylene Oxidation. *Science* **2010,** *327*, 566-571.

(45)   White, M. C., Adding Aliphatic C–H Bond Oxidations to Synthesis. *Science* **2012,** *335* (6070), 807.

(46)   Prat, I.; Gomez, L.; Canta, M.; Ribas, X.; Costas, M., An iron catalyst for oxidation of alkyl c-h bonds showing enhanced selectivity for methylenic sites. *Chem. Eur. J.* **2013,** *19* (6), 1908-13.

(47)   Gomez, L.; Garcia-Bosch, I.; Company, A.; Benet-Buchholz, J.; Polo, A.; Sala, X.; Ribas, X.; Costas, M., Stereospecific CH Oxidation with H2O2 Catalyzed by a Chemically Robust Site-Isolated Iron Catalyst. *Angew. Chem. Int. Ed.* **2009,** *48* (31), 5720-5723.

(48)   Bigi, M. A.; Reed, S. A.; White, M. C., Directed Metal (Oxo) Aliphatic C–H Hydroxylations: Overriding Substrate Bias. *J. Am. Chem. Soc.* **2012,** *134* (23), 9721-9726.

(49)   Hong, B.; Luo, T.; Lei, X., Late-Stage Diversification of Natural Products. *ACS Cent. Sci.* **2020,** *6* (5), 622-635.

(50)   Caron, S.; Dugger, R. W.; Ruggeri, S. G.; Ragan, J. A.; Ripin, D. H. B., Large-Scale Oxidations in the Pharmaceutical Industry. *Chem. Rev.* **2006,** *106* (7), 2943-2989.

(51) Vitaku, E.; Smith, D. T.; Njardarson, J. T., Analysis of the Structural Diversity, Substitution Patterns, and Frequency of Nitrogen Heterocycles among U.S. FDA Approved Pharmaceuticals. *J. Med. Chem.* **2014,** *57* (24), 10257-10274.

(52) Howell, J. M.; Feng, K.; Clark, J. R.; Trzepkowski, L. J.; White, M. C., Remote Oxidation of Aliphatic C–H Bonds in Nitrogen-Containing Molecules. *J. Am. Chem. Soc.* **2015,** *137* (46), 14590-14593.

(53) Nanjo, T.; de Lucca, E. C.; White, M. C., Remote, Late-Stage Oxidation of Aliphatic C–H Bonds in Amide-Containing Molecules. *J. Am. Chem. Soc.* **2017,** *139* (41), 14586-14591.

(54) Milan, M.; Bietti, M.; Costas, M., Highly Enantioselective Oxidation of Nonactivated Aliphatic C–H Bonds with Hydrogen Peroxide Catalyzed by Manganese Complexes. *ACS Cent. Sci.* **2017**.

(55) Dantignana, V.; Milan, M.; Cussó, O.; Company, A.; Bietti, M.; Costas, M., Chemoselective Aliphatic C–H Bond Oxidation Enabled by Polarity Reversal. *Acs Cent. Sci.* **2017,** *3* (12), 1350-1358.

(56) White, M. C.; Doyle, A. G.; Jacobsen, E. N., A Synthetically Useful, Self-Assembling MMO Mimic System for Catalytic Alkene Epoxidation with Aqueous H2O2. *J. Am. Chem. Soc.* **2001,** *123* (29), 7194-7195.

(57) Mas-Ballesté, R.; Que, L., Iron-Catalyzed Olefin Epoxidation in the Presence of Acetic Acid: Insights into the Nature of the Metal-Based Oxidant. *J. Am. Chem. Soc.* **2007,** *129* (51), 15964-15972.

(58) Oloo, W. N.; Que, L., Bioinspired Nonheme Iron Catalysts for C–H and C=C Bond Oxidation: Insights into the Nature of the Metal-Based Oxidants. *Acc. Chem. Res.* **2015,** *48* (9), 2612-2621.

(59) Murphy, A.; Dubois, G.; Stack, T. D. P., Efficient Epoxidation of Electron-Deficient Olefins with a Cationic Manganese Complex. *J. Am. Chem. Soc.* **2003,** *125* (18), 5250-5251.

(60) Murphy, A.; Pace, A.; Stack, T. D. P., Ligand and pH Influence on Manganese-Mediated Peracetic Acid Epoxidation of Terminal Olefins. *Org. Lett.* **2004,** *6* (18), 3119-3122.

(61) Ottenbacher, R. V.; Talsi, E. P.; Bryliakov, K. P., Mechanism of Selective C–H Hydroxylation Mediated by Manganese Aminopyridine Enzyme Models. *ACS Catal.* **2015,** *5* (1), 39-44.

(62) Li, X.-X.; Guo, M.; Qiu, B.; Cho, K.-B.; Sun, W.; Nam, W., High-Spin Mn(V)-Oxo Intermediate in Nonheme Manganese Complex-Catalyzed Alkane Hydroxylation Reaction: Experimental and Theoretical Approach. *Inorg. Chem.* **2019,** *58* (21), 14842-14852.

(63)   Ottenbacher, R. V.; Samsonenko, D. G.; Talsi, E. P.; Bryliakov, K. P., Highly Efficient, Regioselective, and Stereospecific Oxidation of Aliphatic C-H Groups with H2O2, Catalyzed by Aminopyridine Manganese Complexes. *Org. Lett.* **2012,** *14* (17), 4310–4313.

Chapter II.

Objectives

The use of catalysts based on first row transition metals as a tool in organic synthesis has emerged as a valuable alternative to traditional catalysis based in precious metals because the former are highly abundant and exhibit a minor environmental impact than their heavier counterparts. Therefore, these reactions are especially valuable from a sustainability perspective. In addition, first row transition metals often exhibit a singular enhanced reactivity that may be used to promote new reactions, still inaccessible for precious metals. Catalyst design is necessary to exert control and make use of this reactivity. Based in these general considerations, the general objective of this thesis has been the development of first row transition metal catalysts with utility in organic synthesis.

Within this framework, the specific objectives of this thesis are;

The objective of **Chapter III** is the development of an iron catalyzed selective *syn*-dihydroxylation reaction of olefins with broad substrate scope and which could proceed in short reaction time using H_2O_2 as oxidant. This objective will be addressed by synthetizing a sterically encumbered iron catalyst. It was hypothesized that the steric encumbrance will limit catalyst deactivation paths which constitute a major drawback for the development of the iron catalyzed reaction.
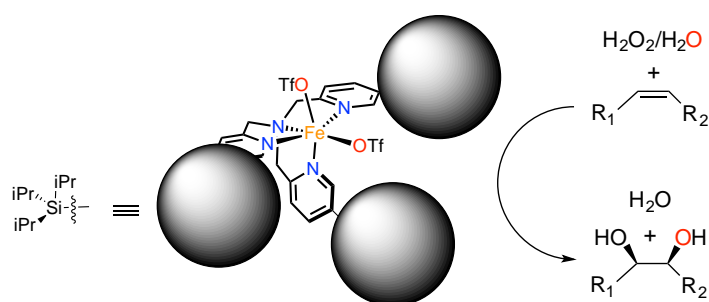
Scheme II.1. Development of a sterically encumbered iron catalyst for *syn*-dihydroxylation reaction.

A second goal (**Chapter IV)** will be exploring the suitability of green solvents as a valid media for selective *syn*-dihydroxylation reactions.
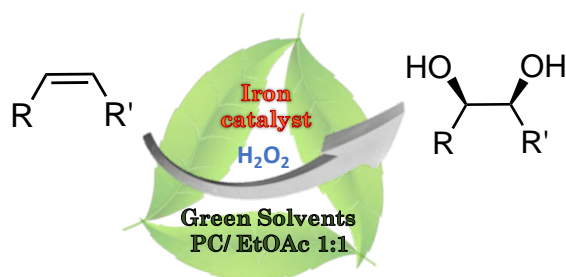
Scheme II.2. Selective *syn*-dihydroxylation of a broad substrate scope using green solvents as solvent media.

It has been proposed that $Fe^V(O)(OH)$ species are the responsible for a *syn*-dihydroxylation reaction in enzymatic and synthetic systems. However, the inability to accumulate this intermediate in solution has thus far prevented its characterization. In **Chapter V**, we will use gas phase ion spectroscopy methods to provide the first spectroscopic and chemical characterization of a $Fe^V(O)(OH)$ species.
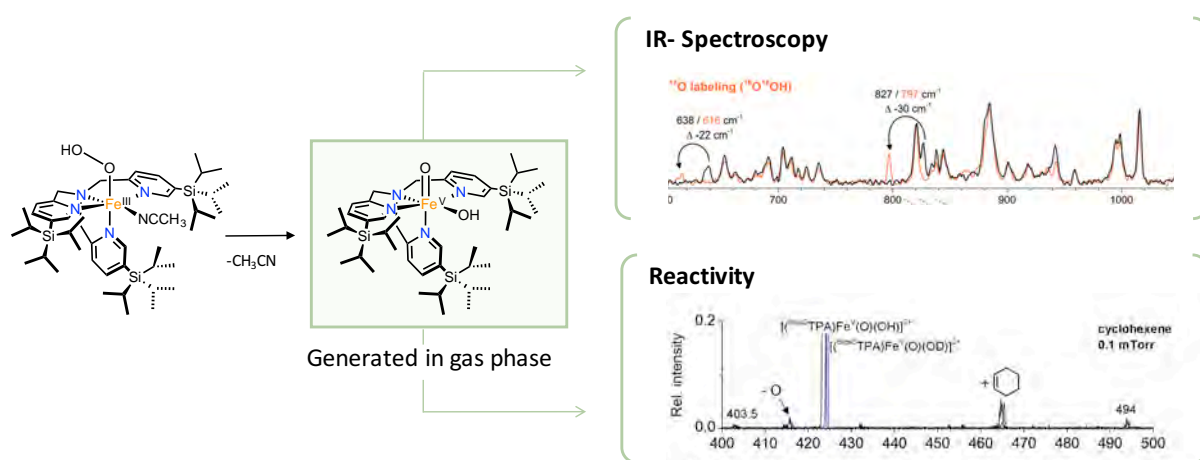
Scheme II.3. Schematic representation of the characterization of $Fe^V(O)(OH)$ and they reactivity in gas phase.

The objective in **Chapter VI** is the development of chemoselective C-H oxidation methodologies of polyhydroxylated molecules. This will be pursued by performing iron and manganese catalyzed oxidations with hydrogen peroxide using a fluorinated alcohol as the solvent media. This solvent will induce a polarity reversal protecting effect in the a priori oxidation sensitive hydroxyl moieties, favoring instead site selective and product chemoselective C-H oxidation at remote positions.
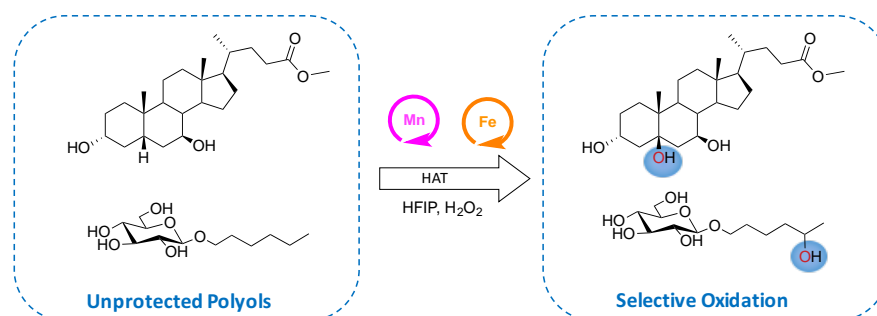
Scheme II. 4. Chemoselective C-H oxidation at the remote position using fluorinated alcohols as solvent.

Chapter III.

Mechanistically Driven Development of an Iron Catalyst for Selective *Syn*-Dihydroxylation of Alkenes with Aqueous Hydrogen Peroxide
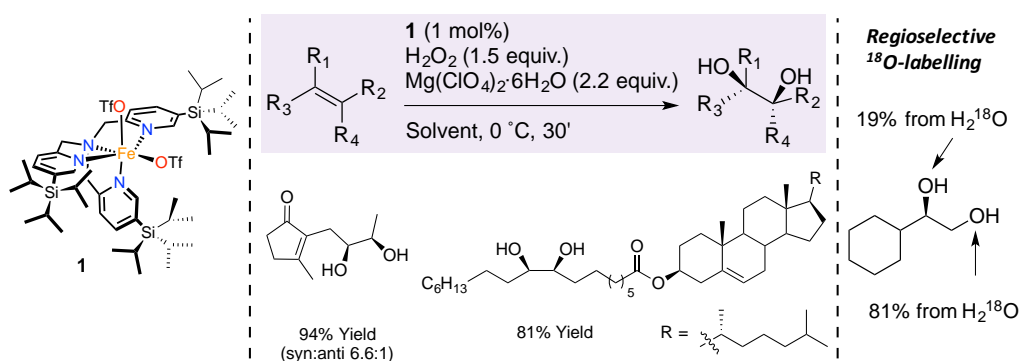
This chapter corresponds to the following publication:

Margarida Borrell, Miquel Costas. *J. Am. Chem. Soc.* **2017**, 139, 36, 12821-12829.

Reprinted with permission from ACS publications.

Mechanistically Driven Development of an Iron Catalyst for Selective *Syn*-Dihydroxylation of Alkenes with Aqueous Hydrogen Peroxide

Margarida Borrell and Miquel Costas*

Institut de Química Computacional i Catàlisi (IQCC) and Departament de Química, Universitat de Girona, Campus Montilivi, Girona E-17071, Catalonia, Spain

S *Supporting Information*
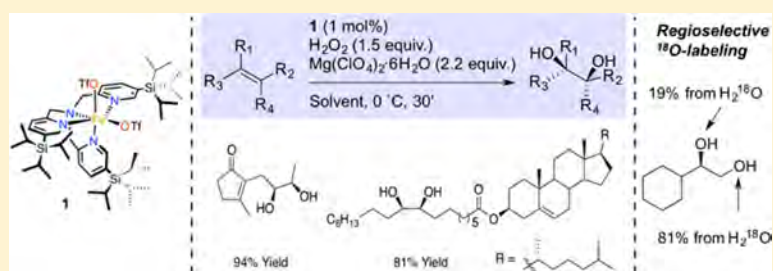
ABSTRACT: Product release is the rate-determining step in the arene *syn*-dihydroxylation reaction taking place at Rieske oxygenase enzymes and is regarded as a difficult problem to be resolved in the design of iron catalysts for olefin *syn*-dihydroxylation with potential utility in organic synthesis. Toward this end, in this work a novel catalyst bearing a sterically encumbered tetradentate ligand based in the tpa (tpa = tris(2-methylpyridyl)amine) scaffold, [Fe^{II}(CF$_3$SO$_3$)$_2$($^{5\text{-tips3}}$tpa)], **1** has been designed. The steric demand of the ligand was envisioned as a key element to support a high catalytic activity by isolating the metal center, preventing bimolecular decomposition paths and facilitating product release. In synergistic combination with a Lewis acid that helps sequestering the product, **1** provides good to excellent yields of diol products (up to 97% isolated yield), in short reaction times under mild experimental conditions using a slight excess (1.5 equiv) of aqueous hydrogen peroxide, from the oxidation of a broad range of olefins. Predictable site selective *syn*-dihydroxylation of diolefins is shown. The encumbered nature of the ligand also provides a unique tool that has been used in combination with isotopic analysis to define the nature of the active species and the mechanism of activation of H$_2$O$_2$. Furthermore, **1** is shown to be a competent synthetic tool for preparing O-labeled diols using water as oxygen source.

■ INTRODUCTION

Syn-dihydroxylation is a very important reaction in organic synthesis because olefins are readily available feedstocks and diols are versatile synthetic intermediates.[1] *Syn*-dihydroxylation is reliably performed using stoichiometric or catalytic amounts of heavy metal oxides, specially OsO$_4$[1b,c] and RuO$_4$,[2] as well as catalysts based in these metals.[3] However, the cost and toxicity of these metals motivate the development of more sustainable alternatives such as metal-free methods[4] and catalytic methodologies based on first row transition metals.[1a] Along this direction, permanganate is the traditional textbook stoichiometric *syn*-dihydroxylating reagent, but overoxidation is a common limitation.[5] Manganese catalysts have shown promising activity,[6,7] although substrate scope and chemoselectivity remain critical aspects.

Rieske dioxygenases are nonheme iron enzymes that catalyze the stereo- and regiospecific, O$_2$-dependent conversion of aromatic substrates into *cis*-dihydrodiols (Scheme 1).[8] These enzymes have provided inspiration for the development of iron-based *syn*-dihydroxylating catalysts.[9]

The first functional model for this class of enzymes was described by Que and Chen, who performed the *syn*-

dihydroxylation of olefins, using the substrate in large excess (1000 equiv) and H$_2$O$_2$ (10 equiv) as oxidant.[10] This work marked the starting point of research efforts to uncover the reaction mechanism[9,11] and also to develop catalysts that could have utility in synthesis.[12] The latter aspect has proven particularly challenging; very few examples exist that could operate under substrate-limiting conditions, potentially amenable for synthesis (Scheme 2a). Rapid catalyst deactivation and limited chemoselectivity are critical problems when reactions are performed under substrate-limiting conditions; competitive epoxidation and overoxidation reactions consistently result in modest product yields. Good product yields and chemoselectivities have been obtained only in two examples described by Che and are basically limited to electron-deficient (ED) olefins; [Fe^{III}(Cl)$_2$(LN$_4$Me$_2$)]$^+$ (Scheme 2a) employs oxone (2 equiv) to oxidize ED olefins with excellent yields and chemoselectivities, but more modest yields and competitive overoxidation are observed with other types of substrates, specially aliphatic olefins. Hydrogen peroxide is a more

Scheme 1. Proposed Catalytic Cycle of Naphthalene Dioxygenase (NDO)[a]
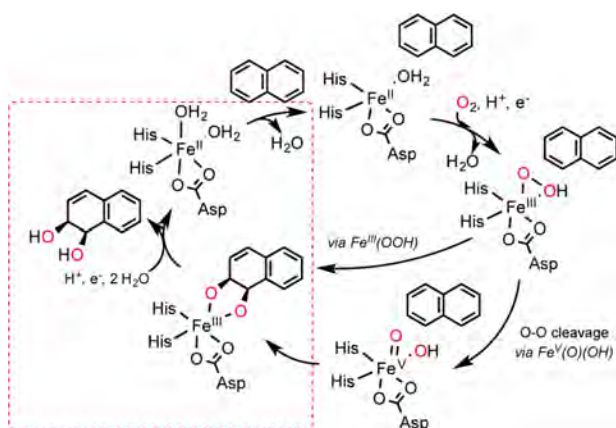
[a]Red frame indicates the rate-determining step under catalytic conditions.

convenient oxidant, but only very recently high yielding *syn*-dihydroxylation of ED olefinic substrates with H_2O_2 has been described with the (S,S)-$[Fe^{II}(OTf)_2(bqcn)]$ catalyst (OTf = trifluoromethanesulfonate anion, Scheme 2a). Interestingly, high enantioselectivities were obtained for these reactions.[12]

We reasoned that the catalyst deactivation and product overoxidation commonly observed with iron catalysts may originate from a rate-determining release of the product, because a strong binding of the diol to the ferric center is favored by the formation of a five-member chelate ring cycle and the high oxophilicity of the ferric center.[11j,12b,13] Indeed, product release appears to be a critical step not limited to iron but also to ruthenium-based *syn*-dihydroxylation reactions.[14] In

Rieske dioxygenases, diol release is rate-determining and is triggered by reduction of the ferric center, which presumably attenuates its oxophilicity.[8c,15] The reaction of the reduced center with O_2 is strictly regulated and only takes place once a new substrate molecule enters the active center, avoiding overoxidation. For synthetic catalysts, an analogous mechanism is not operative, iron (hydrogen) glycolate species rapidly accumulate,[11j,12b,13] and overoxidation of the substrate is difficult to avoid.

We considered that product release may be facilitated by making the ligand sterically more demanding, a common strategy in standard organometallic catalysis. Furthermore, this element will also limit formation of oxo-bridged diferric species, that are catalytically poorly active thermodynamic sinks. Overall, the activity and chemoselectivity of the catalyst would be favored. Taking these considerations into account we have designed an iron catalyst based on the archetypical $[Fe(tpa)]$ architecture tpa = tris(2-pyridylmethyl)amine, for which catalytic *syn*-dihydroxylation activity has been thoughtfully studied,[10,11j,12c] building sterically demanding triisopropylsilyl (tips) groups in position 5 of the pyridine rings (Scheme 2b and Figure 1). We have previously described that incorporation of these bulky groups in chiral iron and manganese catalysts result in highly active epoxidation and C−H oxidation catalysts, exhibiting remarkable regio- and enantioselective properties.[16] Moreover, building on the same mechanistic analysis, herein we show that addition of $Mg(ClO_4)_2 \cdot 6H_2O$ improves product yields and chemoselectivities by binding and sequestering the diol. Overall, this analysis has resulted in an iron-based catalytic system that enables fast and high yield *syn*-dihydroxylation of a broad range of olefins under mild experimental conditions, using H_2O_2 as oxidant. Remarkably, it is also shown that **1** introduces one oxygen atom originating from water in the dihydroxylated olefin, as shown by means of isotopic labeling experiments using $H_2^{18}O$.

Scheme 2. (a) Previous Iron Catalysts Employed in *Syn*-Dihydroxylation under Substrate-Limiting Conditions. (b) Characteristics of the Current System
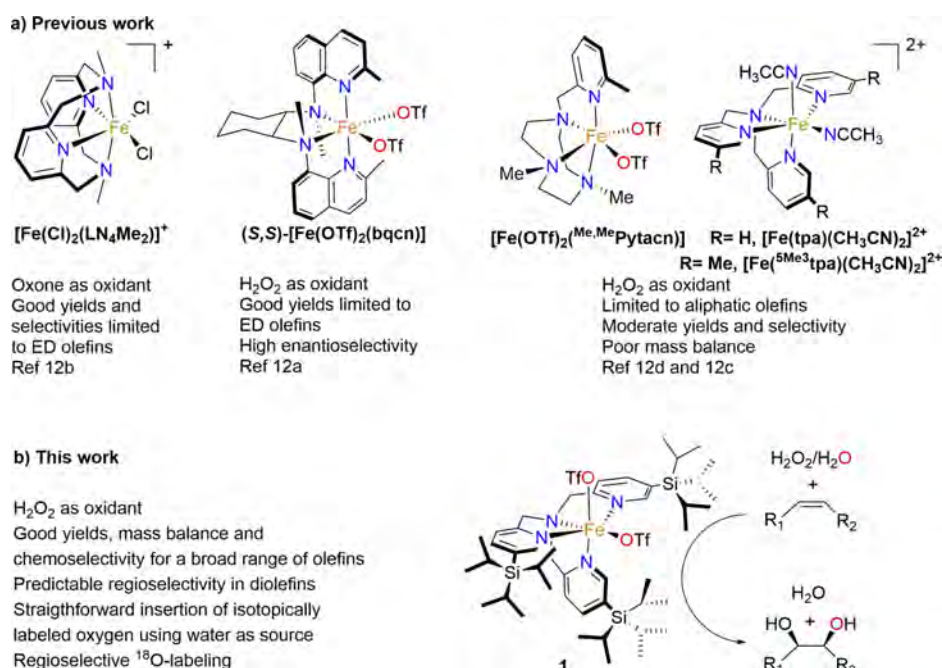
Furthermore, analysis of the isotope distribution of the latter reactions, applied to unsymmetric olefins, uncovers fundamental aspects of the nature of the iron active species and the mechanism by which they are formed.
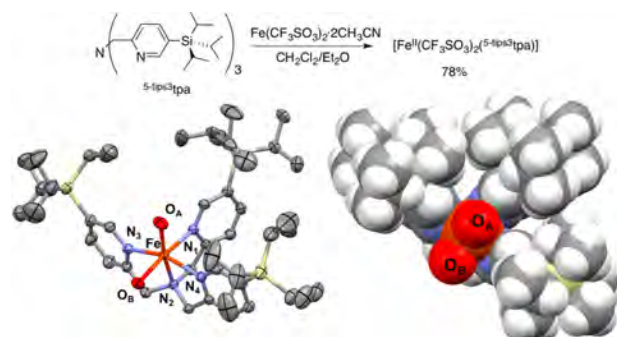
Figure 1. ORTEP diagram of $[Fe^{II}(CF_3SO_3)_2(^{5\text{-tips3}}tpa)]$, **1** (left), and space-filling diagram (right), showing the different steric constrains at O_A (surrounded by three tips groups) and O_B (open to the bulk). Triflate anions are omitted except for the oxygen atoms directly bound to the iron center; thermal ellipsoids are set at 50% probability level and hydrogen atoms omitted for clarity. Selected bond distances; Fe−N1:2.192(2), Fe−N2:2.220(2), Fe−N3:2.160(2), Fe−N4:2.158(2), Fe−O_A: 2.049(2), Fe−O_B: 2.171(2).

■ RESULTS AND DISCUSSION

Synthesis and Characterization of the Catalyst. Standard procedures were used to assemble the bulky tetradentate $^{5\text{-tips3}}$tpa ligand (see Supporting Information (SI) for details). Toward this end, the silyl-substituted picolyl chloride and the silyl-substituted picolyl amine building blocks were conveniently obtained on a gram scale (see SI) following recently described methods.[16a]

The tetradentate $^{5\text{-tips3}}$tpa ligand was then reacted with $Fe(CF_3SO_3)_2 \cdot 2CH_3CN$ to prepare the corresponding iron complex with formula $[Fe^{II}(CF_3SO_3)_2(^{5\text{-tips3}}tpa)]$, **1** (Figure 1 top), that was obtained as a yellow crystalline solid in 78% yield. The X-ray crystal structure of **1** shows a distorted octahedral ferrous center, with the $^{5\text{-tips3}}$tpa ligand coordinated in a tripodal manner (Figure 1). Average Fe−N distances are 2.2 Å and are indicative of a high-spin ferrous center.[17] Two *cis* labile positions are occupied by triflate anions. Most interestingly, the sterically demanding tips groups flank these two positions in a nonequivalent manner (Figure 1). While one of the two *cis* labile positions (O_A), *trans* to the aliphatic amine (N2), is surrounded and hindered by the tips groups corresponding to each of the three pyridine rings of the catalyst, the second one (O_B), *trans* to one of the pyridines (N1), is flanked by only two of the tips groups and appears to be spatially quite more accessible.

Catalytic Reaction Development. Catalytic olefin oxidation reactions were first performed under air by adding 1.5 equiv of H_2O_2 (commercially available 50% w/w solution diluted in acetonitrile) via syringe pump over 30 min at 0 °C to an acetonitrile solution containing 1-octene (**S1**) and 1 mol % of **1** as catalyst. Results are collected in Table 1. Under these conditions, 1-octene was nearly consumed (98% conversion) and the corresponding 1,2-diol (**P1b**) was obtained in a rewarding 74% yield (entry 1), along with 23% of 1,2-epoxyoctane (**P1c**). No significant changes in product yields were observed when the reaction was performed under argon

Table 1. Optimization Conditions for Oxidation of S1 Using Different Iron Catalysts[a]

entry	cat./additive	conv (%)	yield of P1b (%)	yield of P1c (%)	MB[b] (%)
1	**1**/−	98	74	23	99
2	**2**/−	71	47	10	80
3[c]	**2**/−	83	59	13	87
4	**3**/−	66	30	15	68
5	**4**/−	28	2	<1	−
6	**1**/$LiClO_4 \cdot 3H_2O$[d]	62	51	8	95
7	**1**/$Zn(OTf)_2$[d]	99	75	21	97
8	**1**/$Mg(ClO_4)_2 \cdot 6H_2O$[d]	100	87	13	>99
9	**1**/$Mg(ClO_4)_2$[d]	53	43	10	>99
10	**1**/$Mg(OTf)_2$[d]	94	77	17	>99
11	**1**/H_2O[e]	50	26	6	64
12	**2**/$Mg(ClO_4)_2 \cdot 6H_2O$[d]	35	20	4	69
13	**3**/$Mg(ClO_4)_2 \cdot 6H_2O$[d]	74	42	11	72
14	**4**/$Mg(ClO_4)_2 \cdot 6H_2O$[d]	27	<1	<1	−

[a]1 mol % catalyst, 1.5 equiv of H_2O_2 added by syringe pump during 30 min followed by 30 min stirring at 0 °C; substrate conversion (conv) and product yields determined by GC, calibrated with independently prepared products. [b]Mass balance. [c]Conditions employed in ref 12c: 3 mol % catalyst, 4 equiv of H_2O_2. [d]2.2 equiv. [e]13 equiv.

or nitrogen atmosphere. Besides the fact that the yield of diol is the best described for an iron-catalyzed dihydroxylation of an aliphatic substrate, the good mass balance of the reaction (99%) is also extraordinary, even when substrate conversion was high. The excellent performance of **1** is best appreciated when compared with other relevant iron dihydroxylating catalysts (Scheme 2a, and Table 1 entries 2−5) under analogous conditions; the simpler $[Fe^{II}(tpa)(CH_3CN)_2](ClO_4)_2$ (**2**) provides a more modest 47% of diol (entry 2) that can be improved up to 59% (entry 3) by using a larger catalyst loading and up to 4 equiv of H_2O_2. The triazacyclononane-based catalyst $[Fe^{II}(CF_3SO_3)_2(^{Me,Me}Pytacn)]$ (**3**, see Scheme 2a) also provides a modest yield of diol (30%, entry 4), and $[Fe^{II}_2(LN_4Me_2)]$ (**4**, see Scheme 2a left for a diagram of the parent $[Fe^{III}(Cl)_2(LN_4Me_2)]^+$) turns out to be basically inactive in combination with H_2O_2 (entry 5). In sharp contrast to **1**, conversion of the substrate into minor amounts of multiple oxidation products was detected when **2**−**4** were employed as catalysts, resulting in less satisfactory mass balances.

We considered the possibility that accumulation of the diol in the reaction may be compromising the chemoselectivity exhibited by **1**, presumably by binding to the iron center, as previously documented for several iron catalysts.[11j,13] We envisioned that improved yields may be obtained if the diol product could be separated,[12d] or at least sequestered from the reaction mixture. With this proposal in mind, reactions were conducted in the presence of different Lewis acids, to induce binding to the diol (see Table S4 for details on the different Lewis acids tested). Addition of $LiClO_4 \cdot 3H_2O$ (Table 1, entry 6) improved the selectivity toward the diol ([diol]/[epoxide] ∼ 6/1) while retaining an excellent mass balance, but provided an overall reduced yield (51%). Use of $Zn(CF_3SO_3)_2$ (entry 7) did not elicit significant changes. However, a remarkably high yield of diol (87%, entry 8) was obtained when $Mg(ClO_4)_2 \cdot 6H_2O$

(2.2 equiv) was used (see Table S5). The epoxide appears as a minor product (13%), and the mass balance of the reaction remained excellent (99%). Of interest, when 1,2-epoxyoctane (**P1c**) was subjected to these reaction conditions (1 mol % catalyst, 1.5 equiv of H_2O_2, 2.2 equiv of $Mg(ClO_4)_2 \cdot 6H_2O$), diol **P1b** was not formed, indicating that the diol observed in our reaction does not come from an epoxide ring opening. Consistent improvements in yields and selectivities for the diol product were observed for different substrates when reactions were conducted in the presence of $Mg(ClO_4)_2 \cdot 6H_2O$ (see Table S7). Finally, slightly improved yields (92%) and chemoselectivities toward the diol were obtained when reactions were performed in 1 mmol scale and the product was isolated. Remarkably, **1** retains excellent performance at low catalyst loadings; a noticeable good yield (75%) of the corresponding diol (along with 25% of the epoxide) was obtained with 0.25 mol % catalyst (**1**:**S1**:H_2O_2 ratio of 1:400:600). This yield translates into 300 turnover numbers (TN) of diol, which to the best of our knowledge is the largest value described to date for any iron catalyst.

The impact of $Mg(ClO_4)_2 \cdot 6H_2O$ on the catalytic activity of **1** was further investigated. Control experiments showed that the positive effect of $Mg(ClO_4)_2 \cdot 6H_2O$ is not reproduced by adding comparable amounts of water (13 equiv, entry 11), and use of anhydrous sources of Mg^{2+} ions also provided reduced product yields (entries 9 and 10).

The activity of catalyst **3** is also improved with the addition of $Mg(ClO_4)_2 \cdot 6H_2O$. A higher yield of diol product (**P1b**) and a larger [diol]/[epoxide] ratio is observed (compare entry 13 with entry 4), but these numbers are still far from those obtained with **1**. On the other hand, unlike **1** and **3**, the activity of catalysts **2** and **4** could not be improved by the addition of $Mg(ClO_4)_2 \cdot 6H_2O$ (entries 12 and 14).

A positive effect of H_2O in the *syn*-dihydroxylation ability of **3** has been previously observed.[12d] It was reasoned that water can help in the activation of H_2O_2 (see below for details on the reaction mechanism), and can also facilitate product release. However, in the case of **1**, the sole addition of water does not improve the overall performance of the catalyst, and Mg^{2+} ions appear to exert an important beneficial role, which is best evidenced in higher product yields and a robust selectivity toward *syn*-dihydroxylation, even when large amounts of diols accumulate in the reaction mixture. The positive effect of the Mg^{2+} ions can actually be rationalized by considering their Lewis acidity and oxophilicity, which must ensure strong binding to the diol, limiting their interaction to the iron species. Interestingly, the diol binding ability of Mg^{2+} was well supported by mass spectrometry analysis of the reactions, which revealed spectra dominated by multiple and intense cluster ions combining diol and Mg^{2+} ions (see Figure S1 for spectra).

Further evidence in favor of the diol-sequestering role of Mg^{2+} ions and its translation into improved catalytic performance was obtained by performing the oxidation of 1-octene (**S1**) under standard reaction conditions but in the presence of varied amounts (20 and 50 mol %) of *cis*-cyclooctene-1,2-diol (Scheme 3). In the absence of $Mg(ClO_4)_2 \cdot 6H_2O$, addition of cyclooctene-1,2-diol (20 and 50 mol %) produces an inhibition of the reaction, and diol **P1b** is produced in small yields (28% and 16%, respectively). However, addition of $Mg(ClO_4)_2 \cdot 6H_2O$ (2.2 equiv) rescues the catalytic activity, and **P1b** is obtained in good yield (73−74%) and improved selectivity.

Scheme 3. Evidence of the Positive Role of $Mg(ClO_4)_2 \cdot 6H_2O$ by Sequestering the Diol

x mol%	$Mg(ClO_4)_2 \cdot 6H_2O$	P1b (%)	P1c (%)	[P1b]/[P1c]
20 mol%	-	28	6	4.7
	2.2 equiv.	74	12	6.2
50 mol%	-	16	3	4.8
	2.2 equiv.	73	13	5.6
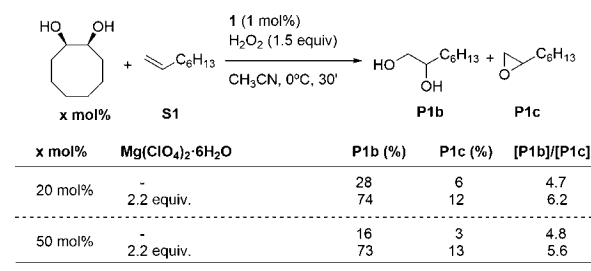
Comparative Analysis of Catalysts 1 and 2. A time course analysis of a catalytic olefin oxidation performed under the optimized reaction conditions (Figure 2) permits us to elucidate different key aspects of the improved performance of **1** when compared with **2**. Analysis of oxidation products at different times shows that the two catalysts are active during all the time course of H_2O_2 addition, but **1** consistently exhibits a more efficient use of H_2O_2, providing higher product yields, which increase linearly with H_2O_2 addition.
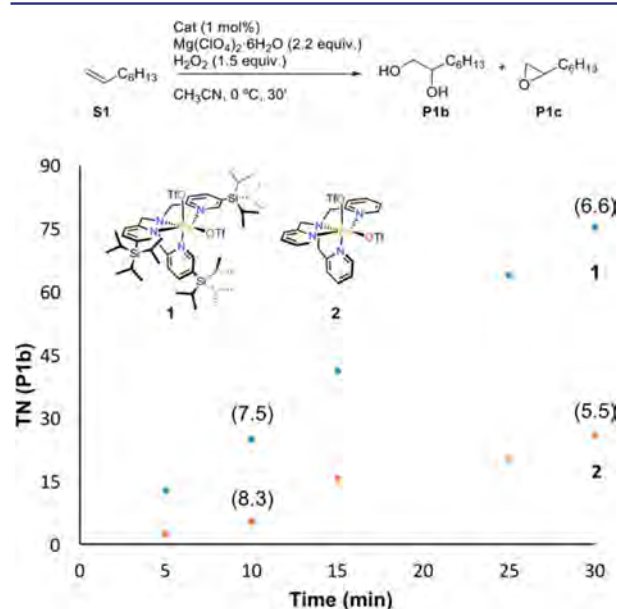
Figure 2. Time course of the catalytic oxidation of 1-octene **S1** with catalysts **1** (blue dots) and **2** (orange dots). H_2O_2 (1.5 equiv delivered by syringe pump at 0 °C) is added to a solution of substrate, $Mg(ClO_4)_2 \cdot 6H_2O$ (2.2 equiv), and catalyst (1 mol %) in acetonitrile. Values in parentheses correspond to [diol]/[epoxide] ratio at different reaction times.
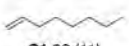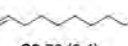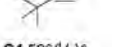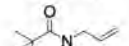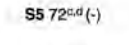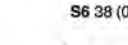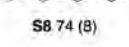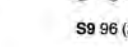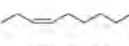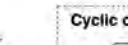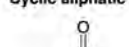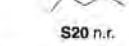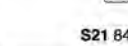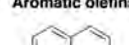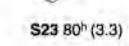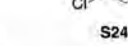
For both catalysts, the chemoselectivity toward the diol (estimated by the [diol]/[epoxide] ratio) is eroded as the reaction progresses, and diol accumulates in solution; for **1** and **2**, [diol]/[epoxide] ratios are very similar at 10 min (7.5 and 8.3, respectively) and decrease to 6.6 and 5.5 at 30 min. Interestingly, the better chemoselectivity displayed by **1** is attained even when substrate conversion is basically quantitative, and a large concentration of diol has accumulated in the reaction mixture. Instead, the selectivity observed with **2** is obtained under experimentally less demanding conditions with regard to the latter parameters. The sum of these data suggests

that under optimal conditions (initial points of the reaction when substrate concentration is large and diol concentration is small), **1** and **2** show quite similar chemoselectivity in the oxidation of **S1**, but **1** appears to be more efficient in activating H_2O_2 in an effective manner to perform the dihydroxylation reaction. In addition, as the reaction progresses, **1** is more resistant against deactivation of the dihydroxylation channel, presumably caused by diol accumulation and binding to the iron center.

Substrate Scope. Dihydroxylation of different families of substrates was then explored under the optimized conditions (Table 2). For comparison purposes, the best results described so far in the literature with an iron catalyst are collected in Table S1. In general, the data shows that **1** yields substantially improved yields when compared with the state-of-the-art iron catalysts. Aliphatic substrates with different substitution patterns are oxidized to the corresponding diol in good to excellent isolated product yields (up to 97%). This includes terminal olefins (**S1**−**S6**, 38−92%), *trans*-olefins (**S7**, **S8**, and **S14**, 74−92%), *cis*-olefins (**S9**−**S13**, 67−97%), and cyclic olefins (**S15** and **S16**, 81−89%). The good mass balance of these reactions (>95%) compares favorably with the values attained with any iron catalyst described to date. In general, substrate conversions are complete, and epoxides are formed as minor products, accounting for the rest of the oxidation products. A 1,1-dialkyl-substituted olefin (**S6**) appears to be a singular case, because its oxidation produces a 1:1 mixture of diol and epoxide (which can be readily converted in the corresponding diol by reaction with an acid), with an excellent 80% combined yield. A particularly remarkable feature is that reactions proceed with stereoretention, forming diol resulting from a *syn*-dihydroxylation reaction. Remarkably, the reaction is tolerant to different functional groups including an amide (**S5**, 72%), an alcohol (**S10**, 86%), a halide (**S11**, 76%), and an ester (**S13**, 97%). Interestingly, the electron-poor dimethyl fumarate (**S14**) and dimethyl maleate (**S12**) are also oxidized with excellent chemoselectivity to the corresponding *syn*-diols (92% and 67%, respectively). Efficient oxidation of maleate (**S12**) requires that the oxidation reaction is performed in the absence of Mg^{2+} ions presumably because favorable chelation to maleate (as ascertained by ESI-MS analysis, see Figure S2) deactivates the substrate. Oxidation of these very electron-poor substrates finds precedent in Che's *syn*-dihydroxylation catalyst $[Fe^{III}(Cl)_2(LN_4Me_2)]^+$ (Scheme 2a), which operates with oxone[12b] and is particularly remarkable because these substrates are inert toward iron epoxidation catalysts that use H_2O_2 and can be seen as structurally related to **1**.[16b] On the other hand, substrates bearing sterically impeded olefins exhibit reduced reactivity; 3,3-dimethyl-1-butene (**S4**) is oxidized to the diol in 53% yield, and 2,3-dimethyl-3-butene probed unreactive, suggesting sensitivity of the catalyst to substrate sterics.

Interestingly, cyclic aliphatic enones (**S17**−**S22**) are also viable substrates and are oxidized to the corresponding *syn*-diol with excellent chemoselectivity (>90%) and moderate to excellent product yields (60−99%). These substrates are valuable synthons in the elaboration of natural products, and their cyclic nature makes the *syn*-diol difficult to obtain by other methods. Of remark, the reaction proceeds satisfactorily for six- to eight-membered ring substrates (**S17**−**S19** and **S21**−**S22**). Again, steric hindrance on the substrate appears to impact the efficiency of the reaction to a different extent; substrates with *gem*-dimethyl groups installed in the cyclohexanone ring (**S18**−**S20**) are oxidized with good but reduced yields of *syn*-diol

Table 2. Substrate Scope of Different Alkenes Using Catalyst 1 and H_2O_2. Isolated yield (%)[a] ([diol]/[epoxide] ratio)[b]

[a]Reaction conditions: 1 equiv of substrate (1 mmol), 1 mol % catalyst, 1.5 equiv of H_2O_2 (50% w/w solution), added via syringe pump during 30 min, 10 mL of CH_3CN, at 0 °C, plus 30 min stirring. [b][diol]/[epoxide] ratio (in parentheses) determined by GC in 1 mmol substrate reactions. [c]Yields determined by GC. [d]Two additions of 1 mol % catalyst and 1.5 equiv of H_2O_2. [e]Epoxide is not formed. [f]Isolated yields using standard conditions; **S10** (77), **S12** (57), **S17** (75), **S19** (55), **S27** (82), **S29** (56), **S31** (53). [g]Oxidation performed without $Mg(ClO_4)_2·6H_2O$. [h]2 mol % of catalyst. [i]1 equiv of H_2O_2. [j]2 mol % of catalyst in the first addition. n.r. = not reactive. Stereoselectivities were determined by GC analyses of the crude reaction mixtures. Stereochemistry of diols resulting from oxidation of **S7**, **S8**, **S9**, **S17**, **S23**, and **S32** was determined by comparison to diols prepared by Sharpless dihydroxylation and by epoxide ring opening.[1b,20] Stereochemistry of diols resulting from oxidation of **S12**, **S14**, **S15**, **S16**, and **S22** was determined by comparison with spectroscopic and GC retention time of commercially available diols.

when compared with **S17**, but substitutions at the olefinic site (**S20**) make the corresponding substrates unreactive. Therefore, while **1** generates very powerful oxidizing species, they are remarkably sensitive to steric hindrance, a conclusion that can be rationalized because of the high steric demand imposed by the $^{5\text{-tips}3}$tpa ligand.

In the absence of deactivating electron-withdrawing groups, aromatic olefins are quite delicate substrates for iron oxidation catalysis.[11i,j,12b,d,18] However, nondeactivated styrenes appear also to be suitable substrates for the current system, and the corresponding diols are obtained in moderate to good (**S23**–**S26**, 44–80%) product yields. Following the same pattern observed for aliphatic substrates, a *cis*-aromatic olefin (**S23**) is oxidized with a substantially better yield (80%, dr 95:5) than the corresponding *trans* isomer (**S26**), and styrene **S24** (a terminal olefin) is oxidized to the corresponding diol in 58% yield. Aromatic olefins with electron-withdrawing groups (**S27**–**S29** and **S31**) are oxidized with improved product yields (57–99%) and excellent chemoselectivity toward the corresponding *syn*-diol. Again, as observed for aliphatic olefins, oxidation of trisubstituted olefins (**S28** and **S30**) provide reduced yields, an effect that is most obvious when comparing **S28** with the *trans*-disubstituted analogue (**S27**).

Previous mechanistic studies have revealed that iron catalyzed *syn*-dihydroxylation can involve electrophilic and nucleophilic species, depending on the nature of the catalyst.[11i] To address this question, the competitive oxidation of cyclooctene (**S15**) and cyclohexenone (**S17**) with **1** was performed (see Table S2 for details), revealing exclusive oxidation of the former. This observation is in agreement with the exclusive site-selective oxidation of **S13** at the most electron-rich site (Table 2) and overall is evidence of an electrophilic nature of the oxidizing species. Further studies were directed toward establishing the relative reactivity of **1** against aliphatic olefins bearing different substitution patterns. Competitive oxidation of pairs of aliphatic olefins (see Table S2) permits the establishment of the following pattern of relative reactivity; *cis* and terminal olefins are more reactive than *trans* (*cis*-2-octene **S9** and 1-octene **S1** are roughly three and two times more reactive than *trans*-2-octene **S8**, respectively). Moreover *cis*-2-octene **S9** is 1.5 times more reactive than cyclooctene **S15**. These competitive studies reveal a preferential reactivity for *cis*-olefins, and most significantly the relatively high reactivity of a terminal olefin, which are recognized as a more difficult class of substrates to oxidize by electrophilic oxidants than internal olefins,[18,19] suggesting that the steric demand of the substrate is a major component in dictating relative reactivity.

Understanding the selectivity properties of **1** permits its use in the predictable selective oxidation of more complex substrates such as small natural products, bearing more than one olefinic site (Scheme 4). Oxidation of *cis*-jasmone (**S32**, contains 8% *trans* isomer) proceeds with an excellent 94% isolated yield of the diol (92:8 dr, see SI section 11) resulting from oxidation at the most electron-rich site. More significantly, oxidation of the steroidal substrate (**S33**), bearing a fatty acid-derived chain, takes place with excellent selectivity toward the sterically less congested *cis*-site in 81% isolated yield, without any detectable oxidation at the more electron-rich double bond but congested trisubstituted site. These results underscore the potential utility of **1** in organic synthesis.

Scheme 4. Site Selective *Syn*-Dihydroxylation of Natural Products
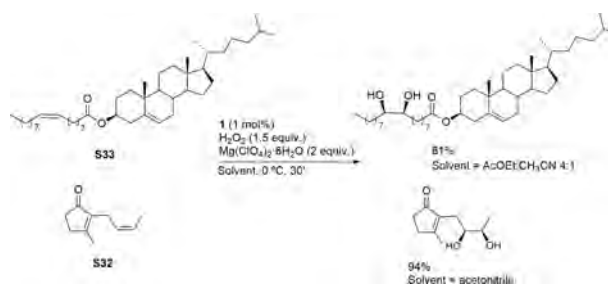
■ MECHANISTIC STUDIES

Regioselective Labeling. Previous mechanistic studies in the reaction of *syn*-dihydroxylation catalyzed by iron coordination complexes have led to the organization of catalysts in two classes (Scheme 5a).[11i,j] For class A catalysts, the resulting diol contains one oxygen atom that originates from H_2O_2 and the second one from H_2O, while diols formed with class B catalysts contain two oxygen atoms derived from the same molecule of H_2O_2. Class A catalysts contain tetradentate strong field ligands, while class B bear weak field ligands.[11i] It can be expected that the introduction of the bulky silyl groups at the fifth position of the pyridines will not perturb in a substantial manner the crystal field and electronic properties of the iron center in **1** when compared with **2**, and therefore both catalysts will likely operate via a common mechanism. Indeed, the latter can be seen as the prototypical example of a class A catalyst. Isotopic labeling analysis confirms this prediction. Catalytic oxidation of a series of olefins by **1** with H_2O_2 in the presence of $H_2^{18}O$ (7.5 equiv) produces the corresponding *syn*-diol that is 90% singly ^{18}O-labeled (Scheme 5b).

Class A catalysts operate via a $Fe^V(O)(OH)$ species formed via water-assisted O−O cleavage of a $Fe^{III}OOH$ species (Scheme 5a).[11j] Most interestingly, **1** is unique because its two labile sites possess quite different structural constraints (see Scheme 5c). It was envisioned that this structural feature may permit us to interrogate at which position (O_A or O_B) is located the oxygen atom from H_2O_2 and H_2O in the $Fe^V(O)(OH)$ oxidant. Because O_A is sterically more hindered than O_B, it is expected that an unsymmetric olefin will react by approaching the sterically less demanding olefin carbon site to O_A and the sterically more congested carbon site to O_B.

To test this model, oxidations of a series of substrates were performed under standard catalytic conditions in the presence of 7.5 equiv of $H_2^{18}O$, and the resulting diols were analyzed by GC-MS (Scheme 5b and Table S8). Ionization by electron impact fragments the diol and allows us to interrogate the position of the ^{18}O oxygen atom. Almost a 1:1 ratio between the two positions is measured for *erythro-vic*-2,3-octanediol (43:57) resulting from oxidation of *cis*-2-octene (**S9**), but most interestingly, preferential introduction of the ^{18}O atom at the less congested carbon is observed, as the difference between the steric demand of the two olefinic carbon sites is accentuated (from 33:66 to 16:84). For example, dihydroxylation of vinylcyclohexane (**S3**) yields predominantly the diol where the terminal carbon atom is regioselectively ^{18}O-labeled with a 19:81 ratio. For comparison, the oxidation of vinylcyclohexane was also studied with **2** in the presence of $H_2^{18}O$, yielding a 55:45 ratio of ^{18}O-labeled that denotes a modest, opposite regioselectivity.

Scheme 5. (a) Mechanistic Typology of Iron-Based *Syn*-Dihydroxylation Catalysts.[11i,j] (b) Results from Isotopic Labeling Analysis of the Oxidation of a Series of Substrates by 1.[a] (c) Schematic Model Rationalizing the Favorable and Disfavorable Approach of the Olefin to the Catalyst on the Basis of Steric Interactions[b]
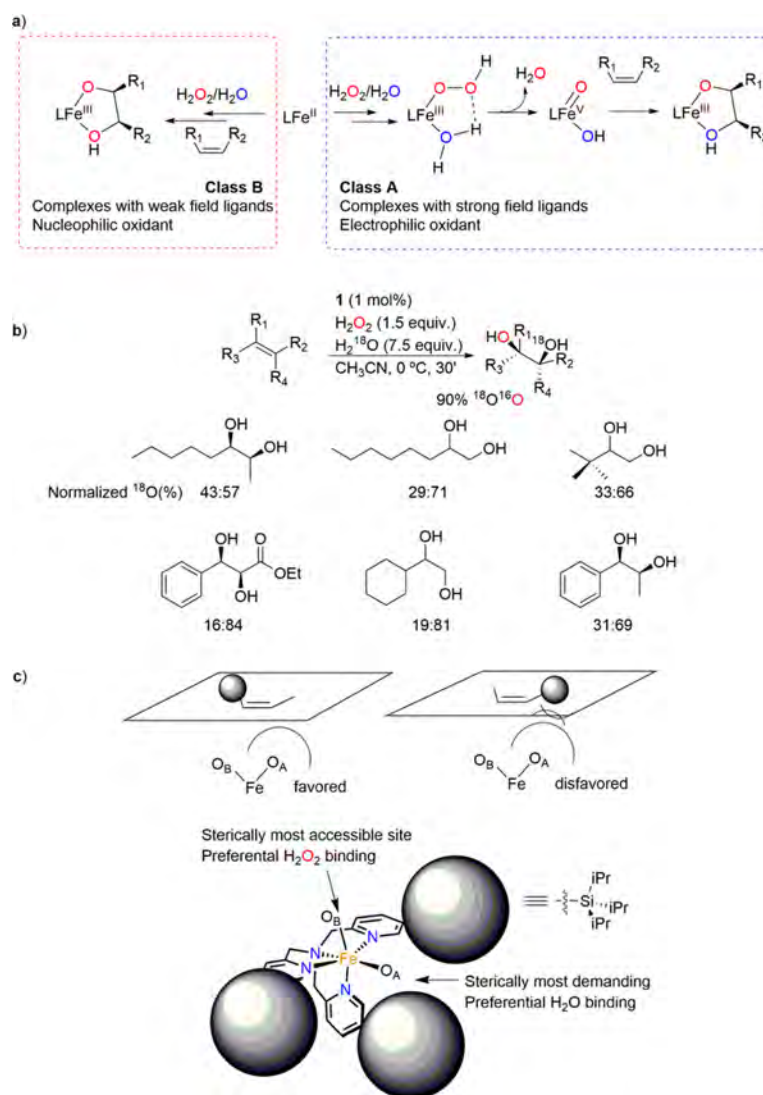
[a]Relative ^{18}O incorporation into the two oxygen atoms of the diol is displayed. [b]The proposed site of H_2O_2 and H_2O binding to the catalysts derived from the isotopic labeling study is also shown.
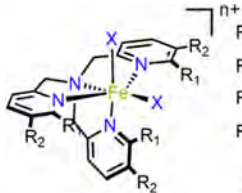
Therefore, the distinct structural constraints of the two labile sites in **1** translate into a distinctive isotopic labeling, strongly pointing out that the oxygen atoms from water and hydrogen peroxide occupy positions O_A and O_B, respectively, in the $[Fe^V(O)(OH)(^{5\text{-tips3}}tpa)]^{2+}$ active species (Scheme 5c). Identification of the latter brings novel insights into the mechanism of H_2O_2 activation operating at this catalyst and in particular on the nature of the ferric hydroperoxide species that evolves into the $Fe^V(O)(OH)$ oxidant.[11j] The isotopic labeling data indicate that the oxygen atom derived from H_2O_2 binds at the spatially more exposed site of the catalyst, *trans* to a pyridine, forming $[Fe^{III}(O_BOH)(O_AH_2)(^{5\text{-tips3}}tpa)]^{2+}$, that then evolves into $[Fe^V(O_B)(O_AH)(^{5\text{-tips3}}tpa)]^{2+}$ via a water-assisted O–O cleavage.[11j] Fast oxo-hydroxo tautomerism can then result in the formation of the tautomeric isomer $[Fe^V(O_BH)(O_A)\cdot(^{5\text{-tips3}}tpa)]^{2+}$.

A tentative rationale for the dominant H_2O_2 activation at O_B may be put forward by considering the relative lability of the two available binding sites. Pyridine is a π-acceptor ligand and exerts a stronger *trans* effect than an aliphatic amine. This should translate into a higher lability of the *trans*-site to the pyridine (O_B), facilitating H_2O_2 binding. On the other hand, the corresponding terminal oxo ligand is expected to be thermodynamically less stable, also because of the stronger *trans* effect exerted by the pyridine. Therefore, it is likely that the dominant activation of H_2O_2 at position O_B during catalysis results from a kinetically preferred peroxide binding, along with the formation of a more reactive high valent iron-oxo isomer.

Finally, the chemoselectivity toward the *syn*-dihydroxylation reaction exhibited by **1** deserves consideration. In general, iron catalysts react with H_2O_2 oxidizing aliphatic olefins to mixtures of epoxides and diols.[11j] The parent catalyst **2** constitutes a prototypical case that yields a modest preference for the diol

([diol]/[epoxide] ∼ 3−1, representative examples are collected in Table 3).[11j,12c] A systematic improvement of the selectivity toward the diol (usually studied in the oxidation of cyclo-octene) can be gained by introducing methyl groups in the α position of the pyridines in the ligand, but this modification results in catalysts with weaker N_{Py}−Fe bonds, which are labile and exhibit poor stability against demetalation, which in turn translates into poor activity.[11d,j,k,12c] On the other hand, the introduction of alkyl groups in the β position does not compromise the stability of the catalyst but has a modest effect in the selectivity toward syn-dihydroxylation.[11j,12c] The high chemoselectivity toward syn-dihydroxylation exhibited by **1**, which can be regarded as a β-trialkylsilyl-substituted version of **2**, while retaining high catalytic performance, is unprecedented and suggests that epoxidation is minimized by the steric crowding of the catalyst. This behavior may be tentatively explained on the basis of at least two factors: (a) the steric isolation of the iron center is envisioned to promote product release and also to limit oligomerization reactions, in turn facilitating the retention, during catalysis, of the two labile sites required for dihydroxylation activity, and (b) steric isolation is attained without compromising the strength of the Fe−N_{py} bonds and therefore the stability of the catalyst. Both of these aspects find strong experimental support in the catalytic behavior exhibited by **1** over time, illustrated in Figure 2.

Table 3. Comparison between the [Diol]/[Epoxide] Ratio Exhibited by Different Iron Catalysts with tpa Type of Ligands

substrate/catalyst	[diol]/[epoxide]			
	1[a]	**2**[b]	**5**[c,d]	**6**[e,b]
1-octene	6.6	2.4	3.3	−
vinylcyclohexane	3.8	2.0	3.5	−
cis-2-octene	24	−	−	−
cis-2-heptene	−	1.4	3.0	10
trans-2-octene	8	−	−	−
trans-2-heptene	−	2.2	4.3	10
cyclooctene	4	1.2	−	7−14[c]

[a]This work. [b]Data from ref 11j. [c]**5** corresponds to [Fe^{II}(CF$_3$SO$_3$)$_2$(^{5Me3}tpa)], ^{5Me3}tpa = tris(5-methyl-2-pyridylmethyl)-amine. [d]Data from ref 12c. [e]**6** corresponds to [Fe^{II}(^{6Me3}tpa)-(CH$_3$CN)$_2$](ClO$_4$)$_2$, ^{6Me3}tpa = tris(6-methyl-2-pyridylmethyl)amine.

However, comparison of our data with the literature precedents (Table 3) also strongly suggests that the Fe^V(O)-(OH) oxidant in **1** and **2** must exhibit an innate different chemoselectivity, the former being similar to that attained with **6**. A rationale for this effect can be found in computational studies in the epoxidation and cis-dihydroxylation reaction performed by [Fe^V(O)(OH)(tpa)]$^{2+}$.[21] These studies indicate that epoxidation is initiated by an attack of the oxo ligand over the olefin, while syn-dihydroxylation is initiated by an attack of the hydroxide. In this scenario, because the Fe=O bond is shorter than the Fe−OH bond, it can be proposed that

epoxidation, when compared with syn-dihydroxylation, will require a closer approach of the substrate to the iron center. Therefore, introduction of sterically demanding groups in either the α or β position of the pyridine can favor the syn-dihydroxylation reaction. It is interesting to note that this is actually a topological effect, meaning that different substitution patterns or shape of the olefin substrate must also affect their approach to the reactive iron-oxo species, translating into different [diol]/[epoxide] ratios. Results collected in Tables 2 and 3 provide experimental evidence in favor of this hypothesis. It is also important to notice that this effect is independent of the one that occurs when the catalyst changes from class A to class B by weakening of the crystal field.[11i] It is envisioned that manipulation of both elements may serve in the near future to design catalysts with improved chemoselectivities.

CONCLUSION

This work describes the development of a sterically encumbered iron catalyst that permits the high yield, selective syn-dihydroxylation of a broad range of olefins at short reaction times using aqueous H$_2$O$_2$ as oxidant. The combination of its excellent performance as a synthetic tool in combination with the fact that it employs water as an oxygen source can make this catalyst a valuable tool for a convenient O-labeling of organic substrates. For example, considering the interest of ^{17}O-labeled compounds in biological sciences,[22] along with the fact that H$_2$^{17}O is by far the most economically accessible source of ^{17}O, this catalyst may be of interest to these fields. Furthermore, besides providing a novel tool that can enable more sustainable synthetic organic chemistry, the work discloses new mechanistic perspectives. The structure of this bulky catalyst is uniquely suitable to provide details of the molecular and topological composition of the active species, which could only be previously proposed on the basis of computational analyses.[11h,21] The improved understanding of the catalytically active species that emerges from the current work may also represent a valuable tool to rationally design, in the near future, the catalytic active site to pursue selectivity on the basis of structural aspects such as molecular shape or olefin substitution patterns.

ASSOCIATED CONTENT

Ⓢ Supporting Information

The Supporting Information is available free of charge on the ACS Publications website at DOI: 10.1021/jacs.7b07909.

CIF file corresponding to **1** (CIF)

Experimental details for the preparation and characterization of the catalysts, experimental procedures for the catalytic reactions, and spectroscopic data for the products (PDF)

AUTHOR INFORMATION

Corresponding Author

*miquel.costas@udg.edu.

ORCID Ⓘ

Miquel Costas: 0000-0001-6326-8299

Notes

The authors declare no competing financial interest.

■ REFERENCES

(1) (a) Bataille, C. J. R.; Donohoe, T. J. *Chem. Soc. Rev.* **2011**, *40*, 114. (b) Kolb, H. C.; VanNieuwenhze, M. S.; Sharpless, K. B. *Chem. Rev.* **1994**, *94*, 2483. (c) Zaitsev, A. B.; Adolfsson, H. *Synthesis* **2006**, 1725.

(2) (a) Shing, T. K. M.; Tam, E. K. W.; Tai, V. W. F.; Chung, I. H. F.; Jiang, Q. *Chem. - Eur. J.* **1996**, *2*, 50. (b) Shing, T. K. M.; Tai, V. M. F.; Tam, E. K. W. *Angew. Chem., Int. Ed. Engl.* **1994**, *33*, 2312.

(3) (a) Sugimoto, H.; Kitayama, K.; Mori, S.; Itoh, S. *J. Am. Chem. Soc.* **2012**, *134*, 19270. (b) Yip, W.-P.; Ho, C.-M.; Zhu, N.; Lau, T.-C.; Che, C.-M. *Chem. - Asian J.* **2008**, *3*, 70. (c) Yip, W. P.; Yu, W. Y.; Zhu, N. Y.; Che, C. M. *J. Am. Chem. Soc.* **2005**, *127*, 14239.

(4) (a) Rawling, M. J.; Tomkinson, N. C. O. *Org. Biomol. Chem.* **2013**, *11*, 1434. (b) Colomer, I.; Barcelos, R. C.; Christensen, K. E.; Donohoe, T. J. *Org. Lett.* **2016**, *18*, 5880. (c) Griffith, J. C.; Jones, K. M.; Picon, S.; Rawling, M. J.; Kariuki, B. M.; Campbell, M.; Tomkinson, N. C. O. *J. Am. Chem. Soc.* **2010**, *132*, 14409. (d) Giglio, B. C.; Schmidt, V. A.; Alexanian, E. J. *J. Am. Chem. Soc.* **2011**, *133*, 13320. (e) Schmidt, V. A.; Alexanian, E. J. *Angew. Chem., Int. Ed.* **2010**, *49*, 4491. (f) Emmanuvel, L.; Shaikh, T. M. A.; Sudalai, A. *Org. Lett.* **2005**, *7*, 5071. (g) Fujita, M.; Wakita, M.; Sugimura, T. *Chem. Commun.* **2011**, *47*, 3983. (h) Kang, Y.-B.; Gade, L. H. *J. Am. Chem. Soc.* **2011**, *133*, 3658. (i) Zhong, W.; Yang, J.; Meng, X.; Li, Z. *J. Org. Chem.* **2011**, *76*, 9997. (j) Haubenreisser, S.; Woste, T. H.; Martinez, C.; Ishihara, K.; Muniz, K. *Angew. Chem., Int. Ed.* **2016**, *55*, 413.

(5) Dash, S.; Patel, S.; Mishra, B. K. *Tetrahedron* **2009**, *65*, 707.

(6) (a) De Vos, D. E.; de Wildeman, S.; Sels, B. F.; Grobet, P. J.; Jacobs, P. A. *Angew. Chem., Int. Ed.* **1999**, *38*, 980. (b) Saisaha, P.; Pijper, D.; van Summeren, R. P.; Hoen, R.; Smit, C.; de Boer, J. W.; Hage, R.; Alsters, P. L.; Feringa, B. L.; Browne, W. R. *Org. Biomol. Chem.* **2010**, *8*, 4444. (c) de Boer, J. W.; Browne, W. R.; Harutyunyan, S. R.; Bini, L.; Tiemersma-Wegman, T. D.; Alsters, P. L.; Hage, R.; Feringa, B. L. *Chem. Commun.* **2008**, 3747. (d) de Boer, J. W.; Browne, W. R.; Brinksma, J.; Alsters, P. L.; Hage, R.; Feringa, B. L. *Inorg. Chem.* **2007**, *46*, 6353. (e) de Boer, J. W.; Brinksma, J.; Browne, W. R.; Meetsma, A.; Alsters, P. L.; Hage, R.; Feringa, B. L. *J. Am. Chem. Soc.* **2005**, *127*, 7990.

(7) Chow, T. W.-S.; Liu, Y.; Che, C.-M. *Chem. Commun.* **2011**, *47*, 11204.

(8) (a) Karlsson, A.; Parales, J. V.; Parales, R. E.; Gibson, D. T.; Eklund, H.; Ramaswamy, S. *Science* **2003**, *299*, 1039. (b) Barry, S. M.; Challis, G. L. *ACS Catal.* **2013**, *3*, 2362. (c) Wolfe, M. D.; Parales, J. V.; Gibson, D. T.; Lipscomb, J. D. *J. Biol. Chem.* **2001**, *276*, 1945. (d) Kovaleva, E. G.; Lipscomb, J. D. *Nat. Chem. Biol.* **2008**, *4*, 186.

(9) Feng, Y.; Ke, C.-y.; Xue, G.; Que, L., Jr. *Chem. Commun.* **2009**, 50.

(10) Chen, K.; Que, L., Jr. *Angew. Chem., Int. Ed.* **1999**, *38*, 2227.

(11) (a) Garcia-Bosch, I.; Codolà, Z.; Prat, I.; Ribas, X.; Lloret-Fillol, J.; Costas, M. *Chem. - Eur. J.* **2012**, *18*, 13269. (b) Feng, Y.; England, J.; Que, L., Jr. *ACS Catal.* **2011**, *1*, 1035. (c) Oldenburg, P. D.; Feng, Y.; Pryjomska-Ray, I.; Ness, D.; Que, L., Jr. *J. Am. Chem. Soc.* **2010**, *132*, 17713. (d) Suzuki, K.; Oldenburg, P. D.; Que, L., Jr. *Angew. Chem., Int. Ed.* **2008**, *47*, 1887. (e) Barry, S. M.; Rutledge, P. J. *Synlett* **2008**, *2008*, 2172. (f) Bautz, J.; Comba, P.; Lopez de Laorden, C.; Menzel, M.; Rajaraman, G. *Angew. Chem., Int. Ed.* **2007**, *46*, 8067. (g) Oldenburg, P. D.; Shteinman, A. A.; Que, L., Jr. *J. Am. Chem. Soc.* **2005**, *127*,

15672. (h) Bassan, A.; Blomberg, M. R. A.; Siegbahn, P. E. M.; Que, L., Jr. *Angew. Chem., Int. Ed.* **2005**, *44*, 2939. (i) Fujita, M.; Costas, M.; Que, L., Jr. *J. Am. Chem. Soc.* **2003**, *125*, 9912. (j) Chen, K.; Costas, M.; Kim, J.; Tipton, A. K.; Que, L., Jr. *J. Am. Chem. Soc.* **2002**, *124*, 3026. (k) Costas, M.; Tipton, A. K.; Chen, K.; Jo, D.-H.; Que, L., Jr. *J. Am. Chem. Soc.* **2001**, *123*, 6722. (l) Bruijnincx, P. C. A.; Buurmans, I. L. C.; Huang, Y.; Juhasz, G.; Viciano-Chumillas, M.; Quesada, M.; Reedijk, J.; Lutz, M.; Spek, A. L.; Muenck, E.; Bominaar, E. L.; Klein Gebbink, R. J. M. *Inorg. Chem.* **2011**, *50*, 9243. (m) Bruijnincx, P. C. A.; Buurmans, I. L. C.; Gosiewska, S.; Moelands, M. A. H.; Lutz, M.; Spek, A. L.; van Koten, G.; Klein Gebbink, R. J. M. *Chem. - Eur. J.* **2008**, *14*, 1228. (n) Folkertsma, E.; de Waard, E. F.; Korpershoek, G.; van Schaik, A. J.; Solozabal Miron, N.; Borrmann, M.; Nijsse, S.; Moelands, M. A. H.; Lutz, M.; Otte, M.; Moret, M. E.; Klein Gebbink, R. J. M. *Eur. J. Inorg. Chem.* **2016**, *2016*, 1319. (o) Chatterjee, S.; Paine, T. K. *Angew. Chem., Int. Ed.* **2015**, *54*, 9338. (p) Kejriwal, A.; Biswas, S.; Biswas, A. N.; Bandyopadhyay, P. *J. Mol. Catal. A: Chem.* **2016**, *413*, 77. (q) Comba, P.; Rajaraman, G. *Inorg. Chem.* **2008**, *47*, 78.

(12) (a) Zang, C.; Liu, Y.; Xu, Z.-J.; Tse, C.-W.; Guan, X.; Wei, J.; Huang, J.-S.; Che, C.-M. *Angew. Chem., Int. Ed.* **2016**, *55*, 10253. (b) Chow, T. W.-S.; Wong, E. L.-M.; Guo, Z.; Liu, Y.; Huang, J.-S.; Che, C.-M. *J. Am. Chem. Soc.* **2010**, *132*, 13229. (c) Ryu, J. Y.; Kim, J.; Costas, M.; Chen, K.; Nam, W.; Que, L., Jr. *Chem. Commun.* **2002**, *12*, 1288. (d) Prat, I.; Font, D.; Company, A.; Junge, K.; Ribas, X.; Beller, M.; Costas, M. *Adv. Synth. Catal.* **2013**, *355*, 947.

(13) Prat, I.; Mathieson, J. S. J. S.; Güell, M.; Ribas, X.; Luis, J. M. J. M.; Cronin, L.; Costas, M. *Nat. Chem.* **2011**, *3*, 788.

(14) (a) Plietker, B.; Niggemann, M. *J. Org. Chem.* **2005**, *70*, 2402. (b) Plietker, B.; Niggemann, M.; Pollrich, A. *Org. Biomol. Chem.* **2004**, *2*, 1116. (c) Plietker, B.; Niggemann, M. *Org. Biomol. Chem.* **2004**, *2*, 2403. (d) Plietker, B.; Niggemann, M. *Org. Lett.* **2003**, *5*, 3353.

(15) (a) Neibergall, M. B.; Stubna, A.; Mekmouche, Y.; Munck, E.; Lipscomb, J. D. *Biochemistry* **2007**, *46*, 8004. (b) Wolfe, M. D.; Altier, D. J.; Stubna, A.; Popescu, C. V.; Münck, E.; Lipscomb, J. D. *Biochemistry* **2002**, *41*, 9611.

(16) (a) Font, D.; Canta, M.; Milan, M.; Cusso, O.; Ribas, X.; Klein Gebbink, R. J. M.; Costas, M. *Angew. Chem., Int. Ed.* **2016**, *55*, 5776. (b) Cusso, O.; Cianfanelli, M.; Ribas, X.; Klein Gebbink, R. J. M.; Costas, M. *J. Am. Chem. Soc.* **2016**, *138*, 2732. (c) Milan, M.; Bietti, M.; Costas, M. *ACS Cent. Sci.* **2017**, *3*, 196.

(17) (a) Prat, I.; Company, A.; Corona, T.; Parella, T.; Ribas, X.; Costas, M. *Inorg. Chem.* **2013**, *52*, 9229−9244. (b) Zang, Y.; Kim, J.; Dong, Y.; Wilkinson, E. C.; Appelman, E. H.; Que, L., Jr. *J. Am. Chem. Soc.* **1997**, *119*, 4197. (c) Diebold, A.; Hagen, K. S. *Inorg. Chem.* **1998**, *37*, 215.

(18) White, M. C.; Doyle, A. G.; Jacobsen, E. N. *J. Am. Chem. Soc.* **2001**, *123*, 7194.

(19) Murphy, A.; Pace, A.; Stack, T. D. P. *Org. Lett.* **2004**, *6*, 3119.

(20) Wang, Z.; Cui, Y.-T.; Xu, Z.-B.; Qu, J. *J. Org. Chem.* **2008**, *73*, 2270.

(21) (a) Bassan, A.; Blomberg, M. R. A.; Siegbahn, P. E. M.; Que, L., Jr. *Chem. - Eur. J.* **2005**, *11*, 692. (b) Bassan, A.; Blomberg, M. R. A.; Siegbahn, P. E. M.; Que, L., Jr. *J. Am. Chem. Soc.* **2002**, *124*, 11056.

(22) (a) Antzutkin, O. N.; Iuga, D.; Filippov, A. V.; Kelly, R. T.; Becker-Baldus, J.; Brown, S. P.; Dupree, R. *Angew. Chem., Int. Ed.* **2012**, *51*, 10289. (b) Wu, G. *Solid State Nucl. Magn. Reson.* **2016**, *73*, 1. (c) Young, R. P.; Caulkins, B. G.; Borchardt, D. N.; Bulloch, D. N.; Larive, C. K.; Dunn, M. F.; Mueller, L. J. *Angew. Chem., Int. Ed.* **2016**, *55*, 1350. (d) Wong, A.; Poli, F., Solid-State O-17 NMR Studies of Biomolecules. In *Annual Reports on NMR Spectroscopy*; Webb, G. A., Ed.; Elsevier Academic Press Inc: San Diego, 2014; Vol. 83, pp 145.

Chapter   IV.

Greening Oxidation Catalysis: Iron Catalyzed
Alkene *syn*-Dihydroxylation with Aqueous Hydrogen
Peroxide in Green Solvents
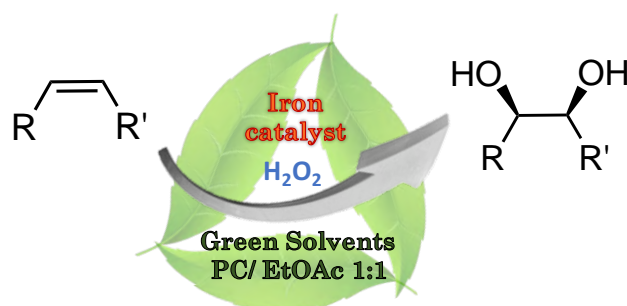
This chapter corresponds to the following publication:

Margarida Borrell, Miquel Costas. *ACS Sustainable Chem. Eng*. **2018**, 6, 7, 8410-8416.

Reprinted with permission from ACS publications.

Greening Oxidation Catalysis: Iron Catalyzed Alkene *syn*-Dihydroxylation with Aqueous Hydrogen Peroxide in Green Solvents

Margarida Borrell and Miquel Costas*

Institut de Química Computacional i Catàlisi (IQCC) and Departament de Química, Universitat de Girona, Campus Montilivi, Girona E-17071, Catalonia, Spain

S Supporting Information

ABSTRACT: Herein, we disclose the application of green solvents in a biologically inspired oxidation reaction. In a mixture of propylene carbonate and ethyl acetate, iron catalyzed *syn*-dihydroxylation of olefins with aqueous hydrogen peroxide proceeds in short reaction times with excellent yields and chemoselectivity. The current report showcases the suitability of this sustainable media to this class of important reactions.
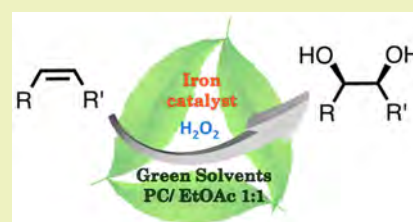
KEYWORDS: *Oxidation catalysis, syn-Dihydroxylation, Hydrogen peroxide, Iron, Green solvents*

INTRODUCTION

Solvents represent the major component of the chemicals employed in conventional organic synthesis, and because of that, the use of green solvents is one of the most efficient ways to reduce the environmental impact of organic reactions. Propylene carbonate (PC) constitutes an ideal alternative to traditional solvents. It has been ranked as the greenest solvent in green solvents guides; it contains only carbon, hydrogen, and oxygen in its structure, so it does not generate NOx and SOx in its incineration. It is known to be nontoxic and is prepared by 100% atom economical reactions.[1] Ethyl acetate (AcOEt) shares most of the positive aspects of PC and it is also regarded as one of the most convenient organic solvents from a green chemistry perspective. Use of green solvents, especially PC in technologically metal catalyzed reactions, is a topic of current interest.[2−7]

Hydrocarbon oxidation reactions are important tools in organic synthesis,[8−10] and development of green oxidation methods is a subject of current importance. The development of sustainable oxidation methodologies ideally needs to target the use of oxidants that produce no waste, catalysts based on nonexpensive and nontoxic metals, mild reaction conditions, and no explosive or toxic volatile solvents. Surprisingly, there is only a single reported example of the use of green solvents such as PC in oxidation reactions.[11]

Olefin *syn*-dihydroxylation represents a paradigmatic case of an important oxidation reaction for which sustainable reaction conditions are needed. It constitutes a cornerstone in traditional organic chemistry, but current methodologies for this transformation are mainly based on heavy metal oxides such as Os and Ru,[8−10,12,13] which hamper the use of the reaction because of sustainability. Metal-free methodologies and the use of catalysts based on first row transition metals that are highly abundant and exhibit a minor environmental impact

constitute promising alternatives.[10,14−24] Particularly interesting are methods employing hydrogen peroxide as oxidant.[25−27]

Iron catalyzed *syn*-dihydroxylation constitutes an interesting option, given the availability and limited cost and toxicity of this metal.[28−30] Taking inspiration from iron dependent arene *syn*-dihydroxylating enzymes present in nature,[31−33] iron coordination complexes have been largely explored as catalysts,[34−51] and a few examples provide synthetically valuable yields (Figure 1).[52−56] A common limitation of these reactions in terms of
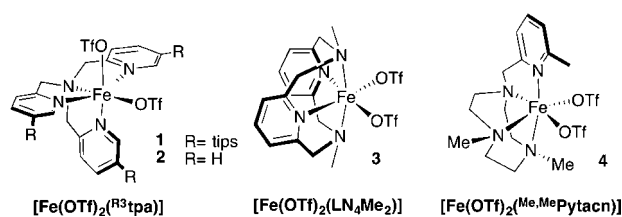
Figure 1. Iron complexes studied in this work as *syn*-dihydroxylation catalysts in green solvents reactions. tips = tris-isopropylsilyl, OTf = trifluoromethanesulfonate anion.

sustainability is that they operate in volatile and toxic solvents, most often acetonitrile. This drawback is actually quite general to iron catalyzed oxidation reactions and constitutes one of the major concerns of these reactions in terms of sustainability.

Iron complexes **1−4** (Figure 1) constitute prototypical examples of catalysts that have been explored in acetonitrile.[56]

Herein, we investigate their activity in green solvents, finding that **1** exhibits excellent activity in EtOAc/PC solvent mixtures. A broad range of olefins are converted into the corresponding

diols with good yields and selectivities, in short reaction times using a slight excess of hydrogen peroxide as oxidant, under mild experimental conditions. The potential utility of the reaction is showcased in the gram-scale *syn*-dihydroxylation of a natural product. Overall, the current report highlights the suitability of this sustainable media for this class of important reactions.

■ EXPERIMENTAL SECTION

Materials and Methods. Materials were purchased from SDS, Sigma-Aldrich, Fluorochem, and Scharlab. All substrates used were of commercially available reagent quality unless stated otherwise, and the liquid ones were filtered through a basic alumina plug before being used. The solvents used were of HPLC grade. Chromatographic analyses were done by GC with a 7820A gas chromatograph, using an Agilent HP-5 column and an FID detector. Oxidation products were identified by comparison of their GC retention time with those of authentic compounds synthesized according to a reported procedure.[56]

Synthesis of the Catalysts. Catalysts **1–4** were synthesized according to the procedures reported in literature.[52–54,56]

Reaction Conditions for Iron-Catalyzed *syn*-Dihydroxylation of Alkenes. The substrate (45 μmol, 1 equiv), the catalyst (0.45 μmol, 1 mol %), and $Mg(ClO_4)_2 \cdot 6H_2O$ (99 μmol, 2.2 equiv) were dissolved with a 1/1 mixture of PC and EtOAc (800 μL) in a 3 mL vial equipped with a stir bar, and the resulting mixture was cooled with an ice bath. Then, 114 μL (67.5 μmol, 1.5 equiv) of 0.58 M H_2O_2 solution in PC (diluted from 50% in aqueous solution) was directly added by syringe pump over 30 min. Then, the solution was stirred for further 30 min.

At this point, 0.1 mL of methyl imidazole and 1 mL of acetic anhydride were added and stirred for 15 min at room temperature to esterify the *syn*-diol product. After 15 min, some ice was added to the solution, and it was stirred for 15 min more. Then, an internal standard (biphenyl) was added to the solution and was extracted in 2 mL of EtOAc. The organic phase was washed with 2 mL of 1 M H_2SO_4. After the vial was shaken vigorously, the organic phase was washed first with 2 mL of $NaHCO_3$ and then with 2 mL of water. The resultant organic phase was dried with $MgSO_4$, filtered, and injected directly to gas chromatograph. GC analysis of the solution provided substrate conversions and product yields relative to the internal standard integration of the substrate.

Iron-Catalyzed *syn*-Dihydroxylation of Alkenes Using an in Situ Generated Catalyst. Iron triflate $(Fe(OTf)_2(CH_3CN)_2)$ (2.6 μmol, 0.01 equiv) and [5-tips3]tpa (2.6 μmol, 0.01 equiv) were dissolved in a 1/1 mixture of PC and EtOAc (1 mL) in a 3 mL vial equipped with a stir bar, and it was stirred at room temperature for 5 min. After this time, the substrate (263 μmol, 1 equiv) and $Mg(ClO_4)_2 \cdot 6H_2O$ (579 μmol, 2.2 equiv) were added, and the resulting mixture was cooled with an ice bath. 666 μl (394 μmol, 1.5 equiv) of 0.58 M H_2O_2 solution in PC (diluted from 50% in aqueous solution) was directly added by syringe pump over 30 min. Then, the solution was stirred for further 30 min.

At this point, 0.1 mL of methyl imidazole and 1 mL of acetic anhydride were added and stirred for 15 min at room temperature to esterify the *syn*-diol product. After 15 min, some ice was added to the solution, and it was stirred for 15 min more. Then, an internal standard (biphenyl) was added to the solution and was extracted in 2 mL of EtOAc. The organic phase was washed with 2 mL of 1 M H_2SO_4. After the vial was shaken vigorously, the organic phase was washed first with 2 mL of $NaHCO_3$ and then with 2 mL of water. The resultant organic phase was filtered through a $MgSO_4$ plug and injected directly to the gas chromatograph. GC analysis of the solution provided substrate conversions and product yields relative to the internal standard integration of the substrate.
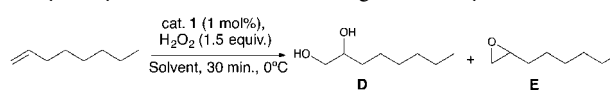
General Procedure for the Isolation of a Complex Organic Molecule. Cholesteryl oleate (6.1 mmol, 1 equiv), the catalyst (60.9 μmol, 1 mol %), and $Mg(ClO_4)_2 \cdot 6H_2O$ (13.3 mmol, 2.2 equiv) were dissolved with a 3:8 mixture of PC and EtOAc (1 mL) in a 50 mL

round-bottom flask and stirred at room temperature. Then, 887 μL (9.2 mmol, 1.5 equiv) of 10.3 M H_2O_2 solution in PC (diluted from 50% aqueous solution) was added by syringe pump during 30 min. Then, the solution was stirred for further 30 min. At this point, 0.3 mL of methyl imidazole and 2 mL of acetic anhydride were added, and the solution was stirred for 15 min at room temperature to esterify the *syn*-diol product. After 15 min, ice (1 g) is added to the solution, and it was stirred for 15 min more. The solution was extracted with 2 mL of EtOAc, and the organic phase was washed with 2 mL of 1 M H_2SO_4. After the vial was shaken vigorously, the organic layer was washed first with 2 mL of $NaHCO_3$ and then with 2 mL of water. The resultant organic phase was dried with $MgSO_4$ and filtered. Finally, the organic fractions were combined and evaporated by distillation using a Kugelrohr to remove the PC. The resulting residue was purified by flash chromatography on silica gel (hexane/EtOAc: 8/2) to obtain the product as a colorless oil (4.8 mmol, 79% isolated yield). Spectroscopic data are in agreement with a previous literature report.[56]

■ RESULTS AND DISCUSSION

Among the series of complexes **1–4**, we chose to initiate our study on the oxidation of olefins with catalyst **1** because it was envisioned that the hydrophobic character of the *tris*-isopropylsilyl (tips) groups will favor its solubility in organic solvents. Dihydroxylation of 1-octene catalyzed by **1** (1 mol %) was initially explored by delivering H_2O_2 (1.5 equiv) via syringe pump during 30 min to a solution of the catalyst at 0 °C. The reaction was tested in different solvents (Table 1) with the aim to find a green solvent that could replace acetonitrile, the common solvent for this class of reactions.[12–14]

Table 1. Screening of Different Solvents for the Dihydroxylation of 1-Octene Using the Catalyst 1

entry	solvent	conv. (%)	yield D (%)	yield E (%)	ratio D/E
1	acetonitrile[b]	97	74	15	4.9
2	acetone[c]	60	19	12	1.6
3	γ-butyrolactone	91	63	27	2.3
4	ethyl hexanoate[c]	82	68	12	5.7
5	EtOAc[c]	60	36	6	6.0
6	PC	83	62	18	3.4
7	EtOAc/PC (1/1)	94	78	15	5.2
8	EtOAc/γ-butyrolactone (1/1)	92	77	14	5.5
9	EtOAc/ethyl hexanoate[c] (1/1)	72	62	9	6.8

[a]Conversions and yields determined by GC, calibrated with authentic standards. [b]From ref 56. [c]The H_2O_2 was solved in CH_3CN due to problems of solubility of the H_2O_2 in the solvent (114 μL (67.5 μmol, 1.5 equiv) of 0.58 M H_2O_2 solution in CH_3CN (diluted from 50% in aqueous solution)). Product yields are the average of 2–3 runs with the error of <9%.

1 is extraordinarily active and selective, and the reaction in acetonitrile provides a mixture of diol and epoxide ([diol]: [epoxide] = 4.9) in 89% combined yield (entry 1). When acetone was used, product yields decrease substantially, and the catalyst loses the chemoselectivity between diol and epoxide (entry 2). Practically full conversion and moderate to good yields were obtained with γ-butyrolactone (entry 3). Remarkably, good chemoselectivity for the diol was obtained in ethyl acetate and ethyl hexanoate (entries 4 and 5). Finally, in PC,

Table 2. Dihydroxylation of 1-Octene in EtOAc/PC or CH₃CN Catalyzed by Different Iron Catalysts[a]
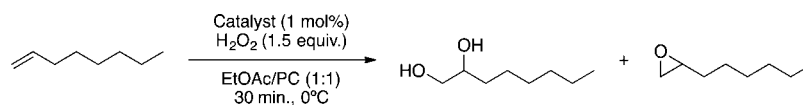
entry	catalyst	conv. (%)	yield D (%)	yield E (%)	ratio D/E
1	1	82	65	13	5.0
	1[b,c]	94	74	23	3.2
2	2	60	50	10	5.0
	2[b,c]	71	47	10	4.7
3	3	15	0.5	1	2.0
	3[b,c]	28	2	<1	
4	4	21	10	11	0.9
	4[b,c]	66	30	15	2.0
5[d]	1	94	78	15	5.2
	1[b,c]	100	86	14	6.1

[a]Conversions and yields determined by GC using the responsive constants of the products. [b]Acetonitrile was used as solvent instead of EtOAc/PC. [c]From ref 56. [d]Using 2.2 equiv of Mg(ClO₄)₂·6H₂O. Products yields are the average of 2−3 runs with the error <8%.

Table 3. Substrate Scope
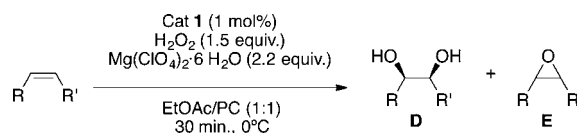
[a]Entry	Substrate	Conv. (%)	Yield D (%)	Yield E (%)	Ratio D/E
1		94	78	15	5.2
2		82	65	17	4
3		99	86	13	6
4		100	70	21	3
5		82	76	4	19
6[b]		100	93	3	22
7[b]		100	69	31	2.2
8		82	64	6	10
9		95	91	3	30
10[c]		95	83	-	-

[a]Conversions and yields determined by GC using the responsive constants of the products. [b]Second addition of 1 mol % of catalyst and 1.5 equiv of H₂O₂. [c]Conversion and yield determined by NMR. Product yields are the average of 2−3 runs with the error of <5%.

good conversion and yields were obtained, and moreover, the mass balance of the reaction is excellent (entry 6). Trying to combine the chemoselectivity toward the diol provided by EtOAc and the good yields observed in PC, γ-butyrolactone and ethyl hexanoate a 1/1 v/v mixture of EtOAC with each of the latter solvents was tested (entries 7−9), and much to our delight, good product yields and selectivities, comparable to those attained in acetonitrile were obtained when EtOAc was combined with PC or γ-butyrolactone (entries 7 and 8).
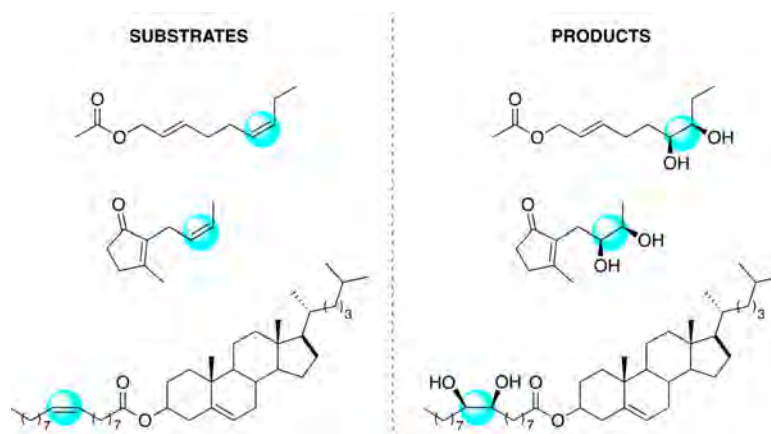
Figure 2. Regioselective *syn*-dihydroxylation of substrates bearing two olefinic sites.

Table 4. Dihydroxylation of in Situ Generated Catalyst 1

[a]Entry	Substrate	Conv. (%)	Yield D (%)	Yield E (%)	Ratio D/E
1		80	65	15	4.3
2		73	63	9	7.0
3		100	72	2	36
4		75	69	4	17

[a]Conversions and yields determined by GC using the responsive constants of the products. Product yields are the average of 2−3 reactions with the error of <8%.

Further studies were performed with the EtOAc/PC (1/1) solvent mixture.

Encouraged by these results, we then tested the same experimental conditions with the best iron dihydroxylating catalysts reported in literature (Table 2). In the case of catalysts **1** and **2** (Figure 1), both based in the tpa (tpa = tris(2-pyridylmethyl)amine) ligand frame, no significant changes were observed between reactions performed in EtOAc/PC 1/1 and the same using acetonitrile (entries 1, 2, and 5). Catalyst **3** is a variation of $[Fe(Cl)_2(LN_4Me_2)]^+$, which requires oxone for efficient operation,[16] and appears to be poorly active in acetonitrile and EtOAc/PC 1/1 (entry 3). Instead, catalyst **4** shows moderate activity in acetonitrile, but both yields and conversions dropped very substantially in EtOAc/PC 1/1 (entry 4). Probably, this is due to the poor solubility of the catalyst in the EtOAc/PC solvent mixture. Most interestingly, when the reaction catalyzed by **1** is conducted in the presence of $Mg(ClO_4)_2 \cdot 6H_2O$ (2.2 equiv), excellent product yields, chemoselectivity toward the diol, and mass balance is obtained. Presumably, addition of $Mg(ClO_4)_2 \cdot 6H_2O$ binds and protects the diol from overoxidation reactions, as recently seen in reactions conducted in acetonitrile.[56]

Dihydroxylation of different olefins catalyzed by **1** was then explored using the best conditions using a EtOAc/PC (1/1) solvent mixture, and results are collected in Table 3.

It was found that using these conditions, good to excellent yields were obtained in a diverse range of representative substrates, including linear aliphatic olefins with terminal (entry 1), *trans* (entry 2), and *cis* substituted olefinic sites (entry 3) as well as cyclic olefins (entry 4). Electron-deficient olefins such as dimethyl fumarate (entry 5) and cyclic aliphatic enones (entry 6) were also oxidized, providing satisfactory yields of the corresponding diols. Oxidation of *cis*-β-methylstyrene also proceeds with moderate yields (entry 7), and remarkably, the reaction proceeds with stereoretention. Of notice, the analysis of the stereochemistry of the diol products shows that the reaction is always a *syn*-dihydroxylation (see Supporting Information).

Remarkably, the catalyst is regioselective when two olefinic sites are present in the same molecule. For example, oxidation occurs at the more electron-rich site of *trans*-2-*cis*-6-nonadienylacetate (entry 8), and the same selectivity is observed in the oxidation of the natural product *cis*-jasmone (entry 9). In addition, the oxidation of cholesteryl oleate (entry 10) occurs selectively at the sterically less impeded site. In all these substrates bearing two olefinic sites, no other regioisomers have been detected (Figure 2).

For comparison, analogous reactions conducted in acetonitrile as solvent and also in 1/1 EtOAc/PC containing catalytic amounts of acetonitrile have been included as Supporting Information, Table S1. Most importantly, reactions conducted in the two solvent mixtures provide comparable results in terms of product yields and chemoselectivities. Significantly lower yields (10−15%) were observed in few examples (entries 2, 4, and 5), but with the single exception of *trans*-2-*cis*-6-nonadienylacetate (entry 8, 90% yield in acetonitrile), the differences are modest. Improved yields of diol with respect to acetonitrile was also observed (entry 9).

Iron complexes with aminopyridine ligands are moderately oxygen sensitive, and because of that, in situ generation of the catalyst can represent an important aspect to make the reactions practical from a synthetic point of view. In this regard, it was interesting to see that a good yield of diol (up to 72%) was also obtained from the *syn*-dihydroxylation of different substrates using standard conditions but previously generating catalyst **1** in situ, from the combination of iron triflate (Fe(OTf)$_2$(CH$_3$CN)$_2$) and the $^{5\text{-tips3}}$tpa ligand, both of which are bench stable, oxygen nonsensitive compounds (Table 4). When the commercially available Fe(OTf)$_2$·2CH$_3$CN was used without the ligand, no oxidation products were obtained.

Use of stoichiometric amounts of Mg(ClO$_4$)$_2$·6H$_2$O may be regarded as a drawback with regard to the atom economy of the reactions, but the addition of this additive significantly improves product yields and chemoselectivity of the reactions. Overall, the latter aspects translate into more efficient and arguably more sustainable transformations. On the other hand, perchlorate anions are potentially explosive, and because of that, other salts were tested to replace this additive (Table 5).

Table 5. Screening of Different Lewis Acids

entry^a	Lewis acid	conv. (%)	yield D (%)	yield E (%)	ratio D/E
1	MgO	58	48	8	6.0
2	Mg(OTf)$_2$	89	74	15	4.9
3	Zn(OTf)$_2$	94	75	19	3.9
4	Mg(ClO$_4$)$_2$·6H$_2$O	94	78	15	5.2

^{a}Conversions and yields determined by GC using the responsive constants of the products. Product yields are the average of 2 reactions with the error of <6%.
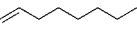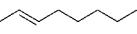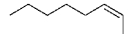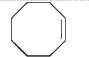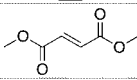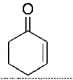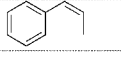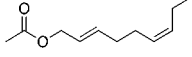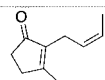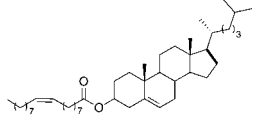
Interestingly, both Mg(OTf)$_2$ (entry 2) and Zn(OTf)$_2$ (entry 3) provide comparable yields of diol to the one obtained with Mg(ClO$_4$)$_2$·6H$_2$O. Interestingly, change of Mg(ClO$_4$)$_2$·6H$_2$O by Mg(OTf)$_2$ does not affect the chemoselectivity of the reaction, as shown by the similar mass balance and D/E ratios.

We explored the utility of the system in synthetically relevant gram-scale reactions. As an example, the gram-scale *syn*-dihydroxylation of cholesteryl oleate was performed (Scheme 1). The reaction proceeds with a good product conversion, obtaining a 79% isolated yield of the corresponding *syn*-diol. Of note, with this steroidal substrate, reaction conditions need to be slightly altered by adding a larger amount of ethyl acetate to solubilize the substrate. This aspect actually suggests that the catalyst is quite robust and unusually tolerant in terms of solvent composition, so the EtOAc/PC mixture could be adjusted depending on the solubility of the substrate, with no significant impact on the catalyst performance.

Finally, we calculate the *E* factor and the atom economy (AE) of the system (Table 6). These green metrics are the

simplest and most popular used to measure the greenness of the reaction.[57]

Table 6. *E* Factor and AE for the Reactions Described in Table 3

Entry	Substrate	E factor	AE (%)
1		197	89
2		237	89
3		179	89
4		223	90
5		167	91
6		186	88
7		214	89
8		162	92
9		125	92
10		40	97

The *E* factor values obtained for the oxidation reactions, with the standard conditions, is relatively high in nearly all the cases (from 125 to 237), but not in the case of cholesteryl oleate (entry 10). The relatively high *E* factors can be traced to the low molecular weight of the substrates employed in the screening and the relatively low concentration of substrate that is used under these conditions. When the total volume of the reaction is decreased 3-fold (300 μL), the *E* factor values obtained are in an acceptable range (between 74 and 100). On the other hand, considering that hydrogen peroxide is used as oxidant and only water is produced as byproduct, the AE obtained in the oxidation reactions is in all the cases very high.

In conclusion, this work describes the first example of an iron catalyzed oxidation reaction in green solvents, demonstrating the suitability of this media for this class of important reactions. The potential utility of the system has been showcased in the gram-scale *syn*-dihydroxylation of a steroidal substrate. The combination of an iron-based catalyst, which can be prepared in

Scheme 1. Gram-Scale Reaction of Cholesteryl Oleate with H$_2$O$_2$ Catalyzed by 1
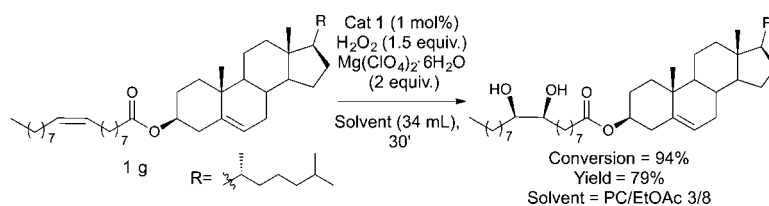
situ from bench stable compounds, a waste-free oxidant, mild experimental conditions, and a green solvent mixture makes this system particularly appealing from a sustainability perspective. Straightforward expansion toward other important oxidation reactions such as epoxidation or C−H hydroxylation[58−60] currently being explored in acetonitrile with related iron catalysts is envisioned.

■ ASSOCIATED CONTENT

Ⓢ Supporting Information

The Supporting Information is available free of charge on the ACS Publications website at DOI: 10.1021/acssuschemeng.8b00542.

> Experimental details for the preparation and characterization of the complexes and experimental procedure for the catalytic reactions, comparative data for reactions performed in acetonitrile, determination of E factors, and spectroscopic and chromatographic data of the products (PDF)

■ AUTHOR INFORMATION

Corresponding Author

*Phone: (+34)972419842; E-mail: miquel.costas@udg.edu.

ORCID Ⓓ

Miquel Costas: 0000-0001-6326-8299

Notes

The authors declare no competing financial interest.

■ ACKNOWLEDGMENTS

■ REFERENCES

(1) Prat, D.; Hayler, J.; Wells, A. A survey of solvent selection guides. *Green Chem.* **2014**, *16* (10), 4546−4551.

(2) North, M.; Pasquale, R. Mechanism of Cyclic Carbonate Synthesis from Epoxides and CO2. *Angew. Chem., Int. Ed.* **2009**, *48* (16), 2946−2948.

(3) North, M.; Omedes-Pujol, M. Catalytic, asymmetric cyanohydrin synthesis in propylene carbonate. *Tetrahedron Lett.* **2009**, *50* (31), 4452−4454.

(4) Lenden, P.; Ylioja, P. M.; Gonzalez-Rodriguez, C.; Entwistle, D. A.; Willis, M. C. Replacing dichloroethane as a solvent for rhodium-catalysed intermolecular alkyne hydroacylation reactions: the utility of propylene carbonate. *Green Chem.* **2011**, *13* (8), 1980−1982.

(5) Yu, B.; Diao, Z.-F.; Guo, C.-X.; Zhong, C.-L.; He, L.-N.; Zhao, Y.-N.; Song, Q.-W.; Liu, A.-H.; Wang, J.-Q. Carboxylation of terminal alkynes at ambient CO2 pressure in ethylene carbonate. *Green Chem.* **2013**, *15* (9), 2401−2407.

(6) Parker, H. L.; Sherwood, J.; Hunt, A. J.; Clark, J. H. Cyclic Carbonates as Green Alternative Solvents for the Heck Reaction. *ACS Sustainable Chem. Eng.* **2014**, *2* (7), 1739−1742.

(7) Neubert, P.; Fuchs, S.; Behr, A. Hydroformylation of piperylene and efficient catalyst recycling in propylene carbonate. *Green Chem.* **2015**, *17* (7), 4045−4052.

(8) Kolb, H. C.; VanNieuwenhze, M. S.; Sharpless, K. B. Catalytic Asymmetric Dihydroxylation. *Chem. Rev.* **1994**, *94*, 2483−2547.

(9) Zaitsev, A. B.; Adolfsson, H. Recent developments in asymmetric dihydroxylations. *Synthesis* **2006**, *11*, 1725−1756.

(10) Bataille, C. J. R.; Donohoe, T. J. Osmium-free direct syn-dihydroxylation of alkenes. *Chem. Soc. Rev.* **2011**, *40*, 114−128.

(11) Pieber, B.; Kappe, C. O. Direct aerobic oxidation of 2-benzylpyridines in a gas-liquid continuous-flow regime using propylene carbonate as a solvent. *Green Chem.* **2013**, *15* (2), 320−324.

(12) Shing, T. K. M.; Tai, V. M. F.; Tam, E. K. W. Practical and rapid vicinal hydroxylation of alkenes by catalytic ruthenium tetraoxide. *Angew. Chem., Int. Ed. Engl.* **1994**, *33* (22), 2312−2313.

(13) Shing, T. K. M.; Tam, E. K. W.; Tai, V. W. F.; Chung, I. H. F.; Jiang, Q. Ruthenium-catalyzed cis-dihydroxylation of alkenes: Scope and limitations. *Chem. - Eur. J.* **1996**, *2* (1), 50−57.

(14) Emmanuvel, L.; Shaikh, T. M. A.; Sudalai, A. NaIO4/LiBr-mediated Diastereoselective Dihydroxylation of Olefins: A Catalytic Approach to the Prevost−Woodward Reaction. *Org. Lett.* **2005**, *7* (22), 5071−5074.

(15) Schmidt, V. A.; Alexanian, E. J. Metal-Free, Aerobic Dioxygenation of Alkenes Using Hydroxamic Acids. *Angew. Chem., Int. Ed.* **2010**, *49* (26), 4491−4494.

(16) Griffith, J. C.; Jones, K. M.; Picon, S.; Rawling, M. J.; Kariuki, B. M.; Campbell, M.; Tomkinson, N. C. O. Alkene Syn Dihydroxylation with Malonoyi Peroxides. *J. Am. Chem. Soc.* **2010**, *132* (41), 14409−14411.

(17) Giglio, B. C.; Schmidt, V. A.; Alexanian, E. J. Metal-Free, Aerobic Dioxygenation of Alkenes Using Simple Hydroxamic Acid Derivatives. *J. Am. Chem. Soc.* **2011**, *133* (34), 13320−13322.

(18) Fujita, M.; Wakita, M.; Sugimura, T. Enantioselective Prevost and Woodward reactions using chiral hypervalent iodine(iii): switch-over of stereochemical course of an optically active 1,3-dioxolan-2-yl cation. *Chem. Commun.* **2011**, *47* (13), 3983−3985.

(19) Kang, Y.-B.; Gade, L. H. The Nature of the Catalytically Active Species in Olefin Dioxygenation with PhI(OAc)2: Metal or Proton? *J. Am. Chem. Soc.* **2011**, *133* (10), 3658−3667.

(20) Zhong, W.; Yang, J.; Meng, X.; Li, Z. BF3·OEt2-Promoted Diastereoselective Diacetoxylation of Alkenes by PhI(OAc)2. *J. Org. Chem.* **2011**, *76* (24), 9997−10004.

(21) For a representative recent paper using heterogeneous metal-based catalysts in *syn*-dihydroxylations, see: Schoenfeldt, N. J.; Ni, Z.; Korinda, A. W.; Meyer, R. J.; Notestein, J. M. Manganese Triazacyclononane Oxidation Catalysts Grafted under Reaction Conditions on Solid Cocatalytic Supports. *J. Am. Chem. Soc.* **2011**, *133* (46), 18684−18695.

(22) Rawling, M. J.; Tomkinson, N. C. O. Metal-free syn-dioxygenation of alkenes. *Org. Biomol. Chem.* **2013**, *11* (9), 1434−1440.

(23) Colomer, I.; Barcelos, R. C.; Christensen, K. E.; Donohoe, T. J. Orthogonally Protected 1,2-Diols from Electron-Rich Alkenes Using Metal-Free Olefin syn-Dihydroxylation. *Org. Lett.* **2016**, *18* (22), 5880−5883.

(24) Haubenreisser, S.; Wöste, T. H.; Martínez, C.; Ishihara, K.; Muñiz, K. Structurally Defined Molecular Hypervalent Iodine Catalysts for Intermolecular Enantioselective Reactions. *Angew. Chem., Int. Ed.* **2016**, *55* (1), 413−417.

(25) De Vos, D. E.; de Wildeman, S.; Sels, B. F.; Grobet, P. J.; Jacobs, P. A. Selective alkene oxidation with H2O2 and a heterogenized Mn catalyst: Epoxidation and a new entry to vicinal cis-diols. *Angew. Chem., Int. Ed.* **1999**, *38* (7), 980−983.

(26) de Boer, J. W.; Brinksma, J.; Browne, W. R.; Meetsma, A.; Alsters, P. L.; Hage, R.; Feringa, B. L. cis-Dihydroxylation and Epoxidation of Alkenes by [Mn2O(RCO2)2(tmtacn)2]: Tailoring the Selectivity of a Highly H2O2-Efficient Catalyst. *J. Am. Chem. Soc.* **2005**, *127* (22), 7990−7991.

(27) Saisaha, P.; Pijper, D.; van Summeren, R. P.; Hoen, R.; Smit, C.; de Boer, J. W.; Hage, R.; Alsters, P. L.; Feringa, B. L.; Browne, W. R. Manganese catalyzed cis-dihydroxylation of electron deficient alkenes with H2O2. *Org. Biomol. Chem.* **2010**, *8* (19), 4444−4450.

(28) Enthaler, S.; Junge, K.; Beller, M. Sustainable Metal Catalysis with Iron: From Rust to a Rising Star? *Angew. Chem., Int. Ed.* **2008**, *47* (18), 3317−3321.

(29) Bauer, I.; Knölker, H.-J. Iron Catalysis in Organic Synthesis. *Chem. Rev.* **2015**, *115* (9), 3170−3387.

(30) Fürstner, A. Iron Catalysis in Organic Synthesis: A Critical Assessment of What It Takes To Make This Base Metal a Multitasking Champion. *ACS Cent. Sci.* **2016**, *2* (11), 778−789.

(31) Haddock, J. D.; Horton, J. R.; Gibson, D. T. Dihydroxylation and Dechlorination of Chlorinated Biphenyls by Purified Biphenyl 2,3-Dioxygenase from Pseudomonas sp. Strain LB400. *J. Bacteriol.* **1995**, *177* (1), 20−26.

(32) Kovaleva, E. G.; Lipscomb, J. D. Versatility of biological non-heme Fe(II) centers in oxygen activation reactions. *Nat. Chem. Biol.* **2008**, *4* (3), 186−193.

(33) Barry, S. M.; Challis, G. L. Mechanism and Catalytic Diversity of Rieske Non-Heme Iron-Dependent Oxygenases. *ACS Catal.* **2013**, *3* (10), 2362−2370.

(34) Chen, K.; Que, L., Jr. cis-Dihydroxylation of Olefins by a Non-Heme Iron Catalyst: A Functional Model for Rieske Dioxygenases. *Angew. Chem., Int. Ed.* **1999**, *38* (15), 2227−2229.

(35) Costas, M.; Tipton, A. K.; Chen, K.; Jo, D.-H.; Que, L., Jr. Modeling Rieske Dioxygenases. The First Example of Iron-Catalyzed Asymmetric *cis*-Dihydroxylation of Olefins. *J. Am. Chem. Soc.* **2001**, *123*, 6722−6723.

(36) Chen, K.; Costas, M.; Kim, J.; Tipton, A. K.; Que, L., Jr. Olefin cis-dihydroxylation versus epoxidation by non-heme iron catalysts: Two faces of an FeIII-OOH coin. *J. Am. Chem. Soc.* **2002**, *124* (12), 3026−3035.

(37) Fujita, M.; Costas, M.; Que, L., Jr. Iron Catalyzed Olefin Cis-Dihydroxylation by H2O2: Electrophilic versus Nucleophilic Mechanisms. *J. Am. Chem. Soc.* **2003**, *125* (33), 9912−9913.

(38) Bassan, A.; Blomberg, M. R. A.; Siegbahn, P. E. M.; Que, L., Jr. Two faces of a biomimetic non-heme HO-FeV=O oxidant: Olefin epoxidation versus cis-dihydroxylation. *Angew. Chem., Int. Ed.* **2005**, *44* (19), 2939−2941.

(39) Oldenburg, P. D.; Shteinman, A. A.; Que, L., Jr. Iron-Catalyzed Olefin cis-Dihydroxylation Using a Bio-Inspired N,N,O-Ligand. *J. Am. Chem. Soc.* **2005**, *127* (45), 15672−15673.

(40) Comba, P.; Rajaraman, G. Epoxidation and 1,2-Dihydroxylation of Alkenes by a Nonheme Iron Model System − DFT Supports the Mechanism Proposed by Experiment. *Inorg. Chem.* **2008**, *47* (1), 78−93.

(41) Suzuki, K.; Oldenburg, P. D.; Que, L., Jr. Iron-Catalyzed Asymmetric Olefin cis-Dihydroxylation with 97% Enantiomeric Excess. *Angew. Chem., Int. Ed.* **2008**, *47* (10), 1887−1889.

(42) Barry, S. M.; Rutledge, P. J. cis-dihydroxylation of alkenes by a non-heme iron enzyme mimic. *Synlett* **2008**, *14*, 2172−2174.

(43) Bruijnincx, P. C. A.; Buurmans, I. L. C.; Gosiewska, S.; Moelands, M. A. H.; Lutz, M.; Spek, A. L.; van Koten, G.; Gebbink, R. J. M. K. Iron(II) complexes with bio-inspired N,N,O ligands as oxidation catalysts: Olefin epoxidation and cis-dihydroxylation. *Chem. - Eur. J.* **2008**, *14* (4), 1228−1237.

(44) Oldenburg, P. D.; Feng, Y.; Pryjomska-Ray, I.; Ness, D.; Que, L., Jr. Olefin Cis-Dihydroxylation with Bio-Inspired Iron Catalysts. Evidence for an FeII/FeIV Catalytic Cycle. *J. Am. Chem. Soc.* **2010**, *132* (50), 17713−17723.

(45) Feng, Y.; England, J.; Que, L., Jr. Iron-Catalyzed Olefin Epoxidation and cis-Dihydroxylation by Tetraalkylcyclam Complexes: the Importance of cis-Labile Sites. *ACS Catal.* **2011**, *1* (9), 1035−1042.

(46) Bruijnincx, P. C. A.; Buurmans, I. L. C.; Huang, Y.; Juhasz, G.; Viciano-Chumillas, M.; Quesada, M.; Reedijk, J.; Lutz, M.; Spek, A. L.; Muenck, E.; Bominaar, E. L.; Gebbink, R. J. M. K. Mono- and Dinuclear Iron Complexes of Bis(1-methylimidazol-2-yl)ketone (bik): Structure, Magnetic Properties, and Catalytic Oxidation Studies. *Inorg. Chem.* **2011**, *50* (19), 9243−9255.

(47) Garcia-Bosch, I.; Codolà, Z.; Prat, I.; Ribas, X.; Lloret-Fillol, J.; Costas, M. Iron-catalyzed C-H hydroxylation and olefin cis-dihydroxylation using a single-electron oxidant and water as the oxygen-atom source. *Chem. - Eur. J.* **2012**, *18* (42), 13269−13273.

(48) Spannring, P.; Prat, I.; Costas, M.; Lutz, M.; Bruijnincx, P. C. A.; Weckhuysen, B. M.; Klein Gebbink, R. J. M. Fe(6-Me-PyTACN)-catalyzed, one-pot oxidative cleavage of methyl oleate and oleic acid into carboxylic acids with H2O2 and NaIO4. *Catal. Sci. Technol.* **2014**, *4* (3), 708−716.

(49) Chatterjee, S.; Paine, T. K. Olefin cis-Dihydroxylation and Aliphatic CH Bond Oxygenation by a Dioxygen-Derived Electrophilic Iron-Oxygen Oxidant. *Angew. Chem., Int. Ed.* **2015**, *54* (32), 9338−9342.

(50) Folkertsma, E.; de Waard, E. F.; Korpershoek, G.; van Schaik, A. J.; Miron, N. S.; Borrmann, M.; Nijsse, S.; Moelands, M. A. H.; Lutz, M.; Otte, M.; Moret, M. E.; Gebbink, R. Mimicry of the 2-His-1-Carboxylate Facial Triad Using Bulky N,N,O-Ligands: Non-Heme Iron Complexes Featuring a Single Facial Ligand and Easily Exchangeable Co-Ligands. *Eur. J. Inorg. Chem.* **2016**, *9*, 1319−1332.

(51) Kejriwal, A.; Biswas, S.; Biswas, A. N.; Bandyopadhyay, P. cis-Dihydroxylation of electron deficient olefins catalysed by an oxo-bridged diiron(III) complex with H2O2. *J. Mol. Catal. A: Chem.* **2016**, *413*, 77−84.

(52) Ryu, J. Y.; Kim, J.; Costas, M.; Chen, K.; Nam, W.; Que, L., Jr. High Conversion of Olefins to cis-Diols by Non-heme Iron Catalysts and H2O2. *Chem. Commun.* **2002**, *12*, 1288−1289.

(53) Chow, T. W.-S.; Wong, E. L.-M.; Guo, Z.; Liu, Y.; Huang, J.-S.; Che, C.-M. cis-Dihydroxylation of Alkenes with Oxone Catalyzed by Iron Complexes of a Macrocyclic Tetraaza Ligand and Reaction Mechanism by ESI-MS Spectrometry and DFT Calculations. *J. Am. Chem. Soc.* **2010**, *132* (38), 13229−13239.

(54) Prat, I.; Font, D.; Company, A.; Junge, K.; Ribas, X.; Beller, M.; Costas, M. Fe(PyTACN)-Catalyzedcis-Dihydroxylation of Olefins with Hydrogen Peroxide. *Adv. Synth. Catal.* **2013**, *355* (5), 947−956.

(55) Zang, C.; Liu, Y.; Xu, Z.-J.; Tse, C.-W.; Guan, X.; Wei, J.; Huang, J.-S.; Che, C.-M. Highly Enantioselective Iron-Catalyzed cis-Dihydroxylation of Alkenes with Hydrogen Peroxide Oxidant via an FeIII-OOH Reactive Intermediate. *Angew. Chem., Int. Ed.* **2016**, *55* (35), 10253−10257.

(56) Borrell, M.; Costas, M. Mechanistically Driven Development of an Iron Catalyst for Selective Syn-Dihydroxylation of Alkenes with Aqueous Hydrogen Peroxide. *J. Am. Chem. Soc.* **2017**, *139* (36), 12821−12829.

(57) Sheldon, R. A. Metrics of Green Chemistry and Sustainability: Past, Present, and Future. *ACS Sustainable Chem. Eng.* **2018**, *6* (1), 32−48.

(58) White, M. C. Adding Aliphatic C−H Bond Oxidations to Synthesis. *Science* **2012**, *335* (6070), 807.

(59) Oloo, W. N.; Que, L. Bioinspired Nonheme Iron Catalysts for C−H and C=C Bond Oxidation: Insights into the Nature of the Metal-Based Oxidants. *Acc. Chem. Res.* **2015**, *48* (9), 2612−2621.

(60) Olivo, G.; Cussó, O.; Borrell, M.; Costas, M. Oxidation of alkane and alkene moieties with biologically inspired nonheme iron catalysts and hydrogen peroxide: from free radicals to stereoselective transformations. *JBIC, J. Biol. Inorg. Chem.* **2017**, *22* (2), 425−452.

Chapter V.

Characterized *cis*-Fe^V(O)(OH) Intermediate Mimics Enzymatic Oxidations in the Gas Phase

This chapter corresponds to the following publication:

Characterized *cis*-Fe^V(O)(OH) intermediate mimics enzymatic oxidations in the gas phase

Margarida Borrell[1], Erik Andris[2], Rafael Navrátil[2], Jana Roithová[2,3] & Miquel Costas [1]

Fe^V(O)(OH) species have long been proposed to play a key role in a wide range of biomimetic and enzymatic oxidations, including as intermediates in arene dihydroxylation catalyzed by Rieske oxygenases. However, the inability to accumulate these intermediates in solution has thus far prevented their spectroscopic and chemical characterization. Thus, we use gas-phase ion spectroscopy and reactivity analysis to characterize the highly reactive [Fe^V(O)(OH)(^{5tips3}tpa)]$^{2+}$ (**3^{2+}**) complex. The results show that **3^{2+}** hydroxylates C–H bonds via a rebound mechanism involving two different ligands at the Fe center and dihydroxylates olefins and arenes. Hence, this study provides a direct evidence of Fe^V(O)(OH) species in non-heme iron catalysis. Furthermore, the reactivity of **3^{2+}** accounts for the unique behavior of Rieske oxygenases. The use of gas-phase ion characterization allows us to address issues related to highly reactive intermediates that other methods are unable to solve in the context of catalysis and enzymology.

[1] Institut de Quimica Computacional I Catalisi and Departament de Química, Universitat de Girona. Facultat de Ciències, Campus de Montilivi, 17071 Girona, Spain. [2] Department of Organic Chemistry, Faculty of Science, Charles University, Hlavova 2030/8128 43 Prague 2Czech Republic. [3] Institute for Molecules and Materials, Radboud University Nijmegen, Heyendaalseweg 135, 6525 AJ Nijmegen, The Netherlands. These authors contributed equally: Margarida Borrell, Erik Andris. Correspondence and requests for materials should be addressed to J.R. (email: j.roithova@science.ru.nl) or to M.C. (email: miquel.costas@udg.edu)

High-valent iron species are highly reactive molecules involved in numerous oxidative processes of synthetic and biological relevance[1,2]. In particular, Fe(V) intermediates have been proposed as the oxidation agents in key organic synthesis reactions, such as C–H, C=C and arene oxidations, and in energy-related transformations, including water oxidation[3]. Moreover, iron-dependent enzymes such as cytochrome P450 and Rieske oxygenases presumably use formal Fe(V) intermediates to oxidize inert substrates, including alkanes or arenes. Cytochrome P450 has been shown to use an oxoiron(IV) porphyrin cation radical intermediate termed compound I (cpd I) in C–H oxidation reactions[4], whereas Rieske oxygenases may use a non-detectable oxoiron(V) intermediate in the *syn*-dihydroxylation of arenes and in metabolic C–H oxidations, although no direct evidence has been reported thus far[5–7]. Oxoiron(V) complexes are extremely challenging targets for synthetic inorganic chemistry because of their high reactivity. Accordingly, no crystal

structure is available, and spectroscopically characterized examples remain exceedingly rare[8–13].

Inspired by iron oxygenases, chemists have intensively exploited iron coordination complexes as catalysts, also thanks to the availability of this metal[14]. Complexes with tetradentate aminopyridine ligands are particularly interesting because they can use hydrogen peroxide to catalyze enzyme-like stereoretentive C–H and C=C oxidations (Fig. 1a)[15–17]. Extensive mechanistic studies based on product analysis, isotopic labeling and computations have indirectly shown that these complexes operate via $Fe^V(O)(X)$ (X = alkyl carboxylate or OH) reactive species[18–21].

Carboxylic acids assist the heterolytic cleavage of the O–O bond (Fig. 1b), forming a reactive $Fe^V(O)(O_2CR)$ (R = alkyl) intermediate (**IIIb** in Fig. 1b) that epoxidizes olefins and hydroxylates alkanes[20,22]. Quite recently, this $Fe^V(O)(O_2CR)$ intermediate was accumulated using a robust ligand frame, enabling its spectroscopic and chemical characterization
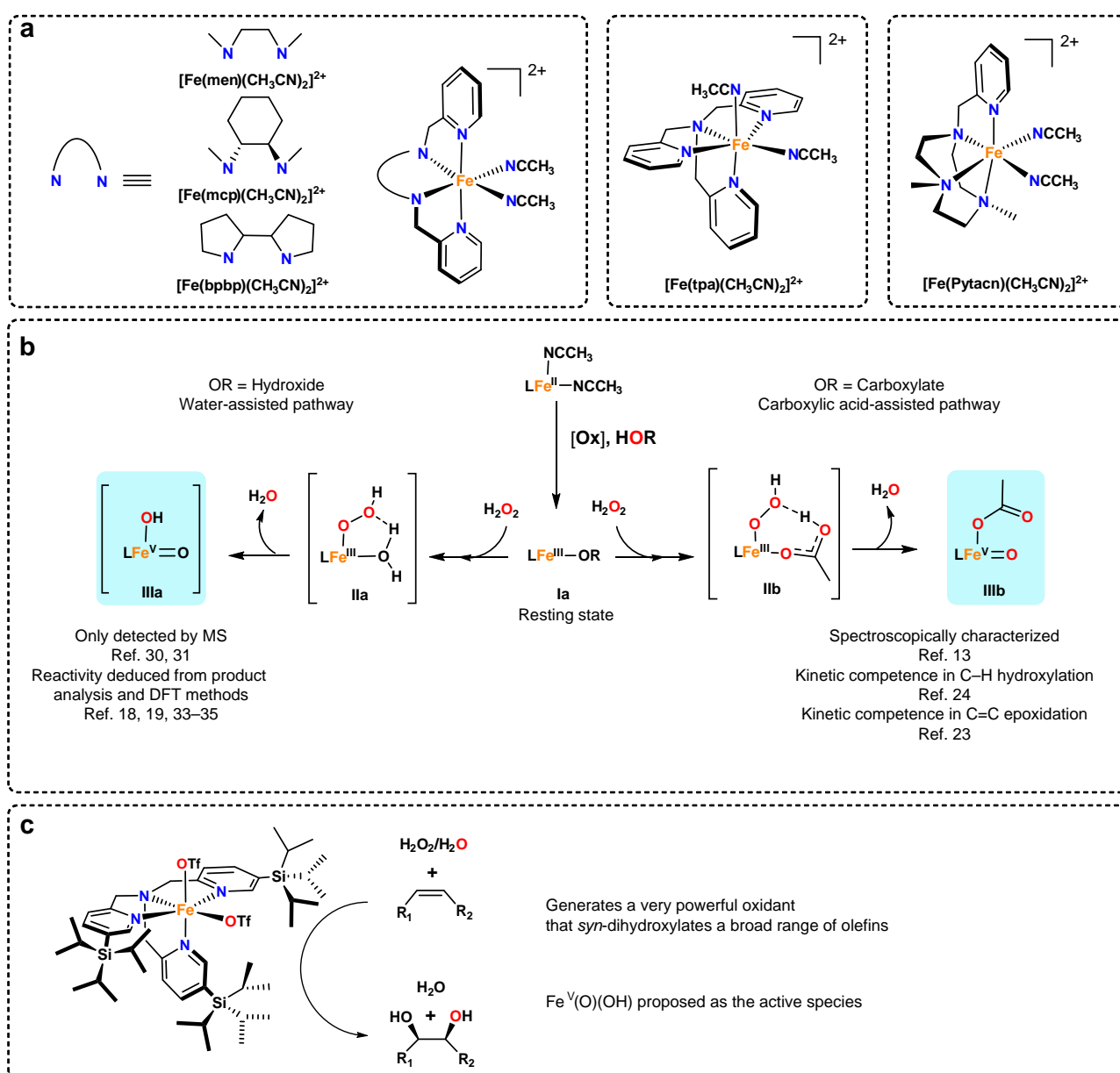
Fig. 1 Mechanistic frame of iron-catalyzed oxidations with tetradentate aminopyridine ligands. **a** Iron catalysts based on tetradentate aminopyridine ligands that catalyze stereoretentive C–H and C=C oxidations. **b** Mechanistic frame for the generation of Fe(V) species in the presence (right) or absence (left) of carboxylic acids. **c** Schematic diagram of [$Fe^{II}(CF_3SO_3)_2$(^{5tips3}tpa)] (**1**) and its catalytic oxidation activity

and, therefore, providing a solid foundation for the mechanistic proposal[13,23,24].

In the absence of carboxylic acids, O–O cleavage may be assisted by a water molecule, forming an $Fe^V(O)(OH)$ (**IIIa** in Fig. 1b) intermediate that hydroxylates alkanes and engages in the *syn*-dihydroxylations of olefins[25]. These $Fe^V(O)(OH)$ species have also been proposed to oxidize the water molecule under low pH condition[3]. Moreover, no $Fe^V(O)(OH)$ species accumulate in solution, consistently with their high reactivity.

The complex $[Fe^{II}(CF_3SO_3)_2(^{5tips3}tpa)]$, **1** (Fig. 1c, $^{5tips3}tpa = tris(5-(triisopropyl)silyl-2-methylpyridyl)amine$ is a remarkable example of a catalyst operating through $Fe^V(O)(OH)$ intermediates. It efficiently catalyzes the *syn*-dihydroxylation of various olefins with H_2O_2[26,27] and is, thus, a sustainable alternative to traditional, Os- and Ru-based *syn*-dihydroxylating agents[28,29]. In addition, this catalyst shows outstanding selectivity properties; for example, olefins are highly chemoselectively *syn*-dihydroxylated while epoxidation is largely minimized. Moreover, electron-deficient olefins, and arenes, unreactive to Os-based reagents, are instantaneously dihydroxylated, thus indicating the involvement of extraordinarily powerful oxidizing species.

Before the present study, $Fe^V(O)(OH)$ species have been detected only by mass spectrometry (MS), and their formulation was derived from experiments using isotopically labeled reagents ($H_2^{18}O$ and $H_2^{18}O_2$)[30,31]. Although their reactivity has been inferred from MS analysis of catalytic reaction mixtures, their spectroscopic characterization and direct assessment of their reactivity has not been performed yet.

Herein, we spectroscopically characterized the proposed $[Fe^V(O)(OH)(^{5tips3}tpa)]^{2+}$ reactive intermediate in the gas phase by helium tagging infrared photodissociation (IRPD) spectroscopy[32]. We conclusively identify the terminal $Fe^V=O$ and $Fe^V–OH$ stretching vibrations of the $Fe(O)(OH)$ unit. Furthermore, we confirm that $[Fe^V(O)(OH)(^{5tips3}tpa)]^{2+}$ hydroxylates C–H bonds in a rebound mechanism and performs the *syn*-dihydroxylation of alkenes and arenes. These reactions, previously described in enzymes and bioinspired oxidation catalysts, have only been previously understood based on product analysis and computational methods[5,6,19,30,33–35].

Thus, the present study reports the experimental characterization of the $Fe^V(O)(OH)$ species and demonstrates its chemical competence in bioinspired reactions, particularly in reactions relevant to Rieske oxygenases.

Results

Generation and ion-spectroscopy characterization of intermediates. The reaction of **1** (0.4 mM) with H_2O_2 (10 equiv.) in acetonitrile at −40 °C, monitored by ultraviolet-visible (UV–vis) spectroscopy, produces a metastable purple species **2** ($\lambda_{max} = 544$ nm, $\varepsilon = 1300$ M^{-1} cm^{-1}) (Fig. 2 and Supplementary Fig. 2). After **2** was formed in acetonitrile solution, the reaction mixture was analyzed by electrospray ionization mass spectrometry (ESI-

MS). Two peaks at $m/z = 444$ and 424 stand out in the ESI-MS spectrum (Supplementary Fig. 1). The former corresponds to the expected dicationic species $[Fe^{III}(OOH)(CH_3CN)(^{5tips3}tpa)]^{2+}$ (**2**[2+])[25], whereas the latter can be tentatively formulated as either $[Fe^{III}(OOH)(^{5tips3}tpa)]^{2+}$ (**2a**[2+]) or $[Fe(O)(OH)(^{5tips3}tpa)]^{2+}$ (**3**[2+]), wherein the O–O bond has been broken. Using helium-tagging IRPD spectroscopy[32] we were able to measure IR spectra of the mass-selected ions with m/z 424 generated by electrospray ionization from the solution of **2** and ascertain that these indeed correspond to $[Fe^V(O)(OH)(^{5tips3}tpa)]^{2+}$ (**3**[2+]).

We measured the IRPD spectrum of the ions (corresponding to the iron(V) intermediate **3**[2+]) generated from the reaction mixture of **1** and $H_2^{16}O_2$. The spectrum was assigned by comparison with the spectra of isotopically labeled ions resulting from the oxidation of **1** with $H_2^{18}O_2$, $H_2^{16}O^{18}O$, and $D_2^{16}O_2$ (the mass-selected complexes contained the ^{56}Fe isotope if not mentioned otherwise, Fig. 3). We also analyzed the spectrum of naturally occurring ^{54}Fe-labeled ions (**3**[2+](^{54}Fe), Supplementary Fig. 3). The IRPD spectrum of $[Fe^V(^{16}O,^{16}OH)(^{5tips3}tpa)]^{2+}$ (**3**[2+], m/z 424) (Fig. 3a, black) shows bands at 827 cm^{-1} and 638 cm^{-1} that shift to 797 cm^{-1} and 616 cm^{-1}, respectively, upon double ^{18}O labeling $[Fe^V(^{18}O,^{18}OH)(^{5tips3}tpa)]^{2+}$, (**3**[2+]($^{18}O^{18}O$), m/z 426, Fig. 3a). These bands can be interpreted as either Fe=O and Fe–OH stretching vibrations[9,13,36,37] or as O–O stretching and O–O–H bending vibrations (see the comparison with the theoretically predicted IR spectra in Fig. 3c)[38]. The frequencies of the characteristic n(Fe–O) and n(O–O) bands of $[Fe^{III}(OOH)(tpa)(S)]^{2+}$ (S = solvent) have been determined by resonance Raman to be 626 cm^{-1} and 789 cm^{-1}[38], respectively, which may be considered in reasonable agreement with those observed for **3**. To differentiate {Fe(O)(OH)} and {Fe(OOH)} binding motifs, we measured the IRPD spectrum of singly ^{18}O labeled ions $[Fe^V(^{16/18}O,^{18/16}OH)(^{5tips3}tpa)]^{2+}$ (**3**[2+]($^{16}O^{18}O$), m/z 425). If the 827 cm^{-1} band would correspond to the O–O stretching mode, the band should redshift (the bond would be always labeled by ^{18}O). Conversely, if the band would correspond to the Fe=O stretch, only half the band should disappear (the Fe=O bond is ^{18}O labeled in only 50% ions). Indeed, the second variant is observed in the experiment (Fig. 3b). This result allows us to assign the IRPD spectra to the $[Fe^V(O)(OH)(^{5tips3}tpa)]^{2+}$ intermediates. Fully consistent with this interpretation, the vibrational spectrum of **3**[2+](^{54}Fe) ($m/z = 423$) shows that both bands are blueshifted by 3 cm^{-1}, as expected for spectral shifts of Fe–O bonds (Supplementary Fig. 3). Interestingly, Hooke's Law analysis of a Fe–O oscillator predicts shifts of 3 cm^{-1} for both vibrations

The vibrational features of **3**[2+] agree well with the DFT spectra of the $[Fe^V(O)(OH)(^{5tips3}tpa)]^{2+}$ complex with the S = 3/2 ground state as predicted at the B3LYP-D3/def2TZVP level (^{4}**3**[2+], Fig. 3c, e). In addition to reproducing the experimentally determined energy and isotopic shifts of Fe=O and Fe–OH stretching vibrations, the computations predict a distinctive δ-OH
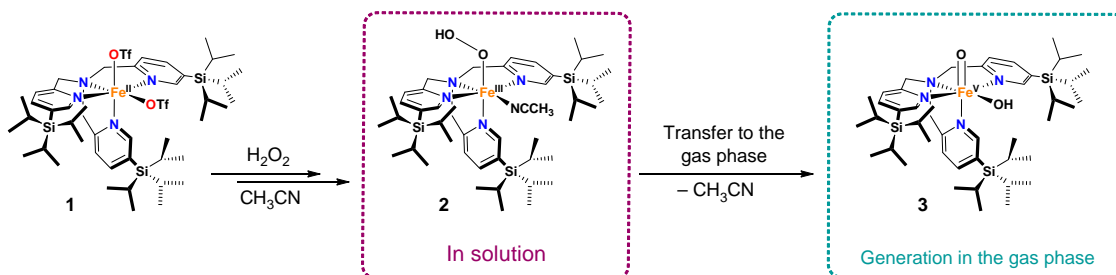
Fig. 2 Generation of the iron(V) intermediate **3**. Schematic diagram of the formation of ferric hydroperoxide species **2** in solution and subsequent transfer of this species to the gas phase where the Fe^V species **3** is generated
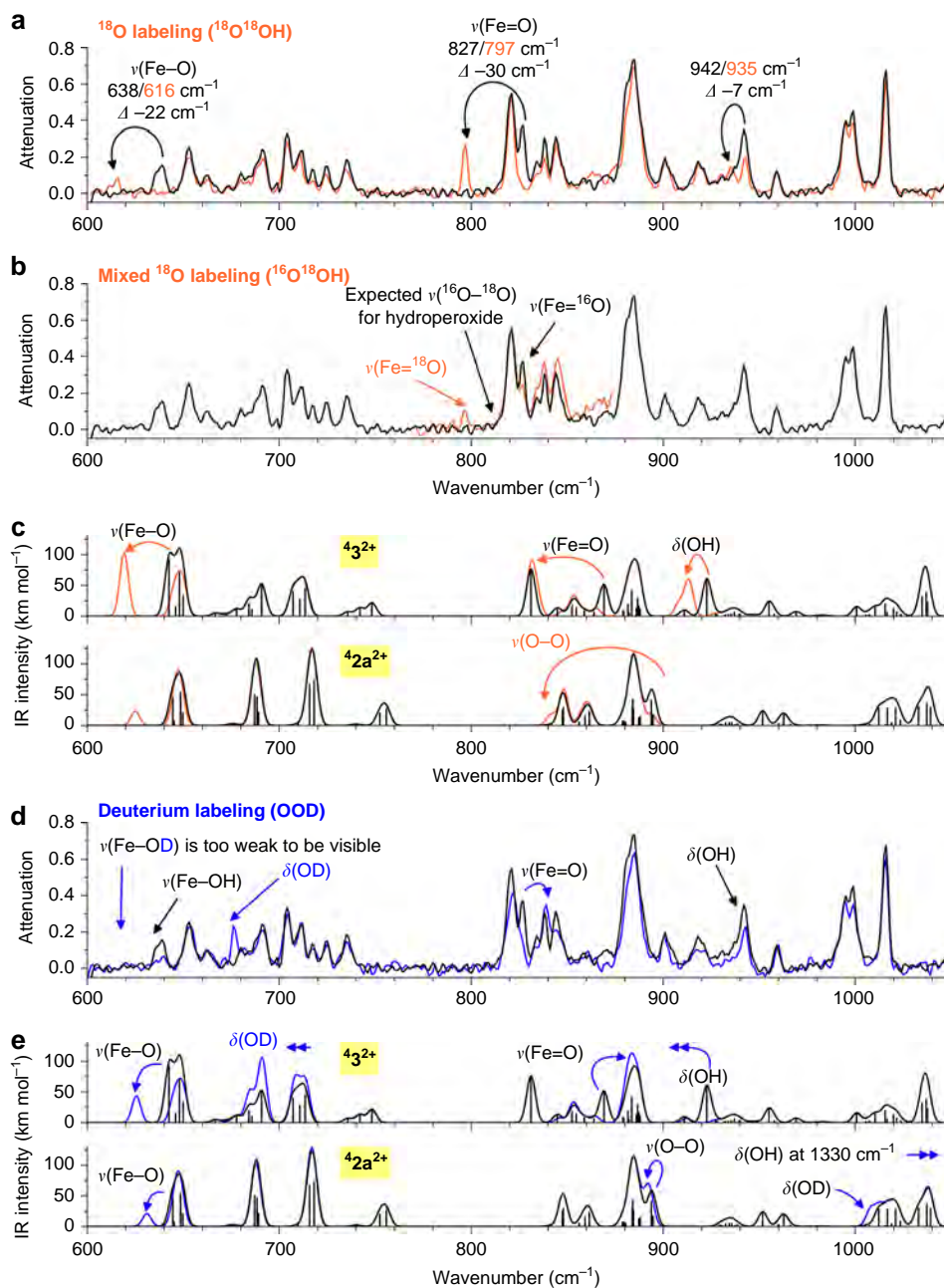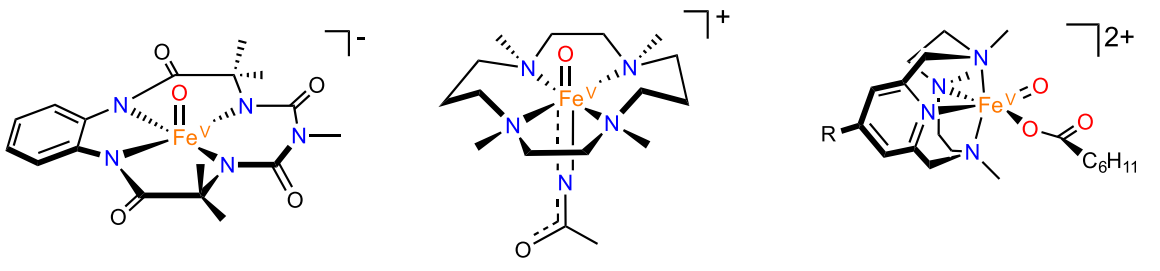
Fig. 3 IRPD spectrum of the ions generated from the reaction mixture of **1** with H_2O_2 and their prediction. **a** IRPD spectra of 3^{2+} (black trace) and $3^{2+}(^{18}O^{18}O)$ (orange trace). **b** IRPD spectra of 3^{2+} and $3^{2+}(^{18}O^{16}O)$. **c** B3LYP-D3/def2TZVP predictions of the IR spectra for the 3^{2+} and $2a^{2+}$ complexes. **d** IRPD spectra of 3^{2+} and $3^{2+}(^2H)$. **e** B3LYP-D3/def2TZVP predictions of the IR spectra of 3^{2+} and $2a^{2+}$ complexes

vibration, sensitive to deuteration, and a blueshift of the Fe=O stretch in $3^{2+}(^2H)$. The blueshift of the Fe=O stretch in $3^{2+}(^2H)$ (Fig. 3d) is caused by coupling between the $v(Fe=O)$ and $\delta(OH)$ vibrations; this coupling is also evident when we calculate the IR spectrum of 3^{2+} labeled only at the Fe=O oxygen, wherein the $\delta(OH)$ vibration redshifts (Supplementary Fig. 4e). We also considered the doublet state, but the calculations predict that this state is 12.3 kcal mol⁻¹ higher in energy than the quartet state. Its predicted IR spectrum is quite similar to that of the quartet state complex, except for a higher frequency of the Fe=O stretching vibration (Supplementary Fig. 4b).

The computed spectroscopic features of the $[Fe^{III}(OO(H/D)(^{5tips3}tpa)]^{2+}$ species were also considered. Interestingly, the computed O–O stretching frequency is basically insensitive to

deuteration of the hydroperoxide ligand, in line with the resonance Raman analysis of $[Fe^{III}(OO(H/D)(N4Py)]^{2+}$ [39], (N4Py = (1,1-di(pyridin-2-yl)-N,N-bis(pyridin-2-ylmethyl) methanamine)) and in sharp contrast with the shift of $[Fe^V(O)(OD)(^{5tips3}tpa)]^{2+}$. In conclusion, the vibrational spectra provide compelling evidence that 3^{2+} must be formulated as $[Fe^V(O)(OH)(^{5tips3}tpa)]^{2+}$, wherein the iron center is in the quartet state. This formulation actually reproduces the structure and spin ground state predicted by Siegbahn and Que for the parent $[Fe^V(O)(OH)(tpa)]^{2+}$, based on DFT calculations [40].

The isotopic composition of 3^{2+} shows that both oxygen atoms originate from a single H_2O_2 molecule, thus indicating that its formation is not assisted by a water molecule (Fig. 1b). In contrast, isotopic analyzes of diol products formed in catalytic

Table 1 Structural and spectroscopic features of previously described Fe^V(O) complexes

[(bTAML)Fe^V (O)]$^-$ [(TMC)Fe^V (O)(NC(O)CH$_3$)]$^+$ [(R-PyNMe$_3$)Fe^V (O)(O$_2$CC$_6$H$_{11}$)]$^{2+}$

Complex	S	Fe–O (Å)	Fe=O ν (cm^{-1})	Ref.
[Fe(O)(bTAML)]$^-$	1/2	1.64^a	862	37
[Fe(O)(TMC)(NC(O)CH$_3$)]$^+$	1/2	(1.65–1.70)^b	798	9, 41
[(R-PyNMe$_3$)Fe(O)(O$_2$CR)]$^{2+}$	1/2	(1.63^a−1.66)^b	815	13
3^{2+}	3/2^b	(1.63–1.64)^b	827	This work

^{a}From EXAFS
^{b}Computed

olefin oxidation reactions conducted in acetonitrile show that **3^{2+}** is formed in solution with the assistance of a water molecule, that is, **3^{2+}** contains one oxygen atom from H$_2$O$_2$ and another from water[26]. Therefore, **3^{2+}** must be formed by different mechanisms in solution and in gas phase. DFT calculations suggest that **3^{2+}** is more than 6 kcal mol^{-1} lower in energy than **2a^{2+}** in the gas phase (see Supplementary Table 1). Therefore, elimination of acetonitrile from **2^{2+}** in the gas phase may likely lead directly to the rearranged product **3^{2+}**.

The electronic spectrum of **3^{2+}** could be also determined by photodissociation spectroscopy (Supplementary Fig. 5). The spectrum is characterized by two absorption bands at 440 nm and 530 nm, corresponding to a charge transfer transition, which is also well reproduced by TD-DFT calculations of **^{4}3^{2+}**.

The complex **^{4}3^{2+}** is one of the few spectroscopically characterized Fe^V=O complexes thus far (Table 1) and the first example of an Fe^V(O)(OH) species. These species are frequently postulated as catalytic intermediates in iron-catalyzed biomimetic oxidations[16] and in the catalytic cycle of Rieske oxygenases[6]. In addition, **3^{2+}** is also the single experimentally characterized example of an Fe(V) complex with a postulated S = 3/2 spin state. The energy of the Fe=O stretch in the doublet state complexes range from 798 cm^{-1} to 862 cm^{-1} [8,13]; thus, the energy of the Fe–O bond of **^{4}3^{2+}** falls within the same range. Moreover, Fe^{IV}=O complexes show Fe–O vibrations from 798 cm^{-1} to 850 cm^{-1} [2]. This suggests that the strength of the Fe=O bond is unaffected by electron removal from Fe^{IV}=O presumably because the electron is removed from non-bonding orbitals, with respect to the Fe=O bond (electronic configuration of S = 1 Fe^{IV}=O: d$_{xy}^2$ d$_{xz}^1$ d$_{yz}^1$; of S = 3/2 Fe^V=O: d$_{xy}^1$ d$_{xz}^1$ d$_{yz}^1$; Fe=O bond is along z-axis). Interestingly, the related iron(V) complex with oxo and acyloxo ligands had the doublet ground state (Table 1)[13]. According to our calculations, replacing of OH by CH$_3$COO in **3^{2+}** would result in the spin change of the ground state to S = ½. This change is also associated with an energetic preference for the closed {LFe^{III}(OOCOCH$_3$)} form over the open, high valent {LFe^V(O)(OCOCH$_3$)} in the gas phase (see in the Supplementary Discussion and Supplementary Fig. 8)[42].

Reactivity studies. After establishing the structure of the iron(V) intermediate, we probed its reactivity with a series of substrates in collisional experiments in the gas phase[43,44]. We studied reactions of mass-selected ions where each ion interacted with only one molecule of a given reactant R. The detected ionic products are thus formed from a well-defined reactant complex [**^{4}3^{2+}**·R] without involvement of any additional molecules such as water or another reactant molecule. The reactions of **^{4}3^{2+}** proceed efficiently, attesting its high reactivity. Remarkably, when the ion corresponding to [Fe^{III}(OOH)(CH$_3$CN)(^{5tips3}tpa)]$^{2+}$ (**2^{2+}**, m/z = 444.3) was tested in similar experiments, no reactivity was observed (Supplementary Fig. 7). This lack of reactivity of the hydroperoxide species against organic molecules reproduces well the rather sluggish oxidant character of these species in solution[25,45].

The reaction of **^{4}3^{2+}**(^{2}H) with cyclohexene (Fig. 4a) yields two products. The dominant product (m/z 465.3, 84%), an adduct between cyclohexene and **^{4}3^{2+}**(^{2}H), corresponds to a dihydroxylation reaction (Supplementary Table 2). The second ion product (m/z = 416.3, 16%) results from the oxygen transfer from **^{4}3^{2+}**(^{2}H) to olefin, most likely in an epoxidation reaction. Thus, these findings are in line with experimental results under catalytic oxidation conditions, thus showing that **1** catalyzes olefin oxidation, largely favoring syn-dihydroxylation over epoxidation reactions[26].

The reaction of **^{4}3^{2+}** with 1,3-cyclohexadiene also dominantly leads to the adduct resulting from the dihydroxylation of an olefinic site alongside with the oxygen transfer reaction (Supplementary Table 2). The addition reaction is accompanied in approximately 10% by subsequent water elimination probably driven by restoring the conjugated double bond system.

We rationalized the reaction pathways based on experiments with deuterated complex ([Fe^V(O)(OD)(^{5tips3}tpa)]$^{2+}$ (**^{4}3^{2+}** (^{2}H), Fig. 4b). The deuterium atom allows us to follow the subsequent fragmentation pathways. The initially formed adduct complex (the dihydroxylation product) is long-lived and therefore allows for hydrogen scrambling (complex is isolated in the gas phase and does not interact with any other molecules/ions)[46,47]. Note that this complex is isolated in the gas phase, therefore contains the

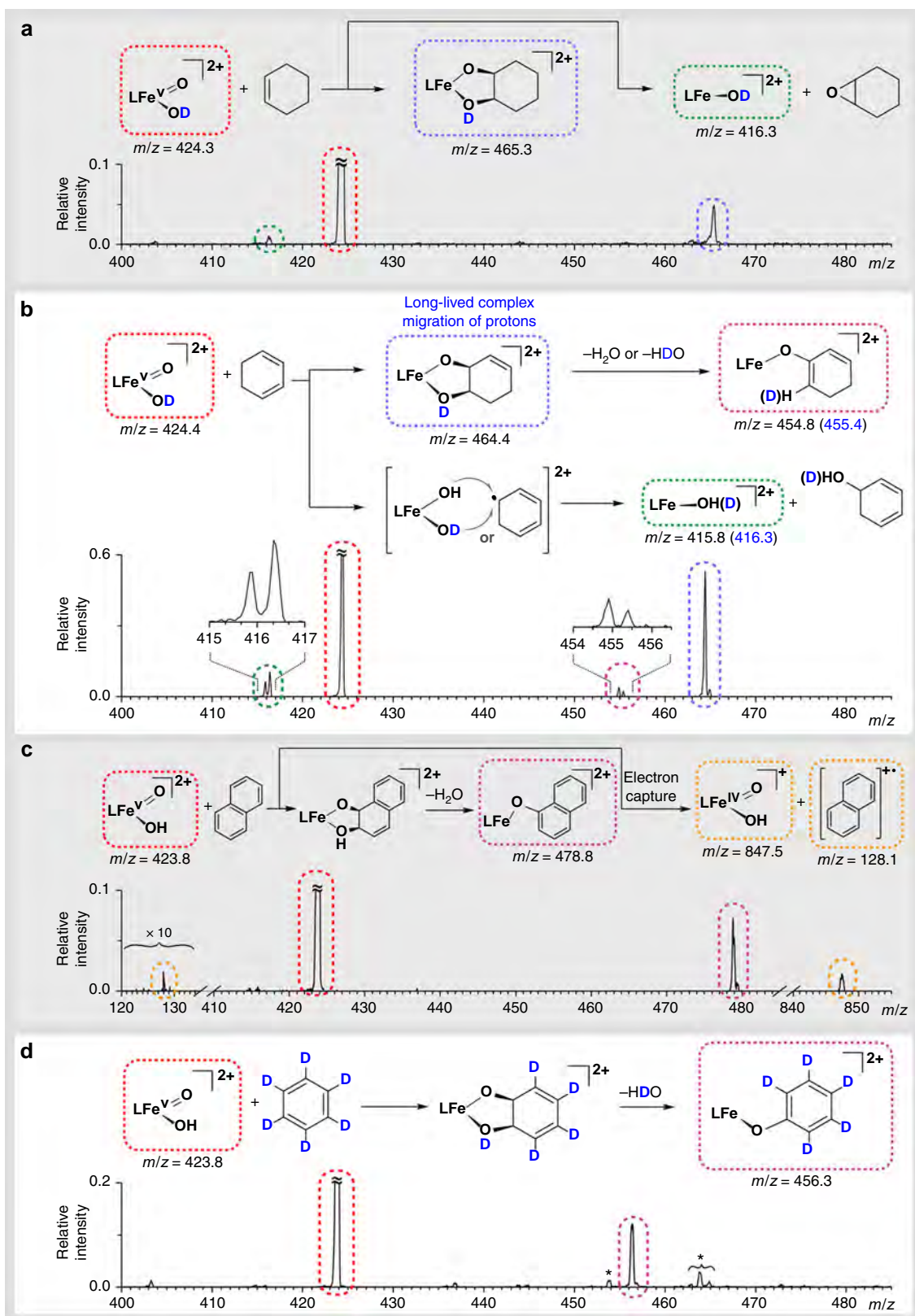**Fig. 4** Ion-molecule reactivity of **3²⁺** and **3²⁺(²H)** in the gas phase. **a** 0.1 mTorr of cyclohexene, **b** 0.1 mTorr of 1,3-cyclohexadiene, **c** < 0.1 mTorr of naphthalene, and **d** 0.2 mTorr benzene (asterisks indicate impurities from previous measurements). All reactions were measured at nominally zero-collision energy determined from the retarding potential analysis

energy released by the exothermic interaction between the reactants and cannot dissipate this energy by interaction with other molecules. The subsequent dehydration of the adduct thus features as elimination of HDO or H_2O in the 3:2 ratio.

Most interestingly, in the formal oxygen transfer reaction, $\mathbf{4}\mathbf{3}^{2+}(^2H)$ yielded not only the expected product ([$Fe^{III}(OD)$ ($^{5tips3}tpa$)]$^{2+}$, $m/z = 416.3$), but also a product in which the OD group was replaced by OH (i.e. [$Fe^{III}(OH)(^{5tips3}tpa)$]$^{2+}$, $m/z = 415.8$). This observation can be explained by a two-step rebound mechanism. In the first step, hydrogen atom abstraction generates [$Fe^{IV}(OD)(OH)(^{5tips3}tpa)$]$^{2+}$ and a short-lived carbon-centered radical. The radical can be then rebound with either OH or OD from the Fe(OH)(OD) unit, to finally form the corresponding alcohol. The observation of rebound mechanism contrasts with the previously-reported reactivity of iron(IV)-oxo complexes in the gas phase, where the observed oxygen transfer is exclusively due to the epoxidation of C=C double bonds[36]. The opening of the C–H activation pathway in the reaction with 1,3-cyclohexadiene increases the overall abundance of the formal oxygen atom transfer channel over cyclohexene (see Supplementary Table 2). This path occurs in the reaction with 1,3-cyclohexadiene but not with cyclohexene because the latter has a stronger C–H bond ($BDE_{C-H} = 74.3$ vs 87.0 kcal mol^{-1})[48]. Exactly the same product pattern, identified in all previous reaction channels, was also observed in the reaction of $\mathbf{4}\mathbf{3}^{2+}(^2H)$ with 1,4-cyclohexadiene (Supplementary Fig. 6).

Lastly, we investigated reactions of $\mathbf{4}\mathbf{3}^{2+}$ with aromatic compounds. Reactions with benzene and naphthalene yield addition products followed by water elimination. Furthermore, only in the case of naphthalene, we also observed a single electron transfer reaction, yielding the naphthalene radical cation and a product of single-electron reduced $\mathbf{4}\mathbf{3}^{2+}$[49,50]. Because gas phase reactions only occur when they are exothermic, the electron affinity of $\mathbf{4}\mathbf{3}^{2+}$ must be higher than ionization energy of naphthalene (8.14 eV.)[51]. In turn, this value is higher than the electron affinities of oxoiron(IV) porphyrin cation radicals (cpdI models), which are always lower than 7.5 eV, thus indicating that $\mathbf{4}\mathbf{3}^{2+}$ is a stronger one-electron oxidant than oxoiron(IV) porphyrin cation radicals[50,52]. The addition/water elimination reaction is similar to reactions with cyclohexadiene reactants, but the reaction fully shifts towards final water elimination. The final product regains aromaticity, thereby likely driving the dehydration step kinetically and thermodynamically. This is particularly relevant in the gas phase because the initially formed *syn*-dihydroxylated product cannot be stabilized by interaction with solvent molecules. On the contrary, we observed the catalytic *syn*-dihydroxylation of naphthalene by complex **1** and H_2O_2 in solution (see supporting information) as also previously observed in reactions with the [$Fe(CH_3CN)_2(tpa)$]$^{2+}$ complex[53]. We also probed the reaction of $\mathbf{3}^{2+}$ with D_6-benzene, and we observed addition followed by HDO elimination with almost 100% selectivity (Fig. 4d). This reaction is highly interesting because these substrates are inert against high-valent Ru and Os oxides and, therefore, show the uniquely powerful oxidation ability of $\mathbf{4}\mathbf{3}^{2+}$.

Discussion

The current study describes the vibrational and electronic spectroscopic characterization of $Fe^V(O)(OH)$ species with a key role in biomimetic oxidations. These $Fe^V(O)(OH)$ species have long been proposed to be ultimately responsible for a wide array of oxidations, including enzymatic reactions. However, the inability to accumulate them in solution has thus far prevented their spectroscopic and chemical characterization. Herein, we used gas phase ion spectroscopy methods to address this problem. The electronic and vibrational spectra of these species were finally determined, providing experimental data to unambiguously determine its atomic and electronic structure. Gas-phase reactivity analysis of these well-defined species showed their competence in C–H hydroxylation and *syn*-dihydroxylation of olefins and arenes. Overall, the data highlights that the particular architecture of the $Fe^V(O)(OH)$ species, featuring two reactive ligands in *cis*-relative positions, translates into singular reactivity properties, unattainable with hemes. For example, high-valent heme iron-oxo complexes consistently epoxidize olefins[4]. However, the current study shows that $Fe^V(O)(OH)$ species readily engage in *syn*-dihydroxylation rather than in epoxidation reactions and, most remarkably, react with arenes. Furthermore, gas phase studies on the hydroxylation of C–H bonds provide direct experimental evidence of a stepwise rebound mechanism, wherein rebound can occur with two different ligands at the Fe center. This behavior differs from that observed in reactions with previously described synthetic $Fe^{IV}=O$ complexes, which engage in HAT followed by diffusion of the carbon-centered radical[36,54,55]. Furthermore, this study provides experimental evidence of the rebound of the carbon-centered radical with the two *cis*-labile ligands at the iron center, which is not possible for hemes because HAT and rebound can only occur at the same oxygen atom[4]. Conversely, in non-heme iron-dependent enzymes and model complexes[56], the presence of labile sites adjacent to the Fe=O moiety enables the transfer of the incipient hydroxyl ligand, or of ligands adjacent to the ferryl. For example, halides, azides and nitrates are transferred in non-heme halogenases[57,58].

Finally, the report shows that gas-phase ion characterization can address questions relevant to catalysis and enzymology, related to highly reactive intermediates, currently unanswerable by other methods.

Methods

Generation of intermediate 2. Initially, 15 µL of a 0.22 M H_2O_2 solution in acetonitrile (diluted from 30% in aqueous solution) were directly added over a 2 mL acetonitrile solution of catalyst **1** (0.2 mM). The resulting mixture was cooled to −40 °C with a CH_3CN/N_2 (l) bath. At this point, the characteristic purple color of **2** was observed. The solution was kept at −33 °C during the measurements in a two-stage Peltier cooler device.

Gas phase reactivity. Mass-spectrometric measurements were performed in a TSQ 7000 quadrupole–octopole–quadrupole spectrometer[43,44]. The ions were transferred to the gas phase using an ESI ion source. Ionization conditions were typically: 6 kV spray voltage, 0 V capillary voltage, 90 V tube lens voltage, 150 °C capillary temperature, 30 psi sheath gas pressure, 300 l h^{-1} auxiliary gas flow. The spray voltage was connected directly to the solution in the vial with a stainless steel wire. The solution was kept at −33 °C and was pumped into the ESI source through a 30-cm-long fused-silica capillary with a 100-µm internal diameter by ~1 psi overpressure of nitrogen gas in the vial with the solution. The ions of interest were mass-selected by the first quadrupole and transferred to the octopole equipped with a collision cell; collision gas pressure was determined using a baratron. The collision energy was set to nominally zero, as determined by retarding potential analysis. The products were extracted from the octopole to the second quadrupole, mass-analyzed and detected with a Daly-type detector.

Helium-tagging infrared/visible photodissociation (IRPD/visPD) spectroscopy. IRPD/visPD spectra were measured with the ISORI instrument based on the TSQ 7000 platform[32,59,60]. The ions were generated and mass selected exactly as above. The mass-selected ions were transferred via a quadrupole bender and octopole to a cryogenic ion trap operating at 3 K. The ions were trapped with 250 µs helium pulse and formed weakly bound complexes with helium. The trapped ions were irradiated by IR light from an OPO/OPA system or by visible light from a continuum laser wavelength-filtered by acusto-optic tunable filter. After irradiation, all ions were ejected from the trap, mass-analyzed in a second quadrupole and counted by a Daly-type detector. IRPD spectra are plotted as wavenumber-dependent attenuation of the number of helium complexes $(1 - N_i(v)/N_{i0})$. The total number of the helium complexes (N_{i0}) was obtained in alternative cycles with blocked photon beam. The visPD spectra were corrected by dividing the attenuation by the laser power.

DFT calculations. DFT calculations were performed with Gaussian 09[61] at B3LYP-D3/def2TZVP level. All structures were fully optimized and characterized by frequency calculations. The frequencies in IR spectra were scaled by 0.99. Reported energies include zero-point vibrational energy corrections; the molecular coordinates are provided in the Supplementary Note 1 and the relative energies in Supplementary Table 3.

Data availability

The authors declare that the data supporting the findings of this study are available within the paper and its supplementary information. Further information is also available from the corresponding authors upon reasonable request.

References

1. Hohenberger, J., Ray, K. & Meyer, K. The biology and chemistry of high-valent iron–oxo and iron–nitrido complexes. *Nat. Commun.* **3**, 720 (2012).
2. McDonald, A. R. & Que, L. High-valent nonheme iron-oxo complexes: Synthesis, structure, and spectroscopy. *Coord. Chem. Rev.* **257**, 414–428 (2013).
3. Fillol, J. L. et al. Efficient water oxidation catalysts based on readily available iron coordination complexes. *Nat. Chem.* **3**, 807 (2011).
4. Huang, X. & Groves, J. T. Oxygen activation and radical transformations in heme proteins and metalloporphyrins. *Chem. Rev.* **118**, 2491–2553 (2018).
5. Chakrabarty, S., Austin, R. N., Deng, D., Groves, J. T. & Lipscomb, J. D. Radical intermediates in monooxygenase reactions of Rieske dioxygenases. *J. Am. Chem. Soc.* **129**, 3514–3515 (2007).
6. Barry, S. M. & Challis, G. L. Mechanism and catalytic diversity of Rieske non-heme iron-dependent oxygenases. *ACS Catal.* **3**, 2362–2370 (2013).
7. Perry, C., de los Santos, EmmanuelL. C., Alkhalaf, L. M. & Challis, G. L. Rieske non-heme iron-dependent oxygenases catalyse diverse reactions in natural product biosynthesis. *Nat. Prod. Rep.* **35**, 622–632 (2018).
8. de Oliveira, F. T. et al. Chemical and spectroscopic evidence for an FeV-oxo complex. *Science* **315**, 835 (2007).
9. Van Heuvelen, K. M. et al. One-electron oxidation of an oxoiron(IV) complex to form an [O=FeV=NR]+ center. *Proc. Natl Acad. Sci.USA* **109**, 11933 (2012).
10. Ghosh, M. et al. Formation of a room temperature stable FeV(O) complex: reactivity toward unactivated C–H bonds. *J. Am. Chem. Soc.* **136**, 9524–9527 (2014).
11. Mills, M. R., Weitz, A. C., Hendrich, M. P., Ryabov, A. D. & Collins, T. J. NaClO-generated iron(IV)oxo and iron(V)oxo TAMLs in pure water. *J. Am. Chem. Soc.* **138**, 13866–13869 (2016).
12. Collins, T. J. & Ryabov, A. D. Targeting of high-valent iron-TAML activators at hydrocarbons and beyond. *Chem. Rev.* **117**, 9140–9162 (2017).
13. Fan, R. et al. Spectroscopic and DFT characterization of a highly reactive nonheme FeV–oxo intermediate. *J. Am. Chem. Soc.* **140**, 3916–3928 (2018).
14. Bauer, I. & Knölker, H.-J. Iron catalysis in organic synthesis. *Chem. Rev.* **115**, 3170–3387 (2015).
15. Talsi, E. P. & Bryliakov, K. P. Chemo- and stereoselective CH oxidations and epoxidations/cis-dihydroxylations with H2O2, catalyzed by non-heme iron and manganese complexes. *Coord. Chem. Rev.* **256**, 1418–1434 (2012).
16. Olivo, G., Cussó, O., Borrell, M. & Costas, M. Oxidation of alkane and alkene moieties with biologically inspired nonheme iron catalysts and hydrogen peroxide: from free radicals to stereoselective transformations. *J. Biol. Inorg. Chem.* **22**, 425–452 (2017).
17. White, M. C. & Zhao, J. Aliphatic C–H oxidations for late-stage functionalization. *J. Am. Chem. Soc.* **140**, 13988–14009 (2018).
18. Chen, K. & Que, J. L. Stereospecific alkane hydroxylation by non-heme iron catalysts: mechanistic evidence for an FeV=O active species. *J. Am. Chem. Soc.* **123**, 6327–6337 (2001).
19. Chen, K., Costas, M., Kim, J., Tipton, A. K. & Que, L. Olefin cis-dihydroxylation versus epoxidation by non-heme iron catalysts: two faces of an FeIII–OOH coin. *J. Am. Chem. Soc.* **124**, 3026–3035 (2002).
20. Mas-Ballesté, R. & Que, L. Iron-catalyzed olefin epoxidation in the presence of acetic acid: insights into the nature of the metal-based oxidant. *J. Am. Chem. Soc.* **129**, 15964–15972 (2007).
21. Bigi, M. A., Reed, S. A. & White, M. C. Directed metal (oxo) aliphatic C–H hydroxylations: overriding substrate bias. *J. Am. Chem. Soc.* **134**, 9721–9726 (2012).
22. Lyakin, O. Y., Zima, A. M., Samsonenko, D. G., Bryliakov, K. P. & Talsi, E. P. EPR spectroscopic detection of the elusive FeV=O intermediates in selective

23. catalytic oxofunctionalizations of hydrocarbons mediated by biomimetic ferric complexes. *ACS Catal.* **5**, 2702–2707 (2015).
23. Serrano-Plana, J. et al. Exceedingly fast oxygen atom transfer to olefins via a catalytically competent nonheme iron species. *Angew. Chem. Int. Ed.* **55**, 6310–6314 (2016).
24. Serrano-Plana, J. et al. Trapping a highly reactive nonheme iron intermediate that oxygenates strong C—H bonds with stereoretention. *J. Am. Chem. Soc.* **137**, 15833–15842 (2015).
25. Oloo, W. N., Fielding, A. J. & Que, L. Rate-determining water-assisted O–O bond cleavage of an FeIII-OOH intermediate in a bio-inspired nonheme iron-catalyzed oxidation. *J. Am. Chem. Soc.* **135**, 6438–6441 (2013).
26. Borrell, M. & Costas, M. Mechanistically driven development of an iron catalyst for selective syn-dihydroxylation of alkenes with aqueous hydrogen peroxide. *J. Am. Chem. Soc.* **139**, 12821–12829 (2017).
27. Borrell, M. & Costas, M. Greening oxidation catalysis: iron catalyzed alkene syn-dihydroxylation with aqueous hydrogen peroxide in green solvents. *ACS Sustain. Chem. Eng.* **6**, 8410–8416 (2018).
28. Kolb, H. C., VanNieuwenhze, M. S. & Sharpless, K. B. Catalytic asymmetric dihydroxylation. *Chem. Rev.* **94**, 2483–2547 (1994).
29. Shing, T. K. M., Tam, E. K. W., Tai, V. W. F., Chung, I. H. F. & Jiang, Q. Ruthenium-catalyzed cis-dihydroxylation of alkenes: scope and limitations. *Chem. Eur. J.* **2**, 50–57 (1996).
30. Prat, I. et al. Observation of Fe(V)=O using variable-temperature mass spectrometry and its enzyme-like C–H and C=C oxidation reactions. *Nat. Chem.* **3**, 788–793 (2011).
31. Xu, S. et al. Detection of a transient FeV(O)(OH) species involved in olefin oxidation by a bio-inspired non-haem iron catalyst. *Chem. Commun.* **54**, 8701–8704 (2018).
32. Roithová, J., Gray, A., Andris, E., Jašík, J. & Gerlich, D. Helium tagging infrared photodissociation spectroscopy of reactive ions. *Acc. Chem. Res.* **49**, 223–230 (2016).
33. Bassan, A., Blomberg, M. R. A., Siegbahn, P. E. M. & Que, L. Two faces of a biomimetic non-heme HO-FeV=O oxidant: Olefin epoxidation versus cis-dihydroxylation. *Angew. Chem. Int. Ed.* **44**, 2939–2941 (2005).
34. Bassan, A., Blomberg, M. R. A., Siegbahn, P. E. M. & Lawrence Que, J. A density functional study on a biomimetic non-heme iron catalyst: insights into alkane hydroxylation by a formally HOFeVO oxidant. *Chem. Eur. J.* **11**, 692–705 (2005).
35. Roy, L. Theoretical insights into the nature of oxidant and mechanism in the regioselective syn-dihydroxylation of an alkene with a Rieske oxygenase inspired iron catalyst. *ChemCamChem* **10**, 3683–3688 (2018).
36. Andris, E. et al. Chasing the evasive Fe=O stretch and the spin state of the iron(IV)–Oxo complexes by photodissociation spectroscopy. *J. Am. Chem. Soc.* **139**, 2757–2765 (2017).
37. Pattanayak, S. et al. Spectroscopic and reactivity comparisons of a pair of bTAML complexes with FeV=O and FeIV=O units. *Inorg. Chem.* **56**, 6352–6361 (2017).
38. Ho, R. Y. N., Roelfes, G., Feringa, B. L. & Que, L. Raman evidence for a weakened O–O bond in mononuclear low-spin iron(III)–hydroperoxides. *J. Am. Chem. Soc.* **121**, 264–265 (1999).
39. Roelfes, G. et al. End-on and side-on peroxo derivatives of non-heme iron complexes with pentadentate ligands: models for putative intermediates in biological iron/dioxygen chemistry. *Inorg. Chem.* **42**, 2639–2653 (2003).
40. Bassan, A., Blomberg, M. R. A., Siegbahn, P. E. M. & Que, L. Jr. A density functional study of O-O bond cleavage for a biomimetic non-heme iron complex demonstrating an FeV-intermediate. *J. Am. Chem. Soc.* **124**, 11056–11063 (2002).
41. Mondal, B., Neese, F., Bill, E. & Ye, S. Electronic structure contributions of non-heme oxo-iron(V) complexes to the reactivity. *J. Am. Chem. Soc.* **140**, 9531–9544 (2018).
42. Oloo, W. N. et al. Identification of a low-spin acylperoxoiron(III) intermediate in bio-inspired non-heme iron-catalysed oxidations. *Nat. Commun.* **5**, 3046 (2014).
43. Ducháčková, L. & Roithová, J. The interaction of zinc(II) and hydroxamic acids and a metal-triggered lossen rearrangement. *Chem. Eur. J.* **15**, 13399–13405 (2009).
44. Jašíková, L. & Roithová, J. Interaction of the gold(I) cation Au(PMe3)+ with unsaturated hydrocarbons. *Organometallics* **31**, 1935–1942 (2012).
45. Park, M. J., Lee, J., Suh, Y., Kim, J. & Nam, W. Reactivities of mononuclear non-heme iron intermediates including evidence that iron(III)–hydroperoxo species is a sluggish oxidant. *J. Am. Chem. Soc.* **128**, 2630–2634 (2006).
46. Kuck, D. Half a century of scrambling in organic ions: complete, incomplete, progressive and composite atom interchange11Dedicated to Seymour Meyerson on the occasion of his 85th birthday. *Int. J. Mass. Spectrom.* **213**, 101–144 (2002).
47. Roithová, J., Ricketts, C. & Schröder, D. Reactions of the dications C7H62+ C7H72+, and C7H82+ with methane: predominance of doubly charged intermediates. *Int. J. Mass. Spectrom.* **280**, 32–37 (2009).

48. Xue, X.-S., Ji, P., Zhou, B. & Cheng, J.-P. The essential role of bond energetics in C–H activation/functionalization. *Chem. Rev.* **117**, 8622–8648 (2017).
49. Mathur, D. Multiply charged molecules. *Phys. Rep.* **225**, 193–272 (1993).
50. Sainna, M. A. et al. A comprehensive test set of epoxidation rate constants for iron(iv)–oxo porphyrin cation radical complexes. *Chem. Sci.* **6**, 1516–1529 (2015).
51. Cockett, M. C. R., Ozeki, H., Okuyama, K. & Kimura, K. Vibronic coupling in the ground cationic state of naphthalene: a laser threshold photoelectron [zero kinetic energy (ZEKE)-photoelectron] spectroscopic study. *J. Chem. Phys.* **98**, 7763–7772 (1993).
52. Chiavarino, B. et al. Probing the compound I-like reactivity of a bare high-valent oxo iron porphyrin complex: the oxidation of tertiary amines. *J. Am. Chem. Soc.* **130**, 3208–3217 (2008).
53. Feng, Y., Ke, C.-Y., Xue, G. & Que, L. Jr. Bio-inspired arene cis-dihydroxylation by a non-haem iron catalyst modeling the action of naphthalene dioxygenase. *Chem. Commun.* https://doi.org/10.1039/B817222F (2008).
54. Cho, K.-B., Hirao, H., Shaik, S. & Nam, W. To rebound or dissociate? This is the mechanistic question in C–H hydroxylation by heme and nonheme metal–oxo complexes. *Chem. Soc. Rev.* **45**, 1197–1210 (2016).
55. Andris, E., Jašík, J., Gómez, L., Costas, M. & Roithová, J. Spectroscopic characterization and reactivity of triplet and quintet iron(IV) oxo complexes in the gas phase. *Angew. Chem. Int. Ed.* **128**, 3701–3705 (2016).
56. Company, A. et al. Alkane hydroxylation by a nonheme iron catalyst that challenges the heme paradigm for oxygenase action. *J. Am. Chem. Soc.* **129**, 15766–15767 (2007).
57. Wong, S. D. et al. Elucidation of the Fe(iv)=O intermediate in the catalytic cycle of the halogenase SyrB2. *Nature* **499**, 320 (2013).
58. Matthews, M. L. et al. Direct nitration and azidation of aliphatic carbons by an iron-dependent halogenase. *Nat. Chem. Biol.* **10**, 209–215 (2014).
59. Jašík, J., Žabka, J., Roithová, J. & Gerlich, D. Infrared spectroscopy of trapped molecular dications below 4K. *Int. J. Mass. Spectrom.* **354-355**, 204–210 (2013).
60. Jašík, J., Navrátil, R., Němec, I. & Roithová, J. Infrared and visible photodissociation spectra of rhodamine ions at 3K in the gas phase. *J. Phys. Chem. A* **119**, 12648–12655 (2015).
61. Gaussian 16 Rev. A.03 (Wallingford, CT, 2016).

Author contributions

M.C. and J.R. devised the project, designed the experiments and analyzed the data. M.B. and E.A. performed the experiments and analyzed the data and contributed equally to the manuscript. These authors contributed to the writing of the manuscript. R.N. performed initial DFT calculations and assisted with the IR measurements.

Additional information

Supplementary Information accompanies this paper at https://doi.org/10.1038/s41467-019-08668-2.

Competing interests: The authors declare no competing interests.

Reprints and permission information is available online at http://npg.nature.com/reprintsandpermissions/

Journal peer review information: *Nature Communications* thanks the anonymous reviewers for their contribution to the peer review of this work. Peer reviewer reports are available.

Publisher's note: Springer Nature remains neutral with regard to jurisdictional claims in published maps and institutional affiliations.

Chapter VI.

Site-Selective and Product Chemoselective Aliphatic C-H Bond Hydroxylation of Polyhydroxylated Substrates

This chapter corresponds to the following publication:

Margarida Borrell, Sergio Gil-Caballero, Massimo Bietti, Miquel Costas. *ACS Catal.* **2020**, 10, 8, 4702-4709.

For this publication M.B. synthesized, isolated and characterized starting materials and products. Moreover, M.B performed the catalytic reactions with alkenes and analyzed the data. S.G-C. supervised the NMR experiments. M.Bietti and M.C. designed the project. Besides, M.B. contributed in writing the manuscript and was involved in argumentations and discussions.

Site-Selective and Product Chemoselective Aliphatic C−H Bond Hydroxylation of Polyhydroxylated Substrates

Margarida Borrell, Sergio Gil-Caballero, Massimo Bietti,* and Miquel Costas*

Read Online

ACCESS | Metrics & More | Article Recommendations | Supporting Information
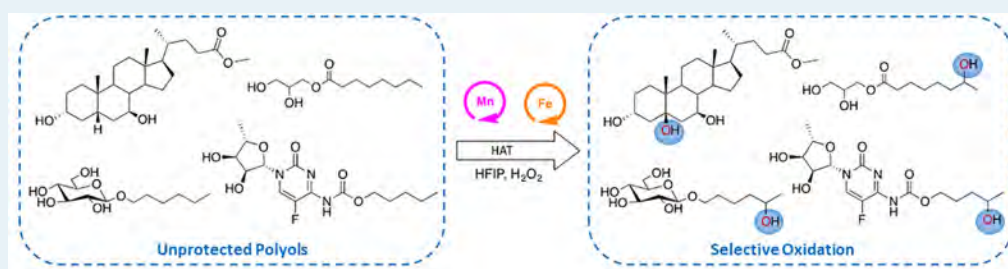
ABSTRACT: Site-selective and product chemoselective aliphatic C−H bond oxidation of 1,2-diols and of polyhydroxylated substrates using iron and manganese catalysts and hydrogen peroxide as terminal oxidant is described. The reaction capitalizes on the use of fluorinated alcohol solvents such as 2,2,2-trifluoroethanol (TFE) and 1,1,1,3,3,3-hexafluoro-2-propanol (HFIP), which exert a strong polarity reversal in the hydroxyl moieties of 1,2-diols via hydrogen bonding, in turn translating into a strong deactivation of proximal C−H bonds against a HAT initiated oxidation by the putative high-valent and electrophilic metal-oxo species. As a result, site-selective and product chemoselective oxidation of complex polyfunctional molecules such as steroids, sugars, and pharmaceuticals is described, where exclusive or predominant C−H bond hydroxylation at a remote and nonactivated site takes place. The current report discloses HAT initiated hydroxylations in fluorinated alcohol solvents as methods displaying orthogonal chemoselectivity to contemporary alcohol oxidations providing a useful tool for synthetic planning in densely functionalized molecules.

KEYWORDS: *Aliphatic hydroxylation, polarity reversal, fluorinated alcohol solvents, hydrogen atom transfer, polyols, manganese, hydrogen peroxide*

A large number of molecules of biological relevance, including natural products, feature polyhydroxylated moieties, that represent a versatile structural motif amenable to a number of important synthetic transformations. The selective oxidation of these compounds at sites that are remote from the polyhydroxylated moiety represents a synthetically important yet challenging transformation.[1] Chemoselective hydroxylation of unactivated aliphatic C−H bonds is traditionally regarded as incompatible with the presence in the substrate of C−H bonds that are activated by adjacent electron rich groups such as hydroxyl, which typically undergo preferential oxidation.[1a−e,2] Furthermore, 1,2-diols easily undergo oxidative C−C cleavage reactions, and these transformations find wide utility both in fine chemistry and in the bulk manipulation of olefin derived substrates.[3] It is therefore not surprising that selective oxidation at unactivated C−H bonds in polyhydroxylated substrates without the assistance of protecting groups constitutes a yet unmet challenging target of relevance in organic synthesis (Scheme 1).

Herein we address this problem by describing site-selective and product chemoselective oxidation of unactivated aliphatic C−H bonds in 1,2-diols and in polyhydroxylated molecules

using iron and manganese catalysts (Scheme 2B) and hydrogen peroxide as terminal oxidant. C−H hydroxylation with these catalysts entails initial hydrogen atom transfer (HAT) from a substrate C−H bond to a high valent metal-oxo species.[4] (Scheme 2A) We show that these reactions, when conducted in fluorinated alcohol solvents, display orthogonal chemoselectivity to contemporary alcohol oxidation methods.[5]

We and others have previously described that by engaging in hydrogen bonding, hydrogen bond donor (HBD) solvents such as fluorinated alcohols can strongly deactivate the electron rich C−H bonds that are α- to hydroxyl groups of simple primary and secondary aliphatic alcohols toward electrophilic HAT reagents, preventing their overoxidation to form aldehydes and ketones.[6] Based on this precedent, we

Scheme 1. Possible Oxidation Paths for Polyhydroxylated Molecules, Exemplified in 1,2-Diols
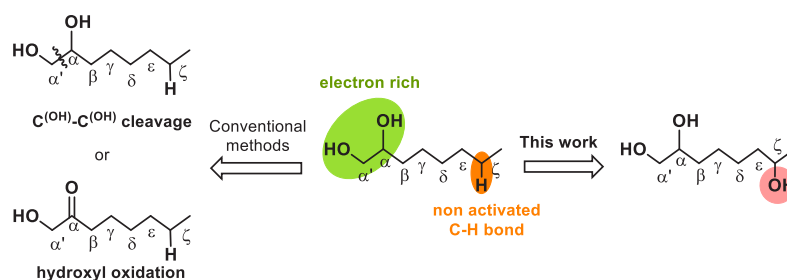
Scheme 2. (A) Proposed Mechanistic Cycle. (B) Structure of the Catalysts Used in This Work
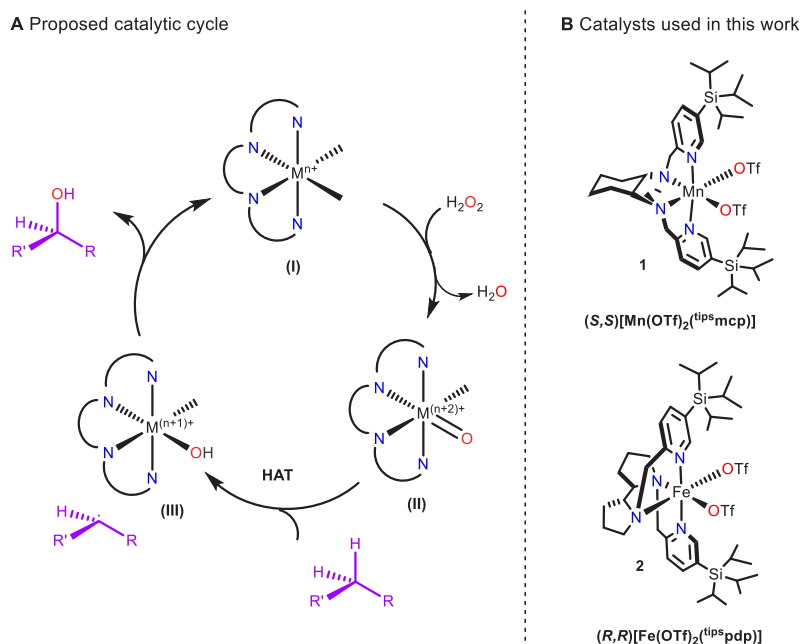
Table 1. Catalytic Oxidation of 1,2-Octanediol (S1) in Different Solvents
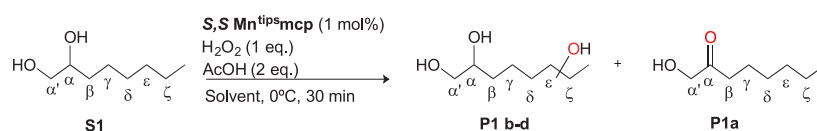
Solvent[a]	Conversion (%)	P1b−d Yield (%) (δ:ε:ζ ratio)	P1a Yield (%)
CH$_3$CN	28	0	21
TFE	52	22 (6:25:69)	5
HFIP	77	62 (5:16:79)	1
HFIP[b]	79	72 (4:18:78)	1

[a]Conversion and yields determined by GC. [b]Urea-hydrogen peroxide was used as oxidant.

considered the oxidation of 1,2-diols and unprotected polyhydroxylated molecules, which represent more challenging targets because their metal chelating ability adds to the well-established oxidation sensitivity of the C−H bonds that are α-to hydroxyl groups.[7] Furthermore, polyhydroxylated carbon skeletons are common in organic molecules of biological interest, with glycosides being a paradigmatic example. Bearing these considerations in mind, catalytic oxidation of model substrate 1,2-octanediol (S1) was first performed using MeCN, TFE, and HFIP as solvents. In a typical reaction, 1 equiv of H$_2$O$_2$ (diluted from an aqueous solution in the solvent of

choice), was added via syringe pump during 30 min at 0 °C to a solution of the substrate (1.5 mmol, 1 equiv) and catalyst ((S,S)-**Mn^{tips}mcp**, 1 mol %, Table 1).[8]

When the reaction was performed in MeCN, modest substrate conversion was observed (28%), leading to formation of 1-hydroxy-2-octanone **P1a** in 21% yield, as the only oxidation product detected. Instead, when the same reaction was performed in TFE and HFIP, significantly higher substrate conversions were observed, with the reaction chemoselectivity that drastically changed. 1,2,7-Octanetriol **P1b**, resulting from oxidation at the most remote methylene site, now represents

Scheme 3. Catalytic Oxidation of 1,2-Diol Substrates*
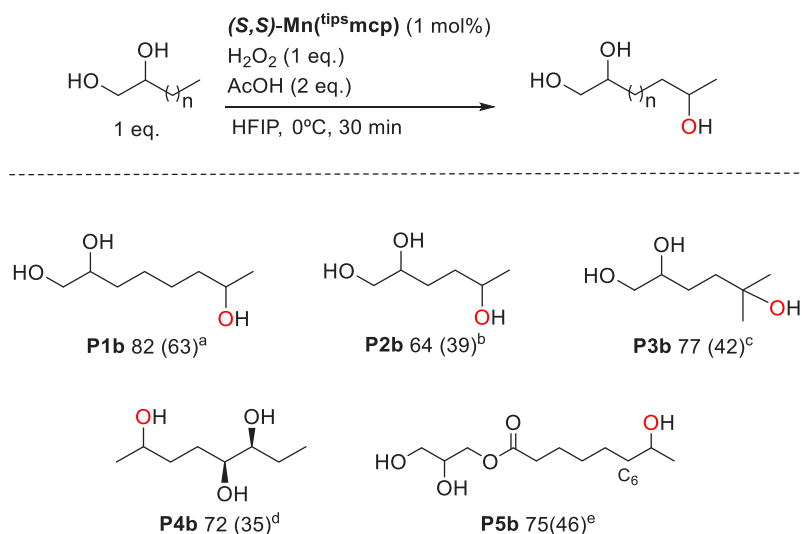
*Unless indicated, isolated yields are reported. Conversion (isolated yield %). [a]Isolated with 14% ε-hydroxylated **P1c**. [b]11% of 1-hydroxy-2-hexanone (**P2a**). [c]55% GC yield of **P3b** and 5% GC yield of 1-hydroxy-5-methyl-2-hexanone **P3a**; also in this oxidation, two hydroxyketones are identified by GC-MS analysis (~13% combined yield). [d]7% and 6% of isomeric hydroxyketones (**P4a** and **P4a'**). [e]Isolated with C-6 (**P5c**, 10%) and C-5 (**P5d**, 4%) hydroxylated products.

the largely dominant product, accompanied by smaller amounts of isomeric triols **P1c** and **P1d**, whereas hydroxyketone **P1a** is formed in only trace amounts. Remarkably, as compared to TFE, in HFIP yield and selectivity toward **P1b** increase. Use of larger amounts of peroxide (3–5 equiv) resulted in a mixture of carbonyl containing overoxidized products and a loss of mass balance in the reaction. Delivering the peroxide during 15 or 60 min does not change significantly product yields and selectivities, but an improvement in yields was observed when urea-hydrogen peroxide was employed as oxidant.[9] On the other hand, a 1:1 combination of HFIP with other solvents (AcOEt, CH3CN, and CH2Cl2) resulted in lower product yields and erosion of the chemoselectivity (see Table S3 in the SI for details). The higher conversions observed in the fluorinated alcohol solvents when compared to acetonitrile can be explained in terms of the strong HBD ability of the former solvents that hampers the metal binding ability of the 1,2-diol moiety, preventing catalyst deactivation. In addition, the stronger HBD ability of HFIP as compared to TFE[10] accounts for the higher selectivity toward hydroxylation at the most remote methylenic site. In addition, it is also possible that HFIP helps in activating the H2O2[11] and that its strong hydrogen donor ability enhances the electrophilicity of the putative high valent manganese-oxo responsible for the initial HAT.[12]

It is interesting to notice that the trends in chemoselectivity and product yields observed in the oxidation of diol **S1** are basically reproduced when 2-octanol (**S0**) was used as substrate, although the formation of significant amounts of 2-octanone (5%) and 2,5-octanediol (10%) suggests an enhanced deactivation in the case of the diol (see Table S6 in the SI for details).

The oxidation of **S1** in HFIP was further explored with a series of related iron and manganese catalysts (see Table S1 in the SI).[13] Related iron catalysts have been pioneered by White in late stage aliphatic C−H oxidation reactions.[14] While all the catalysts exhibited the same product profile, manganese

catalysts systematically delivered higher product yields than the iron counterparts in the oxidation of this substrate. (S,S)-Mn^tips^mcp[8] was chosen for further exploration of the reaction.

A series of 1,2-diol substrates containing alkyl chains and a glycerol monoester were then subjected to oxidation under the optimized conditions on a 1.5 mmol scale (Scheme 3) in order to allow isolation of products. Oxidation of 1,2-hexanediol (**S2**) gives preferentially 1,2,5-hexanetriol (**P2b**, 39% yield) resulting from hydroxylation at the most remote methylenic site, over 1-hydroxy-2-hexanone (**P2a**, 11% yield) formed by HAT initiated α-C−H bond hydroxylation. Analogously, with 5-methyl-1,2-hexanediol (**S3**), hydroxylation occurs preferentially at the remote tertiary C−H bond to give triol **P3b** in 42% yield (55% GC yield) over 1-hydroxy-5-methyl-2-hexanone **P3a** (5% GC yield).[15] With 3,4-octanediol (**S4**), oxidation occurs preferentially at the most remote δ-methylene site, delivering 2,5,6-octanetriol (**P4b**) in 35% yield, along with the two hydroxyketone products (**P4a** and **P4a'**) in a combined 13% yield. Partial oxidation of the diol moiety, while retaining intact the ethyl group, indicates that secondary aliphatic C−H bond oxidation starts to be competitive with diol oxidation only when this site is spaced by at least two methylene groups from the closest OH group. More proximal C−H bonds are deactivated toward HAT to the high valent metal-oxo species by the electron-withdrawing character of the hydrogen bonded diol moiety. Interestingly, as the length of the alkyl chain is increased, both product yield and chemoselectivity for the remote C−H hydroxylation product are improved. For example, oxidation of 1,2-octanediol (**S1**) gives 1,2,7-octanetriol (**P1b**) in 63% yield along with 1,2,6-octanetriol (**P1c**) in 14% yield, while **P1a** is formed in <1%. Analogous observations derive from the oxidation of the glycerol monoester drug monoctanoin (**S5**). Oxidation occurs selectively at the most remote methylenic position delivering the hydroxylation product at C-7 (**P5b**) in 46% yield, along with the isomeric products hydroxylated at C-6 and C-5 in 10% and 4% yield (**P5c** and **P5d**). In line with previous

Scheme 4. Catalytic Oxidation of 1,2-Cycloalkanediols*
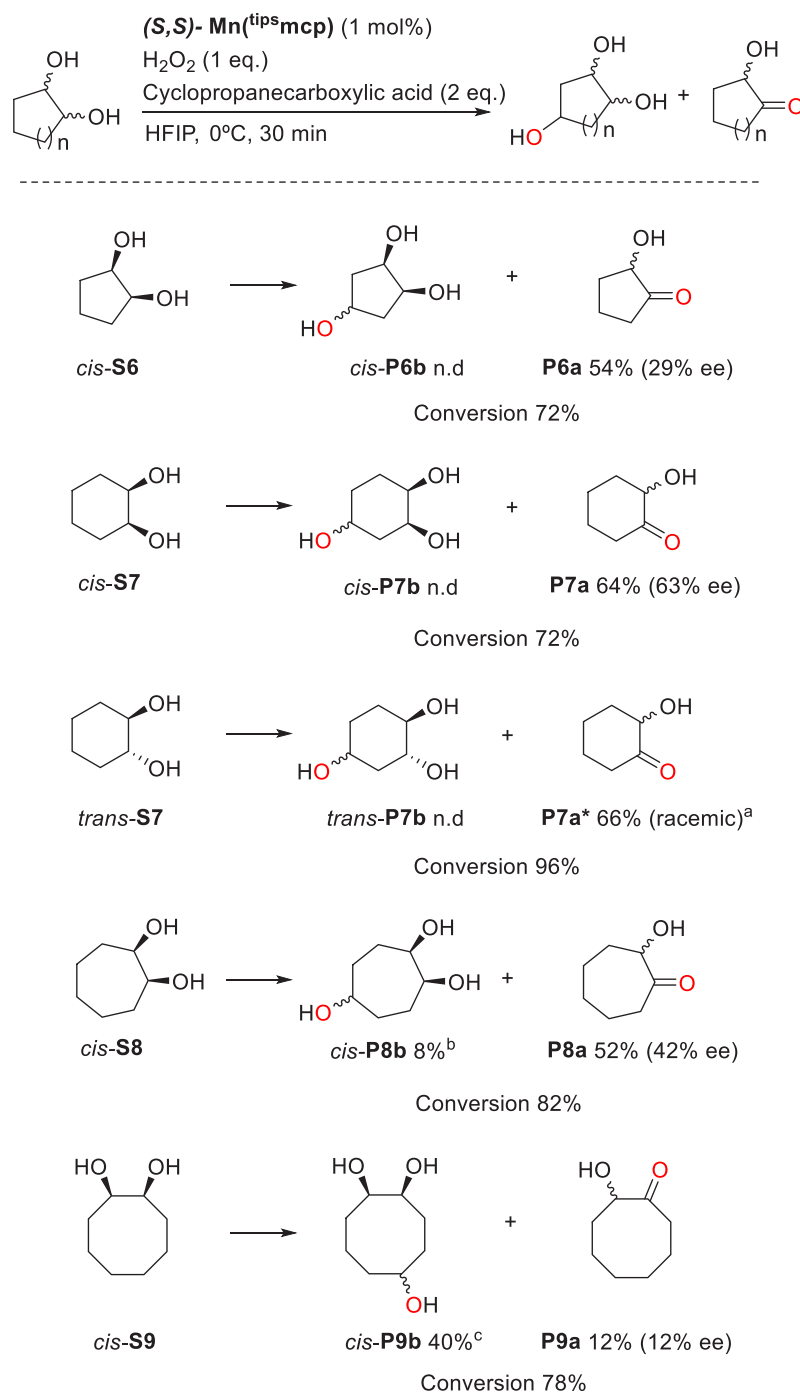
*Unless indicated, isolated yields are reported (ee%). [a]Yield determined by GC. [b]1:1 d.r. isolated with traces of 1,2,4-cycloheptanetriol. [c]1:1 d.r., isolated with 17% of 1,2,4-cyclooctanetriol triol cis-P9c (total yield 69%). n.d. stands for not detected.

observations, no products deriving from oxidation of the glycerol moiety are observed. These observations can be explained on the basis of the progressive decrease of the deactivating effect exerted by the hydrogen bonded 1,2-diol moiety on the C−H bonds of the alkyl chain as these bonds are further spaced from this strong electron withdrawing moiety.

The reaction was then explored in the oxidation of a series of cyclic 1,2-diol substrates (Scheme 4). Cyclopropanecarboxylic acid was used instead of acetic acid in order to promote enantioselectivity in the reactions.[8] Oxidation of cis-1,2-cyclopentanediol (cis-S6) and cis-1,2-cyclohexanediol (cis-S7) occurs exclusively at the diol moiety producing the corresponding hydroxyketones (P6a and P7a) in 54% and 64% yield. Oxidation of these compounds proceeds with

Scheme 5. Oxidation of Glycosides and Related Polyfunctional Molecules*
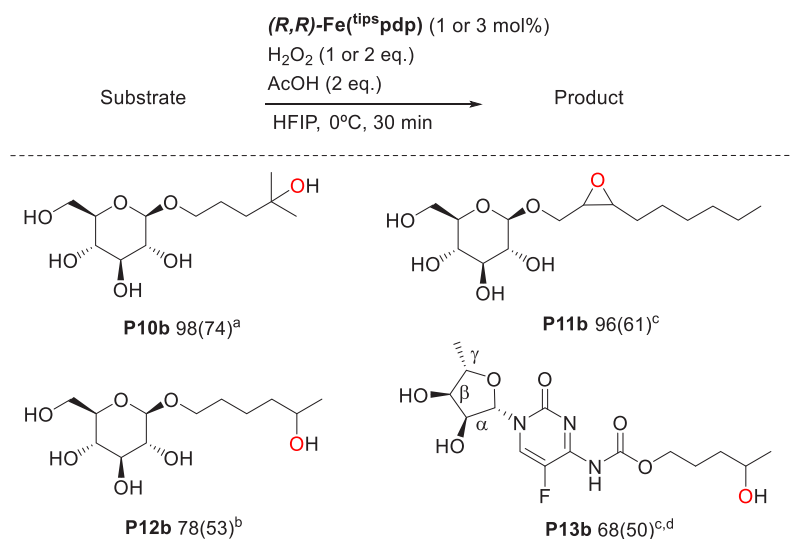
*Conversion (isolated yield %). [a]2 × (3 mol % catalyst/1 equiv. H$_2$O$_2$). [b]3 mol % catalyst/1 equiv H$_2$O$_2$. Isolated with δ-hydroxylated product **P12c** (12% yield, total yield 65%). [c]1 mol % catalyst/1 equiv H$_2$O$_2$. [d]Along with 12% of the corresponding carbonyl derivative (total yield 62%).

Scheme 6. Oxidation of Hydroxylated Steroidal Substrates
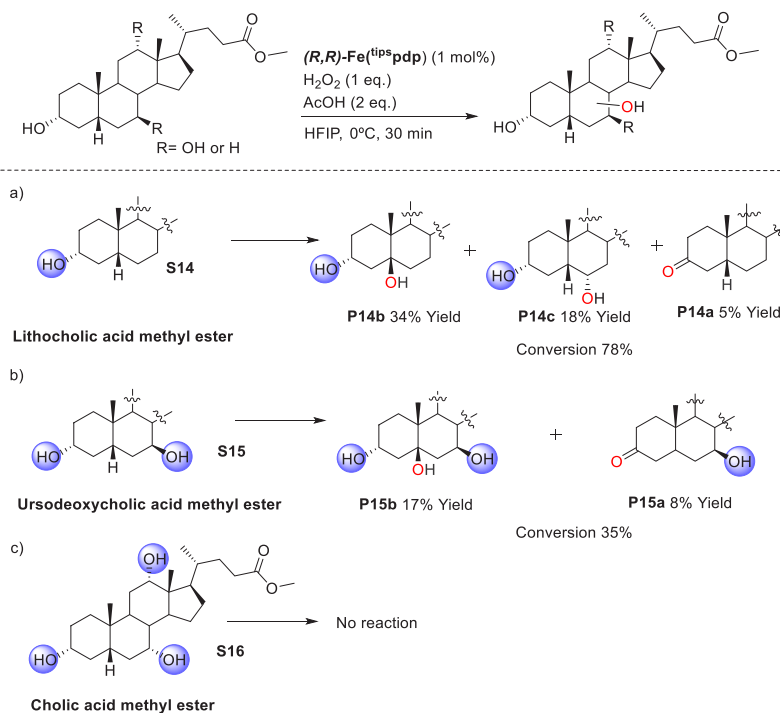
modest to good levels of enantioselectivity (29% and 63% ee for **P6a** and **P7a**, respectively).[16] Instead, oxidation of a racemic mixture of *trans*-1,2-cyclohexanol (*trans*-**S7**) produces racemic hydroxyketone **P7a** in 66% yield.

As ring size is increased, the reaction chemoselectivity is systematically changed in favor of triol products deriving from remote C−H hydroxylation. Oxidation of *cis*-1,2-cyclohepta-nediol (*cis*-**S8**) yields the corresponding hydroxyketone (**P8a**) in 52% yield (42% ee), along with 1,2,5-cycloheptanetriol *cis*-**P8b** (8%, 1:1 d.r.). Instead, oxidation of *cis*-1,2-cyclooctanediol (*cis*-**S9**) provides preferentially 1,2,5-cyclooctanetriol (*cis*-**P9b**,

40%, 1:1 dr), along with 17% of 1,2,4-cyclooctanetriol (*cis*-**P9c**), while the hydroxyketone product (**P9a**) is only obtained as a minor product (12% yield, 12% ee). Taken together, the data collected in Scheme 4 further indicate that C−H bond deactivation exerted by the hydrogen bonded 1,2-diol moiety extends effectively up to position γ, leading to chemoselective oxidation of the diol. δ-C−H bonds experience instead a weaker deactivation and undergo preferential oxidation over the diol moiety.

The chemoselectivity observed in the remote oxidation of relatively simple 1,2-diol substrates led us to consider the

application of the reaction to carbohydrates (Scheme 5). Their selective oxidation in unprotected form is a challenging issue in carbohydrate manipulation.[17] A short optimization protocol identified (R,R)-Fe^{tips}pdp[13d] as the optimum catalyst (see Table S1 and S2 in the SI). Effectively, (4-methyl)-1-pentyl β-D-glucopyranoside S10 and 1-hexyl β-D-glucopyranoside S12 undergo selective C−H hydroxylation at the exocyclic alkyl chain, without affecting the densely oxygenated glucose moiety, characterized in both cases by 9 C−H bonds that are α- to oxygen atoms. Oxidation of S10 leads to the exclusive formation of P10b deriving from hydroxylation at the remote tertiary C−H bond in 74% yield. Oxidation of S12 leads instead to the formation of product P12b, deriving from hydroxylation at the most remote methylene site (53%), accompanied by 12% of the corresponding product (P12c) deriving from hydroxylation at the next methylene site. The reaction is thus orthogonal to previously described glycoside oxidation methods, that operate on 1,2-diol moieties.[17] Furthermore, S10 and S12 are interesting targets for late stage C−H hydroxylation because they can be viewed as models for lipopolysaccharides, endotoxins of Gram-negative bacteria.[18] On the other hand, epoxidation of the C═C bond in alkenyl β-D-glucopyranoside S11 delivers the corresponding epoxide (P11b) in 61% yield, again retaining the sugar moiety.

Anticancer drug Capecitabine S13 exhibits several features which are recognized as recurrent standing problems in the metal catalyzed chemical manipulation of small molecule pharmaceuticals.[19] Capecitabine contains a highly polar, functional group rich core, composed by an a priori oxidation sensitive five membered cyclic ether bearing a tertiary C−H bond at C_γ, and a 1,2-syn-diol moiety at C_β and C_α. This ether is connected to a fluorinated N-heterocycle, in turn ligated to an alkyl carbamate moiety. Several 4, 5, and 6 membered metal chelating units can be identified, potentially capable of deactivating metal catalysts. Most remarkably, when S13 was subjected to the standard conditions, oxidation at the remote methylenic site of the alkyl chain proceeds smoothly (68% conversion), leaving the densely functionalized core intact, yielding hydroxylation product P13b in 50% yield, along with 12% of the corresponding carbonyl derivative.

The reaction was finally tested in the oxidation of steroidal substrates containing hydroxyl groups (Scheme 6).[13d20] Oxidation of unprotected lithocholic acid methyl ester S14 in HFIP yields two major diol products in a combined 52% yield where the hydroxyl group of the parent substrate is left intact: diol P14b (34%), resulting from hydroxylation at the bridgehead C-5 methine, and hyodeoxycholic acid methyl ester P14c (18%), where stereoselective hydroxylation has taken place at the equatorial C−H bond at the C-6 methylene. Ketone P14a, deriving from oxidation of the hydroxyl group at C-3, is detected in only minor amounts (5%). In contrast, P14a is the single product (37% yield) in acetonitrile. Hydroxylation of ursodeoxycholic acid methyl ester S15, a substrate bearing two hydroxyl groups at C-3 and C-7, also proceeds preferentially at the C-5 methine C−H, albeit with modest substrate conversion (35%) and product yields (17% isolated yield of P15b and 8% of P15a), a behavior that reasonably reflects the combined deactivation effect of the two hydrogen bonded hydroxyl groups. Along the same path, no reaction takes place when cholic acid methyl ester S16, a substrate bearing three hydroxyl groups at C-3, C-7, and C-12, is employed as substrate, in line with the operation of a

stronger deactivation of all the steroidal skeletal C−H bonds determined by the three hydrogen bonded hydroxyl groups.

Summarizing, the current work describes site-selective and product chemoselective C−H bond oxidation of di- and polyhydroxylated substrates with hydrogen peroxide catalyzed by iron and manganese complexes in fluorinated alcohol solvents. The reaction can be applied to sugars, steroids, and other densely functionalized substrates, without the need to protect the hydroxyl functionalities, which become deactivating groups by solvent hydrogen bonding, and play a directing role toward oxidation at remote and unactivated aliphatic C−H bonds. Overall, the reaction opens a new entry for the straightforward construction of functionality at unactivated sites in complex organic molecules via late stage hydroxylation of aliphatic moieties, providing a new and powerful tool to be rapidly implemented in synthetic planning.

■ ASSOCIATED CONTENT

Ⓢ Supporting Information

The Supporting Information is available free of charge at https://pubs.acs.org/doi/10.1021/acscatal.9b05423.

> Experimental details on the reaction procedures and reaction optimization, product characterization data, GC spectra for determining ratios of regioisomers, and X-ray determined structure of P14b (PDF)

■ AUTHOR INFORMATION

Corresponding Authors

Massimo Bietti − Dipartimento di Scienze e Tecnologie Chimiche, Università "Tor Vergata", 1 I-00133 Rome, Italy; ⓞ orcid.org/0000-0001-5880-7614; Email: bietti@uniroma2.it

Miquel Costas − Institut de Química Computacional i Catàlisi (IQCC) and Departament de Química, Universitat de Girona, Girona E-17071, Catalonia, Spain; ⓞ orcid.org/0000-0001-6326-8299; Email: miquel.costas@udg.edu

Authors

Margarida Borrell − Institut de Química Computacional i Catàlisi (IQCC) and Departament de Química, Universitat de Girona, Girona E-17071, Catalonia, Spain

Sergio Gil-Caballero − Serveis Tècnics de Recerca (NMR), Universitat de Girona, Parc científic i tecnològic de la UdG, Girona E-17003, Catalonia, Spain

Complete contact information is available at:
https://pubs.acs.org/10.1021/acscatal.9b05423

Notes

The authors declare no competing financial interest.

■ REFERENCES

(1) (a) Plietker, B.; Niggemann, M. The RuO4-catalysed dihydroxylation, ketohydroxylation and mono oxidation—novel oxidation reactions for the synthesis of diols and α-hydroxy ketones.

Org. Biomol. Chem. **2004**, *2*, 2403−2407. (b) Plietker, B. The RuO4-Catalyzed Ketohydroxylation. Part 1. Development, Scope, and Limitation. *J. Org. Chem.* **2004**, *69*, 8287−8296. (c) Maki, T.; Iikawa, S.; Mogami, G.; Harasawa, H.; Matsumura, Y.; Onomura, O. Efficient Oxidation of 1,2-Diols into *α*-Hydroxyketones Catalyzed by Organotin Compounds. *Chem. - Eur. J.* **2009**, *15*, 5364−5370. (d) Painter, R. M.; Pearson, D. M.; Waymouth, R. M. Selective Catalytic Oxidation of Glycerol to Dihydroxyacetone. *Angew. Chem., Int. Ed.* **2010**, *49*, 9456−9459. (e) Chung, K.; Banik, S. M.; De Crisci, A. G.; Pearson, D. M.; Blake, T. R.; Olsson, J. V.; Ingram, A. J.; Zare, R. N.; Waymouth, R. M. Chemoselective Pd-Catalyzed Oxidation of Polyols: Synthetic Scope and Mechanistic Studies. *J. Am. Chem. Soc.* **2013**, *135*, 7593−7602. (f) Hung, K.; Condakes, M. L.; Morikawa, T.; Maimone, T. J. Oxidative Entry into the Illicium Sesquiterpenes: Enantiospecific Synthesis of (+)-Pseudoanisatin. *J. Am. Chem. Soc.* **2016**, *138*, 16616−16619. (g) Hill, C. K.; Hartwig, J. F. Site-selective oxidation, amination and epimerization reactions of complex polyols enabled by transfer hydrogenation. *Nat. Chem.* **2017**, *9*, 1213. (h) Hung, K.; Condakes, M. L.; Novaes, L. F. T.; Harwood, S. J.; Morikawa, T.; Yang, Z.; Maimone, T. J. Development of a Terpene Feedstock-Based Oxidative Synthetic Approach to the Illicium Sesquiterpenes. *J. Am. Chem. Soc.* **2019**, *141*, 3083−3099.

(2) Bietti, M. Activation and Deactivation Strategies Promoted by Medium Effects for Selective Aliphatic C-H Bond Functionalization. *Angew. Chem., Int. Ed.* **2018**, *57*, 16618−16637.

(3) Spannring, P.; Bruijnincx, P. C. A.; Weckhuysen, B. M.; Gebbink, R. J. M. K. Transition metal-catalyzed oxidative double bond cleavage of simple and bio-derived alkenes and unsaturated fatty acids. *Catal. Sci. Technol.* **2014**, *4*, 2182−2209.

(4) (a) Serrano-Plana, J.; Oloo, W. N.; Acosta-Rueda, L.; Meier, K. K.; Verdejo, B.; García-España, E.; Basallote, M. G.; Münck, E.; Que, L.; Company, A.; Costas, M. Trapping a Highly Reactive Nonheme Iron Intermediate That Oxygenates Strong C—H Bonds with Stereoretention. *J. Am. Chem. Soc.* **2015**, *137*, 15833−15842. (b) Ottenbacher, R. V.; Talsi, E. P.; Bryliakov, K. P. Mechanism of Selective C-H Hydroxylation Mediated by Manganese Aminopyridine Enzyme Models. *ACS Catal.* **2015**, *5*, 39−44.

(5) (a) Sheldon, R. A.; Arends, I. W. C. E.; ten Brink, G.-J.; Dijksman, A. Green, Catalytic Oxidations of Alcohols. *Acc. Chem. Res.* **2002**, *35*, 774−781. (b) Ryland, B. L.; Stahl, S. S. Practical Aerobic Oxidations of Alcohols and Amines with Homogeneous Copper/TEMPO and Related Catalyst Systems. *Angew. Chem., Int. Ed.* **2014**, *53*, 8824−8838.

(6) (a) Roberts, B. P. Polarity-reversal catalysis of hydrogen-atom abstraction reactions: concepts and applications in organic chemistry. *Chem. Soc. Rev.* **1999**, *28*, 25−35. (b) Wang, D.; Shuler, W. G.; Pierce, C. J.; Hilinski, M. K. An Iminium Salt Organocatalyst for Selective Aliphatic C-H Hydroxylation. *Org. Lett.* **2016**, *18*, 3826−3829. (c) Gaster, E.; Kozuch, S.; Pappo, D. Selective Aerobic Oxidation of Methylarenes to Benzaldehydes Catalyzed by N-Hydroxyphthalimide and Cobalt(II) Acetate in Hexafluoropropan-2-ol. *Angew. Chem., Int. Ed.* **2017**, *56*, 5912−5915. (d) Dantignana, V.; Milan, M.; Cussó, O.; Company, A.; Bietti, M.; Costas, M. Chemoselective Aliphatic C-H Bond Oxidation Enabled by Polarity Reversal. *ACS Cent. Sci.* **2017**, *3*, 1350−1358. (e) Ottenbacher, R. V.; Talsi, E. P.; Rybalova, T. V.; Bryliakov, K. P. Enantioselective Benzylic Hydroxylation of Arylalkanes with H2O2 in Fluorinated Alcohols in the Presence of Chiral Mn Aminopyridine Complexes. *ChemCatChem* **2018**, *10*, 5323−5330. (f) Adams, A. M.; Du Bois, J. Organocatalytic C-H hydroxylation with Oxone® enabled by an aqueous fluoroalcohol solvent system. *Chem. Sci.* **2014**, *5*, 656−659 It has been proposed that hydrogen peroxide forms microdroplets in HFIP. (g) Hollóczki, O.; Berkessel, A.; Mars, J.; Mezger, M.; Wiebe, A.; Waldvogel, S. R.; Kirchner, B. The Catalytic Effect of Fluoroalcohol Mixtures Depends on Domain Formation. *ACS Catal.* **2017**, *7*, 1846−1852 For an alternative role of HFIP in organocatalytic C—H oxidations, forming microdoplets that concentrate reagents and improve catalyst stability see:. (h) Adams, A. M.; Du Bois, J. Organocatalytic C-H

hydroxylation with Oxone® enabled by an aqueous fluoroalcohol solvent system. *Chem. Sci.* **2014**, *5*, 656−659.

(7) Borrell, M.; Costas, M. Mechanistically Driven Development of an Iron Catalyst for Selective Syn-Dihydroxylation of Alkenes with Aqueous Hydrogen Peroxide. *J. Am. Chem. Soc.* **2017**, *139*, 12821−12829.

(8) Milan, M.; Bietti, M.; Costas, M. Highly Enantioselective Oxidation of Nonactivated Aliphatic C-H Bonds with Hydrogen Peroxide Catalyzed by Manganese Complexes. *ACS Cent. Sci.* **2017**, *3*, 196−204.

(9) We thank an anonymous reviewer for suggesting this experiment.

(10) Abraham, M. H.; Grellier, P. L.; Prior, D. V.; Duce, P. P.; Morris, J. J.; Taylor, P. J. Hydrogen bonding. Part 7. A scale of solute hydrogen-bond acidity based on log K values for complexation in tetrachloromethane. *J. Chem. Soc., Perkin Trans. 2* **1989**, 699−711.

(11) Berkessel, A.; Adrio, J. A. Dramatic Acceleration of Olefin Epoxidation in Fluorinated Alcohols: Activation of Hydrogen Peroxide by Multiple H-Bond Networks. *J. Am. Chem. Soc.* **2006**, *128*, 13412−13420.

(12) Lee, Y.-M.; Kim, S.; Ohkubo, K.; Kim, K.-H.; Nam, W.; Fukuzumi, S. Unified Mechanism of Oxygen Atom Transfer and Hydrogen Atom Transfer Reactions with a Triflic Acid-Bound Nonheme Manganese(IV)-Oxo Complex via Outer-Sphere Electron Transfer. *J. Am. Chem. Soc.* **2019**, *141*, 2614−2622.

(13) (a) Ottenbacher, R. V.; Samsonenko, D. G.; Talsi, E. P.; Bryliakov, K. P. Highly Efficient, Regioselective, and Stereospecific Oxidation of Aliphatic C-H Groups with H2O2, Catalyzed by Aminopyridine Manganese Complexes. *Org. Lett.* **2012**, *14*, 4310−4313. (b) Cussó, O.; Garcia-Bosch, I.; Ribas, X.; Lloret-Fillol, J.; Costas, M. Asymmetric Epoxidation with H2O2 by Manipulating the Electronic Properties of Non-heme Iron Catalysts. *J. Am. Chem. Soc.* **2013**, *135*, 14871−14878. (c) Cussó, O.; Garcia-Bosch, I.; Font, D.; Ribas, X.; Lloret-Fillol, J.; Costas, M. Highly Stereoselective Epoxidation with H2O2 Catalyzed by Electron-Rich Aminopyridine Manganese Catalysts. *Org. Lett.* **2013**, *15*, 6158−6161. (d) Font, D.; Canta, M.; Milan, M.; Cusso, O.; Ribas, X.; Gebbink, R. J. M. K.; Costas, M. Readily Accessible Bulky Iron Catalysts exhibiting Site Selectivity in the Oxidation of Steroidal Substrates. *Angew. Chem., Int. Ed.* **2016**, *55*, 5776−5779. (e) Milan, M.; Carboni, G.; Salamone, M.; Costas, M.; Bietti, M. Tuning Selectivity in Aliphatic C-H Bond Oxidation of N-Alkylamides and Phthalimides Catalyzed by Manganese Complexes. *ACS Catal.* **2017**, *7*, 5903−5911.

(14) (a) Chen, M. S.; White, M. C. A predictably selective aliphatic C-H oxidation reaction for complex molecule synthesis. *Science* **2007**, *318*, 783−7. (b) White, M. C.; Zhao, J. Aliphatic C-H Oxidations for Late-Stage Functionalization. *J. Am. Chem. Soc.* **2018**, *140*, 13988−14009.

(15) GC yields were determined in order to have an accurate ratio between products.

(16) Milan, M.; Bietti, M.; Costas, M. Enantioselective aliphatic C-H bond oxidation catalyzed by bioinspired complexes. *Chem. Commun.* **2018**, *54*, 9559−9570.

(17) (a) Tsuda, Y.; Hanajima, M.; Matsuhira, N.; Okuno, Y.; Kanemitsu, K. Regioselective Mono-oxidation of Non-protected Carbohydrates by Brominolysis of the Tin Intermediates. *Chem. Pharm. Bull.* **1989**, *37*, 2344−2350. (b) Freimund, S.; Huwig, A.; Giffhorn, F.; Köpper, S. Rare Keto-Aldoses from Enzymatic Oxidation: Substrates and Oxidation Products of Pyranose 2-Oxidase. *Chem. - Eur. J.* **1998**, *4*, 2442−2455. (c) Perlin, A. S. Glycol-Cleavage Oxidation. In *Adv. Carbohydr. Chem. Biochem.* Horton, D., Ed.; Academic Press: 2006; Vol. *60*, pp 183−250. (d) Jäger, M.; Hartmann, M.; de Vries, J. G.; Minnaard, A. J. Catalytic Regioselective Oxidation of Glycosides. *Angew. Chem., Int. Ed.* **2013**, *52*, 7809−7812. (e) Muramatsu, W. Catalytic and Regioselective Oxidation of Carbohydrates To Synthesize Keto-Sugars under Mild Conditions. *Org. Lett.* **2014**, *16*, 4846−4849. (f) Jäger, M.; Minnaard, A. J. Regioselective modification of unprotected glycosides. *Chem. Commun.* **2016**, *52*, 656−664. (g) Shang, W.; He, B.; Niu, D.

Ligand-controlled, transition-metal catalyzed site-selective modification of glycosides. *Carbohydr. Res.* **2019**, *474*, 16−33.

(18) Alexander, C.; Rietschel, E. T. Invited review: Bacterial lipopolysaccharides and innate immunity. *J. Endotoxin Res.* **2001**, *7*, 167−202.

(19) Blakemore, D. C.; Castro, L.; Churcher, I.; Rees, D. C.; Thomas, A. W.; Wilson, D. M.; Wood, A. Organic synthesis provides opportunities to transform drug discovery. *Nat. Chem.* **2018**, *10*, 383−394.

(20) (a) Breslow, R.; Huang, Y.; Zhang, X.; Yang, J. An artificial cytochrome P450 that hydroxylates unactivated carbons with regio- and stereoselectivity and useful catalytic turnovers. *Proc. Natl. Acad. Sci. U. S. A.* **1997**, *94*, 11156−11158. (b) Yang, J.; Gabriele, B.; Belvedere, S.; Huang, Y.; Breslow, R. Catalytic Oxidations of Steroid Substrates by Artificial Cytochrome P-450 Enzymes. *J. Org. Chem.* **2002**, *67*, 5057−5067. (c) Yang, J.; Breslow, R. Selective Hydroxylation of a Steroid at C-9 by an Artificial Cytochrome P-450. *Angew. Chem., Int. Ed.* **2000**, *39*, 2692−2695. (d) Schönecker, B.; Zheldakova, T.; Liu, Y.; Kötteritzsch, M.; Günther, W.; Görls, H. Biomimetic Hydroxylation of Nonactivated CH2 Groups with Copper Complexes and Molecular Oxygen. *Angew. Chem., Int. Ed.* **2003**, *42*, 3240−3244. (e) Biellmann, J.-F. Enantiomeric Steroids: Synthesis, Physical, and Biological Properties. *Chem. Rev.* **2003**, *103*, 2019−2034. (f) Canta, M.; Font, D.; Gómez, L.; Ribas, X.; Costas, M. The Iron(II) Complex [Fe(CF3SO3)2(mcp)] as a Convenient, Readily Available Catalyst for the Selective Oxidation of Methylenic Sites in Alkanes. *Adv. Synth. Catal.* **2014**, *356*, 818−830. (g) See, Y. Y.; Herrmann, A. T.; Aihara, Y.; Baran, P. S. Scalable C-H Oxidation with Copper: Synthesis of Polyoxypregnanes. *J. Am. Chem. Soc.* **2015**, *137*, 13776−13779. (h) Niwa, T.; Murayama, N.; Imagawa, Y.; Yamazaki, H. Regioselective hydroxylation of steroid hormones by human cytochromes P450. *Drug Metab. Rev.* **2015**, *47*, 89−110. (i) Qiu, Y.; Gao, S. Trends in applying C-H oxidation to the total synthesis of natural products. *Nat. Prod. Rep.* **2016**, *33*, 562−581. (j) Gupta, P.; Mahajan, A. Sustainable approaches for steroid synthesis. *Environ. Chem. Lett.* **2019**, *17*, 879−895. (k) Noack, F.; Heinze, R. C.; Heretsch, P. Contemporary Synthetic Strategies towards Secosteroids, abeo -Steroids, and Related Triterpenes. *Synthesis* **2019**, *51*, 2039−2057. (l) Zhao, J. P.; Nanjo, T.; de Lucca, E. C.; White, M. C. Chemoselective methylene oxidation in aromatic molecules. *Nat. Chem.* **2019**, *11*, 213−221.

■ NOTE ADDED AFTER ASAP PUBLICATION

This paper was originally published ASAP on April 2, 2020. Schemes 4 and 5 were updated, and the revised version was reposted on April 6, 2020.
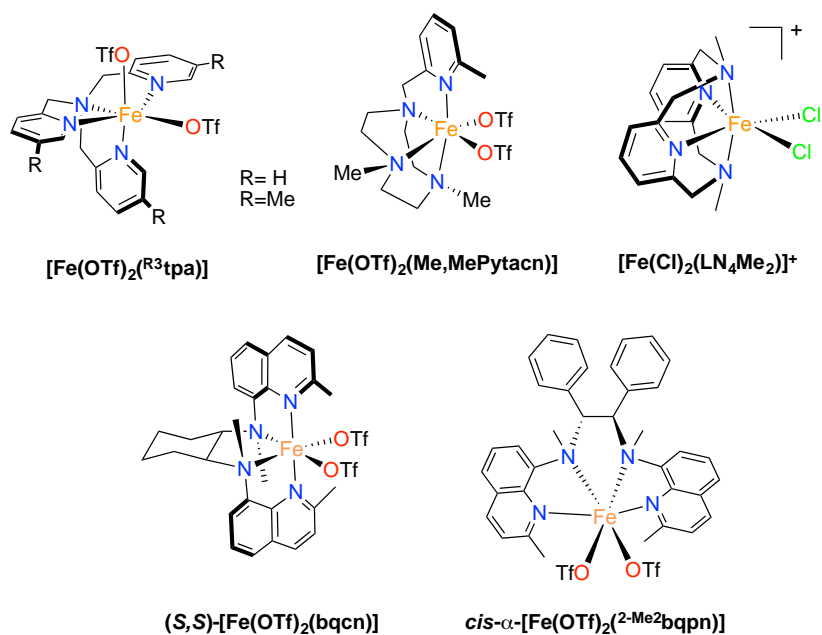
Chapter VII.

Results and Discussion

Note: the numbering of metal complexes and organic compound is consistent within each chapter and refer to the numbering used in the corresponding publication.

VII.1. Mechanistically Driven Development of an Iron Catalyst for Selective *Syn*-Dihydroxylation of Alkenes with Aqueous Hydrogen Peroxide

Olefin *syn*-dihydroxylation is an important oxidation reaction because it transforms widely available feedstocks into valuable building-blocks for bulk and fine chemistry.[1-3] The common methods to perform this reaction use stoichiometric or catalytic amounts of heavy metal oxides such as OsO_4 or RuO_4, which are toxic, expensive and produce heavy metal waste.[4-6] For this reason, in order to improve the sustainability of this transformation, the development of novel methodologies based on first row transition metals is appealing.[1, 7-9] This motivates the development of methodologies based on first row transition metals, which are highly abundant and exhibit a minor environmental impact, and the use of non-toxic oxidants such as hydrogen peroxide, that provides water as residue. Iron and manganese are promising alternatives for catalyst development given their availability and limited cost and toxicity. Manganese catalysts have shown promising activity although the chemoselectivity and the substrate scope are still critical aspects.[10-13]

Taking inspiration from iron dependent arene *syn*-dihydroxylating enzymes present in nature,[14-16] iron coordination complexes have been largely explored as catalysts,[17] but only few examples provide synthetically valuable yields because most systems operate under oxidant-limiting conditions, in the presence of large excess of substrate (Figure VII.1).[18-23]

a) Previous work

[Fe(OTf)$_2$(^{R3}tpa)]

R= H
R=Me

[Fe(OTf)$_2$(Me,MePytacn)]

[Fe(Cl)$_2$(LN$_4$Me$_2$)]$^+$

(*S,S*)-[Fe(OTf)$_2$(bqcn)]

cis-α-[Fe(OTf)$_2$($^{2\text{-Me2}}$bqpn)]

b) This work

[Fe(OTf)₂(⁵⁻ᵗⁱᵖˢ³tpa)]   **Space-filling diagram**
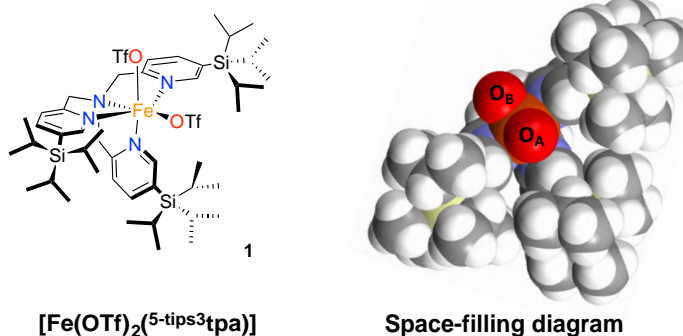
Figure VII.1. Summary of the reported *syn*-dihydroxylation iron catalysts that operate under substrate limiting conditions. a) Catalysts previous to this work. b) this work, [Fe^{II}(OTf)$_2$($^{5\text{-}tips3}$tpa)] (**1**) complex and it's crystal structure space-filling diagram.

VII.1.1. Catalyst design and characterization

In order to develop a novel catalyst, the well-known tetradentate tpa (tpa = tris(2-pyridylmethyl)-amine) ligand was taken as the basic structure,[21, 24-25] and it was modified by introducing the sterically demanding tris(isopropyl)silyl (tips)[26] group in position 5 of each pyridine ring. We envisioned that the introduction of these bulky groups will make a sterically encumbered iron catalyst, a feature that will improve the yields and the chemoselectivity by preventing the coordination of the diol to the iron center. Moreover, the activity of the catalyst may be favored as the bulkiness of the complex would limit the formation of oxo-bridged diferric species, that have been found to be poorly active in catalysis.

The catalyst [Fe(OTf)$_2$($^{5\text{-}tips3}$tpa)] **1** was prepared and characterized. The $^{5\text{-}tips3}$tpa ligand was prepared in 58% yield by reacting two equivalents of 5-silyl-substituted picolyl chloride (**^{tips}PyCH$_2$Cl**,[26] Scheme VII.1) with one equivalent of the 5-silyl-substituted picolyl amine (**^{tips}PyCH$_2$NH$_2$**), both of which were prepared following reported procedures. The $^{5\text{-}tips3}$tpa ligand was directly reacted with Fe(OTf)$_2$·(CH$_3$CN)$_2$ under an inert atmosphere to form the complex, which after crystallization using a mixture of CH$_2$Cl$_2$:hexane, was obtained as yellow crystals in 78% yield.
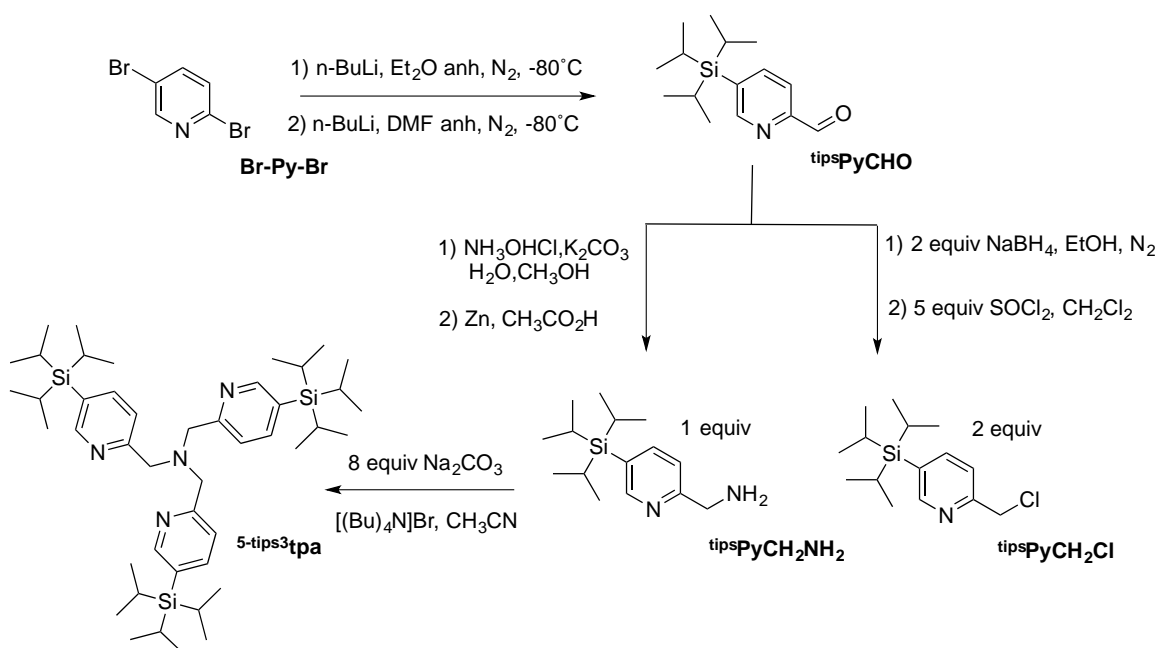
Scheme VII.1. Synthesis of the ligand $^{5\text{-tips3}}$tpa.

X-ray diffraction analysis of the crystals revealed a distorted octahedral iron center geometry, as represented by the *trans* ligand angles of 154.65(2)° for N_3-Fe-N_4, 174.39(3)° for N_1-Fe-O_B, and 156.70(2)° for N_2-Fe-O_A. The stronger coordination of the pyridine moiety cause that the Fe-O bond *trans* to the tertiary amino group (Fe-O_A, 2.049(2) Å) is shorter that the bond *trans* to a pyridyl moiety (Fe-O_B, 2.171(2) Å). Moreover, the longest Fe-N bond derived from the Fe center corresponds to the Fe-N_{amine} (Fe-N2), indicating that the tertiary amine nitrogen is the weaker atom of the complexes. These trends are typical for several tpa complexes,[27-28] and can be observed by comparing the crystal structures of [Fe(OTf)$_2$($^{5\text{-tips3}}$tpa)] and [Fe(OTf)$_2$(tpa)] (Table VII.1). In addition, in both complexes the Fe-N_{pyr} distances range from 2.156(2) to 2.220(2) Å, characteristic of a high-spin Fe(II) center.

Table VII.1. ORTEP diagram of [Fe^{II}(OTf)$_2$($^{5\text{-tips3}}$tpa)], (right) and [Fe^{II}(OTf)$_2$(tpa)], (left). Triflate anions are omitted except for the oxygen atoms directly bound to the iron center; (50% and 30% thermal ellipsoids respectively). Hydrogen atoms omitted for clarity. Selected bond distances (Å) for both catalysts.
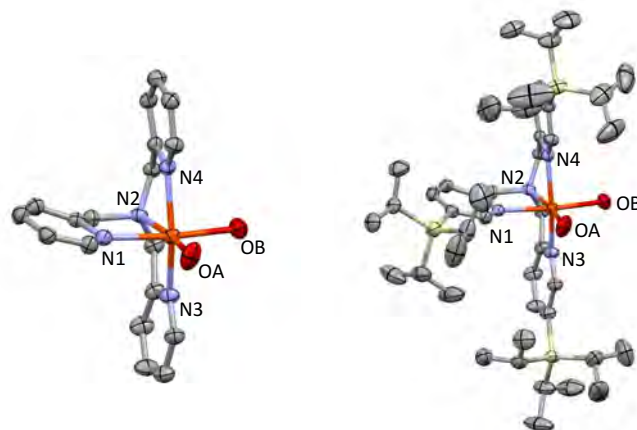
[Fe^{II}(OTf)$_2$(tpa)]		[Fe^{II}(OTf)$_2$($^{5\text{-tips3}}$tpa)]	
Fe-N1	2.179(2)	Fe-N1	2.192(2)
Fe-N2	2.203(2)	Fe-N2	2.220(2)
Fe-N3	2.174(2)	Fe-N3	2.160(2)
Fe-N4	2.156(2)	Fe-N4	2.158(2)
Fe-OA	2.054(2)	Fe-OA	2.049(2)
Fe-OB	2.150(2)	Fe-OB	2.171(2)

VII.1.2. Catalytic activity

VII.1.2.1. Optimization

The new catalyst was then tested in olefin *syn*-dihydroxylation using 1-octene (**S1**) as model substrate. The reaction was carried out under air by adding 1.5 equiv. of H$_2$O$_2$ (commercially available 50% w/w solution diluted in acetonitrile) via syringe pump over 30 min at 0 °C to an acetonitrile solution containing 1 equiv. of substrate and 1 mol% of catalyst. Under these conditions, a 74% yield of 1,2-octandiol (**P1b**) was obtained, together with 23% of 1-epoxide octane (**P1c**) (Entry 1 in Table VII.2). This result is remarkable since the mass balance of the reaction is excellent (98% conversion, 97% total yield) (Entry 1, Table VII.2), indicating that overoxidation reactions are negligible. We considered the possibility that the yields and the chemoselectivity will improve by separating the diol from the mixture, because the accumulation of the diol in solution inhibits the catalytic activity by binding to the catalytic iron center, as was previously documented for several iron catalysts.[23-24, 29] In order to reduce the effective availability of free diol in solution, we performed the reaction in the presence of 2.2

equiv. of different Lewis acids, which could potentially bind the diol and therefore, "sequester" it from the solution (Table VII.2).

Table VII.2. Screening of different Lewis acids, using 1-octene (**S1**) as substrate.

Entry[a]	Additives (2.2 equiv.)	Conversion (%)	Yield *syn*-diol P1b (%)	Yield epoxide P1c (%)	Ratio *syn*-P1b/P1c
1	-	98	74	23	3.2
2	**Mg(ClO$_4$)$_2$·6H$_2$O**	**100**	**86**	**14**	**6.1**
3	Zn(OTf)$_2$	99	75	21	3.6
4	NaOTf	80	59	14	4.2
5	MgO	86	71	15	4.7
6	Mg(OTf)$_2$	94	77	17	4.5
7	Mg(ClO$_4$)$_2$	53	43	10	4.3
8	LiClO$_4$·3H$_2$O	62	51	8	6.4

[a] Yields determined by GC

Among the series of Lewis acids tested (Table VII.2), Mg(ClO$_4$)$_2$·6H$_2$O (Entry 2, Table VII.2) provided the most significant improvement in product yields and selectivity towards the diols, without compromising neither the selectivity nor the mass balance of the reaction. A marginally improved yield of diol was observed when the reaction was performed in the presence of Zn(OTf)$_2$ (Entry 3, Table VII.2) and Mg(OTf)$_2$ (Entry 6, Table VII.2), while the rest of the cases yielded lower yields. The addition of LiClO$_4$·3H$_2$O (Entry 8, Table VII.2) improved the selectivity towards the *syn*-diol product albeit with a reduced yield.

Further investigation was done to evaluate the origin of the impact of Mg(ClO$_4$)$_2$·6H$_2$O; control experiments showed that the single addition of 6 equiv. of water or the use of Mg(ClO$_4$)$_2$ do not reproduce the positive effect of Mg(ClO$_4$)$_2$·6H$_2$O, indicating that both elements contribute in a synergistic manner.

With these results in hands, we tested if the positive effect of Mg(ClO$_4$)$_2$·6H$_2$O is translated to others ion catalysts. We evaluated the effect in the activity of [Fe^{II}(tpa)(CH$_3$CN)$_2$](ClO$_4$)$_2$, [Fe^{II}(CF$_3$SO$_3$)$_2$(^{Me,Me}Pytacn)] and [Fe^{II}(Cl)$_2$(LN4Me$_2$)]$^+$ (Chapter IX, Table IX.1) catalysts under

the same conditions. The results reveal that the activity of catalyst $[Fe^{II}(tpa)(CH_3CN)_2](ClO_4)_2$ and $[Fe^{II}(Cl)_2(LN4Me_2)]^+$ could not be improved but, interestingly, the activity of $[Fe^{II}(CF_3SO_3)_2(^{Me,Me}Pytacn)]$ is also improved, increasing the yield of diol and also the diol/epoxide ratio.

The diol sequestering role of the Lewis acid was confirmed by analysis of the reaction mixture by high resolution mass spectrometry (HRMS) at different times (in Figure VII.2). HRMS analysis were done using 1-octene (**S1**) as a substrate and the standard conditions, this includes 2.2 equiv. of $Mg(ClO_4)_2 \cdot 6H_2O$.

Panel A is the spectrum recorded at 2 minutes of the reaction, two peaks were identified, a first one at *m/z* = 479.80 assigned to $[Fe^{III}\{(C_8H_{16})(O)(OH)\}(^{tips}tpa)]^+$, where a molecule of the monodeprotonated diol binds to the iron center, as previously reported for several iron catalysts,[24, 29] and a second one at *m/z* = 423.74 that corresponds to the hydroperoxide intermediate $[Fe^{III}(OOH)(^{tips}tpa)]^+$. The second spectrum was recorded after 15 minutes of the reaction (panel B). In this spectrum, it can be seen as the *m/z* = 423.74 peak has disappeared. On the contrary, the peak of the diol binding to the iron center dominates the spectrum. Finally, the last spectrum (panel C) was recorded at the end of the reaction (30 minutes). As expected the peaks observed correspond to the adducts between Mg^{2+} and the diol. Interestingly the peak corresponding to the diol binding to the iron center (*m/z* = 479.80) has almost disappeared.
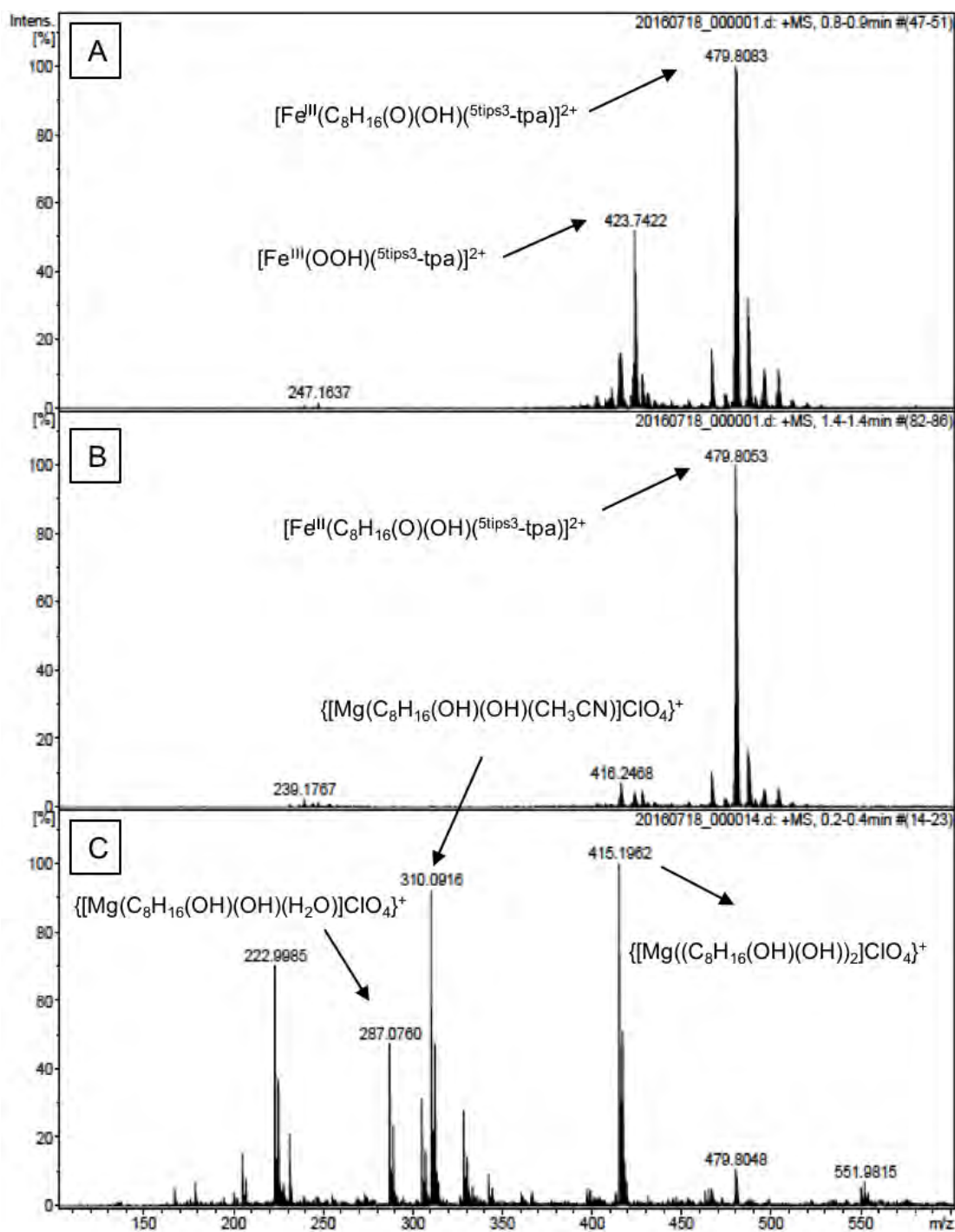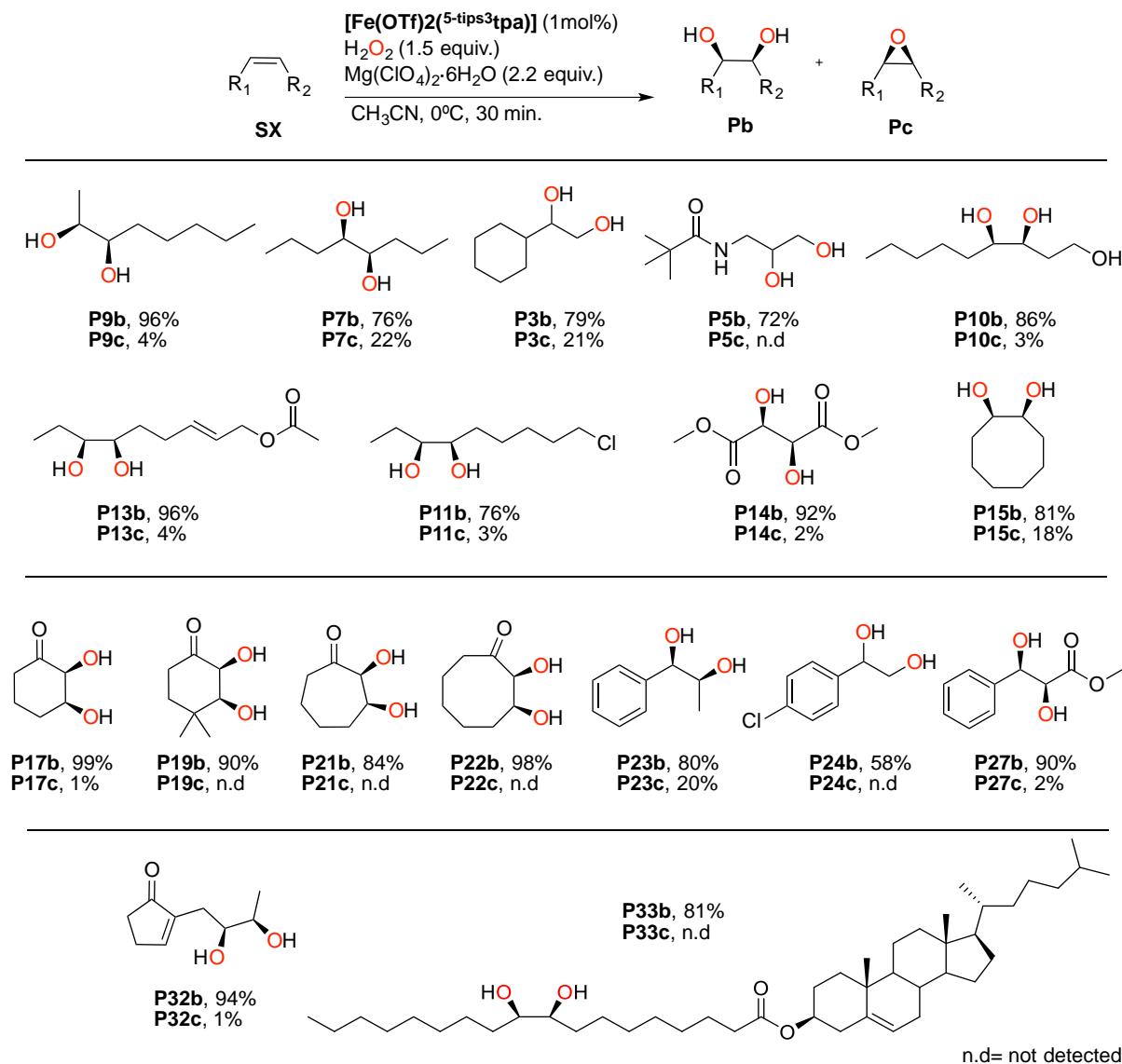
Figure VII.2. HRMS analysis of the reaction using 1-octene (**S1**) as a substrate recorded at different time. Spectrum A was recorded at 2 min, spectrum B at 30 min and spectrum C at 30 min.

VII.1.2.2. Substrate scope

Then, the scope of reaction was evaluated, revealing that our system works efficiently in different families of substrates Scheme VII.2.

Scheme VII.2. Substrate scope of different alkenes using catalyst **1**.

Excellent isolated yields were obtained when aliphatic olefins were used as substrates (up to 97%). Reactions proceeded with outstanding mass balances (>95%). In general, full conversions were achieved, and epoxides are obtained as minor products. These results compare favorably with those obtained with the previously reported catalysts.

The reaction is tolerant to different functional groups, including alcohols (**S10**), halides (**S11**), esters (**S13**), amide (**S5**) and even in electron-poor substrates such as methyl fumarate (**S14**) and methyl maleate (**S12**). Particularly interesting is the *syn*-dihydroxylation of dimethyl

maleate (**S12**), since the reaction only proceeds in good yields when is performed without Mg(ClO$_4$)$_2$·6H$_2$O, presumably because chelation of the Mg^{2+} with the substrate (observed by HRMS) causes deactivation of the substrate (Figure VII.3).

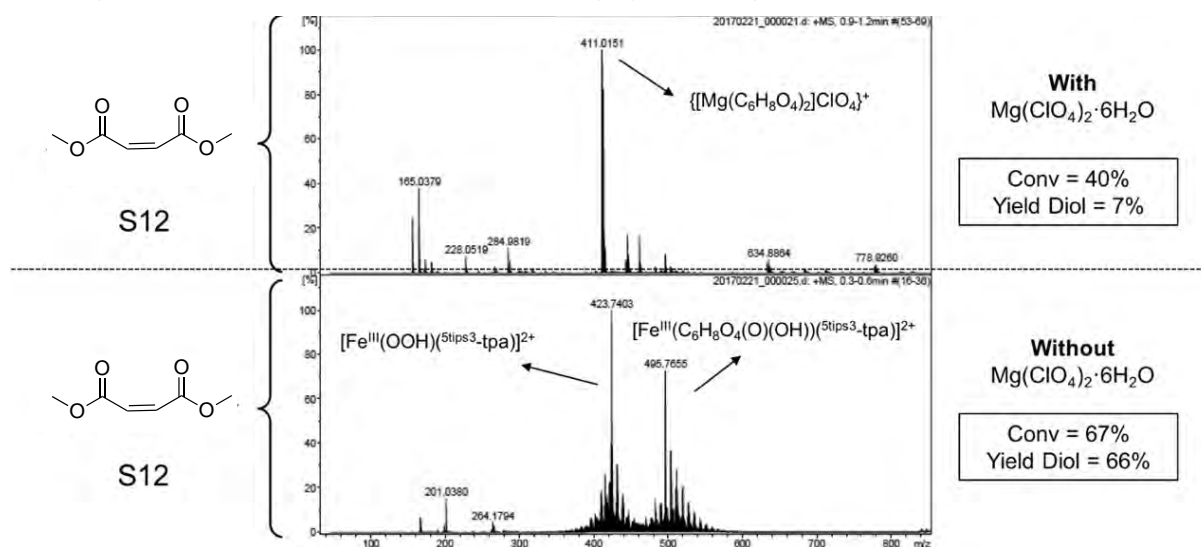**Figure VII.3.** HRMS analysis of the reaction with maleate substrate with Mg(ClO$_4$)$_2$·6H$_2$O and without.

Cyclic aliphatic enones (**S17**, **S19**, **S21, S22**) were also oxidized in good yields and excellent chemoselectivity. Aromatic olefins (**S23**, **S24**, **S27**) were also tolerated and *syn*-diols were obtained in moderate- to good yields. Non-deactivated aromatic rings are oxidized (**S23** and **S24**), albeit with significant amounts of epoxide. Improved yields and chemoselectivities are observed when electron-withdrawing groups are present in the substrate (**S27**). This can be clearly observed by comparing the outcome of the reaction of *cis*-β-methylstyrene (**S23**) and 4-chloro-*cis*-β-mehtylstyrene (**S24**).

More challenging substrates such natural products with two olefinic sites, were finally tested. *Cis*-jasmone (**S32**) and the steroidal substrate (**S33**) were efficiently and selectively oxidized, obtaining only the diol resulting from the *syn*-dihydroxylation of the most electron-rich (in **S32**) and less sterically impeded (in **S33**) olefinic site. These results show the potential of this system to be used in organic synthesis.

VII.1.3. Mechanistic studies

To understand the mechanism of the system, isotope labelling experiments were performed. *Syn*-dihydroxylation of different substrates were performed in presence of H$_2$^{18}O and H$_2$O$_2$, and in all cases the corresponding *syn*-diol was obtained as 90% singly ^{18}O-labelled. This

indicates that the catalyst can be classified as a Class A catalyst. As mentioned in Chapter I, this type of catalysts involved an electrophilic oxidizing species, presumably an $Fe^V(O)(OH)$.[30]

Once ascertained that **1** is a class A catalyst, we wondered if it was possible to predict in which position is located the oxygen atom that originates from H_2O_2 and the one from H_2O in the $Fe^V(O)(OH)$ oxidizing species. Analysis of the crystal structure of the catalyst (Figure VII.1b and table VII.1) reveals that the two *cis*-labile positions at the iron center are non-equivalents in terms of steric bulkiness, mainly imposed by the tips groups. Whereas the O atom *trans* to the aliphatic amine (O_A) is surrounded by the three bulky groups, the O atom *trans* to one of the pyridines (O_B) is surrounded by only two tips groups, making it priori less hindered than the other (Figure VII.4).
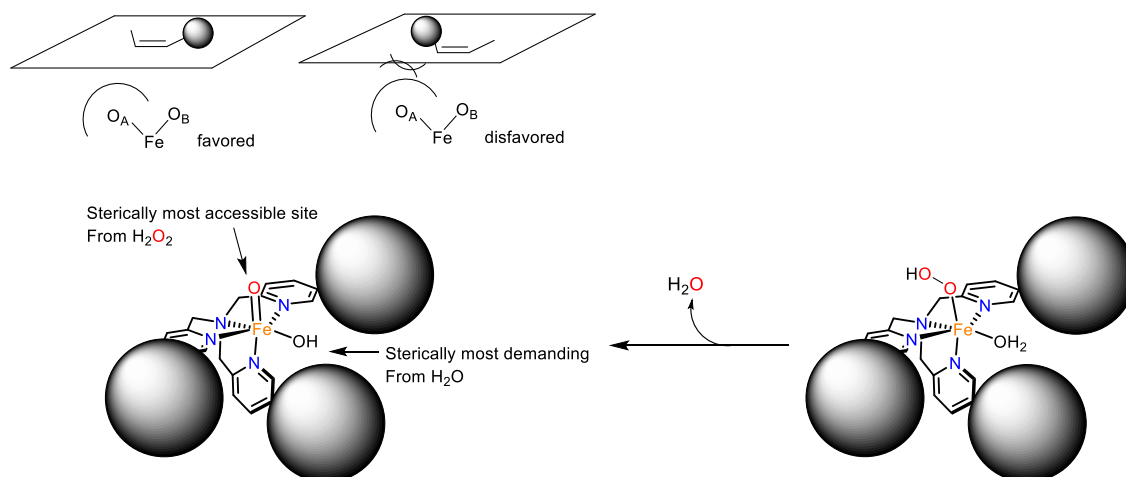

Figure VII.4. Schematic representation of the favorable and disfavorable approach of the olefin to the $Fe^V(O)(OH)$.

This model was used in the analysis of the *syn*-dihydroxylation of unsymmetrical olefins using H_2O_2 and $H_2{}^{18}O$ (Scheme VII.3). Fragmentation of the diol by electron ionization and mass spectrometry analysis of the fragments allowed us to determine the position of the ^{18}O. Consistently, the ^{18}O-atom is preferentially introduced to the less congested carbon, suggesting that this oxygen atom occupies the sterically most demanding site in the catalysts (O_A). The model was further confirmed by using olefins where the size differences between the two olefin substituents is large. For example, the two ($^{18}O,^{16}O$) diol isotopomers obtained in the oxidation of *cis*-2-octene and 1-octene in the presence of $^{18}OH_2$ changes from 1:1 to 1:2, enhancing the proportion of isotopomer where ^{18}O incorporation has taken place at the sterically more congested site.
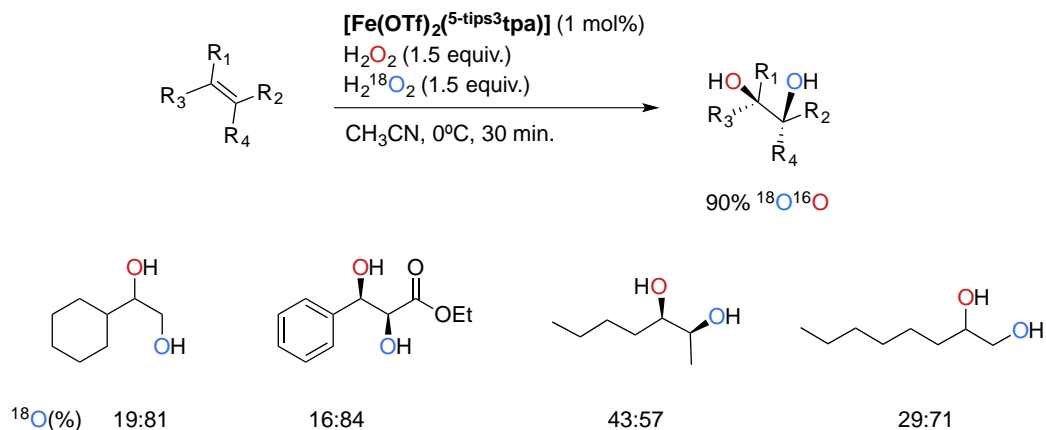
Scheme VII.3. Isotopic labeling analysis of the oxidation of different substrates.

To summarize, a new sterically demanding iron catalyst for *syn*-dihydroxylation of olefins have been prepared. This catalyst performs the *syn*-dihydroxylation of a wide range of olefins using H_2O_2 as oxidant under mild experimental conditions. The nature of the active species could be understood in basis of structural analysis of the catalyst and labelling experiments, which may serve in a near future, as a tool to rationally design new catalysts.

VII.2. Greening Oxidation Catalysis: Iron Catalyzed Alkene *syn*-Dihydroxylation with Aqueous Hydrogen Peroxide in Green Solvents

In terms of sustainability, one of the limitations of oxidation reactions, as well as other conventional organic transformations, is the reaction media. In the case of iron-catalyzed oxidation reactions, the use of volatile and toxic solvents, such as acetonitrile or fluorinated alcohols, is a common practice.[31]

An interesting case to study is the reaction of *syn*-dihydroxylation of olefins. The use of iron catalysts has represented a great advance in terms of environmental impact, because it can avoid the use of heavy metals such as Os and Ru.[4, 32] In addition, iron catalysts can work using H_2O_2, an environmentally harmless compound, as oxidant.[1] However, the iron catalysts described so far operate in acetonitrile, which is a toxic and volatile solvent.[18-21, 23, 33]

The objective of this project is to investigate the possibility of replacing acetonitrile by a green solvent in oxidation reactions. Towards this end, the *syn*-dihydroxylation of olefins with the [Fe(OTf)$_2$($^{5\text{-tips3}}$tpa)] catalyst was chosen, mainly by two reasons. First, and as described in the previous section, this complex is an excellent catalyst in *syn*-dihydroxylation reactions both in terms of activity, chemo- and regioselectivity.[18] On the other hand, the hydrophobic tips groups in the pyridines favor the solubility of the complex in organic solvents, that can be considered a crucial issue in homogeneous catalysis.[26]

VII.2.1. Identification of green solvents compatible with the oxidation reaction

A series of solvents were tested in the *syn*-dihydroxylation of 1-octene (**S1**), using 1 mol % of catalyst and 1.5 equiv. of H_2O_2 in 30 minutes. Results are collected in Table VII.3.

Table VII.3. Screening of different solvents using standard conditions and 1-octene (**S1**) as substrate.

[Fe(OTf)₂(⁵⁻ᵗⁱᵖˢ³tpa)] (1 mol%)
H₂O₂ (1.5 equiv.)

Mg(ClO₄)₂·6H₂O (2.2 equiv.)
Solvent, 0°C, 30 min.

S1 → **P1b** + **P1c**

Entry	Solvent	Conv. (%)[a]	Yield P1b (%)	Yield P1c (%)	Ratio P1b/P1c
1	Acetonitrile	97	74	15	4.9
2	γ-butyrolactone	91	63	27	2.3
3	EtOAc	60	36	6	6.0
4	PC	83	62	18	3.4
5	EtOAc/PC	94	78	15	5.2

[a]Conversions and yields determined by GC, calibrated with authentic standards.

The result obtained when γ-butyrolactone was employed (Entry 2, Table VII.3) reveals the positive ability of this catalyst to work in different solvents apart from acetonitrile. However, neither the yield or the chemoselectivity were improved when compared with acetonitrile (Entry 1, Table VII.3).

Good chemoselectivity was obtained in EtOAc as solvent (Table VII.3, Entry 3) albeit in modest yield, while an opposite trend is observed when propylene carbonate (PC, Entry 4, Table VII.3) is used. Trying to combine the good yields obtained with PC and the good chemoselectivity provided by EtOAc, a 1:1 mixture of these solvents was used (Entry 5, Table VII.3.), achieving in this case improved yield and chemoselectivity in comparison with acetonitrile.

VII.2.2. Substrate scope

Encouraged by these results, we tested the dihydroxylation of different olefins in the mixture of EtOAc/PC (Table VII.4). Good to excellent yields were obtained in a wide range of olefins covering aliphatic olefins with different substitution patterns (Entries 1-4, Table VII.4), enones (Entries 5-6, Table VII.4) and an aromatic olefin (Entry 7, Table VII.4). As found in the previous section, when two olefinic sites are present in the substrate, the system is regioselective towards the more electron rich (Entries 8 and 9) and less sterically impeded (Entry 10, Table VII.4) site. In most cases, yields and chemoselectivities are comparable than those obtained with acetonitrile. The only exception is the *syn*-dihydroxylation of *trans*-2-*cis*-nonadienylacetate, in which a 26% lower diol yield is achieved (Entry 8, Table VII.4).

Table VII.4. Substrate scope with a comparison of CH₃CN vs EtOAc/PC

Reaction scheme: R–CH=CH–R' with **[Fe(OTf)₂(5-tips3tpa)]** (1 mol%), H_2O_2 (1.5 equiv.), $Mg(ClO_4)_2 \cdot 6\,H_2O$ (2.2 equiv.), PC/AcOEt (1/1), 30 min., 0°C → diol **PXb** + epoxide **PXc**

Entry[a]	Substrate	CH₃CN	Conv. (%)	Yield PXb (%)	Yield PXc (%)	Ratio Pxb/ Pxc
1		-	94	78	15	5.2
		100 %[b]	98	81	17	5
2		-	82	65	17	4
		100 %[b]	98	76	22	3.5
3		-	99	86	13	6
		100 %[b]	100	81	15	5.5
4		-	100	70	21	3
		100 %[b]	100	82	17	5
5		-	82	76	4	19
		100%[b]	100	92	5	18
6		-	100	93[c]	3[c]	22
		100 %[b]	100	99	-	-
7		-	100	69[c]	31[c]	2.2
		100 %[b]	75	55	20	2.7
8		-	82	64	6	10
		100 %[b]	99	90	6	15
9		-	95	91	3	30
		100 %[b]	98	88	3	29
10		-	95	83	-	-

[a] Conversions and yields determined by GC using the responsive constants of the products. Reported product yields are the average of 2-3 reactions and the error is <5%. [b] Acetonitrile was used instead of PC:AcOEt. [c]Second addition of 1 mol % catalyst and 1.5 equiv. of H_2O_2.

VII.2.3. Oxidations with in-situ generated catalyst

In order to make this system more suitable form a practical synthesis point of view, we analyzed if the catalyst could be formed in situ. This would represent a more practical methodology because iron complexes bearing tetradentate nitrogen-based ligands are oxygen sensitive. On an opposite manner, the ligand and the iron precursor used to prepare the complex ($Fe(OTf)_2$ are bench-stable compounds. Therefore, the in-situ generation of the complex would facilitate the manipulation of the reagents used in the catalytic reaction.

Taking cholesteryl oleate as an example for a gram-scale reaction, a good yield of the corresponding *syn*-diol (79%) was obtained demonstrating the suitability of the green solvents on *syn*-dihydroxylation reactions and its applicability in organic synthesis. To note, a slightly amount of EtOAc was added in order to solubilizes the substrate.

In situ formation of the catalyst was used in the *syn*-dihydroxylation of different olefins and good yields were obtained (up to 72%). It is important to remark that the reaction using the ligand by itself or the $Fe(OTf)_2$ without the ligand does not proceed.
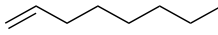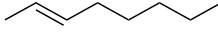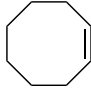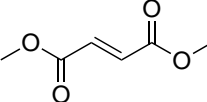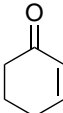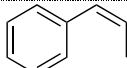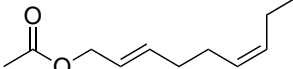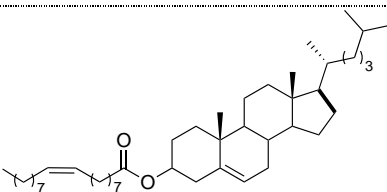
VII.2.4. E-factors considerations

Finally, we evaluate the greenness of the reaction calculating the E factor and atom economy (AE), a two popular green metrics,[34] for different olefins.

The E-factor is the mass ratio of waste to the desired product. Values for the reactions studied are collected in Table VII.5. It can be observed that values are relatively high (except for the cholesteryl acetate Table VII.5 Entry 8), probably because of the low molecular weight of the substrates employed and the low concentration of substrate used in the standard conditions. The E-factor can be decreased by increasing 3-fold the concentration of the reaction solutions, obtaining in this case acceptable values (between 74 and 100).

On the other hand, atom economies obtained are extraordinarily high. It can be said that the use of 2.2 equiv. of $Mg(ClO_4)_2 \cdot 6H_2O$ is not beneficial in terms of atom economy, however, the addition of this Lewis acid significantly improves the yield of *syn*-diol and the chemoselectivity of the reaction, which overall can be translated into more efficient and sustainable transformation.

Table VII.5. E factor and AE of different substrates.

Entry	Substrate	E factor	AE (%)
1		197	89
2		237	89
3		223	90
4		167	91
5		186	88
6		214	89
7		162	92
8		40	97

To summarize, it has been demonstrated that the [Fe(OTf)$_2$($^{5\text{-tips}3}$tpa)] catalyzed *syn*-dihydroxylation of olefins can be efficiently performed using a mixture of PC and EtOAc as solvent, obtaining comparable reaction outcomes with values obtained in acetonitrile. The replacement of acetonitrile by these green solvents, combined with the fact that the catalyst is based on iron, that can be prepared in situ from bench-stable compounds, and that uses H$_2$O$_2$ that does not generate waste, makes this system attractive from a sustainable point of view. The results obtained in this section can be used as a proof of concept to expand the use of green solvents in other iron-catalyzed oxidation reactions, such as C-H hydroxylation and epoxidation.

VII.3. Characterized *cis*-Fe^V(O)(OH) intermediate mimics enzymatic oxidations in the gas phase

Fe^V species are postulated as oxidizing agents in numerous metal-catalyzed oxidation methods and in the reaction mechanism of Rieske oxygenases, bacterial enzymes that oxidize hydrocarbons and arenes.[35] However, the high reactivity of Fe^V(O) species presumably prevents their accumulation in solution and makes their direct experimental identification and characterization extraordinary rare.[36-40]

The oxidizing species in Rieske oxygenases is not known but is postulated to be a Fe^V(O)(OH) transient, where the oxo and the hydroxide ligands are in relative cis-position.[41] In parallel, synthetic iron catalysts capable of *syn*-dihydroxylating olefins and hydroxylating alkanes have been developed over the last decade and they are also proposed to operate via a Fe^V(O)(OH) intermediate.[42-43] Whereas related Fe^V(O)(O$_2$CR) species have been spectroscopic and chemically characterized,[40, 44-45] no direct experimental observation of the Fe^V(O)(OH) species had been reported before the present study. The [Fe^V(O)(OH)(Pytacn)]$^{2+}$ (Pytacn = 1-(2'-pyridylmethyl)-4,7-dimethyl-1,4,7-triazacyclononane) was previously detected by mass spectrometry and formulated on the basis of labelling experiments with H$_2^{18}$O and H$_2^{18}$O$_2$ and theoretical calculations.[29, 46] More recently, Pushkar and co-workers have claimed trapping and spectroscopic characterization by X-ray absorption spectroscopy and EPR analyses of the latter species in catalytic water oxidation reactions.[47]

In this section, the [Fe^V(O)(OH)($^{5-tips3}$tpa)]$^{2+}$ species claimed to be the oxidizing agent in the reactions described in chapters III and IV has been generated and spectroscopically characterized in gas phase using helium tagged infrared photodissociation spectroscopy (IRPD).[48]

VII.3.1. Generation of the Fe(V) species

First, the transient [Fe^{III}(OOH)($^{5-tips3}$tpa)]$^{2+}$ was generated from the reaction of [Fe(OTf)$_2$($^{5-tips3}$tpa)] and H$_2$O$_2$ (10 equiv.) in acetonitrile at -40ºC. The reaction could be followed by UV-vis spectroscopy (Figure VII.5), where the formation of [Fe^{III}(OOH)($^{5-tips3}$tpa)]$^{2+}$ was evidenced by a characteristic intense absorption at λ_{max} = 520 nm associated with peroxide to Fe^{III} charge transfer bands.[18]

The reaction mixture was then analyzed by electrospray ionization mass spectrometry (ESI-MS); two peaks were identified, a first one at *m/z* = 444.12, attributed to the expected dicationic species [Fe^{III}(OOH)(CH$_3$CN)(^{5tips3}tpa)]$^{2+}$,[49] and a second one that could be tentatively assigned to the previous [Fe^{III}(OOH)(^{5tips3}tpa)]$^{2+}$ with a loss of an acetonitrile ligand, or alternatively to an [Fe^{V}(O)(OH)(^{5tips3}tpa)]$^{2+}$ formed after O-O bond cleavage of the hydroperoxide species. (Figure VII.5) To determine which one of these species was formed, we used helium-tagging infrared photodissociation (IRPD) spectroscopy to mass-select the peak at m/z = ~424 and characterized it by IR spectroscopy and isotope labelling experiments.
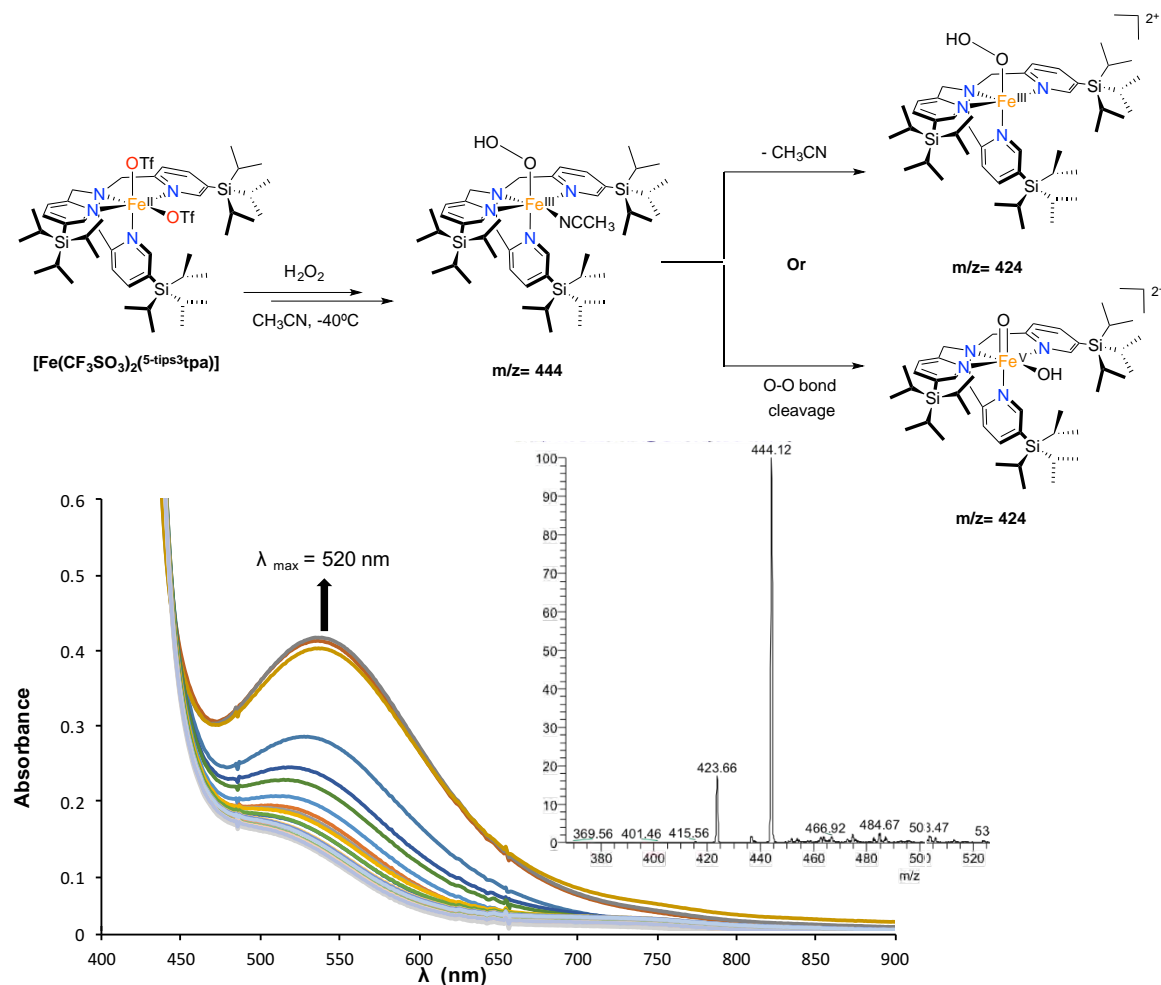
Figure VII.5. Electrospray ionization mass spectrometry (ESI-MS) and UV-Vis spectra of the progressive formation of [Fe^{III}(OOH)(^{5tips3}tpa)]$^{2+}$ or [Fe^{V}(O)OH(^{5tips3}tpa)]$^{2+}$ upon addition of H$_2$O$_2$ at -40ºC.

VII.3.2. Characterization by IRPD spectroscopy.

The IR spectrum was measured when the m/z = ~424 transient species were generated using H_2O_2 (Figure VII.6, black line), labeled $H_2^{18}O$ (Figure VII.6, orange line) and mixed labelled $H_2^{16}O^{18}O$ (a 1:2:1 mixture of $H_2^{16}O_2$:$H_2^{18}O$:$H_2^{16}O^{18}O$, Figure VII.7., orange line). By comparison of these spectra, the signals at 638 and 827 could be assigned. The energy of the first one at 638 cm^{-1} is consistent with a v(Fe-O) stretching or (O-OH) bending vibrations, while the one at 827 matches frequency values expected for v(Fe=O) or v(O-O) stretching vibrations. [38, 50-53] However, the -22 cm^{-1} and -30 cm^{-1} shifts observed in the 638 cm^{-1} and 827 cm^{-1} bands upon ^{18}O labelling are in good agreement with the expected shifts for Fe-O and Fe=O vibrations on the basis of a Hook's law analysis (-28 and -36 cm^{-1}, respectively), providing strong credibility to the v(Fe-O) stretching and v(Fe=O) assignment.
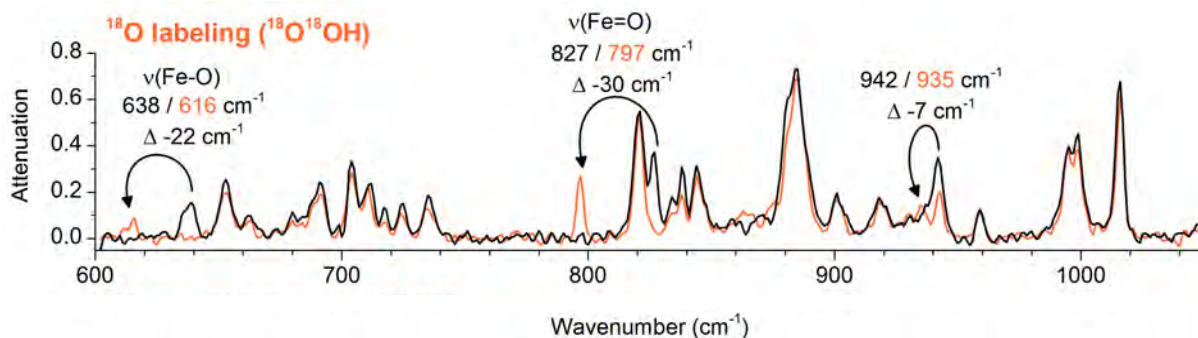
Figure VII.6. IRPD spectrum of the m/z = ~424 ions generated from the reaction mixture of catalyst with H_2O_2 (black trace) and generated with $H_2^{18}O_2$ (orange trace).

To further differentiate between the {Fe(O)(OH)} and {Fe(OOH)} bindings, we measured the spectrum of the m/z = ~424 with a mixture of labeled and non-labeled peroxide ($H_2^{18}O_2$/ $H_2^{18}O^{16}O$/ $H_2^{16}O_2$ 1:2:1 ratio). If the 827 cm^{-1} peak corresponds to a O-O vibration, it will be split in three peaks in a 1:2:1 intensity ratio, corresponding to the ^{16}O-^{16}O, ^{16}O-^{18}O, ^{18}O-^{18}O isotopomer vibrations. If on the contrary, if the band corresponds to a Fe=O vibration, it will be split only in two peaks, corresponding to the Fe=^{16}O and Fe=^{18}O isomers. The latter situation is the one observed experimentally, strongly suggesting that a Fe=O stretching is involved. (Figure VII.7)
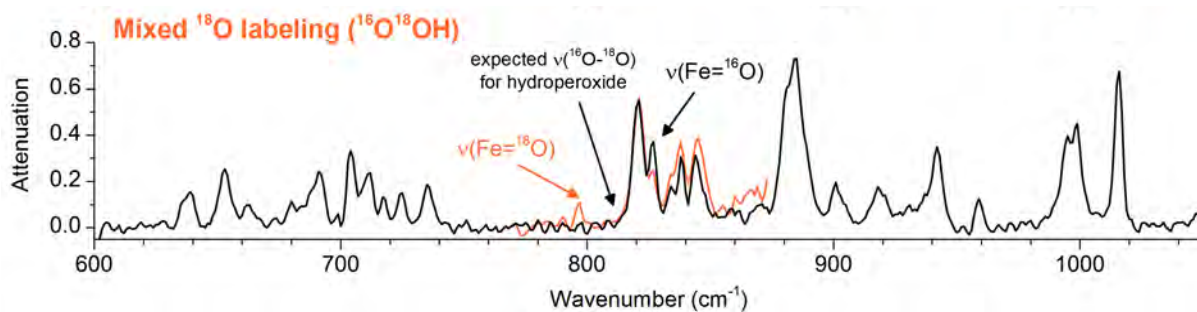
Figure VII.7. IRPD spectrum of the ions generated from the reaction mixture of catalyst with H_2O_2 (black trace) and generated whit $H_2^{16}O^{18}O$ (orange trace).

To confirm the assignation of the bands, the experiment was repeated by mass selecting the [54]Fe-labellled ions. Interestingly, an upfield shift of the 827 and 638 cm^{-1} signals is observed, consistent with the assignment (Figure VII.8).
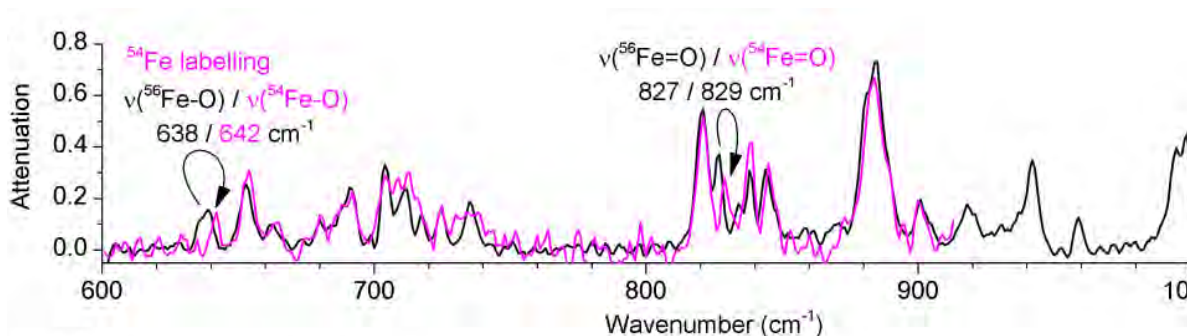

Figure VII.8. IRPD spectrum of the natural abundant of [56]Fe ion generated from the reaction mixture of catalyst with H_2O_2 (black trace) and generated with [54]Fe (purple trace).

All these experiments allowed us to unambiguously assign the peak at m/z=424 as a $[Fe^V(O)(OH)(^{5\text{-tips3}}tpa)]^{2+}$ intermediate, representing the first example of an experimentally spectroscopically characterized $Fe^V(O)(OH)$ species.
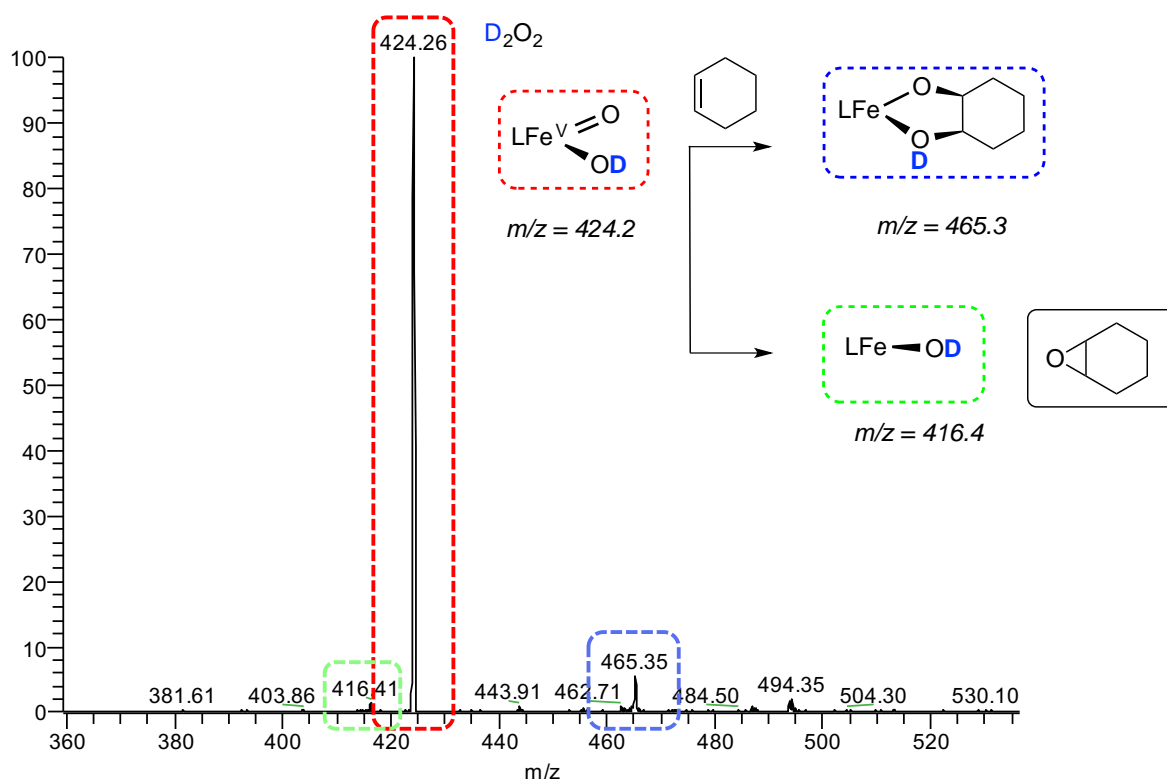
VII.3.3. Gas phase reactivity

Once the intermediate was identified and characterized as an $Fe^V(O)(OH)$ species, its reactivity towards a series of substrates was studied in the gas phase.

Towards this end, the m/z = ~424 was mass selected, brought to a second reaction chamber, and reacted with different substrates. The reaction with cyclohexene substrate gave two products, the first one, with m/z = 465 (84%), which can be viewed as the "adduct" between the substrate and the Fe(V), can be assigned as the product resulting from the olefin dihydroxylation reaction (FigureVII.4). The second product has a m/z = 416 (16%) and can be

understood as the species that form after the Fe(V) species has lost an oxygen atom. This suggests that an oxygen atom transfer from the Fe(V) to the olefin occurred, most likely in an epoxidation reaction, generating a Fe^{III}(OH) species (m/z = 416) (Scheme VII.4). The alternative scenario, entailing hydroxylation of the substrate can be discarded since the reaction did not exhibited a KIE upon using a deuterated substrate.

These results are in agreement with the ones found under catalytic conditions in solution for the Fe(^{tips}tpa) catalyst, in which the *syn*-dihydroxylation reaction is more favorable than epoxidation.[18]

Scheme VII.4. Reactivity of [Fe^V(O)(OD)(^{5tips3}tpa)]$^{2+}$ in the gas phase with 0.1 mTorr of cyclohexene.

The same behavior was observed when, 1,3-cyclohexadiene was used as substrate in a reaction with a deuterated [Fe^V(O)(OD)(^{5tips3}tpa)]$^{2+}$ intermediate (generated from reaction with D$_2$O$_2$), in which *syn*-dihydroxylation predominates over oxygen atom transfer reaction.

More interestingly is the analysis of the peaks that result from the O-transfer channel. In this case, not only the expected product ([Fe^{III}(OD)(^{5tips3}tpa)]$^{2+}$, *m/z* = 416.3) was observed, but in addition, a peak at m/z 415.8 was also found in the spectrum, in accordance with the

replacement of the OD group by an OH. These peaks cannot be fully explained by an epoxidation reaction and instead point towards an additional oxygen atom transfer reaction. The data can be rationalized considering a two-step rebound mechanism, in which a first hydrogen atom abstraction from the allylic position of the substrate is followed by the rebound with the OH or the OD group of the incipient $[Fe^{IV}(OD)(OH)(^{5tips3}tpa)]^{2+}$ intermediate (Scheme VII.5).

Finally, a peak at m/z = 454.90 can be assigned to the product resulting from H_2O/DHO elimination from the initial *syn*-dihydroxylated substrate-complex (m/z = 464, Scheme VII.5b).
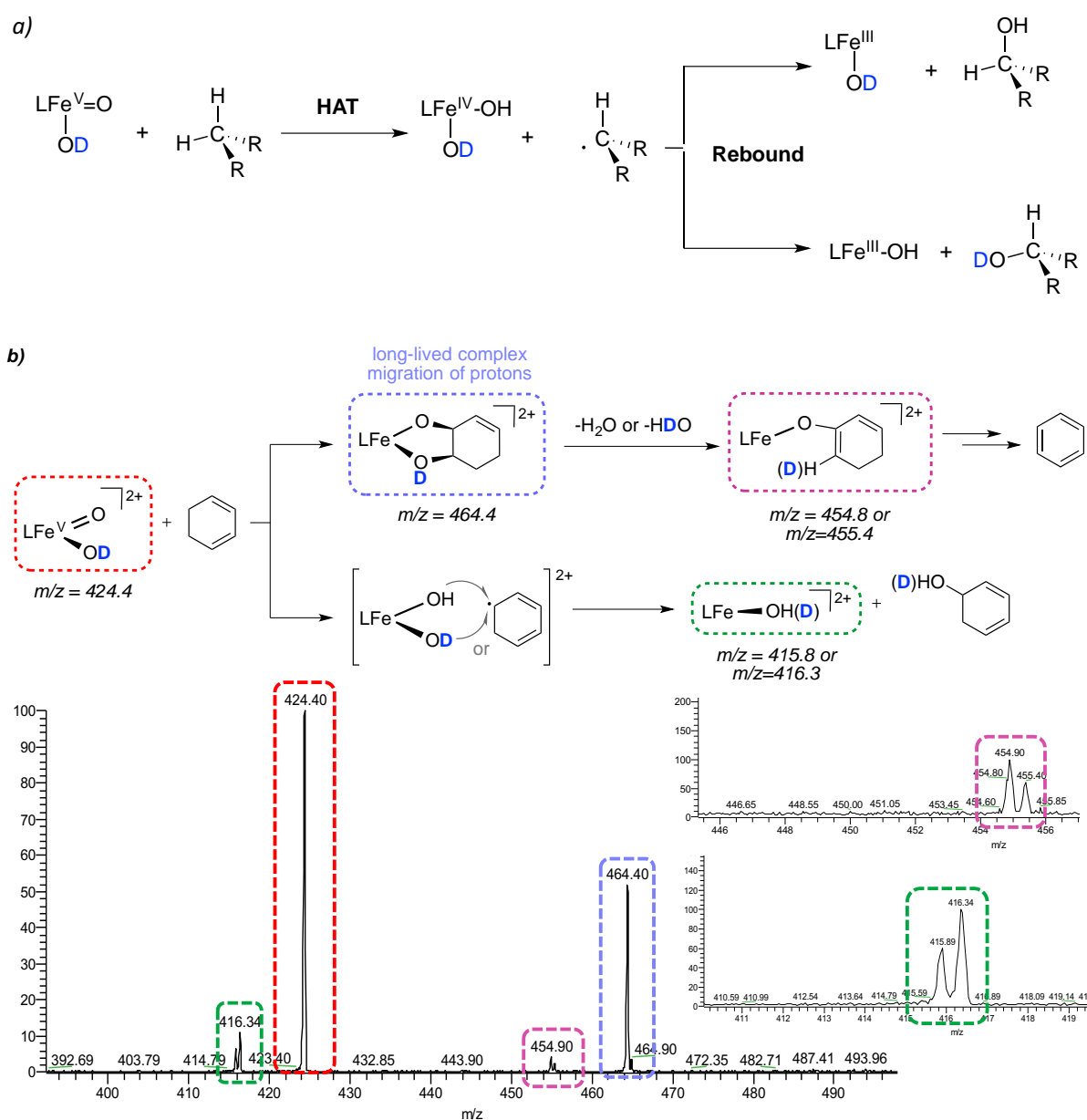
Scheme VII.5. a) Proposed two-steps rebound mechanism. b) Reactivity of $[Fe^V(O)(OD)(^{5\text{-}tips3}tpa)]^{2+}$ in the gas phase with 0.1 mTorr of 1,3-cyclohexadiene.

Finally, the reactivity with aromatic compounds (i.e. deuterated benzene, naphthalene) was investigated. These reactions are interesting because the *syn*-dihydroxylation of these compounds cannot be achieved by conventional methods based on Ru and Os oxides, and is performed exclusively by enzymes. In both cases, the peak corresponding to the intermediate for the addition products followed by dehydration was observed in the spectrum, suggesting that the isolated Fe(V) intermediate can perform *syn*-dihydroxylation in gas phase of these aromatic substrates (Scheme VII.6).

Interestingly, in the case of naphthalene, a monocharged peak at m/z 847 was found in the spectrum, consistent with a $Fe^{IV}(O)(OH)$ species. This represents a single electron transfer reaction between the Fe(V) and the naphthalene, that finally generates a naphthalene radical cation, that is also observed in the mass spectrum (m/z = 128). Therefore, and considering that in gas phase only exothermic reactions occur, the 1e- reduction potential for the $Fe^{V}(O)(OH)$ species can be deduced to be higher than 8.14 eV (ionization energy for naphthalene). If this value is compared with the reduction potential of Fe(IV) porphyrin cation radicals considered as CpdI models, that is always lower than 7.5 eV, it can be concluded that the $Fe^{V}(O)(OH)$ characterized in this section is a more powerful oxidant than the CpdI models.
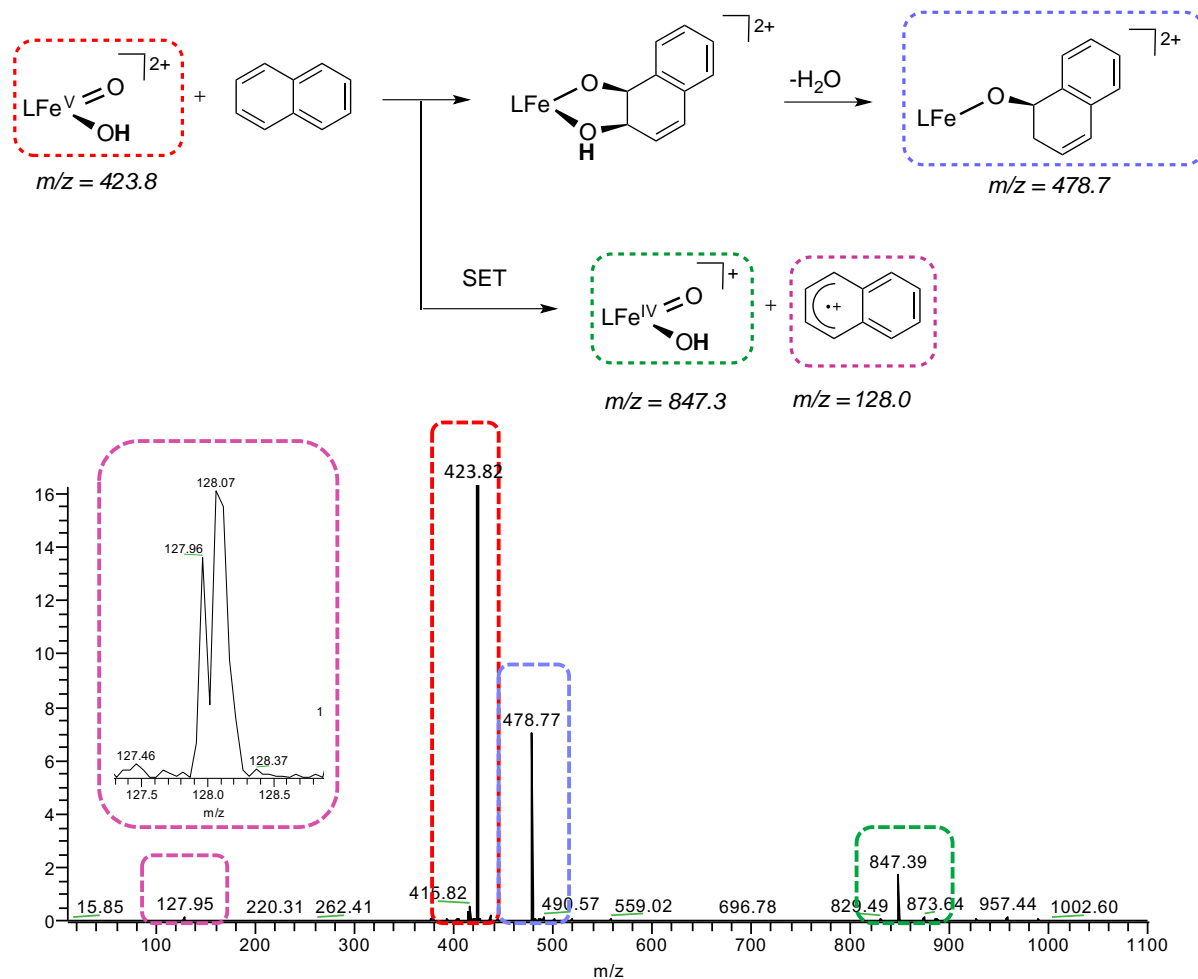
**Scheme VII.6.** Reactivity of [Fe^V(O)(OH)($^{5\text{-tips3}}$tpa)]$^{2+}$ in the gas phase with 0.1 mTorr of naftalene.

To summarize, in this section we described the formation and characterization of a Fe^V(O)(OH) species in the gas phase using helium tagging infrared photodissociation spectroscopy and the [Fe(OTf)$_2$($^{5\text{-tips3}}$tpa)] complex described in previous chapters. The Fe^V=O and Fe^V-OH stretching frequencies have been identified, as well as the vibrational spectroscopic features of the *cis*-Fe^V(O)(OH) unit. In addition, reactivity studies revealed that this intermediate can perform *syn*-dihydroxylation of arenes, as well as the hydroxylation of aliphatic C-H bonds via a rebound mechanism. Overall, this constitutes the first experimental evidence for this type of C-H and C=C functionalization mechanism, that before this work, was only supported computationally. Of notice, the catalyst employed in this study is a prototypical example of a Class A type of catalyst and therefore the conclusions apply to this subgroup of catalysts. The identity of the active species in Class B catalysts remain under discussion.

VII.4. Site-Selective and Product Chemoselective Aliphatic C−H Bond Hydroxylation of Polyhydroxylated Substrates

As discussed in Chapter I, chemoselective and site-selective hydroxylation of unactivated aliphatic C-H bonds is a challenging reaction, mainly due to the multiple C-H bonds presents in most organic molecules, with similar structural characteristics and chemical properties.[54] Furthermore, the higher reactivity of the hydroxyl groups of primary and secondary alcohols in comparison with the C-H bonds of alkyl groups makes overoxidation of the first formed alcohol products difficult to prevent, eroding product chemoselectivity.[55-56] In addition, polyhydroxylated substrates easily undergo oxidative C-C bond cleavage.[57] For these reasons, selective C-H bond hydroxylation in this kind of molecules, without using protecting groups, is an unresolved challenge in organic synthesis.

It has been previously described by our group and others, that the use of fluorinated alcohols as solvents can strongly deactivate the electron rich α-C-H bond to the hydroxyl groups, in simple primary and secondary alcohols.[58-63] This is due to a polarity reversal effect caused by the strong hydrogen donor ability of the O-H bond of the solvent and the hydroxyl group of the alcohol. This interaction removes electron density from the proximal C-H bonds, directing the oxidation towards more remote positions, and thus preventing overoxidation (Scheme VII.7).
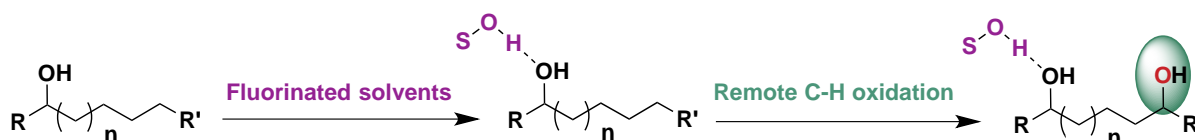
Scheme VII.7. Oxidation path using fluorinated alcohol solvents (S-OH).

Taking advantage of this strategy, we considered the possibility to selectively oxidize aliphatic C-H bonds in unprotected polyhydroxylated molecules. The oxidation of this kind of molecules becomes more difficult because of the number of the hydroxyl groups present, that moreover can interact with the metal catalyst due to their chelating ability.

VII.4.1. Reaction optimization and development

To achieve this challenging goal, we first tested the oxidation of 1,2-octanediol (**S1**), that was chosen as model substrate in different solvents (MeCN, TFE, HFIP) using 1 mol% of (*S,S*)-

[Mn (OTf)$_2$(^{tips}mcp)], (Figure VII.9), 2 equivalents of acetic acid and 1 equivalent of H$_2$O$_2$ solution added by syringe pump during 30 minutes.

(S,S)-[M(OTf)$_2$(^{DMM}pdp)]　　**(S,S)-[M(OTf)$_2$(^{tips}mcp)]**　　**(S,S)-[Mn(OTf)$_2$(^{tips}pdp)]**　　**(R,R)-[Fe(OTf)$_2$(^{tips}pdp)]**
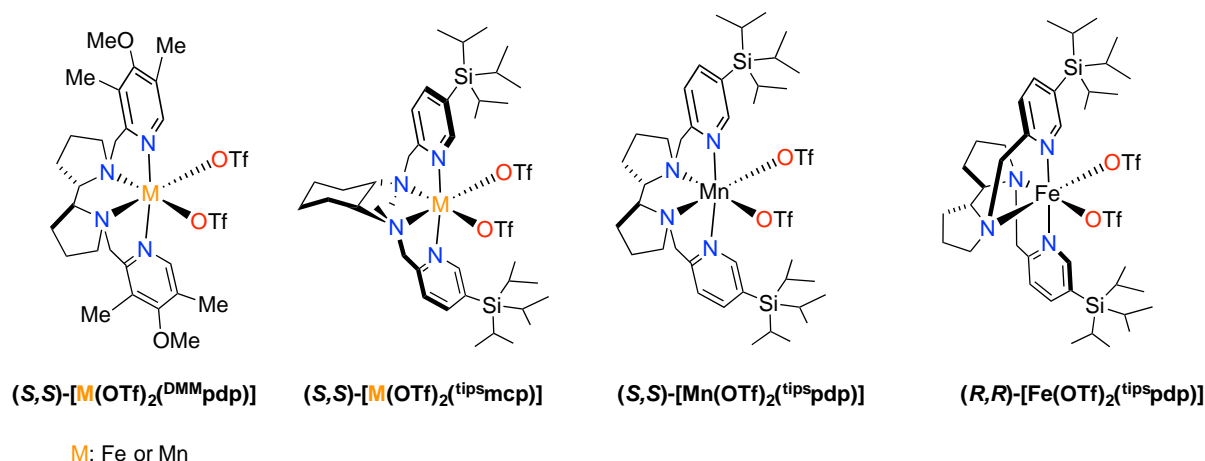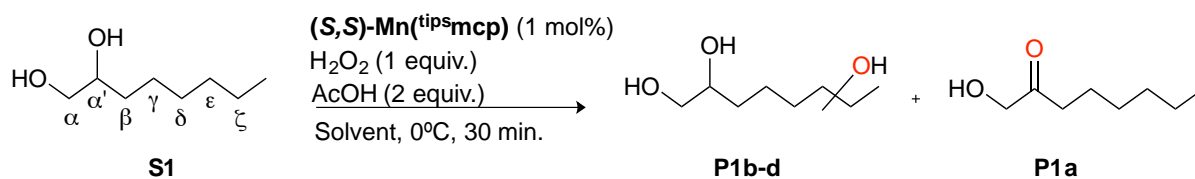
M: Fe or Mn

Figure VII.9. Catalysts tested

The use of MeCN leads to modest substrate conversion and the only oxidation product detected was 1-hydroxy-2-octanone (**P1a**) in 21% yield. This product results from the over oxidation of one of the alcohols of the starting diol, and its formation can be substantially reduced when the reaction was performed in fluorinated alcohol solvents. When TFE and HFIP were used, a higher substrate conversion was obtained and the major oxidation product was the diol **P1b**, resulting from C-H hydroxylation at the most remote methylenic position from the diol moiety, with minor amount of regioisomeric triols in δ (**P1d**) and ε (**P1c**) position. Only trace amounts of ketone **P1a** were detected. It is interesting to notice that the selectivity towards the most remote alcohol is higher with HFIP than TFE, in line with the strength of the hydrogen-bond donor ability of the solvents (Table VII.6).

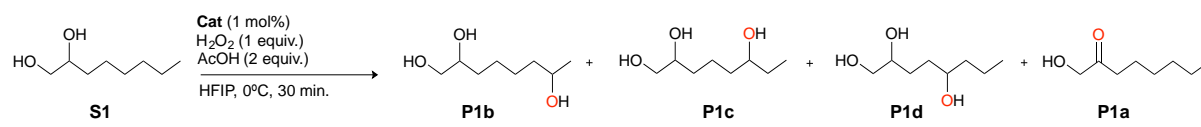**Table VII.6.** Catalytic oxidation of **S1** in different solvents.

Solvent	Conv. (%)[a]	P1b-d Yield (%)[a] (δ:ε:ζ ratio)	P1a Yield (%)[a]
CH$_3$CN	28	0	21
TFE	52	22(6:25:69)	5
HFIP	77	62(5:16:79)	1

[a] Yields determined by GC

The reaction in HFIP was then tested using a series of iron and manganese catalysts previously used in C-H bond hydroxylation reactions (Figure VII.9).[26, 64-66] The same trend in chemo- and regioselectivity is observed in all of them; being the manganese catalysts the ones providing the highest yields. Among them, **Mn(^{tips}mcp)**[67] gave the bests results (Table VII.7).
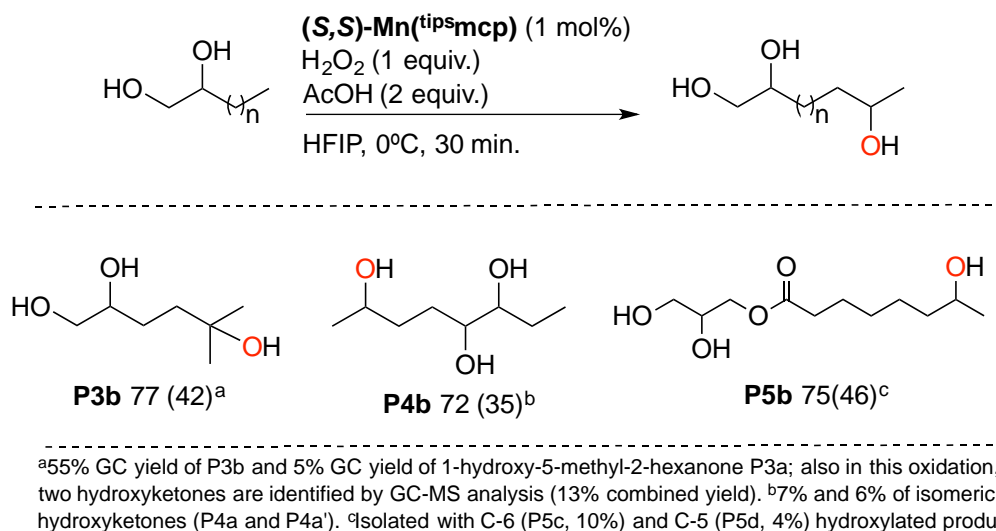
Table VII.7. Screening of a series of related iron and manganese catalysts.

Cat	Conv. (%)[a]	P1b (%)[a]	Yield	P1c (%)[a]	Yield	P1d (%)[a]	Yield	P1a (%)[a]	Yield
S,S Mn^{DMM}pdp	71	49		17		4		2	
***S,S* Mn^{tips}mcp**	**77**	**49**		**10**		**3**		**1**	
S,S Mn^{tips}pdp	73	48		11		3		1	
R,R Fe^{tips}pdp	67	41		14		4		1	
S,S Fe^{DMM}pdp	43	27		9		4		3	
S,S Fe^{tips}mcp	60	36		12		2		2	

[a] Conversion and yields determined by GC. Reactions were run in duplicate. Values included in table **2** represent average values with typical errors being <5%.

Under the optimized conditions we then explored a series of polyhydroxylated molecules. Preferential oxidation at the most remote position was observed with 1,2-diol substrates, and only small amounts of ketoalcohol formed by HAT initiated α-C-H bond hydroxylation are detected (Table VII.7, Figure VII.10 and Scheme VII.8). With 1,2-octanediol (**S1**) as substrate, the oxidation occurs preferentially at the most remote methylenic site in 49% yield (**P1b**), accompanied by small amount of **P1c** and **P1d** (Table VII.7). 1,2-hexanediol (**S2**) gives 39% yield of **P2b**, and only 11% yield of 1-hydroxy-2-hexanone (**P2a**) (Figure VII.6). The same oxidation pattern is observed with 5-methyl-1,2-hexanediol (**S3**), where the major oxidation product is **P3b** in 42% and 5% of 1-hydroxy-5-methyl-2-hexanone **P3a**. Analogous observation derive for the oxidation of **S4** and **S5** substrates, where the major oxidation occurs at the most remote methylenic site in 35% and 45% yield respectively, while hydroxyketone product is obtained as a minor product (**P4a)** in the oxidation of **S4** and 14% yield combined of hydroxylated product **P5c-d** with **S5** as substrate (Scheme VII.8).

(S,S)-Mn(tipsmcp) (1 mol%)
H₂O₂ (1 equiv.)
AcOH (2 equiv.)
HFIP, 0ºC, 30 min.

P3b 77 (42)[a]   **P4b** 72 (35)[b]   **P5b** 75(46)[c]

[a]55% GC yield of P3b and 5% GC yield of 1-hydroxy-5-methyl-2-hexanone P3a; also in this oxidation, two hydroxyketones are identified by GC-MS analysis (13% combined yield). [b]7% and 6% of isomeric hydroxyketones (P4a and P4a'). [c]Isolated with C-6 (P5c, 10%) and C-5 (P5d, 4%) hydroxylated products.

Scheme VII.8. Catalytic oxidation of 1,2-diol substrate.

Interestingly, by comparing the oxidation of **S1** with 1,2-hexanediol (**S2**) it can be deduced that as the larger is the alkyl chain, the higher is the product yield and the chemoselectivity for the remote C-H hydroxylation. (Figure VII.10) Improvement of both parameters can be explained by the reduction of the polarity reversal deactivating effect as C-H bonds are further away from the polar diol moiety.

P2, Conv: 64%   **P1,** Conv: 83%

As the larger is the alkyl chain

Higher Yield
Higher Chemoselectivity
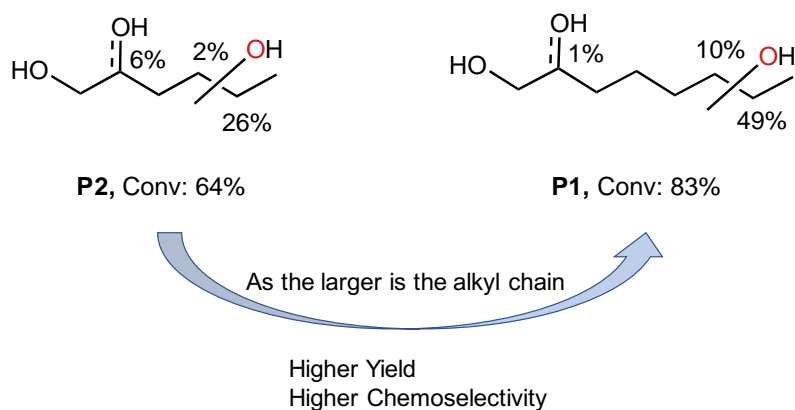
Figure VII.10. Catalytic oxidation of **S1** and **S2** substrates with optimized conditions.

The oxidation of 1,2-cycloalkanediols was then tested. Oxidation of *cis*-1,2-cyclopentanediol (***cis*-S6**) and *cis*-1,2-cyclohexanediol (***cis*-S7**) gave selectively the corresponding hydroxyketone product in a good yield (for **P6a** 54% and for **P7a** 64% yield) and modest to good enantioselectivity (29% and 63% ee, respectively). Oxidation of the racemic mixture of ***trans*-S7** produce a 66% yield of racemic hydroxyketone. The oxidation of ***cis*-S8 (***cis*-1,2-cyclohepta) have a 52% of hdroxyketone (P8a) with 42% ee alone with 7% of 1,2,5-cycloheptanetriol (**P8b**). As ring size increases, the chemoselectivity of the reaction

completely changes, and the triol resulting from the oxidation at the most remote C-H bond is obtained as the major product. These results indicate that the C-H bond deactivation by the hydrogen bond donor ability of the solvent occurs in an effective manner up to position γ, leading to a chemoselective hydroxylation in δ-position. Consequently, the oxidation of *cis*-1,2-cyclooctanediol (*cis*-**S9**) provide a 40% yield of 1,2,5-cyclooctanetriol (*cis*-**P9b**) and 17% yield of 1,2,4-cyclooctanetriol (*cis*-**P9c**) alone with only 17% of kydroxyketone product (**P9a**).
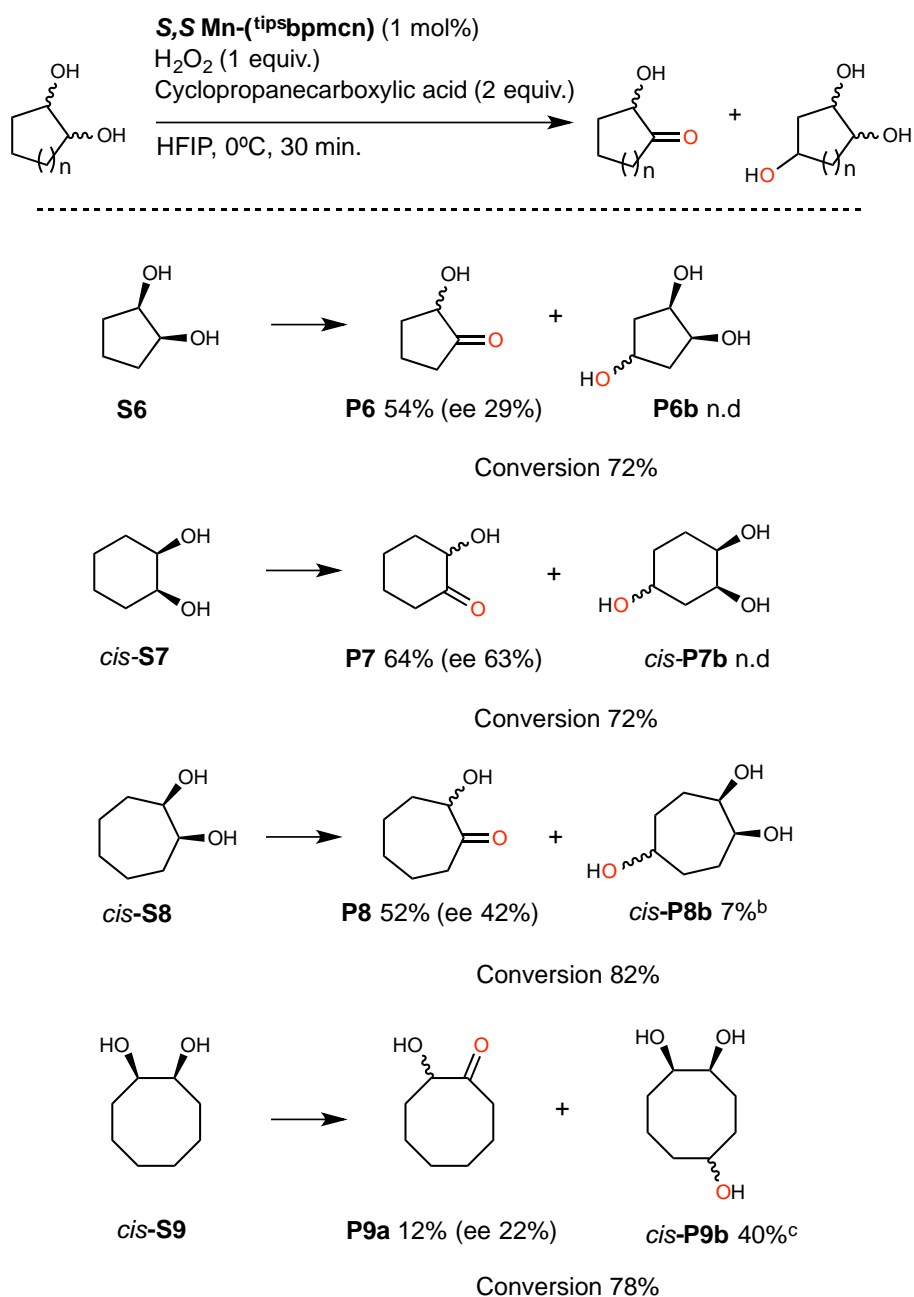
Scheme VII.9. Catalytic oxidation of 1,2-cycloalkanediols.

VII.4.2. Application to complex molecules

The results observed with simple 1,2-diol substrates led us to consider the possibility to translate the chemoselectivity of the reaction to more densely functionalized substrates. To test this hypothesis the oxidation of different unprotected glucoside derivatives was studied.[68] The oxidation of glucopyranoside (**S10**) is selective to the most remote tertiary C-H bond (74 % yield), without affecting the unprotected hydroxyls of the molecule. The same tendency was observed when 1-hexyl β-D-glucopyranoside (**S12**) was tested obtaining a 53 % yield of the polyol resulting from oxidation at the most methylenic site. In addition, oxidation and the next methylenic side was also observed as side product in 12 % yield. After a short optimization we identified that the ((*R,R*)-Fe[tips]pdp) catalyst was the optimum choice for this kind of substrates.

Other interesting substrate was Capecitabine (**P13**), a drug used to treat different types of cancer, including mammarial and rectal ones. Its functionalization is challenging due to its highly functionalized core, composed by a polyhydroxylated five-membered ring, a fluorinated N-heterocycle and different functional groups units such as urea that can easily chelate a metal center and deactivate the catalyst. Remarkably, hydroxylation on this substrate occurs at the most remote methylenic site of the urea substituents without altering the core of the drug.

*a*3 mol % catalyst. Isolated with P12c (12% yield, total yield 65%). *b*Along with 12% of the corresponding carbonyl derivative (total yield 62%).
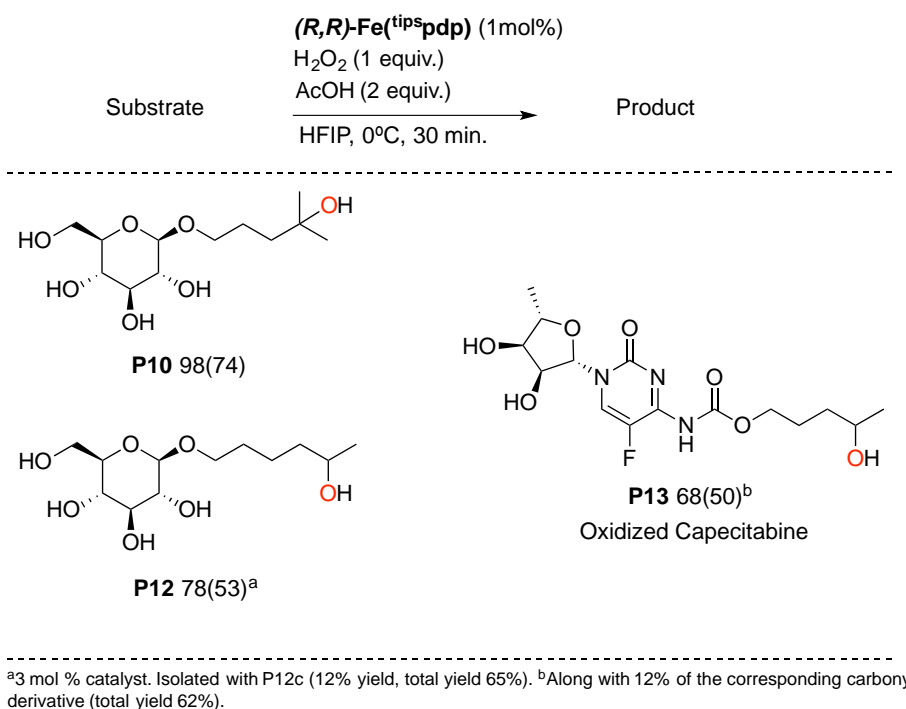
Scheme VII.10. Catalytic oxidation of polyfuntional molecules. Conversion(yield).

Finally, we tested the reaction with steroidal substrates containing hydroxyls groups. To control the selectivity of the oxidation of steroids is an important issue, as it is well-known that the oxidation pattern can modify its recognition in biological systems.

The oxidation of unprotected lithocholic acid methyl ester (**S14**) gave two diol products in a combined 52% yield; the diol resulting from the oxidation of the tertiary C-5 (**P14b**) is obtained in 34% yield and oxidation of the secondary C-6 (**P14c**) is observed in 18% yield. Overoxidation of the alcohol present in the starting substrate is only observed in 5% yield.

Then, the oxidation of ursodeoxycholic acid methyl ester (**S15**), which incorporates an additional hydroxyl group was tested, and the product resulting of the hydroxylation of the tertiary C-5 (**P15b**) was achieved in 17% yield, and again only a small amount of overoxidation of the starting substrate was observed (8% yield). The incorporation of a third hydroxyl group in the substrate as in the cholic acid methyl ester (**S16**) completely deactivate the substrates, avoiding the reaction. The reduced product yields upon introduction of hydroxyl moieties presumably reflects an increased deactivation of the increasingly polarized substrates in the fluorinated alcohol solvents.

To note that, product arising from decarboxylation of the acid where not detected although low molecular weight product may be skipped CG analysis, therefore competitive oxidation of the carboxylic acid cannot be fully discarded.
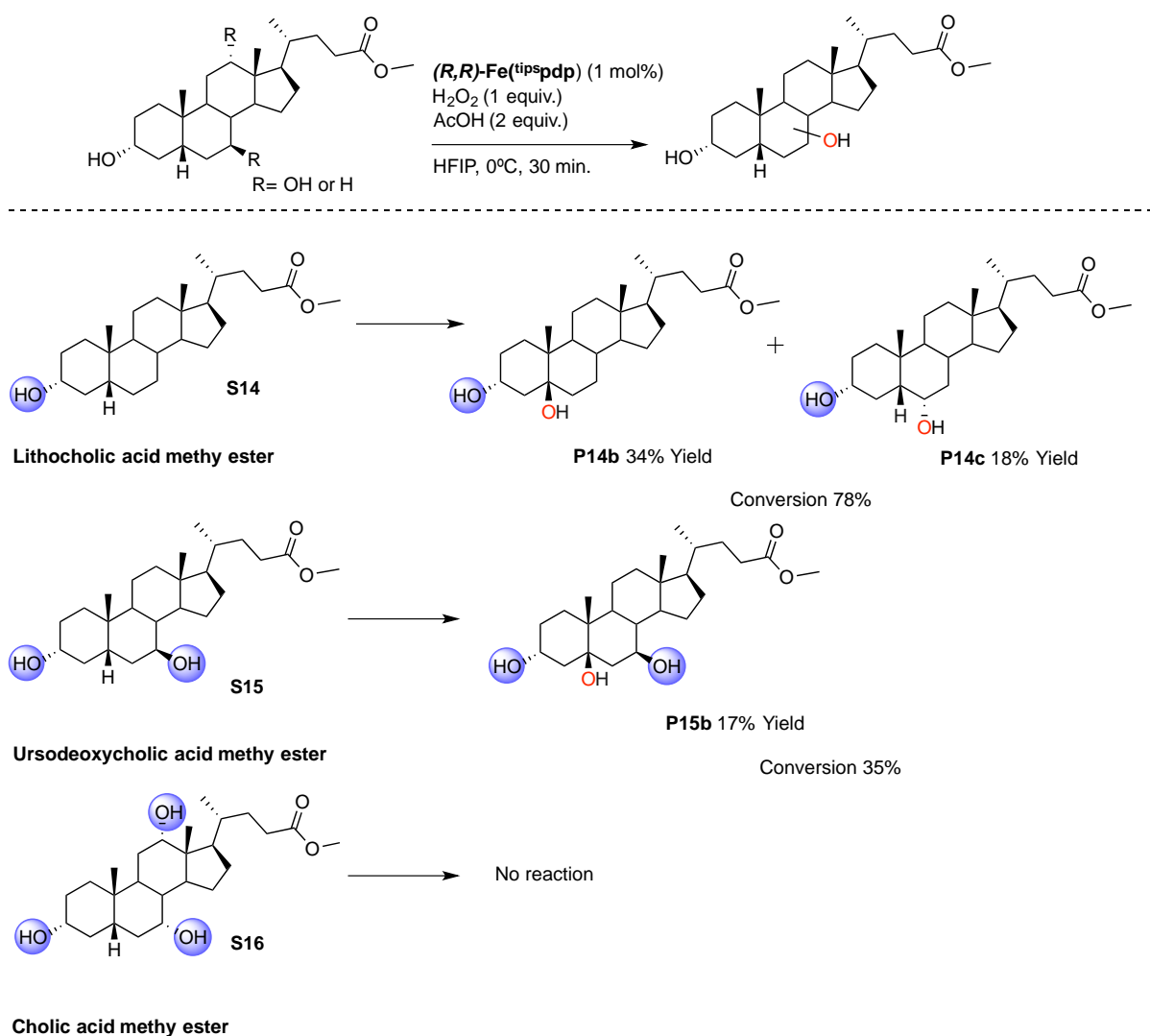
Scheme VII.11. Catalytic oxidation of different steroidal substrates containing hydroxyls groups.

To summarize, in this chapter it has been demonstrated that the use of fluorinated alcohol solvents can be used to control the site-selectivity and the chemoselectivity of the metal-catalyzed hydroxylation of complex polyhydroxylated molecules. HFIP has been found as the best solvent. The solvent interacts via hydrogen bonding with the hydroxyls of the substrate, removing electron density avoiding its overoxidation and deactivating the most proximal sites. Oxidation of complex molecules of biological interest, such as glucosides and steroids, have been performed with high selectivity and good yields.

VII.5. References

(1)   Bataille, C. J. R.; Donohoe, T. J., Osmium-free direct syn-dihydroxylation of alkenes. *Chem. Soc. Rev.* **2011,** *40*, 114-128.

(2)   Kolb, H. C.; VanNieuwenhze, M. S.; Sharpless, K. B., Catalytic Asymmetric Dihydroxylation. *Chem. Rev.* **1994,** *94*, 2483-2547.

(3)   Zaitsev, A. B.; Adolfsson, H., Recent developments in asymmetric dihydroxylations. *Synthesis* **2006,** (11), 1725-1756.

(4)   Shing, T. K. M.; Tam, E. K. W.; Tai, V. W. F.; Chung, I. H. F.; Jiang, Q., Ruthenium-catalyzed cis-dihydroxylation of alkenes: Scope and limitations. *Chem. Eur. J.* **1996,** *2* (1), 50-57.

(5)   Sugimoto, H.; Kitayama, K.; Mori, S.; Itoh, S., An Osmium(III)/Osmium(V) Redox Couple Generating Os-V(O)(OH) Center for cis-1,2-Dihydroxylation of Alkenes with H2O2: Os Complex with a Nitrogen-Based Tetradentate Ligand. *J. Am. Chem. Soc.* **2012,** *134* (46), 19270-19280.

(6)   Yip, W. P.; Ho, C. M.; Zhu, N.; Lau, T. C.; Che, C. M., Homogeneous [RuIII(Me3tacn)Cl3]-Catalyzed Alkene cis-Dihydroxylation with Aqueous Hydrogen Peroxide. *Chem. Asian J.* **2008,** *3* (1), 70-77.

(7)   Rawling, M. J.; Tomkinson, N. C. O., Metal-free syn-dioxygenation of alkenes. *Org. Biomol. Chem.* **2013,** *11* (9), 1434-1440.

(8)   Colomer, I.; Barcelos, R. C.; Christensen, K. E.; Donohoe, T. J., Orthogonally Protected 1,2-Diols from Electron-Rich Alkenes Using Metal-Free Olefin syn-Dihydroxylation. *Org. Lett.* **2016,** *18* (22), 5880-5883.

(9)   Griffith, J. C.; Jones, K. M.; Picon, S.; Rawling, M. J.; Kariuki, B. M.; Campbell, M.; Tomkinson, N. C. O., Alkene Syn Dihydroxylation with Malonoyi Peroxides. *J. Am. Chem. Soc.* **2010,** *132* (41), 14409-14411.

(10)   De Vos, D. E.; de Wildeman, S.; Sels, B. F.; Grobet, P. J.; Jacobs, P. A., Selective alkene oxidation with H2O2 and a heterogenized Mn catalyst: Epoxidation and a new entry to vicinal cis-diols. *Angew. Chem. Int. Ed.* **1999,** *38* (7), 980-983.

(11)   Saisaha, P.; Pijper, D.; Summerren, R. P. v.; Hoen, R.; Smit, C.; Boer, J. W. d.; Hage, R.; Alsters, P. L.; Feringa, B. L.; Browne, W. R., Manganese catalyzed cis-hydroxilation of electron deficient alkenes with H2O2. *Org. Biomol. Chem.* **2010,** *8*, 4444-4450.

(12)   de Boer, J. W.; Browne, W. R.; Harutyunyan, S. R.; Bini, L.; Tiemersma-Wegman, T. D.; Alsters, P. L.; Hage, R.; Feringa, B. L., Manganese catalysed asymmetric cis-dihydroxylation with H2O2. *Chem. Commun.* **2008,** (32), 3747-3749.

(13)   Boer, J. W. d.; Brinksma, J.; Browne, W. R.; Meetsma, A.; Alsters, P. L.; Hage, R.; Feringa, B. L., cis-Dihydroxylation and Epoxidation of Alkenes by [Mn2O(RCO2)2(tmtacn)2]: Tailoring the Selectivity of a Highly H2O2-Efficient Catalyst *J. Am. Chem. Soc.* **2005,** *127* (22), 7990-7991.

(14)   Karlsson, A.; Parales, J. V.; Parales, R. E.; Gibson, D. T.; Eklund, H.; Ramaswamy, S., Crystal Structure of Naphthalene Dioxygenase: Side-on Binding of Dioxygen to Iron. *Science* **2003,** *299*, 1039-1042.

(15)   Wolfe, M. D.; Lipscomb, J. D., Hydrogen Peroxide-coupled cis-Diol Formation Catalyzed by Naphthalene 1,2-Dioxygenase. *J. Biol. Chem.* **2003,** *278* (2), 829-835.

(16)   Kovaleva, E. G.; Lipscomb, J. D., Versatility of biological non-heme Fe(II) centers in oxygen activation reactions. *Nat. Chem. Biol.* **2008,** *4* (3), 186-193.

(17)   Feng, Y.; Ke, C.-y.; Xue, G.; Que Jr., L., Bio-inspired arene cis-dihydroxylation by a non-haem iron catalyst modeling the action of naphthalene dioxygenase *Chem. Commun.* **2009,** (1), 50-52.

(18)   Borrell, M.; Costas, M., Mechanistically Driven Development of an Iron Catalyst for Selective Syn-Dihydroxylation of Alkenes with Aqueous Hydrogen Peroxide. *J. Am. Chem. Soc.* **2017,** *139* (36), 12821-12829.

(19)   Wei, J.; Wu, L.; Wang, H.-X.; Zhang, X.; Tse, C.-W.; Zhou, C.-Y.; Huang, J.-S.; Che, C.-M., Iron-Catalyzed Highly Enantioselective cis-Dihydroxylation of Trisubstituted Alkenes with Aqueous H2O2. *Angew. Chem. Int. Ed.* **2020,** *59* (38), 16561-16571.

(20)   Zang, C.; Liu, Y.; Xu, Z.-J.; Tse, C.-W.; Guan, X.; Wei, J.; Huang, J.-S.; Che, C.-M., Highly Enantioselective Iron-Catalyzed cis-Dihydroxylation of Alkenes with Hydrogen Peroxide Oxidant via an FeIII-OOH Reactive Intermediate. *Angew. Chem. Int. Ed.* **2016,** *55* (35), 10253-10257.

(21)   Ryu, J. Y.; Kim, J.; Costas, M.; Chen, K.; Nam, W.; Que Jr., L., High Conversion of Olefins to cis-Diols by Non-heme Iron Catalysts and H2O2. *Chem. Commun.* **2002,** *12*, 1288-1289.

(22)   Prat, I.; Company, A.; Corona, T.; Parella, T.; Ribas, X.; Costas, M., Assessing the Impact of Electronic and Steric Tuning of the Ligand in the Spin State and Catalytic Oxidation Ability of the Fe. *Inorg. Chem.* **2013,** *52*, 9229−9244-9229−9244.

(23)   Chow, T. W.-S.; Wong, E. L.-M.; Guo, Z.; Liu, Y.; Huang, J.-S.; Che, C.-M., cis-Dihydroxylation of Alkenes with Oxone Catalyzed by Iron Complexes of a Macrocyclic Tetraaza Ligand and Reaction Mechanism by ESI-MS Spectrometry and DFT Calculations. *J. Am. Chem. Soc.* **2010,** *132* (38), 13229-13239.

(24)   Chen, K.; Costas, M.; Kim, J.; Tipton, A. K.; Que, L., Olefin Cis-Dihydroxylation versus Epoxidation by Non-Heme Iron Catalysts: Two Faces of an FeIII−OOH Coin. *J. Am. Chem. Soc.* **2002,** *124* (12), 3026-3035.

(25) Chen, K.; Que Jr., L., cis-Dihydroxylation of Olefins by a Non-Heme Iron Catalyst: A Functional Model for Rieske Dioxygenases. *Angew. Chem. Int. Ed.* **1999,** *38* (15), 2227-2229.

(26) Font, D.; Canta, M.; Milan, M.; Cusso, O.; Ribas, X.; Gebbink, R. J. M. K.; Costas, M., Readily Accessible Bulky Iron Catalysts exhibiting Site Selectivity in the Oxidation of Steroidal Substrates. *Angew. Chem. Int. Ed.* **2016,** *55* (19), 5776-5779.

(27) Kojima, T.; Leising, R. A.; Yan, S.; Que, L., Alkane functionalization at nonheme iron centers. Stoichiometric transfer of metal-bound ligands to alkane. *J. Am. Chem. Soc.* **1993,** *115* (24), 11328-11335.

(28) Jang, H. G.; Cox, D. D.; Que, L., A highly reactive functional model for the catechol dioxygenases. Structure and properties of [Fe(TPA)DBC]BPh4. *J. Am. Chem. Soc.* **1991,** *113* (24), 9200-9204.

(29) Prat, I.; Mathieson, J. S. J. S.; Güell, M.; Ribas, X.; Luis, J. M. J. M.; Cronin, L.; Costas, M., Observation of Fe(V)=O using variable-temperature mass spectrometry and its enzyme-like C–H and C=C oxidation reactions. *Nat. Chem.* **2011,** *3* (10), 788-793.

(30) Fujita, M.; Costas, M.; Que Jr., L., Iron Catalyzed Olefin Cis-Dihydroxylation by H2O2: Electrophilic versus Nucleophilic Mechanisms. *J. Am. Chem. Soc.* **2003,** *125* (33), 9912-9913.

(31) Prat, D.; Hayler, J.; Wells, A., A survey of solvent selection guides. *Green Chem.* **2014,** *16* (10), 4546-4551.

(32) Shing, T. K. M.; Tai, V. M. F.; Tam, E. K. W., Practical and Rapid Vicinal Hydroxylation of Alkenes by Catalytic Ruthenium Tetraoxide. *Angew. Chem. Int. Ed.* **1994,** *33* (22), 2312-2313.

(33) Prat, I.; Font, D.; Company, A.; Junge, K.; Ribas, X.; Beller, M.; Costas, M., Fe(PyTACN)-Catalyzed cis-Dihydroxylation of Olefins with Hydrogen Peroxide. *Adv. Synth. Catal.* **2013,** *355* (5), 947-956.

(34) Sheldon, R. A., Metrics of Green Chemistry and Sustainability: Past, Present, and Future. *ACS Sustainable Chem. Eng.* **2018,** *6* (1), 32-48.

(35) Huang, X.; Groves, J. T., Oxygen Activation and Radical Transformations in Heme Proteins and Metalloporphyrins. *Chem. Rev.* **2018,** *118* (5), 2491-2553.

(36) McDonald, A. R.; Que, L., High-valent nonheme iron-oxo complexes: Synthesis, structure, and spectroscopy. *Coord. Chem. Rev.* **2013,** *257* (2), 414-428.

(37) de Oliveira, F. T.; Chanda, A.; Banerjee, D.; Shan, X.; Mondal, S.; Que, L.; Bominaar, E. L.; Münck, E.; Collins, T. J., Chemical and Spectroscopic Evidence for an FeV-Oxo Complex. *Science* **2007,** *315* (5813), 835.

(38)   Van Heuvelen, K. M.; Fiedler, A. T.; Shan, X.; De Hont, R. F.; Meier, K. K.; Bominaar, E. L.; Münck, E.; Que, L., One-electron oxidation of an oxoiron(IV) complex to form an [O=FeV=NR]+ center. *Proc. Nat. Acad. Sci.* **2012,** *109* (30), 11933.

(39)   Ghosh, M.; Singh, K. K.; Panda, C.; Weitz, A.; Hendrich, M. P.; Collins, T. J.; Dhar, B. B.; Sen Gupta, S., Formation of a Room Temperature Stable FeV(O) Complex: Reactivity Toward Unactivated C–H Bonds. *J. Am. Chem. Soc.* **2014,** *136* (27), 9524-9527.

(40)   Fan, R.; Serrano-Plana, J.; Oloo, W. N.; Draksharapu, A.; Delgado-Pinar, E.; Company, A.; Martin-Diaconescu, V.; Borrell, M.; Lloret-Fillol, J.; García-España, E.; Guo, Y.; Bominaar, E. L.; Que, L.; Costas, M.; Münck, E., Spectroscopic and DFT Characterization of a Highly Reactive Nonheme FeV–Oxo Intermediate. *J. Am. Chem. Soc.* **2018,** *140* (11), 3916-3928.

(41)   Barry, S. M.; Challis, G. L., Mechanism and Catalytic Diversity of Rieske Non-Heme Iron-Dependent Oxygenases. *ACS Catal.* **2013,** *3* (10), 2362-2370.

(42)   Li, F.; Meier, K. K.; Cranswick, M. A.; Chakrabarti, M.; Van Heuvelen, K. M.; Münck, E.; Que, L., Characterization of a High-Spin Non-Heme FeIII–OOH Intermediate and Its Quantitative Conversion to an FeIV=O Complex. *J. Am. Chem. Soc.* **2011,** *133* (19), 7256-7259.

(43)   Olivo, G.; Cussó, O.; Borrell, M.; Costas, M., Oxidation of alkane and alkene moieties with biologically inspired nonheme iron catalysts and hydrogen peroxide: from free radicals to stereoselective transformations. *J. Biol. Inorg. Chem.* **2017,** *22* (2), 425-452.

(44)   Serrano-Plana, J.; Oloo, W. N.; Acosta-Rueda, L.; Meier, K. K.; Verdejo, B.; García-España, E.; Basallote, M. G.; Münck, E.; Que, L.; Company, A.; Costas, M., Trapping a Highly Reactive Nonheme Iron Intermediate That Oxygenates Strong C—H Bonds with Stereoretention. *J. Am. Chem. Soc.* **2015,** *137* (50), 15833-15842.

(45)   Serrano-Plana, J.; Aguinaco, A.; Belda, R.; García-España, E.; Basallote, M. G.; Company, A.; Costas, M., Exceedingly Fast Oxygen Atom Transfer to Olefins via a Catalytically Competent Nonheme Iron Species. *Angew. Chem. Int. Ed.* **2016,** *55* (21), 6310-6314.

(46)   Xu, S.; Veach, J. J.; Oloo, W. N.; Peters, K. C.; Wang, J.; Perry, R. H.; Que, L., Detection of a transient FeV(O)(OH) species involved in olefin oxidation by a bio-inspired non-haem iron catalyst. *Chem. Commun.* **2018,** *54* (63), 8701-8704.

(47)   Ezhov, R.; Ravari, A. K.; Pushkar, Y., Characterization of the FeV=O Complex in the Pathway of Water Oxidation. *Angew. Chem. Int. Ed.* **2020,** *59* (32), 13502-13505.

(48)   Roithová, J.; Gray, A.; Andris, E.; Jašík, J.; Gerlich, D., Helium Tagging Infrared Photodissociation Spectroscopy of Reactive Ions. *Acc. Chem. Res.* **2016,** *49* (2), 223-230.

(49)   Oloo, W. N.; Fielding, A. J.; Que, L., Rate-Determining Water-Assisted O–O Bond Cleavage of an FeIII-OOH Intermediate in a Bio-inspired Nonheme Iron-Catalyzed Oxidation. *J. Am. Chem. Soc.* **2013,** *135* (17), 6438-6441.

(50)   Andris, E.; Navrátil, R.; Jašík, J.; Terencio, T.; Srnec, M.; Costas, M.; Roithová, J., Chasing the Evasive Fe=O Stretch and the Spin State of the Iron(IV)–Oxo Complexes by Photodissociation Spectroscopy. *J. Am. Chem. Soc.* **2017,** *139* (7), 2757-2765.

(51)   Fan, R.; Serrano-Plana, J.; Oloo, W. N.; Draksharapu, A.; Delgado-Pinar, E.; Company, A.; Martin-Diaconescu, V.; Borrell, M.; Lloret-Fillol, J.; García-España, E.; Guo, Y.; Bominaar, E. L.; Que, L.; Costas, M.; Münck, E., Spectroscopic and DFT Characterization of a Highly Reactive Nonheme FeV-oxo Intermediate. *J. Am. Chem. Soc.* **2018**.

(52)   Pattanayak, S.; Jasniewski, A. J.; Rana, A.; Draksharapu, A.; Singh, K. K.; Weitz, A.; Hendrich, M.; Que, L.; Dey, A.; Sen Gupta, S., Spectroscopic and Reactivity Comparisons of a Pair of bTAML Complexes with FeV=O and FeIV=O Units. *Inorg. Chem.* **2017,** *56* (11), 6352-6361.

(53)   Ho, R. Y. N.; Roelfes, G.; Feringa, B. L.; Que, L., Raman Evidence for a Weakened O−O Bond in Mononuclear Low-Spin Iron(III)−Hydroperoxides. *J. Am. Chem. Soc.* **1999,** *121* (1), 264-265.

(54)   Newhouse, T.; Baran, P. S., If C-H Bonds Could Talk: Selective C-H Bond Oxidation. *Angew. Chem. Int. Ed.* **2011,** *50* (15), 3362-3374.

(55)   Bietti, M., Activation and Deactivation Strategies Promoted by Medium Effects for Selective Aliphatic C−H Bond Functionalization. *Angew. Chem. Int. Ed.* **2018,** *57* (51), 16618-16637.

(56)   Hill, C. K.; Hartwig, J. F., Site-selective oxidation, amination and epimerization reactions of complex polyols enabled by transfer hydrogenation. *Nat. Chem.* **2017,** *9*, 1213.

(57)   Spannring, P.; Prat, I.; Costas, M.; Lutz, M.; Bruijnincx, P. C. A.; Weckhuysen, B. M.; Klein Gebbink, R. J. M., Fe(6-Me-PyTACN)-catalyzed, one-pot oxidative cleavage of methyl oleate and oleic acid into carboxylic acids with H2O2 and NaIO4. *Catal. Sci. Technol.* **2014,** *4* (3), 708-716.

(58)   Dantignana, V.; Milan, M.; Cussó, O.; Company, A.; Bietti, M.; Costas, M., Chemoselective Aliphatic C–H Bond Oxidation Enabled by Polarity Reversal. *Acs Cent. Sci.* **2017,** *3* (12), 1350-1358.

(59) P. Roberts, B., Polarity-reversal catalysis of hydrogen-atom abstraction reactions: concepts and applications in organic chemistry. *Chem. Soc. Rev.* **1999,** *28* (1), 25-35.

(60) Wang, D.; Shuler, W. G.; Pierce, C. J.; Hilinski, M. K., An Iminium Salt Organocatalyst for Selective Aliphatic C–H Hydroxylation. *Org. Lett.* **2016,** *18* (15), 3826-3829.

(61) Gaster, E.; Kozuch, S.; Pappo, D., Selective Aerobic Oxidation of Methylarenes to Benzaldehydes Catalyzed by N-Hydroxyphthalimide and Cobalt(II) Acetate in Hexafluoropropan-2-ol. *Angew. Chem. Int. Ed.* **2017,** *56* (21), 5912-5915.

(62) Ottenbacher, R. V.; Talsi, E. P.; Rybalova, T. V.; Bryliakov, K. P., Enantioselective Benzylic Hydroxylation of Arylalkanes with H2O2 in Fluorinated Alcohols in the Presence of Chiral Mn Aminopyridine Complexes. *ChemCamChem* **2018,** *10* (22), 5323-5330.

(63) Adams, A. M.; Du Bois, J., Organocatalytic C–H hydroxylation with Oxone® enabled by an aqueous fluoroalcohol solvent system. *Chem. Sci.* **2014,** *5* (2), 656-659.

(64) Ottenbacher, R. V.; Samsonenko, D. G.; Talsi, E. P.; Bryliakov, K. P., Highly Efficient, Regioselective, and Stereospecific Oxidation of Aliphatic C-H Groups with H2O2, Catalyzed by Aminopyridine Manganese Complexes. *Org. Lett.* **2012,** *14* (17), 4310–4313.

(65) O.Cussó; Garcia-Bosch, I.; Ribas, X.; Lloret-Fillol, J.; Costas, M., Asymmetric Epoxidation with H2O2 by Manipulating the Electronic Properties of Non-heme Iron Catalysts. *J. Am. Chem. Soc.* **2013,** *135* (39), 14871-14878.

(66) Cussó, O.; Garcia-Bosch, I.; Font, D.; Ribas, X.; Lloret-Fillol, J.; Costas, M., Highly Stereoselective Epoxidation with H2O2 Catalyzed by Electron-Rich Aminopyridine Manganese Catalysts. *Org. Lett.* **2013,** *15* (24), 6158-6161.

(67) Milan, M.; Bietti, M.; Costas, M., Highly Enantioselective Oxidation of Nonactivated Aliphatic C-H Bonds with Hydrogen Peroxide Catalyzed by Manganese Complexes. *Acs Cent. Sci.* **2017,** *3* (3), 196-204.

(68) Ogawa, S.; Asakura, K.; Osanai, S., Thermotropic and glass transition behaviors of n-alkyl β-d-glucosides. *RSC Adv.* **2013,** *3* (44), 21439-21446.

Chapter VIII.

Conclusions and Perspectives

In **Chapter III**, the design of a new sterically encumbered iron catalyst permits to achieve high yields and selectivity for *syn*-dihydroxylation reactions of a broad range of olefins, using aqueous H_2O_2 as oxidant. Labelling experiments using $H_2^{18}O$ allows us to identify the position of the oxygen from the water and the oxygen from the H_2O_2 transferred to unsymmetrical olefins. This information has been used to clarify the mechanism of formation of the $Fe^V(O)(OH)$ oxidizing species.

Also, in this **chapter IV** we describe, for the first time, and iron catalyst suitable to perform this transformation in green solvents, achieving similar reactivity and selectivity as observed in acetonitrile media (Chapter III). Remarkably, the in situ generated catalyst performs in a satisfactory manner. For Chapter III and IV, the emerging knowledge from the current work represents a valuable tool to rationally design, in the near future, new catalysts to pursue enantioselectivity. Understanding of the structural aspects of the active species and its molecular shape can serve to identify types of olefins or arenes with matching shapes.

In **Chapter V**, we used gas phase helium tagging infrared photodissociation (IRPD) spectroscopy to characterize the proposed $[Fe^V(O)(OH)(^{5tips3}tpa)]^{2+}$ oxidizing intermediate. These species have long been proposed to be the responsible for oxidation reactions, but the inability to accumulate them in solution, presumably because of their high reactivity has prevented their spectroscopic and chemical characterization. Gas-phase ion spectroscopy characterization methods have allowed us to address this problem. Therefore, this work represents a breakthrough in the field of bioinspired oxidation catalysis, as it provides new information on the nature of the species responsible for the *syn*-dihydroxylation reaction catalyzed by non-heme iron catalysts. However, ideally the next step should be to generate it in a condensed media.

Finally, in **Chapter VI**, site and chemoselective C-H oxidation of polyhdroxylated molecules (such as sugars, steroids and polyfunctional molecules) is described using fluorinated alcohols (TFE and HFIP) as solvents. These solvents exert a strong polarity reversal effect in the hydroxyl moieties via hydrogen bonding and strongly deactivate the proximal C-H bonds. As a result, site-selective and chemoselective oxidation is achieved without having to protect the hydroxyls groups. In order to improve this work,

selectivity patterns induced by the media should be combined with new catalyst structures that reinforce selectivities. For example, steric demand on the catalyst combined with polarity reversal may help concentrate oxidations at the most exposed, remote sites.

Chapter IX.

Experimental Section

Material

Reagents, substrates and solvents used were of commercially available reagent quality unless stated otherwise. Solvents were purchased from SDS, Aldrich, Fluorochem and Scharlab. Solvents were purified and dried by passing through an activated alumina purification system (M-Braun SPS-800) or by conventional distillation techniques. All liquid substrates were filtered through a basic alumina plug before being used.

Instrumentation

NMR experiments were recorded on a Bruker 400 MHz Avance III HD spectrometer equipped with a 5mm BBOF probe. NMR spectra were performed with standard experiments provided in the Bruker release. Spectra were referenced to the residual proto solvents peaks or TMS (tetramethylsilane) for ^{1}H. GC-MS spectral analyses were performed on GS-MS spectral on an Agilent 7890A gas chromatograph interfaced with an Agilent 5975c mass spectrometer with a triple-axis detector. Oxidation products were identified by comparison of their GC retention times, GC analyses were carried out on an Agilent 7820A gas chromatograph (HP5 column, 30m) with a flame ionization detector. Chromatographic resolution of enantiomers was performed on an AgilentGC-7820-A chromatograph using a CYCLOSIL-B column. Elemental analyses of C, H and N were performed using on a PerkinElmer EA2400 series II elemental analyzer. X-ray diffraction analysis were carried out on a BRUKER SMART APEX CCD diffractometer using graphite-monochromated MoKα radiation (λ = 0.71073 Å) from an X-ray Tube. Electrospray ionization mass spectrometry (ESI-MS) experiments were performed on a Bruker Daltonics Esquire 3000 Spectrometer using a 1>mM solution of the analyzed compound. High resolution mass spectrometry (HRMS) were performed on Bruker MicrOTOF-Q^{II} (Q-TOF) instrument with a quadrupole analyzer with positive and negative ionization mode using methanol as mobile phase at Serveis Tècnics of the University of Girona. Samples were introduced into the mass spectrometer ion source by direct infusion through a syringe pump and were externally calibrated using sodium formate. UV-vis absorption spectra were performed by a diode array spectrophotometer Agilent Cary 60 and low temperature control was maintained with a Cryostat from Unisoku Scientific Instruments. Cyclic voltammetry (CV) was performed using a model CHInstruments with three-electrode cell. The working electrode was a glassy carbon disk from BAS (0.07 cm^2), the reference electrode was a saturated KCl calomel electrode, and the auxiliary electrode was platinum wire.

IX.1. Experimental Section for Chapter III

Mechanistically driven development of an iron catalyst for selective syn-dihydroxylation of alkenes with aqueous hydrogen peroxide

IX.1.1. Synthesis of ligand

IX.1.1.1. Synthesis of pyridine synthons

Pyridine synthons ^{tips}PyCHO, ^{tips}PyCH$_2$OH and ^{tips}PyCH$_2$Cl were synthetized following a previously described procedure.[1-2]

Synthesis of ^{tips}PyCH$_2$NH$_2$·HCl
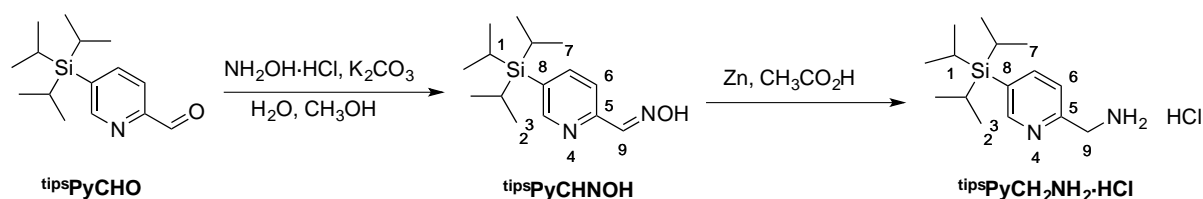
Scheme IX.1. Synthesis of ^{tips}PyCH$_2$NH$_2$·HCl.

^{tips}**PyCHNOH.** The procedure followed is inspired in the method described by Janicki.[3] ^{tips}**PyCHO** (1 g, 3.80 mmol, 1 equiv.), NH$_2$OH·HCl (0.67 g, 9.64 mmol, 2.5 equiv.) and K$_2$CO$_3$ (0.72 g, 5.21 mmol, 1.4 equiv.) were added in a round bottom flask with 25 mL of a H$_2$O:CH$_3$OH (1:2) mixture. The mixture is stirred overnight under reflux at 90°C. After this time, the solvent is removed under vacuum, in order to obtain 0.81 g as a yellow oil. This product is used in the next step without purification. ^{1}H-NMR (CDCl$_3$, 400 MHz) δ, ppm: 1.06 (d, J = 7.9 Hz, 18H$_2$) 1.41 (sept, J = 7.4 Hz , 3H$_1$) 7.70 (d, J= 7.2 Hz, 1H$_6$) 7.88 (d, J = 7.2 Hz, 1H$_7$) 8.45 (s,H$_9$) 8.73 (s, 1H$_3$). ^{13}C{^{1}H}-NMR (CDCl$_3$, 100 MHz) δ, ppm: 10.6, 18.4, 120.1, 131.4, 143.6, 151.4, 155.1. HRMS(ESI-MS): *m/z* calculated for C$_{15}$H$_{25}$NOSi, [M+H]$^+$ 279.1887, found 279.1902.

The crude obtained in the previous reaction (0.81 g, 2.9 mmol, 1 equiv.) is solved in 15 mL of glacial acetic acid at 80%. Then 3 g of Zn powder, previously activated by washing it with one drop of concentrated HCl in H2O, is added in one portion. After stirring for 48h at 40°C, the solution is brought to pH=14 by addition of NaOH(aq) and the crude is extracted with concentrated HCl. The combined aqueous layers were concentrated under vacuum to give 0.45 g (1.50 mmol, 40% yield) of the product as a white solid. 1H-NMR (D2O, 400 MHz) δ, ppm: 0.98 (d, J = 7.2 Hz, 18H2) 1.46 (sept, J = 7.4 Hz, 3H1), 4.48 (s, 2H9), 7.87 (d, J = 7.4 Hz, 1H6), 8.54 (d, J = 7.4 Hz, 1H7), 8.71 (s, 1H3). ^{13}C{^{1}H}-NMR (D$_2$O, 100 MHz) δ, ppm: 9.7, 17.4, 39.7, 125.6, 136.6, 146.2, 147.1, 153.9. HRMS(ESI-MS): m/z Calculated for C$_{15}$H$_{28}$N$_2$Si, [M$^+$H]$^+$ 265.2095, found 265.2100.

IX.1.1.2. Synthesis of ligand $^{5\text{-tips3}}$tpa
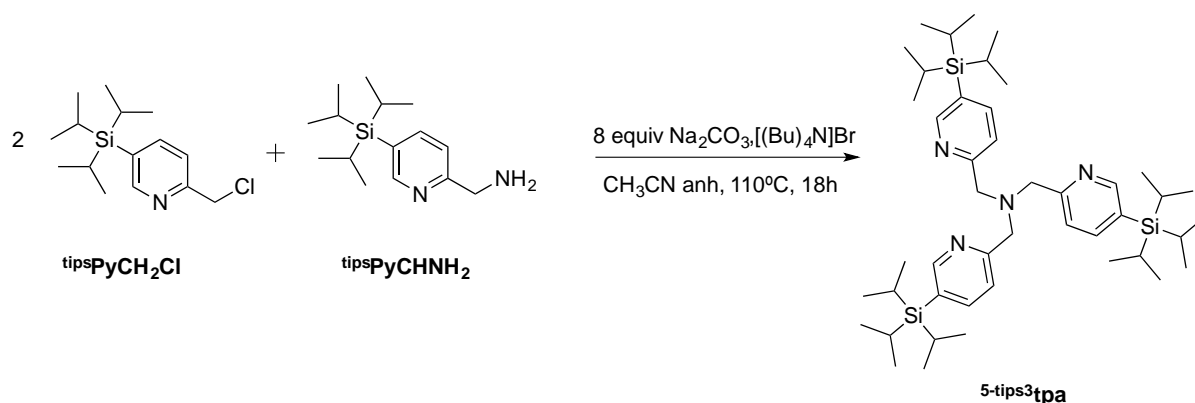
Scheme IX.2. Synthesis of ligand $^{5\text{-tips3}}$tpa.

$^{5\text{-tips3}}$**tpa.** The procedure followed is inspired in the method reported by Que and co-workers.[4] **^{tips}PyCH$_2$Cl** and **^{tips}PyCH$_2$NH$_2$** were first obtained from **^{tips}PyCH$_2$Cl·HCl** and **^{tips}PyCH$_2$NH$_2$·HCl**, respectively, by dissolving them in 25 mL of a mixture of Brine and NaHCO$_3$ (1:1) and extracted with CH$_2$Cl$_2$ (2 x 25 mL), the organic layers were combined, dried with MgSO$_4$ and evaporated under reduced pressure.

2 equiv. of **^{tips}PyCH$_2$Cl** (520 mg, 1.84 mmols) and 1 equiv. of **^{tips}PyCH$_2$NH$_2$** (243 mg, 0.92 mmols) were mixed in a vial and solved in anhydrous CH$_3$CN (15 mL) under a N$_2$ atmosphere. Then Na$_2$CO$_3$ (0.7 g, 6.60 mmol, 8 equiv.) and 1 mg of [(Bu)$_4$N]Br were added directly as solids. The resulting mixture was sealed with a rubber septum and brought to 110°C for 18h. After this time, the excess of Na$_2$CO$_3$ is filtered and the solvent is removed under vacuum. The residue is hydrolyzed with 50 mL of 1M NaOH and extracted with 2x50 mL of CH$_2$Cl$_2$. The combined organic layers were washed with 30 mL of a saturated solution of NaHCO$_3$, dried over MgSO$_4$, concentrated using a rotatory evaporator and purified by silica column chromatography eluting with hexane:ethyl acetate (8:2) to obtain 560 mg of product (0.74 mmol, 58% yield) as a brown oil. ^{1}H-NMR (CDCl$_3$, 400 MHz) δ, ppm: 1.08 (d, *J* = 7.4 Hz, 54H2), 1.42 (sept, *J* = 7.1 Hz, 9H$_1$), 3.86 (s, 4H$_9$), 3.99 (s, 2H$_9$), 7.45 (d, *J* = 7.3 Hz, 3H$_6$), 7.81 (d, *J* = 7.3 Hz, 3H$_7$), 8.64 (s, 3H$_3$). ^{13}C{^{1}H}-NMR (CDCl$_3$, 100 MHz) δ, ppm: 10.6 (C$_2$), 18.4 (C$_1$), 60.1 (C$_9$), 122.0 (C$_6$), 127.8 (C$_4$), 143.5 (C$_7$), 154.8 (C$_3$), 159.3 (C$_5$). HRMS (ESI-MS): *m/z* calculated for C$_{45}$H$_{78}$N$_4$Si$_3$, [M+Na]$^+$ 781.5426, Found 781.5414 Elemental Analysis (%) for C$_{45}$H$_{78}$N$_4$Si$_3$ (MW = 759.38). Calculated N: 10.35, C: 71.17, H: 10.35; obtained N: 9.98, C: 72.22, H: 11.65 FT-IR (ATR) v, cm^{-1}: 2943-2864 (C-H)$_{sp3}$, 1579, 1461, 1343, 1103.5, 1014, 881, 733, 677, 655, 571.5, 514.9.

IX.1.1.3. Synthesis of the complex [Fe^{II}(OTf)$_2$($^{5\text{-tips3}}$tpa)]
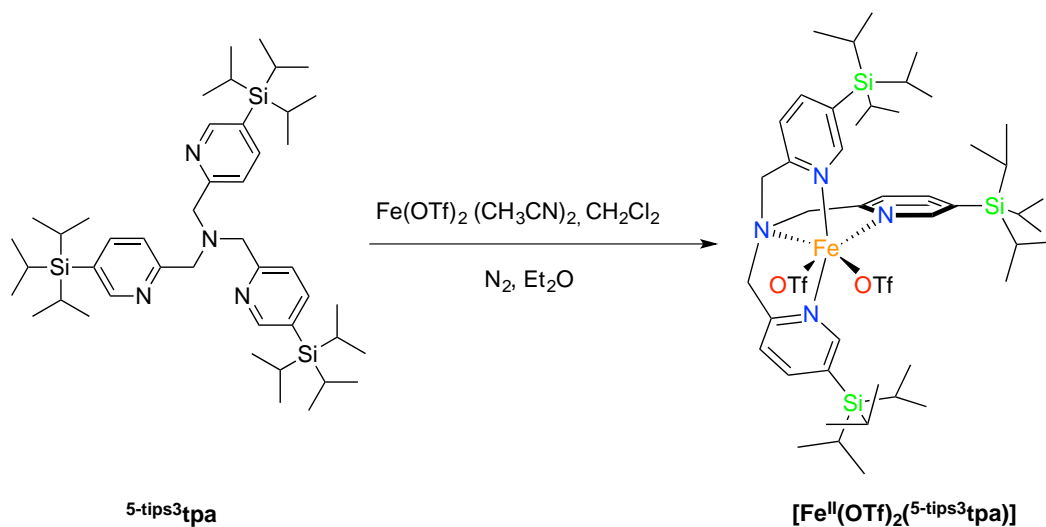
Scheme IX.3. Synthesis of the complex [Fe^{II}(OTf)$_2$($^{5\text{-tips3}}$tpa)].

A suspension of Fe(OTf)$_2$(CH$_3$CN)$_2$ (58 mg, 0.13 mmol, 1 equiv.) in anhydrous CH$_2$Cl$_2$ (1 mL) was added dropwise to a vigorously stirred solution of tris((5-(triisopropylsilyl)piridin-2-yl)methyl)amine ($^{5\text{-tips3}}$tpa) (100 mg, 0.13 mmol, 1 equiv.) in CH$_2$Cl$_2$ (1 mL), forming a brown homogeneous solution. The mixture was stirred for a minimum of 2 hours. The solvent was dried under reduced pressure. The residue obtained is solved again with the minimum volume of anhydrous CH$_2$Cl$_2$ and is filtered through celite©. Slow diethyl ether diffusion over the resulting solution afforded, in a few days, 55 mg (0.10 mmol, 78% yield) of yellow crystals.

HRMS (ESI-TOF): *m/z* calculated for C$_{45}$H$_{78}$F$_6$FeN$_4$S$_6$Si$_3$, [M-OTf]$^+$ 963.4400, Found 963.4375

Elemental Analysis (%) for C$_{45}$H$_{78}$F$_6$FeN$_4$S$_6$Si$_3$ (MW = 1113.37 g/mol). Calculated N: 5.03, C: 50.70, H: 7.06; obtained N: 5.16, C: 50.68, H: 6.70 FT-IR (ATR) v, cm^{-1}: 2943-2866 (C-H)$_{sp3}$, 1591, 1463, 1300, 1232, 1161, 1036, 983, 882, 685, 634, 586, 514.

IX.1.2. Catalytic studies

IX.1.2.1. Reaction conditions for iron-catalyzed *syn*-dihydroxylation of alkenes

An acetonitrile solution (1 mL) of the substrate (90 µmol, 1 equiv.) the catalyst (0.9 µmol, 1 mol%) and $Mg(ClO_4)_2 \cdot 6H_2O$ (198 µmol, 2.2 equiv.) was prepared in a 3 mL vial equipped with a stir bar, and the resulting mixture cooled with an ice bath. 114 µL (135 µmol, 1.5 equiv.) of 0.58M H_2O_2 solution in acetonitrile (diluted from 50% in aqueous solution) were directly added by syringe pump over 30 minutes. Then, the solution was stirred for further 30 minutes.

At this point, 0.1 mL methyl imidazole and 1 mL of acetic anhydride were added and stirred for 15 minutes at room temperature to esterify the *syn*-diol product. After 15 minutes, some ice is added to the solution and it was stirred for 15 minutes more. Then, an internal standard (biphenyl) was added to the solution and was extracted in 2 mL of CH_2Cl_2. The organic layer is treated with 2 mL of 1M H_2SO_4. After shaking vigorously, the vial, the organic layer is treated first with 2 mL of $NaHCO_3$ and then with 2 mL of water. The resultant organic layer is filtered through $MgSO_4$ plug and injected directly to gas chromatograph. GC analysis of the solution provided substrate conversions and product yields relative to the internal standard.

Table IX.1. Substrate scope of different alkenes using catalyst **1** and compared with the best reported iron catalysts.
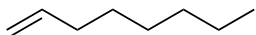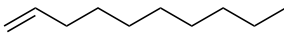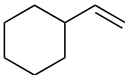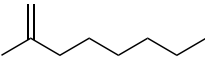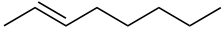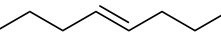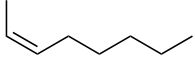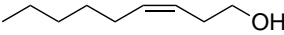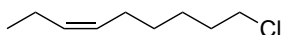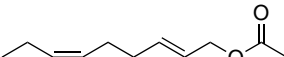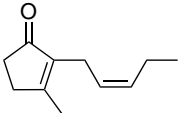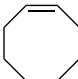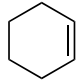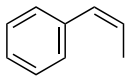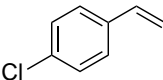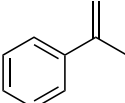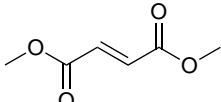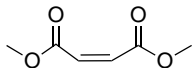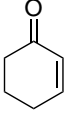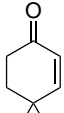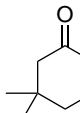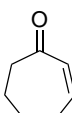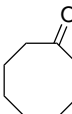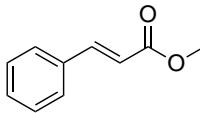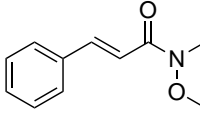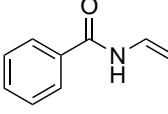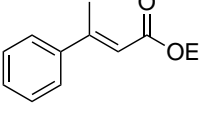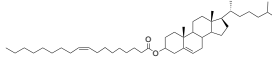
Entry	Alkene	*Syn*-diol Isolated yield (%)	Ratio *Syn*-diol vs. epoxide[b]	Best reported *syn*-diol (%)	
				Conv.	*Syn*-diol[i]
1		92	11	-	67[f]
2		76	6.4	-	62[f]
3		79	3.8	-	57**[f]**
4		38	0.9	66	7[e]
5		74	8	48	43**[d]**
6		76	3.5	50	43**[d]**
7		96	24	98	56[e]
8		77	24	-	-
9		76	14	76	38[e]
10		97	18	88	56[e]
11		94	69	90	45[e]
12		81	4	96	60[e]
13		89	146	-	45**[f]**
14[g]		80	3.3	62	31**[d]**
15		58	(-)	99	65[c]
16[k]		77	(-)	-	-
17		92	40	99	99[c]
18[j], [h]		67	(-)	94	77[c]

Table IX.1. (cont.). Substrate scope of different alkenes using catalyst **1** and compared with the best reported iron catalysts.

Entry [a]	Alkene	*Syn*-diol Isolated yield (%)	Ratio *Syn*-diol vs. epoxide[b]	Best reported *syn*-diol (%)	
				Conv.	*Syn*-diol[i]
19		75	(-)[f]	52	21[d]
20[h]		55	(-)	-	-
21[h]		60	(-)	-	-
22[h]		84	(-)	-	-
23[h]		98	(-)	-	-
24[g]		82	57	97	94[d]
25[g]		53	25	-	-
26[g]		56	(-)	-	-
27[g]		57	(-)	-	-
28		81	(-)	-	-

[a]Reaction conditions: 1 equiv. of substrate, 1mol% catalyst, 2.2 equiv. of Mg(ClO$_4$)$_2$·6H$_2$O and 1.5 equiv. of H$_2$O$_2$ (50% w/w solution) added via syringe pump addition over 30 min, 10 ml of CH$_3$CN, at 0 ºC, plus 30 min stirring. [b]*Syn*-diol/epoxide ratio determined by GC using estimated response factors obtained with the substrate. Best reported examples: [c]from reference[5]; [d]from reference[6]; [e]from reference[7]; [f]from reference[8]. [g]2 mol% of catalyst at room temperature. [h]Yields determined by GC using response factors obtained with independently prepared, or commercially available products. [i]Yields based on starting substrate. [j]Oxidation performed without Mg(ClO$_4$)$_2$·6H$_2$O.[k]1 equiv. H$_2$O$_2$ (50% w/w solution).

IX.1.3. General procedure for isolation of *syn*-diol products

An acetonitrile solution (10 mL) of the substrate (900 µmol, 1 equiv.), the catalyst (9 µmol, 1 mol%) and $Mg(ClO_4)_2 \cdot 6H_2O$ (1.2 mmol, 2.2 equiv.) was prepared in a 25mL round bottom flask equipped with a stir bar and the mixture cooled with an ice bath. 775 µL (1.35 mmol, 1.5 equiv.) of 1.47M H_2O_2 solution in acetonitrile (diluted from 50% aqueous solution) was added by syringe pump during 30 minutes. Then, the solution was stirred for further 30 minutes. At this point, 10 mL of an aqueous $NaHCO_3$ saturated solution were added to the mixture. The resultant solution was extracted with CH_2Cl_2 (3 x 10 mL) and the organic fractions were combined, dried over $MgSO_4$, and the solvent was removed under reduced pressure to afford the oxidized product. The resulting residue was purified by flash chromatography on silica gel (Hexane/AcOEt: 8/2). Purity of obtained products was checked by ^{1}H-NMR, ^{13}C{^{1}H}-NMR, HRMS-TOF and GC. In some cases, the *syn*-diol was acetylated.

For the acetylation, 0.1 mL methyl imidazole and 1 mL of acetic anhydride were added and the mixture stirred for 15 minutes at room temperature. After 15 minutes, some ice is added to the solution and the mixture was stirred for 15 additional minutes. Then, an internal standard (biphenyl) was added to the solution, which was then extracted in 2 mL of CH_2Cl_2. The organic layer is treated with 2 mL of 1M H_2SO_4. After vigorously shaking the vial, the organic layer is separated and treated first with 2 mL of $NaHCO_3$, and then with 2 mL of water. The resultant organic layer is filtered through a $MgSO_4$ plug and analyzed by gas chromatography. GC analysis of the solution provided substrate conversions and product yields relative to the internal standard.

IX.1.3.1. Characterization of isolated *syn*-diols products

For known compounds the analytical data was compared with that described in the literature. The relative configuration of the products was confirmed by comparing NMR spectra with that of independently prepared or commercially available compounds, and GC retention times with that of independently prepared, or commercially available samples.
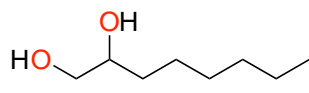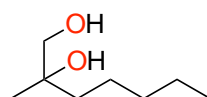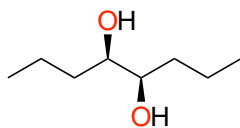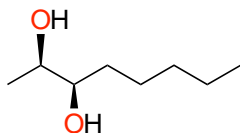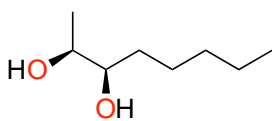
(P1b) Purification by flash chromatography on silica gel (SiO$_2$;Hexane/AcOEt: 8/2) gave the product as a pale yellow oil (92% yield) ^{1}H-NMR (CDCl$_3$, 400 MHz) δ, ppm: 3.70-3.59 (m, 2H), 3.41 (dd, *J* = 11.2, 7.9 Hz, 1H), 1.50-1.23 (m, 10H), 0.94-0.83 (m, 3H). ^{13}C{^{1}H}-NMR (CDCl$_3$, 100 MHz) δ, ppm: 72.38, 66.71, 33.09, 31.78, 29.37, 25.61, 22.59, 14.02. HRMS(ESI+) *m/z* calculated for C$_8$H$_{18}$O$_2$ [M+Na]$^+$ 169.1199, found 169.1205.
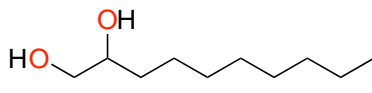
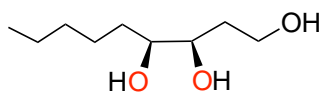**(P2b)** Purification by flash chromatography on silica gel (SiO$_2$;Hexane/AcOEt: 8/2) gave the product as a pale yellow oil (76% yield) ^{1}H-NMR (CDCl$_3$, 400 MHz) δ, ppm: 3.66-3.54 (m, 2H), 3.37 (dd, *J* = 11.3, 7.8 Hz, 1H), 1.38 (s, 3H), 1.24 (s, 11H), 0.85 (t, J= 6.6 HZ, 3H). ^{13}C{^{1}H }-NMR (CDCl$_3$, 100 MHz) δ, ppm:74.43, 35.52, 18.42, 13.96. HRMS(ESI+) *m/z* calculated for C$_{10}$H$_{22}$O$_2$ [M+Na]$^+$ 197.1512, found 197.1527.
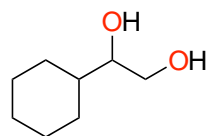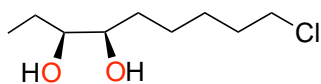

(P3b) Purification by flash chromatography on silica gel (SiO$_2$;Hexane/AcOEt: 8/2) gave the product as a pale yellow oil (79% yield) ^{1}H-NMR (CDCl$_3$, 400 MHz) δ, ppm: 3.70 (dd, *J* = 11.0, 2.6 Hz, 1H), 3.53 (dd, *J* = 11.0, 8.0 Hz, 1H), 3.48-3.40 (m, 1H), 2.96 (s, 2H), 1.92-1.83 (m, 1H), 1.75 (ddd, *J* = 12.0, 8.3, 4.2 Hz, 2H), 1.71-1.60 (m, 2H), 1.47-1.34 (m, 1H), 1.31-1.12 (m, 3H), 1.04 (qd, *J* = 12.2, 3.4 Hz, 2H).^{13}C{^{1}H}-NMR (CDCl$_3$, 100 MHz) δ, ppm: 76.49, 64.74, 40.72, 29.00, 28.67, 26.39, 26.10, 26.01. HRMS(ESI+) *m/z* calculated for C$_8$H$_{16}$O$_2$ [M+Na]$^+$ 167.1043, found 167.1052.
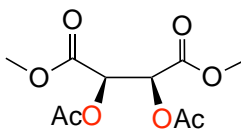

(P6b) Purification by flash chromatography on silica gel (SiO$_2$;Hexane/AcOEt: 8/2) gave the product as a pale yellow oil (38% yield) ^{1}H-NMR (CDCl$_3$, 400 MHz) δ, ppm: 3.51-3.36 (m, 2H), 2.50 (s, 1H), 2.26 (s, 1H), 1.53-1.45 (m, 2H), 1.40-1.23 (m, 6H), 1.17 (s, 3H), 0.91 (t, *J* = 6.7 Hz, 3H). ^{13}C{^{1}H }-NMR (CDCl$_3$, 100 MHz) δ, ppm:20.48, 20.89, 20.95, 28.33, 39.94, 72.30, 76.40, 169.75, 169.91, 201.59. HRMS(ESI+) *m/z* calculated for C$_8$H$_{18}$O$_2$ [M+Na]$^+$ 169.1199, found 169.1203.
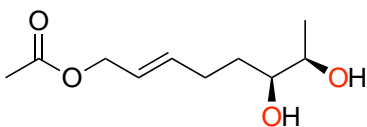
(P7b) Purification by flash chromatography on silica gel (SiO$_2$;Hexane/AcOEt: 8/2) gave the product as a pale yellow oil (76% yield) ^{1}H-NMR (CDCl$_3$, 400 MHz) δ, ppm: 3.54 (s, 2H), 1.43 (d, J = 42.5 Hz, 8H), 0.93 (s, 6H). ^{13}C{^{1}H}-NMR (CDCl$_3$, 100 MHz) δ, ppm: 72.37, 66.72, 33.08, 31.88, 29.73, 29.57, 29.31, 25.66, 22.66, 14.09. HRMS(ESI+) *m/z* calculated for C$_8$H$_{18}$O$_2$ [M+Na]$^+$ 169.1199, found 169.1197.
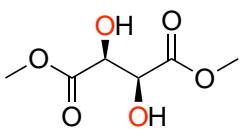

(P8b) Purification by flash chromatography on silica gel (SiO$_2$;Hexane/AcOEt: 8/2) gave the product as a pale yellow oil (74% yield) ^{1}H-NMR (CDCl$_3$, 400 MHz) δ, ppm: 3.60-3.53 (m, 1H), 3.35-3.26 (m, 1H), 3.10 (s, 2H), 1.54-1.42 (m, 2H), 1.41-1.21 (m, 6H), 1.17 (d, J= 6.4Hz, 3H) 0.95-0.83 (m, 3H). ^{13}C{^{1}H}-NMR (CDCl$_3$, 100 MHz) δ, ppm: 76.20, 70.86, 33.87, 25.25, 22.57, 19.44, 13.98. HRMS(ESI+) *m/z* calculated for C$_8$H$_{18}$O$_2$ [M+Na]$^+$ 169.1199, found 169.1204.

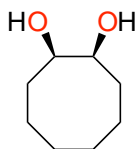**(P9b)** Purification by flash chromatography on silica gel (SiO$_2$;Hexane/AcOEt: 8/2) gave the product as a pale yellow oil (96% yield) ^{1}H-NMR (CDCl$_3$, 400 MHz) δ, ppm: 3.83 (s, 1H), 3.66 (s, 1H), 2.83 (s,2H), 1.52-1.32 (m, 8H), 1.16-1.15 (s, 3H), 0.92-0.89 (m, 3H). ^{13}C{^{1}H}-NMR (CDCl$_3$, 100 MHz) δ, ppm: 74.90, 70.36, 31.85, 25.67, 22.56, 16.34, 13.99, 1.89. HRMS(ESI+) *m/z* calculated for C$_8$H$_{18}$O$_2$ [M+Na]$^+$ 169.1199, found 169.1202.
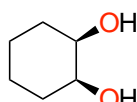

(P10b) Purification by flash chromatography on silica gel (SiO$_2$;Hexane/AcOEt: 8/2) gave the product as a pale yellow oil (77% yield) ^{1}H-NMR (CDCl$_3$, 400 MHz) δ, ppm: 4.00-3.56 (m, 4H), 1.83 (dtd, J = 14.8, 8.8, 4.4 Hz, 1H), 1.71 (ddt, J = 14.7, 5.3, 3.3 Hz, 1H), 1.61-1.24 (m, 8H), 0.92 (td, J = 6.8, 5.8, 3.2 Hz, 3H). ^{13}C{^{1}H}-NMR (CDCl$_3$, 100 MHz) δ, ppm: 74.54, 74.46, 61.44, 32.18, 31.95, 31.84, 25.65, 22.58, 14.03. HRMS(ESI+) *m/z* calculated for C$_9$H$_{20}$O$_3$ [M+Na]$^+$ 199.1303, found 199.1305.

(P11b) Purification by flash chromatography on silica gel (SiO$_2$;Hexane/AcOEt: 8/2) gave the product as a pale yellow oil (76% yield) ^{1}H-NMR (CDCl$_3$, 400 MHz) δ, ppm: 43.54 (t, *J* = 6.7 Hz, 2H), 2.45 (s, 2H), 1.80 (p, *J* = 7.0 Hz, 2H), 1.54-1.39 (m, 6H), 0.99 (t, *J* = 7.4 Hz, 3H). ^{13}C{^{1}H}-NMR (CDCl$_3$, 100 MHz) δ, ppm: 76.29, 74. 31, 45.02, 32.52, 30.94, 26.90, 25.36, 24.25, 10.46. HRMS(ESI+) *m/z* calculated for C$_9$H$_{19}$ClO$_2$ [M+Na]$^+$ 217.0966, found 217.0969.

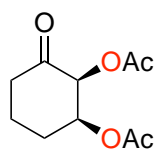**(P12b)** Purification by flash chromatography on silica gel (SiO$_2$;Hexane/AcOEt: 8/2) gave the product as a pale yellow oil (57% yield) ^{1}H-NMR (CDCl$_3$, 400 MHz) δ, ppm: 5.65 (s, 2H), 3.79 (s, 6H), 2.17 (s, 6H) . ^{13}C{^{1}H}-NMR (CDCl$_3$, 100 MHz) δ, ppm: 20.50, 52.91, 70.92, 166.22, 169.58. HRMS(ESI+) *m/z* calculated for C$_{10}$H$_{14}$O$_8$ [M+Na]$^+$ 285.0575, found 285.0581. This product was oxidized with the previous descried methodology but without using Mg(ClO$_4$)$_2$·6H$_2$O.
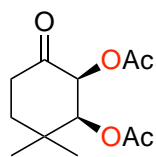
(P13b) Purification by flash chromatography on silica gel (SiO$_2$;Hexane/AcOEt: 8/2) gave the product as a pale yellow oil (97% yield) ^{1}H-NMR (CDCl$_3$, 400 MHz) δ, ppm: 5.83-5.69 (m, 1H), 5.59 (dd, *J* = 14.2, 7.6 Hz, 1H), 4.48 (d, J = 6.2 Hz, 2H), 3.58 (s, 1H), 3.53-3.45 (m, 1H), 2.34-2.22 (m, 1H), 2.11 (dd, *J* = 16.9, 9.5 Hz, 1H), 2.03 (s, 3H), 1.48 (dd, *J* = 26.5, 7.1 Hz, 4H) 0.96 (t, *J* = 7.2 Hz, 3H). ^{13}C{^{1}H}-NMR (CDCl$_3$, 100 MHz) δ, ppm: 171.00, 135.74, 124.41, 76.22, 73.72, 65.16, 30.24, 28.73, 24.37, 21.01, 10.42. HRMS(ESI+) *m/z* calculated for C$_{11}$H$_{20}$O$_4$ [M+Na]$^+$ 239.1254, found 239.1254
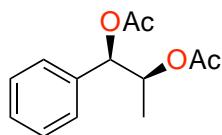
(P14b) Purification by flash chromatography on silica gel (SiO$_2$;Hexane/AcOEt: 8/2) gave the product as a pale yellow oil (92% yield) ^{1}H-NMR (CDCl$_3$, 400 MHz) δ, ppm: 4.56 (s, 2H), 3.87 (d, *J* = 1.3 Hz, 6H). ^{13}C{^{1}H}-NMR (CDCl$_3$, 100 MHz) δ, ppm: 171.91, 71.91, 53.24. HRMS(ESI+) *m/z* calculated for C$_6$H$_{10}$O$_6$ [M+Na]$^+$ 201.0370, found 201.0370.

(P15b) Purification by flash chromatography on silica gel (SiO$_2$;Hexane/AcOEt: 8/2) gave the product as a pale yellow oil (81% yield) ^{1}H-NMR (CDCl$_3$, 400 MHz) δ, ppm: 3.90 (d, *J* = 10.4 Hz, 2H), 3.65 (s, 2H), 1.97-1.79 (m, 2H), 1.75-1.59 (m, 4H), 1.61-1.41(m, 6H). ^{13}C{^{1}H}-NMR (CDCl$_3$, 100 MHz) δ, ppm: 73.09, 30.03, 26.25, 23.74. HRMS(ESI+) *m/z* calculated for C$_8$H$_{16}$O$_2$ [M+Na]$^+$ 167.1043, found 167.1045.

(P16b) Purification by flash chromatography on silica gel (SiO$_2$;Hexane/AcOEt: 8/2) gave the product as a pale yellow oil (89% yield) ^{1}H-NMR (CDCl$_3$, 400 MHz) δ, ppm: 3.80 (s, 2H), 2.21 (s, 2H), 1.46 (d, *J* = 106.4 Hz, 8H). ^{13}C{^{1}H}-NMR (CDCl$_3$, 100 MHz) δ, ppm: 70.64, 29.95, 21.45. HRMS(ESI+) *m/z* calculated for C$_6$H$_{12}$O$_2$ [M+Na]$^+$ 139.0730, found 139.0735.
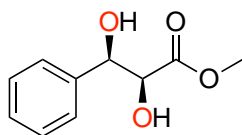

(P17b), isolated as acetylated product. Purification by flash chromatography on silica gel (SiO$_2$;Hexane/AcOEt: 8/2) gave the product as a pale yellow oil (75% yield) ^{1}H-NMR (CDCl$_3$, 400 MHz) δ, ppm: 5.58 (s, 1H), 5.28 (d, *J* = 3.4 Hz, 1H), 2.53 (d, *J* = 11.9 Hz, 1H), 2.47-2.35 (m, 1H), 2.11 (s, 4H), 2.04 (s, 3H), 1.96 (d, *J* = 8.0 Hz, 3H).^{13}C{^{1}H}-NMR (CDCl$_3$, 100 MHz) δ, ppm: 201.59, 169.91, 169.75, 76.40, 73.30, 39.94, 28.33, 20.95, 20.89, 20.48. HRMS(ESI+) *m/z* calculated for C$_{10}$H$_{14}$O$_5$ [M+Na]$^+$ 237.0733, found 237.0743.
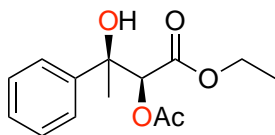

(P19b), isolated as acetylated product. Purification by flash chromatography on silica gel (SiO$_2$;Hexane/AcOEt: 8/2) gave the product as a pale yellow oil (55% yield) ^{1}H-NMR (CDCl$_3$, 400 MHz) δ, ppm: 5.47 (d, *J* = 3.4 Hz, 1H), 5.29-5.19 (m, 1H), 2.53 (td, J = 14.4, 6.6 Hz, 1H), 2.41 (ddd, *J* = 14.9, 5.1, 2.3 Hz, 1H), 2.06 (d, *J* = 13.4 Hz, 6H), 1.96 (dd, *J* = 13.8, 5.1 Hz, 1H), 1.66-1.54 (m, 1H), 1.32 (s, 3H), 0.95 (s, 3H). ^{13}C{^{1}H}-NMR (CDCl$_3$, 100 MHz) δ, ppm: 20.51, 20.67, 23.81, 26.31, 33.99, 35.52, 36.55, 74.13, 79.87, 169.83, 170.12, 201.91. HRMS(ESI+) *m/z* calculated for C$_{12}$H$_{18}$O$_5$ [M+Na]$^+$ 265.1046, found 265.1057.
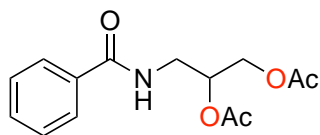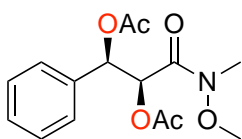
(P23b), isolated as acetylated product. Purification by flash chromatography on silica gel (SiO$_2$;Hexane/AcOEt: 8/2) gave the product as a pale yellow oil (80% yield) ^{1}H-NMR (CDCl$_3$, 400 MHz) δ, ppm: 7.34 (d, *J* = 4.5 Hz, 5H), 5.92 (d, *J* = 4.3 Hz, 1H), 5.26-5.17 (m, 1H), 2.13 (s, 3H), 1.99 (s, 3H), 1.17 (d, *J* = 6.6 Hz, 3H). ^{13}C{^{1}H}-NMR (CDCl$_3$, 100 MHz) δ, ppm: 20.48, 20.89, 20.95, 28.33, 39.94, 73.30, 76.40, 169.75, 169.91, 201.59. HRMS(ESI+) *m/z* calculated for C$_{13}$H$_{16}$O$_4$ [M+Na]$^+$ 259.0941, found 259.0953.
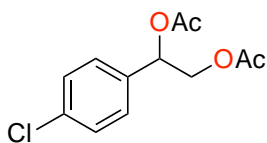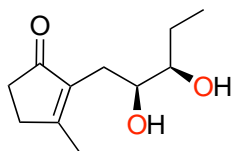

(P24b), isolated as acetylated product. Purification by flash chromatography on silica gel (SiO$_2$;Hexane/AcOEt: 8/2) gave the product as a pale yellow oil (58% yield) 1H-NMR (CDCl3, 400 MHz) δ, ppm: 7.39-7.29 (m, 4H), 5.98 (s, 1H), 4.38-4.22 (m, 2H), 2.13 (s, 3H), 2.06 (s, 3H). ^{13}C{^{1}H}-NMR (CDCl$_3$, 100 MHz) δ, ppm: 20.73, 21.03, 65.76, 72.64, 128.13, 128.87, 134.50, 135.09, 169.91, 170.52. HRMS(ESI+) *m/z* calculated for C$_{12}$H$_{13}$ClO$_4$ [M+Na]$^+$ 279.0395, found 279.0392.

(P27b) Purification by flash chromatography on silica gel (SiO$_2$;Hexane/AcOEt: 8/2) gave the product as a pale yellow oil (82% yield) ^{1}H-NMR (CDCl$_3$, 400 MHz) δ, ppm: 7.39 (dt, *J* = 24.2, 7.3 Hz, 5H), 5.04 (d, *J* = 2.8 Hz, 1H), 4.40 (d, *J* = 2.8 Hz, 1H), 3.83 (s, 3H), 3.21 (s, 1H), 2.91 (s, 1H). ^{13}C{^{1}H}-NMR (CDCl$_3$, 100 MHz) δ, ppm:173.16, 139.91, 128.48, 128.10, 126.20, 74.71, 74.44, 52.87. HRMS(ESI+) *m/z* calculated for C$_{10}$H$_{12}$O$_4$ [M+Na]$^+$ 219.0628, found 219.0630.
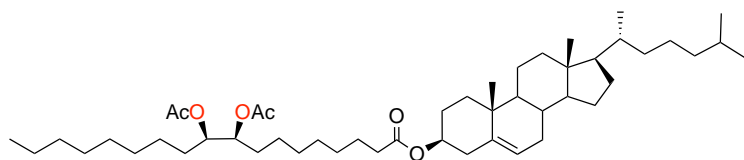

(P28b), isolated as monoacetylated product. Purification by flash chromatography on silica gel (SiO$_2$;Hexane/AcOEt: 8/2) gave the product as a pale yellow oil (57% yield) ^{1}H-NMR (CDCl$_3$, 400 MHz) δ, ppm: 7.50-7,40 (m, 2H), 7.35-7,21 (m, 3H), 5.24 (s, 1H), 4.90 (q, *J* = 7.1 Hz, 2H), 2.04 (s, 3H), 1.61 (s, 3H), 1.10 (t, *J* = 7.1 Hz, 3H). ^{13}C{^{1}H}-NMR (CDCl$_3$, 100 MHz) δ, ppm: 13.86, 20.47, 26.53, 61.60, 74.90, 78.34, 125.01, 127.41, 128.16, 143.90, 160.98, 168.43, 169.90. HRMS(ESI+) *m/z* calculated for C$_{14}$H$_{18}$O$_5$ [M+Na]$^+$ 290.1080, found 290.1091.

(P29b), isolated as acetylated product. Purification by flash chromatography on silica gel (SiO2;Hexane/AcOEt: 8/2) gave the product as a pale yellow oil (56% yield) ^{1}H-NMR (CDCl3, 400 MHz) δ, ppm7.80-7.68 (m, 2H), 7.43 (dt, *J* = 31.1, 7.2 Hz, 3H), 6.80 (s, 1H), 5.18 (p, *J* = 5.4 Hz, 1H), 4.30 (dd, J = 12.1, 4.1 Hz, 1H), 4.19 (dd, *J* = 12.1, 5.6 Hz, 1H), 3.66 (t, *J* = 6.2 Hz, 2H), 2.06 (d, *J* = 1.5 Hz, 6H). ^{13}C{^{1}H}-NMR (CDCl$_3$, 100 MHz) δ, ppm: 20.69, 20.94, 40.18, 63.09, 70.60, 126.98, 128.53, 131.59, 134.05, 167.76, 170.81. HRMS(ESI+) *m/z* calculated for C$_{14}$H$_{17}$O$_5$ [M+Na]$^+$ 302.0999, found 302.1003.

(P31b), isolated as acetylated product. Purification by flash chromatography on silica gel (SiO$_2$;Hexane/AcOEt: 8/2) gave the product as a pale yellow oil (53% yield) ^{1}H-NMR (CDCl$_3$, 400 MHz) δ, ppm: 7.40-7.28 (m, 5H), 6.30 (d, *J* = 4.7 Hz, 1H), 5.64 (d, *J* = 4.0 Hz, 1H), 3.70 (s, 3H), 3.05 (s, 3H), 2.09 (d, *J* = 10.0 Hz, 6H). ^{13}C{^{1}H}-NMR (CDCl$_3$, 100 MHz) δ, ppm: 20.56, 20.96, 32.25, 61.20, 72.34, 73.13, 127.05, 128.34, 128.57, 135.74, 169.75, 170.39. HRMS(ESI+) *m/z* calculated for C$_{15}$H$_{19}$O$_6$ [M+Na]$^+$ 332.1105, found 332.1088.

(P32b) Purification by flash chromatography on silica gel (SiO$_2$;Hexane/AcOEt: 8/2) gave the product as a pale yellow oil (94% yield). The product is isolated with a 85:15 dr, which corresponds to the initial cis/trans composition of the substrate. Spectroscopic data for the major diastereoisomer; ^{1}H-NMR (CDCl$_3$, 400 MHz) δ, ppm: 3.58 (s, 1H), 3.42-3.30 (m, 1H), 2.74-2.29 (m, 6H), 2.09 (s, 3H), 1.52 (d, *J* = 57.3 Hz, 2H), 0.97 (t, *J* = 7.3 Hz, 3H).^{13}C{^{1}H}-NMR (CDCl$_3$, 100 MHz) δ, ppm: 212.59, 174.87, 137.78, 75.38, 73.77, 34.20, 32.29, 25.94, 25.42, 17.57, 10.28. HRMS(ESI+) *m/z* calculated for C$_{11}$H$_{18}$O$_3$ [M+Na]$^+$ 211.0366, found 211.1159.

(P33b), isolated as acetylated product. Purification by flash chromatography on silica gel (SiO$_2$;Hexane/AcOEt: 8/2) gave the product as a pale yellow oil (81% yield) ^{1}H-NMR (CDCl3, 400 MHz) δ, 5.39 (d, *J* = 5.1 Hz, 1H), 5.04-4.93 (m, 2H), 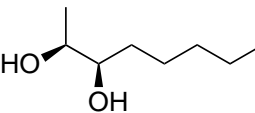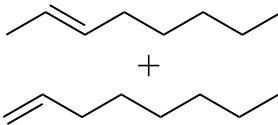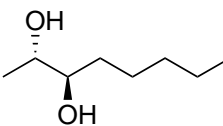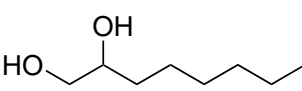4.69-4.57 (m, 1H), 2.35-2.25 (m, 5H), 2.06 (s, 6H), 1.93-1.77 (m, 4H), 1.69-1.47 (m, 15H), 1.34-1.23 (m, 25H), 1.21-1.07 (m, 9H), 0.95-0.88 (m, 13H), 0.70 (s, 3H). ^{13}C{^{1}H}-NMR (CDCl$_3$, 100 MHz) δ, ppm: 11.86, 14.10, 18.72, 19.32, 21.04, 22.56, 22.65, 22.82, 23.83, 24.29, 24.98, 25.52, 25.56, 27.82, 28.01, 28.23, 29.02, 29.09, 29.21, 29.27, 29.21, 29.39, 29.42, 31.83, 31.87, 31.91, 35.79, 36.19, 36.60, 37.00, 38.16, 39.52, 39.74, 42.32, 50.03, 56.14, 56.69, 74.24, 122.58, 170.68. HRMS(ESI+) *m/z* calculated for C$_{49}$H$_{84}$O$_6$ [M+Na]$^+$ 791.6160, found 791.6152. Despite the data is consistent with a single product, most likely the compound consists of an indistinguishable mixture of the two diastereoisomers resulting from *syn*-dihydroxylation at the aliphatic chain.
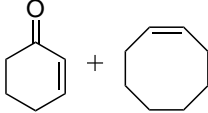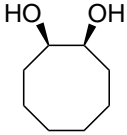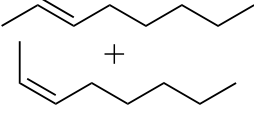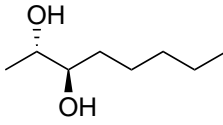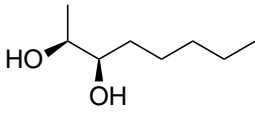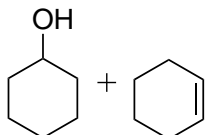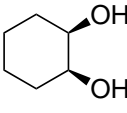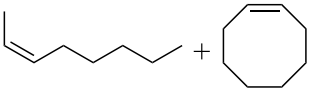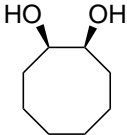
IX.1.4. Competition studies

An acetonitrile solution (1 mL) with the two substrates (45.0 μmol, 0.5 equiv. of each substrate), the catalyst (0.9 μmol, 1 mol%) and Mg(ClO$_4$)$_2$·6H$_2$O (99 μmol, 2.2 equiv.) was prepared in a vial (3 mL) equipped with a stir bar, and the mixture was cooled with an ice bath. 77.5 μL (45.0 μmol, 0.5 equiv.) of 0.58 mM H$_2$O$_2$ solution (diluted from 50% in acetonitrile) was added by syringe pump over 30 minutes. At this point, the solution was stirred for 30 additional minutes. Then, an internal standard (biphenyl) was added to the solution and the resulting mixture was quickly extracted in 2 mL of CHCl$_3$. The organic layer is treated with 2 mL of 1M H$_2$SO$_4$. After shaking the vial vigorously, the organic layer is treated first with 2 mL of NaHCO$_3$ and then with 2 mL of water. The resultant organic layer is filtered through a MgSO$_4$ plug and subjected to gas chromatograph. GC analysis of the solution provided substrate conversions and product yields relative to the internal standard integration.

Competitive reactions have been performed (Table IX.2), revealing the preference of the system to preferentially oxidize the electron rich over the electron poor olefin (Entry 1), also preferentially oxidizes *cis* over *trans* aliphatic olefins (Entry 2). These experiments also show the tolerance of the catalyst in front of alcohols (Entry 3). When cyclic and cis-linear aliphatic olefins are present, the system slightly prefers to oxidize the linear aliphatic olefin (Entry 4). And when a terminal and a *trans* olefin are present the system slightly prefers to oxidize the terminal one (Entry 5).

Table IX.2. Competitive reactions.

Entry [a]	Alkenes	*Syn*-diol product	*Syn*-diol yield[b] (%)	Ratio *Syn*-diol vs. epoxide[c]
1			62	4
2			23	3.5
			66	13
3			65	6
4			32	3.5
			41	10
5			31	2.6
			56	7

[a]Reaction conditions: 1 equiv. of substrate, 1mol% catalyst, 0.5 equiv. of H_2O_2 (50% w/w solution), added via syringe pump addition over 30 min, 1 ml of CH_3CN, at 0ºC, 30 min stirring. [b]Yields determined by GC using estimated response factors derived from the substrates. [c]*Syn*-diol/epoxide ratio determined by GC.

IX.1.5. Optimization reactions

Solvent and additives effects examined for dihydroxylation of 1-octene.

A solution of the corresponding solvent (1 mL), 1-octene as a substrate (90 µmol, 1 equiv.), the catalyst (0.9 µmol, 1 mol%) and $Mg(ClO_4)_2·6H_2O$ (198 µmol, 2.2 equiv.) was prepared in a 3 mL vial equipped with a stir bar, and cooled with an ice bath. 114.2 µL (134.8 µmol, 1.5 equiv.) of 0.58M H_2O_2 solution in acetonitrile (diluted from 50% in aqueous solution) was added by syringe pump during 30 minutes. Then, the solution was stirred for further 30 minutes. (Standard conditions)

At this point, 0.1 mL methyl imidazole and 1 mL of acetic anhydride were added and stirred for 15 minutes at room temperature to esterify the *syn*-diol product. After 15 minutes, some ice is added to the solution and it was stirred for 15 additional minutes. Then, an internal standard (biphenyl) was added to the solution and was extracted in 2 mL of CH_2Cl_2. The organic layer is treated with 2 mL of 1M H_2SO_4. After vigorously shaking the vial, the organic layer is treated first with 2 mL of $NaHCO_3$ and then with 2 mL of water. The resultant organic layer is filtered through a $MgSO_4$ plug and analyzed by gas chromatography. GC analysis of the solution provided substrate conversions and product yields relative to the internal standard integration. Response factors were calculated using commercially available products.

Table IX.3. Solvents screening using catalyst **1**.

Entry	Solvents	Conv. (%)	Yield diol (%)	Yield epoxide (%)	Ratio diol/epoxide
1	CH_3CN/ CH_2Cl_2 (1:1)	61	49	12	4.1
2	Acetone	76	17	17	1.0
3	i-PrCN	65	54	11	4.9
4	$CH_2Cl_2/$ 10% i-PrCN[a]	17	8	3	2.7
5	AcOEt	60	36	6	6.0
6	AcOEt/ 10% i-PrCN[a]	53	42	7	6.0
7	AcOEt/ 5% i-PrCN[a]	56	34	6	5.7
8	PhCN[b]	40	30	10	3.0
9	CH_3CN	98	74	23	3.2
10	CH_3CN/10% i-PrCN[a]	93	67	22	3.0
11	TFE	41	23	17	1.4
12	$CH_3CN/$ AcOEt (1:1)	98	63	17	3.7
13	AcOEt/ 10% *t*-Butanol	n.r.	-	-	-
14	AcOEt/ 10% DMF	n.r.	-	-	-
15	AcOEt/ 10% MeOH	n.r.	-	-	-
16	AcOEt/*t*-BuOH 1:1	n.r.	-	-	-
17	ethyl hexanoate	26	18	3	6.0
18	methyl cyclohexanecarboxylate	14	12	2	6.0
19	1,1,1-trifluoropentan-2-one	6	2	5	0.4
20	dihydrofuran-2(3H)-one	98	58	20	2.9

[a] Isobutyronitrile, [b] Benzonitrile. n.r: not reactive.

Table IX.4. Additive screening.

Entry	Additives (2.2 equiv.)	Conv. (%)	Yield diol (%)	Yield epoxide (%)	Ratio diol/epoxide
1	$LiClO_4 \cdot 3H_2O$	62	51	8	6.4
2	$Mg(ClO_4)_2 \cdot 6H_2O$	100	86	14	6.1
3	$Zn(OTf)_2$	99	75	21	3.6
4	NaOTf	80	59	14	4.2
5	MgO	86	71	15	4.7
6	$Mg(OTf)_2$	94	77	17	4.5
7	$Mg(ClO_4)_2$	53	43	10	4.3

Table IX.5. Screening of different equivalents of $Mg(ClO_4)_2 \cdot 6H_2O$.

Entry	$Mg(ClO_4)_2 \cdot 6H_2O$	Conv. (%)	Yield diol (%)	Yield epoxide (%)	Ratio diol/epoxide
1	0.2 equiv.	93	75	17	4.4
2	0.5 equiv.	100	76	15	5
3	1 equiv.	99	81	18	5
4	1.2 equiv.	80	81	16	5
5	1.7 equiv.	86	84	15	6
6	2.2 equiv.	100	86	14	6.1
7	3 equiv.	100	83	16	6.4

Table IX.6. Time course of the catalytic oxidation of 1-octene with catalysts **1** and **2**.

CATALYST 1		
Time (min)	TN *syn-diol*	TN epoxide
5	13	1
10	25	3
15	41	6
25	64	9
30	75	11
35	78	12

1

[Fe(OTf)$_2$(^{5tips3}tpa)]$^{2+}$
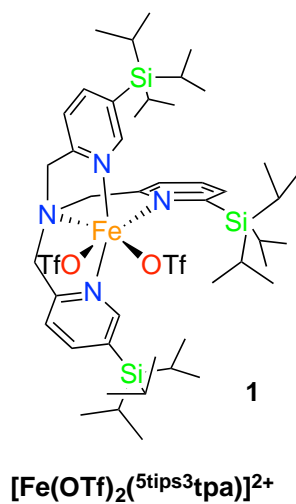
CATALYST 2		
Time (min)	TN *syn-diol*	TN epoxide
5	2	0
10	5	1
15	15	3
20	20	4
30	26	5
35	37	7

2

[Fe(OTf)$_2$(tpa)]$^{2+}$
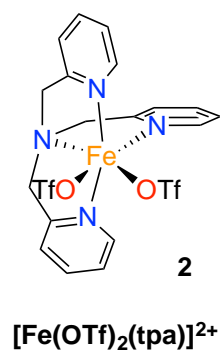
IX.1.5.1. HRMS analysis of the *syn*-dihydroxylation of substrates S12 and S14 in presence and absence of Mg(ClO$_4$)$_2$·6H$_2$O.

A solution of the corresponding solvent (1 mL), substrate **S12** or **S14** (90 µmol, 1 equiv.), the catalyst (0.9 µmol, 1 mol%) and Mg(ClO$_4$)$_2$·6H$_2$O (198 µmol, 2.2 equiv.) or without, was prepared in a 3 mL vial equipped with a stir bar, and the mixture cooled with an ice bath. 114.2 µL (134.8 µmol, 1.5 equiv.) of 0.58M H$_2$O$_2$ solution in acetonitrile (diluted from 50% in aqueous solution) was added by syringe pump over 30 minutes. After 5 minutes of addition, a sample was analyzed by HRMS. The conversion and the yield of diol was calculated at the end of the addition.
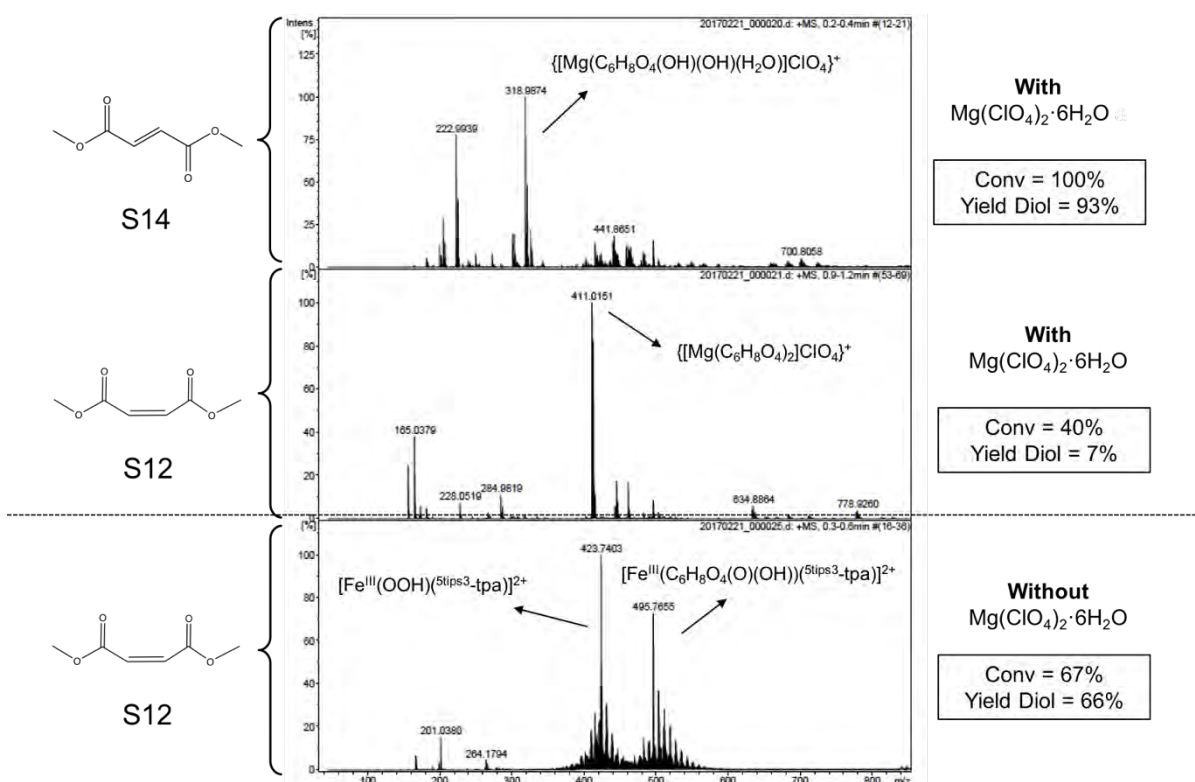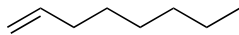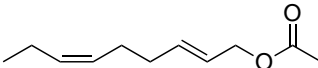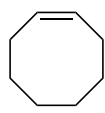

Figure IX.1. HRMS analysis of the reaction using **S12** and **S14** substrates performed with and without Mg(ClO$_4$)$_2$·6H$_2$O.

IX.1.5.2. Comparison of some results obtained with and without Mg(ClO$_4$)$_2$·6H$_2$O

Mg(ClO$_4$)$_2$·6H$_2$O effect examined for dihydroxylation of substrates **S1**, **S13** and **S15**. A solution of acetonitrile (1 mL), the substrate (90 µmol, 1 equiv.), the catalyst (0.9 µmol, 1 mol%) and Mg(ClO$_4$)$_2$·6H$_2$O (198 µmol, 2.2 equiv.) (or in its absence), was prepared in a 3 mL vial equipped with a stir bar, and the mixture cooled with an ice bath. Then 114 µL (135 µmol, 1.5 equiv.) of 0.58M H$_2$O$_2$ solution in acetonitrile (diluted from 50% in aqueous solution) were

directly added by syringe pump over 30 minutes. After stirring for additional 30 minutes, the reaction was analyzed with GC.

Table IX.7. Results of the reaction of different substrates in the presence or absence of $Mg(ClO_4)_2 \cdot 6H_2O$.

	Substrates	Yields with $Mg(ClO_4)_2 \cdot 6H_2O$ [diol, epoxide (conv.)]	Yields without $Mg(ClO_4)_2 \cdot 6H_2O$ [diol, epoxide (conv.)]
S1		86, 14 (100)	74, 23 (98)
S13		90, 6 (99)	57, 8 (84)
S15		87, 11 (98)	47, 22 (76)

IX.1.5.3. Labelling experiments

IX.1.5.3.1. General procedure for the *syn*-dihydroxylation with H_2O_2 and $H_2^{18}O$

An acetonitrile solution (1 mL) with the substrate (1-octene, 45 µmol, 1 equiv.) and the catalyst (0.45 µmol, 1 mol%) was prepared in a vial equipped with stir bar, and 4 µL (225 µmol, 5 equiv.) of $H_2^{18}O$ (97% ^{18}O-isotopic content) were added. The resulting solution was cooled with an ice bath. 114 µL (135 µmol, 0.1 equiv.) of a 0.58 mM H_2O_2 solution (diluted from 50% in acetonitrile) was added by syringe pump during 30 minutes. At this point, the solution was stirred for 30 additional minutes.

Then, 0.1 mL of methyl imidazole and 1 mL of acetic anhydride were added and stirred for 15 minutes at room temperature to esterify the *syn*-diol product. After 15 minutes, some ice is added to the solution and it was stirred for 15 more minutes. Then, an internal standard (biphenyl) was added to the solution and was extracted in 2 mL of CH_2Cl_2. The organic layer is treated with 2 mL of 1M H_2SO_4. After shaking vigorously the vial, the organic layer is treated first with 2 mL of $NaHCO_3$ and then with 2 mL of water. The resultant organic layer is filtered through $MgSO_4$ plug and analyzed with a GC-MS equipped with EI and CI sources. GC-MS analysis of the solution provided m/z peaks of characteristic fragments.

IX.1.5.3.2. GC-MS Analysis

The CI source allows us to determine the ^{18}O-total labeling in the diol. Fragmentation at the EI detector allows us to determine the ^{18}O content in each oxygen atom of the fragment.
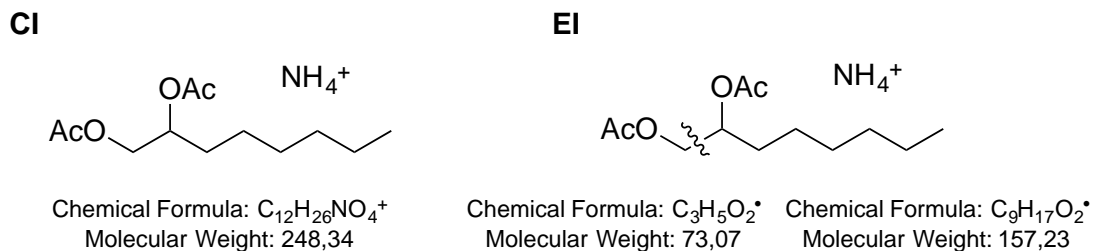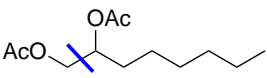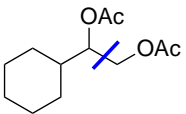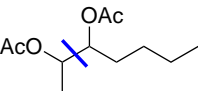

CI

Chemical Formula: $C_{12}H_{26}NO_4^+$
Molecular Weight: 248,34

EI

Chemical Formula: $C_3H_5O_2^{\bullet}$
Molecular Weight: 73,07

Chemical Formula: $C_9H_{17}O_2^{\bullet}$
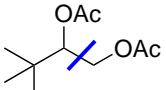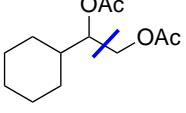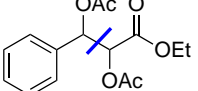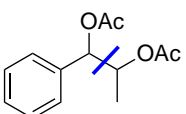Molecular Weight: 157,23

Figure IX.2. GC-MS analysis of the solution provided m/z peaks of characteristic fragments in EI and CI sources.

Table IX.8. Labeling studies with different substrate.

Entry	Substrate	EI			CI		
		Peak	Non labelled (%)	Labelled (%)	Peak	Non labelled (%)	Labelled (%)
1		157	72%	28%	248-250	9.5%	90.5%
2		155	83%	17%	246-248	9.6%	90.1%
3		129	59,4%	38,5%	234-236	15.1%	84.5%
4		129	70,7%	28,5%	220-222	12,6%	86,9%
5[a]		155	44,7%	55,1%	246-248	8,3%	90,9%
6		149	85,3%	14,7%	312-314	10%	89,5%
7		149	73,7%	25,6%	254-256	18,0%	81,3%

[a] Obtained with the [Fe(OTf)$_2$(tpa)] catalyst.

IX.1.6. References

(1)   Cusso, O.; Cianfanelli, M.; Ribas, X.; Gebbink, R.; Costas, M., Iron Catalyzed Highly Enantioselective Epoxidation of Cyclic Aliphatic Enones with Aqueous H2O2. *J. Am. Chem. Soc.* **2016,** *138* (8), 2732-2738.

(2)   Milan, M.; Bietti, M.; Costas, M., Highly Enantioselective Oxidation of Nonactivated Aliphatic C-H Bonds with Hydrogen Peroxide Catalyzed by Manganese Complexes. *ACS Central Sci.* **2017,** *3* (3), 196-204.

(3)   Janicki, R., Synthesis, crystal structure and spectral properties of diammonium dihydrogen N-(methylene-2-pyridine)-N,N,-di-(methylenephosphonate). *J. Molec. Struct.* **2013,** *1036*, 35-41.

(4)   Zang, Y.; Kim, J.; Dong, Y.; Wilkinson, E. C.; Appelman, E. H.; Que Jr., L., Models for Nonheme Iron Intermediates: Structural Basis for Tuning the Spin States of Fe(TPA) Complexes. *J. Am. Chem. Soc.* **1997,** *119*, 4197-4205.

(5)   Chow, T. W.-S.; Wong, E. L.-M.; Guo, Z.; Liu, Y.; Huang, J.-S.; Che, C.-M., cis-Dihydroxylation of Alkenes with Oxone Catalyzed by Iron Complexes of a Macrocyclic Tetraaza Ligand and Reaction Mechanism by ESI-MS Spectrometry and DFT Calculations. *J. Am. Chem. Soc.* **2010,** *132* (38), 13229-13239.

(6)   Zang, C.; Liu, Y.; Xu, Z.-J.; Tse, C.-W.; Guan, X.; Wei, J.; Huang, J.-S.; Che, C.-M., Highly Enantioselective Iron-Catalyzed cis-Dihydroxylation of Alkenes with Hydrogen Peroxide Oxidant via an FeIII-OOH Reactive Intermediate. *Angew. Chem. Int. Ed.* **2016,** *55* (35), 10253-10257.

(7)   Prat, I.; Font, D.; Company, A.; Junge, K.; Ribas, X.; Beller, M.; Costas, M., Fe(PyTACN)-Catalyzedcis-Dihydroxylation of Olefins with Hydrogen Peroxide. *Adv. Synth. Catal.* **2013,** *355* (5), 947-956.

(8)   Ryu, J. Y.; Kim, J.; Costas, M.; Chen, K.; Nam, W.; Que Jr., L., High Conversion of Olefins to cis-Diols by Non-heme Iron Catalysts and H2O2. *Chem. Commun.* **2002,** *12*, 1288-1289.

IX.2. Experimental Section for Chapter IV

Greening oxidation catalysis. Iron catalyzed alkene syn-dihydroxylation with aqueous hydrogen peroxide in green solvents

IX.2.1. Synthesis of the iron complexes 1-4

Iron complexes 1-4 were prepared according to literature procedures.[1-4]

IX.2.2. The effect of the acetonitrile

A solution of substrate (90 µmol, 1 equiv) and catalyst (0.9 µmol, 1 mol%) with the corresponding solvent (1 mL), were prepared in a 3 mL vial equipped with a stir bar, and the resulting mixture was cooled with an ice bath. 114 µL (135 µmol, 1.5 equiv) of 0.58M H_2O_2 solution in the corresponding solvent (diluted from 50% in aqueous solution) were directly added by syringe pump over 30 minutes. At this point, 0.1 mL methyl imidazole and 1 mL of acetic anhydride were added and stirred for 15 minutes at room temperature to esterify the *syn*-diol product. After 15 minutes, some ice was added to the solution and it was stirred for 15 minutes more. Then, an internal standard (biphenyl) was added to the solution and was extracted in 2 mL of AcOEt. The organic layer was washed with 2 mL of 1M H_2SO_4. After shaking vigorously the vial, the organic layer was washed first with 2 mL of $NaHCO_3$ and then with 2 mL of water. The resultant organic layer was dried with $MgSO_4$, filtered and injected directly to gas chromatograph. GC analysis of the solution provided substrate conversions and product yields relative to the internal standard integration of the substrate.

Table IX.9. Effect of the presence of acetonitrile in the reactions.
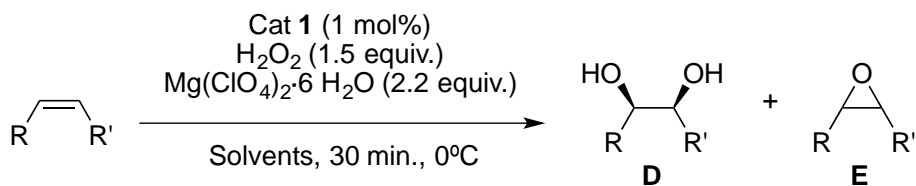
Entry[a]	Substrate	CH_3CN [b]	Conv. (%)	Yield D (%)	Yield E (%)	Ratio D/E
1		0.1 %	93	77	14	5.5
		100 %	98	81	17	5
2		0.1 %	86	75	11	7
		100 %	98	76	22	3.5
3		0.1 %	100	88	12	7
		100 %	100	88	12	7
4		0.1 %	100	69	26	2.6
		100 %	100	81	15	5.5
5		0.1 %	86	81	7	12
		100%	100	92	5	4
6 [c]		0.1 %	73	68	2	34
		100 %	100	99	-	-
7 [c]		0.1 %	-	58	23	2.75
		100 %	75	55	20	2.7
8		0.1 %	88	60	7	9
		100 %	99	90	6	15
9		0.1 %	94	91	0	-
		100 %	98	88	3	29

[a] Conversions and yields determined by GC using the responsive constants of the products, results are the average of 2-3 reactions, and the error is <8%. [b] Solvents employed in the case of 0.1% of acetonitrile are a 1:1 mixture of PC:EtOAc, and 100% of acetonitrile in the other case. [c] Second addition of 1 mol % catalyst and 1.5 equiv. of H_2O_2.

IX.2.3. E factor

E factor (environmental factor) [5]: mass ratio of waste to desired product

$$E\ factor = \frac{Total\ mass\ of\ waste}{Total\ mass\ of\ desired\ product}$$

All the reactions have been done using 45 μmols of substrate,

Volume of the reaction:

$$400\ \mu l\ of\ PC = \frac{1,2\ mg}{1\ \mu l} = 480\ mg\ PC$$

$$400\ \mu l\ of\ EtOAc = \frac{0,9\ mg}{1\ \mu l} = 361\ mg\ of\ EtOAc$$

Volume of PC of the H_2O_2 solution:

$$114\ \mu l\ of\ PC = \frac{1,2\ mg}{1\ \mu l} = 137\ mg\ PC$$

$Mg(ClO_4)_2 \cdot 6H_2O$: 32 mg

Cat: 0.5 mg

Substrate:

Example of the oxidation using 1-octene as a substrate:

$$Substrate = \frac{(100 - Conv) * \mu mol\ of\ substrate * MW\ sub}{10^5}\ mg\ of\ sub$$

$$Substrate = \frac{(100 - 94) * 45 \mu mol * 112.2\ sub}{10^5} = 0.30\ mg\ of\ sub$$

Product (Diol):

$$Product = \frac{Yield\ of\ product * \mu mol\ of\ substrate * MW\ of\ product}{10^5} = mg\ of\ product$$

$$Product = \frac{78 * 45\ \mu mol * 146.2}{10^5} = 5.13\ mg\ of\ product$$

Epoxide:

$$Epoxide = \frac{Yield\ of\ epoxide * \mu mol\ of\ substrate * MW\ of\ epoxide}{10^5} = mg\ of\ epoxide$$

$$Epoxide = \frac{15 * 45\ \mu mol * 128.2}{10^5} = 0.86\ mg\ of\ epoxide$$

$$E\ factor = \frac{480 + 361 + 137 + 32 + 0.5 + 0.30 + 0.86}{5.13} = 197$$

The H_2O is not taken into account

IX.2.4. References

(1)   Borrell, M.; Costas, M., Mechanistically Driven Development of an Iron Catalyst for Selective Syn-Dihydroxylation of Alkenes with Aqueous Hydrogen Peroxide. *J. Am. Chem. Soc.* **2017,** *139* (36), 12821-12829.

(2)   Ryu, J. Y.; Kim, J.; Costas, M.; Chen, K.; Nam, W.; Que Jr, L., High conversion of olefins to cis-diols by non-heme iron catalysts and H2O2. *Chem. Commun.* **2002,** (12), 1288-1289.

(3)   Chow, T. W.-S.; Wong, E. L.-M.; Guo, Z.; Liu, Y.; Huang, J.-S.; Che, C.-M., cis-Dihydroxylation of Alkenes with Oxone Catalyzed by Iron Complexes of a Macrocyclic Tetraaza Ligand and Reaction Mechanism by ESI-MS Spectrometry and DFT Calculations. *J. Am. Chem. Soc.* **2010,** *132* (38), 13229-13239.

(4)   Prat, I.; Font, D.; Company, A.; Junge, K.; Ribas, X.; Beller, M.; Costas, M., Fe(PyTACN)-Catalyzed cis-Dihydroxylation of Olefins with Hydrogen Peroxide. *Adv. Synth. Catal.* **2013,** *355* (5), 947-956.

(5)   Sheldon, R. A., Metrics of Green Chemistry and Sustainability: Past, Present, and Future. *ACS Sustainable Chem. Eng.* **2018,** *6* (1), 32-48.

IX.3. Experimental Section for Chapter V

Characterized cis-Fe^V(O)(OH) Intermediate Mimics

Enzymatic Oxidations in the Gas Phase

IX.3.1. Synthesis of the complex 1

Complex [Fe^{III}(CF$_3$SO$_3$)$_2$($^{5\text{-tips3}}$tpa)] (**1**) was synthetized following previously described procedures.[1]
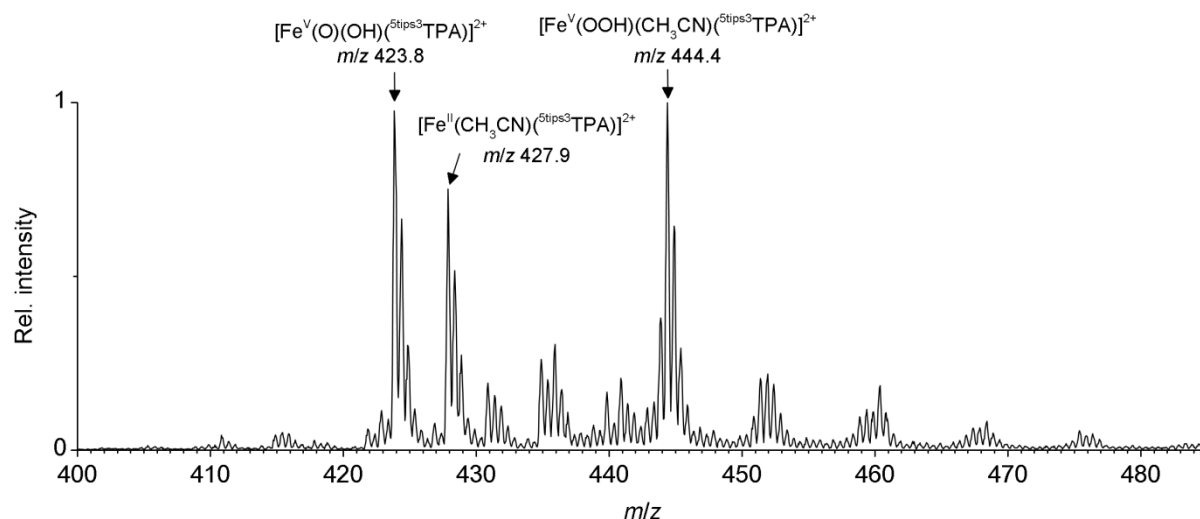
IX.3.2. Generation of intermediate Fe^{III}(OOH)

Figure IX.3. Mass spectrum of the [($^{5\text{-tips3}}$tpa)Fe^{III}(OOH)]$^{2+}$ (**2**) solution.

A 1 mM solution of **1** in dry acetonitrile was prepared inside the glovebox. 2 mL of this solution were placed in a UV-Vis cuvette. The quartz cell was capped with a septum and taken out of the box, placed in the Unisoku cryostat of the UV-Vis spectrophotometer and cooled down to 233 K. After reaching thermal equilibrium, a UV-Vis spectrum of the starting complex was recorded. Then, 10 equiv. H$_2$O$_2$ in dry acetonitrile were added. The formation of a band at λ_{max} = 544 nm was observed.
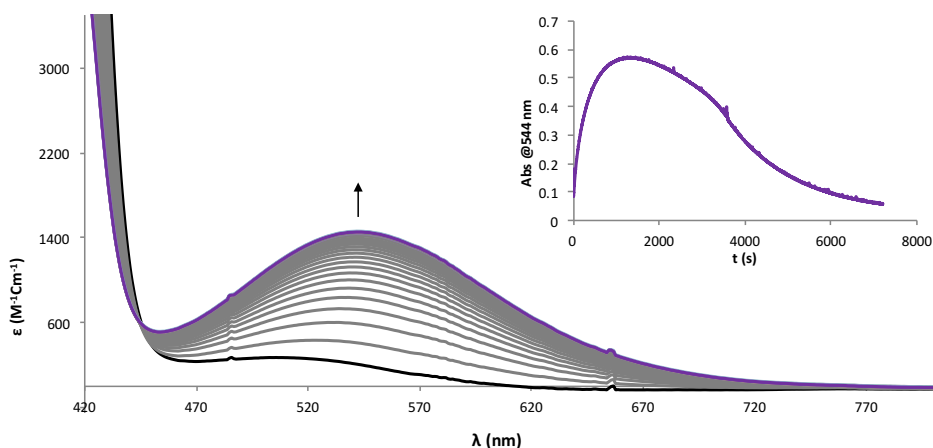
Figure IX.4. UV-Vis spectra of **1** (0.4 mM, black line), **2** (violet line). Solid gray lines show the progressive formation of 2 upon addition of 10 equiv H_2O_2 at -40 ^{o}C in acetonitrile over the course of 126 minutes. Inset: time trace at 544 nm.

IX.3.3. Representative examples of catalytic *syn*-dihydroxylation reactions

General procedure:[1] An acetonitrile solution (1 mL) of substrate (90 μmol, 1 equiv.), the catalyst (0.9 μmol, 1 mol%) and $Mg(ClO_4)_2 \cdot 6H_2O$ (198 μmol, 2.2 equiv.) was prepared in a 3 mL vial equipped with a stir bar, and the resulting mixture cooled with an ice bath. 114 μL (135 μmol, 1.5 equiv.) of 0.58M H_2O_2 solution in acetonitrile (diluted from 50% in aqueous solution) were directly added by syringe pump over 30 minutes. Then, the solution was stirred for further 30 minutes. An internal standard (biphenyl) was added and the solution was immediately filtered through a short silica plug, which was subsequently rinsed with AcOEt. The reaction mixture was then analyzed by GC and GC-MS. Products were identified and quantified by comparison with authentic samples.
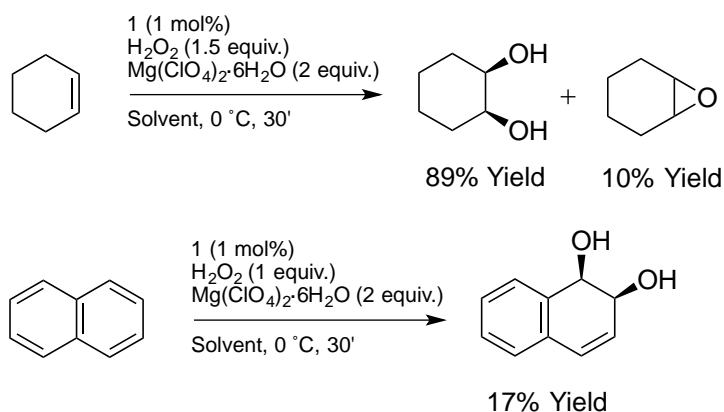
Scheme IX.4. Catalytic *syn*-dihyroxylation of cyclohexene and naphthalene.
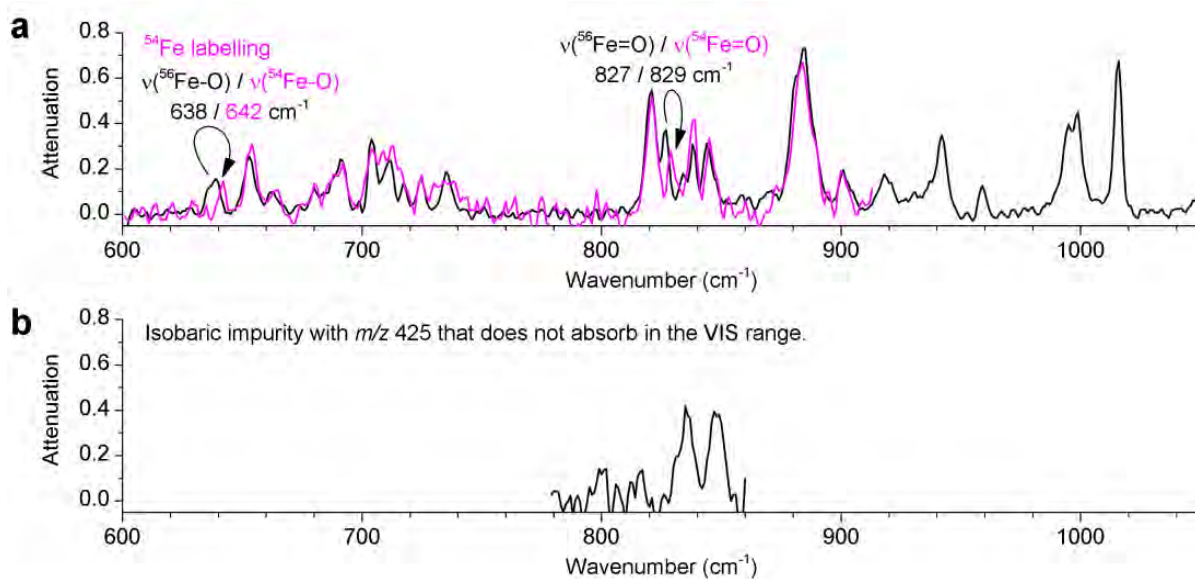
IX.3.4. Supplementary figures

Figure IX.5. (a) IRPD spectra of **3²⁺** and **3²⁺**(^{54}Fe). (b) IRPD spectrum of an isobaric impurity present in **3²⁺**(^{16}O^{18}O) ions with *m/z* 425. The spectrum was obtained by depleting the helium clusters population by irradiation of the ion cloud with a visible laser concurrent with the IR irradiation.
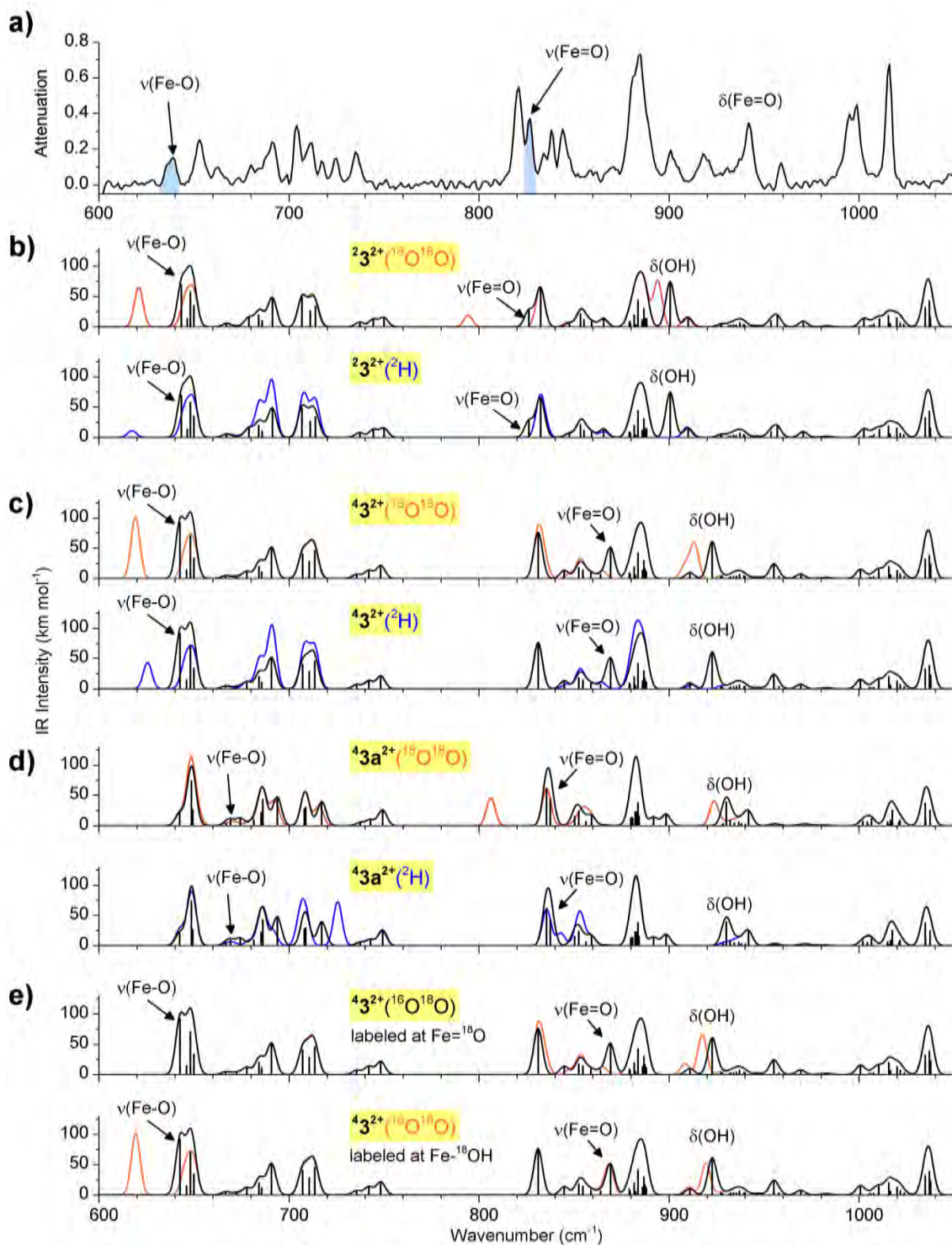
Figure IX.6. (a) IRPD spectrum of 3^{2+}. (b-e) Theoretical predictions of the IR spectra of different isomers and isotopic labeling of 3^{2+}.
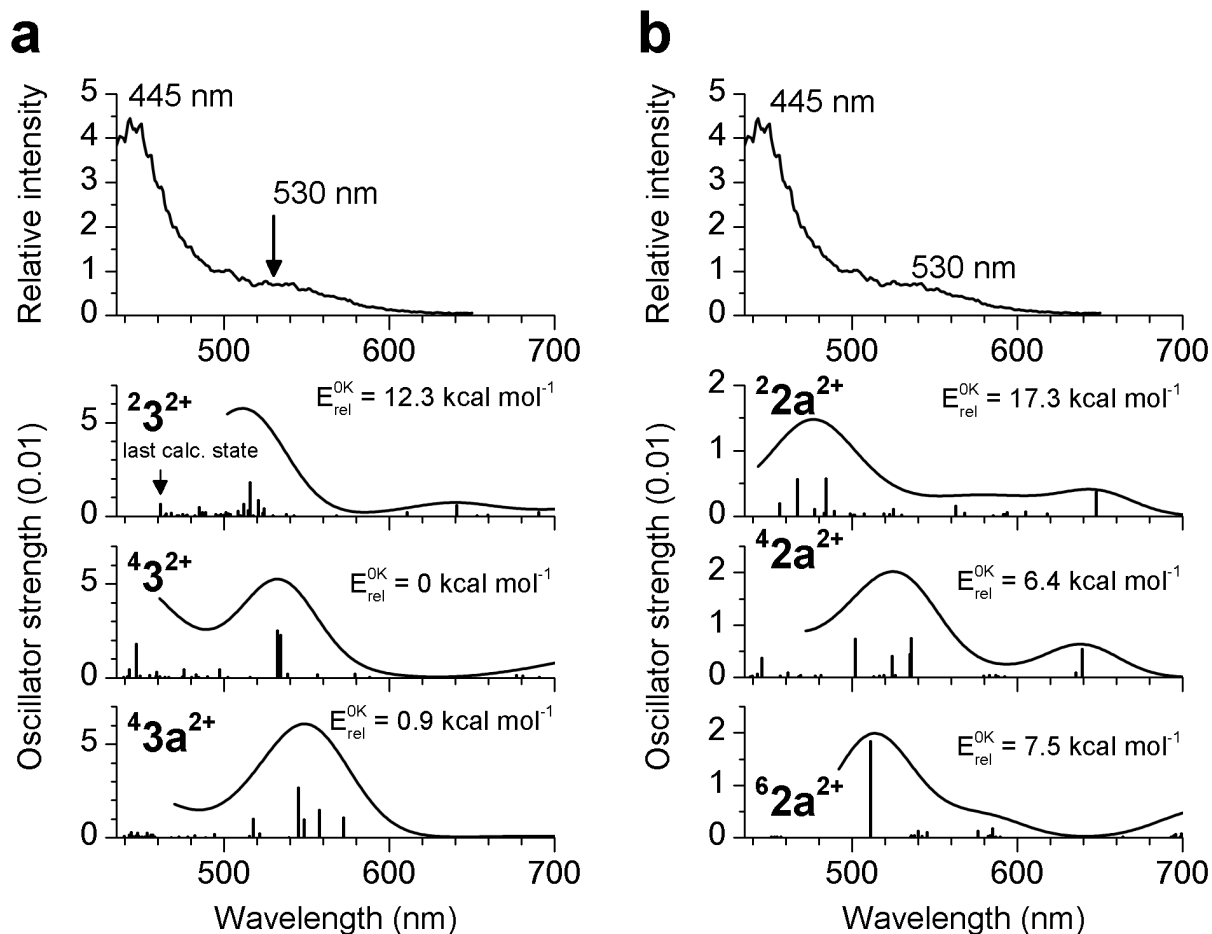
Figure IX.7. Comparison of experimental VIS spectrum of **3** with TD-DFT predictions (B3LYP-D3/def2-TZVP). The convoluted spectrum is only shown to within 40 nm of the last predicted state (there were 64 states). Relative intensity was calculated by dividing the attenuation by the visible laser power in mW and irradiation time (0.780 s).
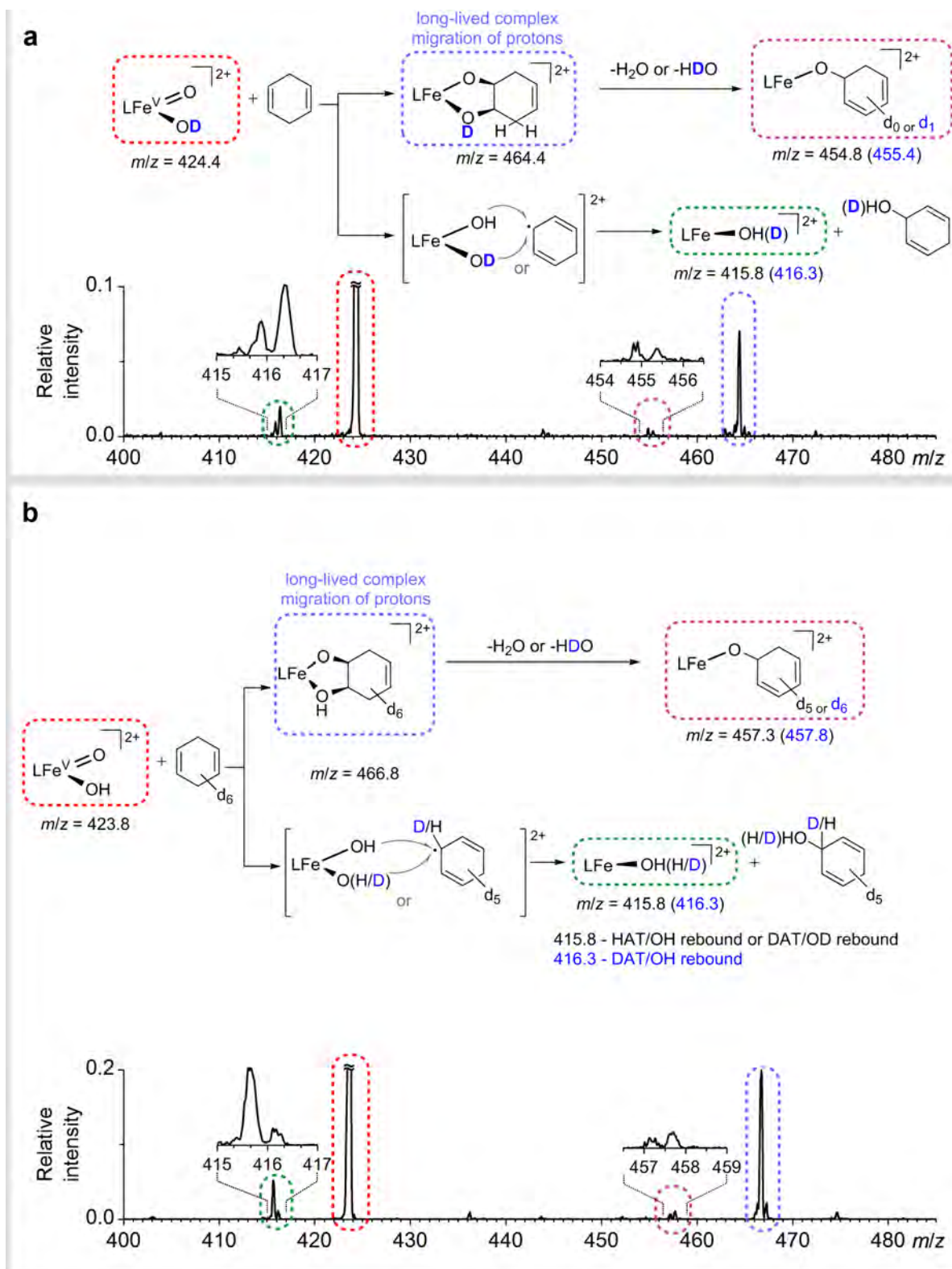
Figure IX.8. Ion-molecule reactivity of $3^{2+}(^2H)$ in the gas phase with 0.1 mTorr of 1,4-cyclohexadiene. The reaction was measured at nominally zero-collision energy determined from the retarding potential analysis.
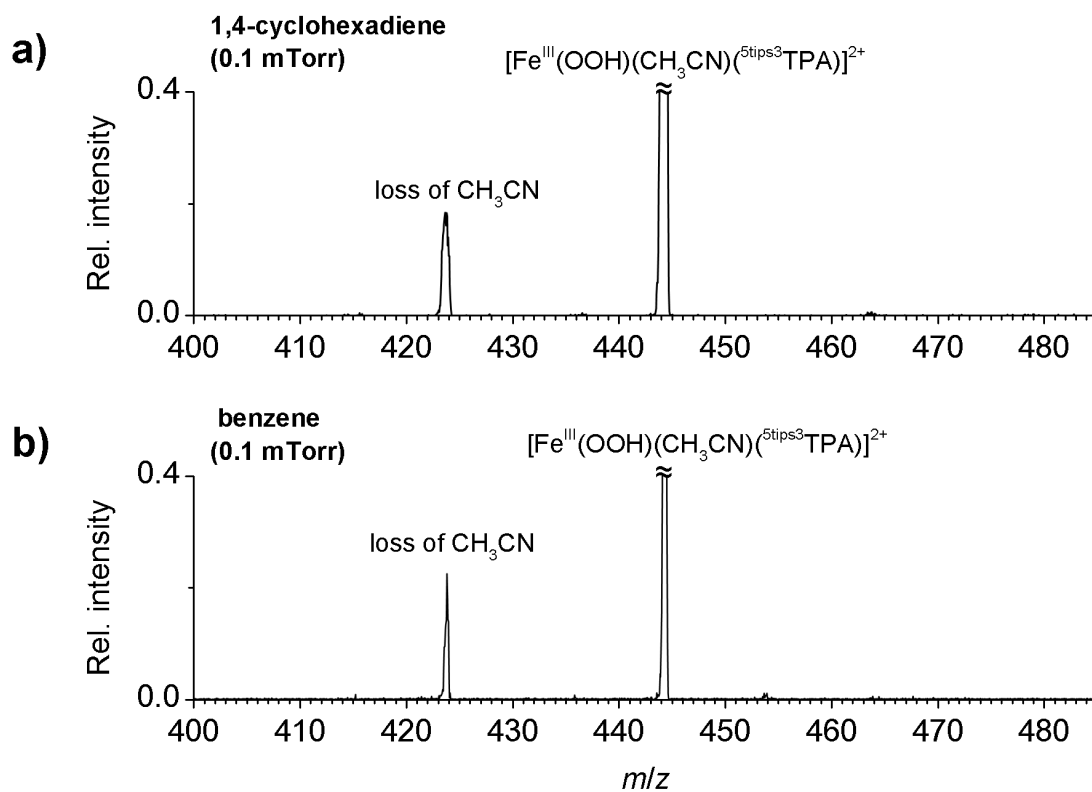
a)

1,4-cyclohexadiene (0.1 mTorr)

$[Fe^{III}(OOH)(CH_3CN)(^{5tips3}TPA)]^{2+}$

loss of CH_3CN

Rel. intensity

0.4

0.0

400   410   420   430   440   450   460   470   480

b)

benzene (0.1 mTorr)

$[Fe^{III}(OOH)(CH_3CN)(^{5tips3}TPA)]^{2+}$

loss of CH_3CN

Rel. intensity

0.4

0.0

400   410   420   430   440   450   460   470   480

m/z

Figure IX.9. Ion-molecule reactivity of **2^{2+}** in the gas phase with (a) 0.1 mTorr of 1,4-cyclohexadiene and (b) 0.1 mTorr of benzene. The reactions were measured at nominally zero-collision energy determined from the retarding potential analysis.

IX.3.5. References

(1)   Borrell, M.; Costas, M., Mechanistically Driven Development of an Iron Catalyst for Selective *Syn*-Dihydroxylation of Alkenes with Aqueous Hydrogen Peroxide. *J. Am. Chem. Soc.* **2017,** *139* (36), 12821-12829.

IX.4. Experimental Section for Chapter VI

Site-selective and product chemoselective aliphatic C-H bond hydroxylation of polyhydroxylated substrates

IX.4.1. Synthesis of the complexes

(*S*,*S*)-[Mn(OTf)$_2$(^{tips}mcp)],[1] OTf = trifluoromethanesulfonate anion, ((**S,S**)-**Mn^{tips}mcp**), (*S*,*S*)-[Fe(OTf)$_2$(^{tips}mcp)][2], ((**S,S**)-**Fe^{tips}mcp**), (*R*,*R*)-[Fe(OTf)$_2$(^{tips}pdp)][2], ((**R,R**)-**Fe^{tips}pdp**), (*S*,*S*)-[Fe(OTf)$_2$(^{DMM}pdp)][3] ((**S,S**)-**Fe^{DMM}pdp**) and (*S*,*S*)-[Mn(OTf)$_2$(^{DMM}pdp)][4] ((**S,S**)-**Mn^{DMM}pdp**) were prepared according to the reported procedure.

IX.4.2. Synthesis of the substrates

The substrates **S1**, **S2**, **S5**, **S6**, **S7, S9** and **S13** are commercially available. The following substrates were prepared according to the reported procedures:

- **S3**, **S4**[5] and **S8**[6]

- The esterification reactions of the steroids (**S14**, **S15** and **S16**) were done according to the reported procedure.[7] Spectral data match with those previously reported for Lithocholic ester, Ursodexycholic ester and Cholic ester.[8-11]

- The synthesis of the different alkyl β-D-glucosides with different alkyl chain lengths (**S10**, **S11** and **S12**).[12]
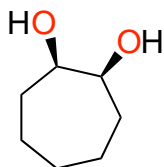
IX.4.2.1. Characterization of the substrates
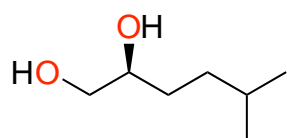
(**S3**)[5] Purification by flash chromatography on silica gel (SiO$_2$;Hexane/AcOEt: 8/2) gave the product as a pale yellow oil (79% yield). ^{1}H-NMR (CDCl$_3$, 400 MHz) δ, ppm: 3.66-3.60 (m, 2H), 3.41 (dd, *J* = 11.1, 7.8 Hz, 1H), 1.61-1.47 (m, 1H), 1.46-1.37 (m, 2H), 1.32 (dt, *J* = 14.7, 6.8 Hz, 1H), 1.25-1.12 (m, 1H), 0.90 (d, *J* = 1.7 Hz, 3H), 0.88 (d, *J* = 1.7 Hz, 3H). ^{13}C{^{1}H}-NMR (CDCl$_3$, 100 MHz) δ, ppm: 72.7, 66.7, 34.7, 31.0, 28.1, 22.5, 22.5. HRMS(ESI+) *m/z* calculated for C$_7$H$_{16}$O$_2$ [M+Na]$^+$ 155.1043, found 155.1047.
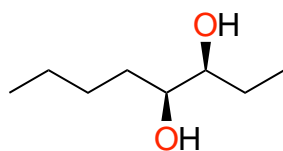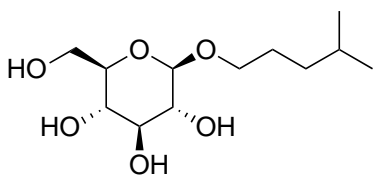

(**S4**)[5] Purification by flash chromatography on silica gel (SiO$_2$;Hexane/AcOEt: 8/2) gave the product as a pale yellow oil (76% yield) ^{1}H-NMR (MeOD, 400 MHz) δ, ppm: 3.40-3.36 (m, 2H), 1.63-1.36 (m, 8H), 0.93 (s, 6H). ^{13}C{^{1}H}-NMR (MeOD, 100 MHz) δ, ppm: 75.5, 73.7, 32.3, 28.0, 25.4, 22.4, 13.1, 9.4. HRMS(ESI+) *m/z* calculated for C$_8$H$_{18}$O$_2$ [M+Na]$^+$ 169.1199, found 169.1203.
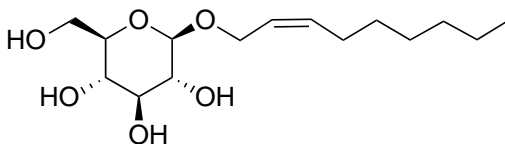
(*cis*-**S8**)[6] Purification by flash chromatography on silica gel (SiO$_2$;Hexane/AcOEt: 8/2) gave the product as a pale yellow oil (81% yield). ^{1}H-NMR (MeOD, 400 MHz) δ, ppm: 3.90 (d, 2H), 2.17 (s, 2H), 1.22-1.80 (m, 10H). ^{13}C{^{1}H}-NMR (MeOD, 100 MHz) δ, ppm: 73.8, 30.9, 27.8, 21.9. HRMS(ESI+) *m/z* calculated for C$_7$H$_{14}$O$_2$ [M+Na]$^+$ 153.0886, found 153.0888.
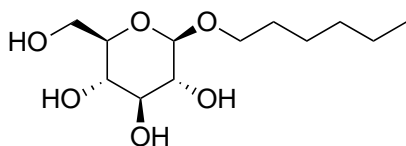

(**S10**)[12] Purification by flash chromatography on silica gel (SiO$_2$;CH$_2$Cl$_2$/MeOH: 6/1) gave the product as a colorless oil (52% yield). ^{1}H-NMR (MeOD, 400 MHz) δ, ppm: 4.28 (d, *J* = 7.8 Hz, 1H), 3.95-3.84 (m, 2H), 3.70 (dd, *J* = 11.9, 5.2 Hz, 1H), 3.54 (dt, *J* = 9.5, 6.8 Hz, 1H), 3.43-3.28 (m, 2H), 3.30-3.16 (m, 1H), 1.71-1.62 (m, 1H), 1.67-1.48 (m, 2H), 1.35-1.22 (m, 2H), 0.92 (d, *J* = 6.6 Hz, 5H). ^{13}C{^{1}H}-NMR (MeOD, 100 MHz) δ, ppm: 102.9, 76.7, 76.4, 73.7, 70.2, 69.8, 61.4, 34.9, 27.7, 27.3, 21.7. HRMS(ESI+) *m/z* calculated for C$_{12}$H$_{24}$O$_6$ [M+Na]$^+$ 551.3029, found 551.3038.

(**S11**)[12] Purification by flash chromatography on silica gel (SiO$_2$;CH$_2$Cl$_2$/MeOH: 6/1) gave the product as a colorless oil (63% yield). ^{1}H-NMR (MeOD, 400 MHz) δ, ppm: 5.52-5.36 (m, 2H), 4.31 (d, *J* = 7.8 Hz, 1H), 3.94-3.82 (m, 2H), 3.72 (dd, *J* = 11.9, 5.2 Hz, 1H), 3.56 (dt, *J* = 9.4, 7.1 Hz, 1H), 3.48-3.29 (m, 2H), 3.31-3.18 (m, 1H), 2.47-2.33 (m, 2H), 2.12-2.02 (m, 2H), 1.44-1.24 (m, 6H), 0.99-0.86 (m, 3H). ^{13}C{^{1}H}-NMR (MeOD, 100 MHz) δ, ppm: 131.5, 125.1, 102.9, 76.6, 76.4, 73.6, 70.1, 69.1, 61.4, 31.3, 29.1, 27.6, 26.9, 22.3, 13.3. HRMS(ESI+) *m/z* calculated for C$_{15}$H$_{28}$O$_6$ [(M)$_2$+Na]$^+$ 631.3664, found 631.3680.

(**S12**)[12] Purification by flash chromatography on silica gel (SiO$_2$; CH$_2$Cl$_2$/MeOH: 6/1) gave the product as a pale yellow oil (60% yield). ^{1}H-NMR (MeOH, 400 MHz) δ, ppm: 4.27 (d, *J* = 7.8 Hz, 1H), 3.97-3.84 (m, 2H), 3.69 (dd, *J* = 11.9, 5.2 Hz, 1H), 3.55 (dt, *J* = 9.5, 6.8 Hz, 1H), 3.43-3.28 (m, 2H), 3.30-3.15 (m, 1H), 1.64 (dq, *J* = 8.4, 6.8 Hz, 2H), 1.47-1.27 (m, 5H), 0.99-0.85 (m, 3H). ^{13}C{^{1}H}-NMR (MeOH, 100 MHz) δ, ppm: 102.9, 76.7, 76.5, 73.7, 70.2, 69.6, 61.8, 31.5, 29.4, 25.4, 22.3, 13.1. HRMS(ESI+) *m/z* calculated for C$_{12}$H$_{24}$O$_6$ [M+Na]$^+$ 287.1465, found 287.1462.

IX.4.3 Reaction protocol for catalysis

Hydrogen peroxide solutions employed in the oxidation reactions were prepared by diluting commercially available hydrogen peroxide (30% H$_2$O$_2$ solution in water, Aldrich) in HFIP (1,1,1,3,3,3-Hexafluoro-2-propanol) to achieve a 0.58 M solution. This solution can be stored in the fridge for a week wo apparent decrease in oxidation performance. Unless explicitly stated, commercially available glacial acetic acid (99-100%) purchased from Riedel-de-Haën was employed. The purity of the substrates synthetized as described above was in all cases >99%.

An HFIP solution (400 µL) of the substrate (50 µmol, 1 equiv) and the corresponding catalyst (0.50 µmol, 1 mol%) was prepared in a 3 mL vial equipped with a stir bar, and the resulting mixture cooled with an ice bath. 6 µL (neat, 2 equiv.) of acetic acid (or the equivalent amount of cyclopropylcarboxylic acid) were added directly to the solution. Then, 86 µL (50 µmol, 1 equiv) of 0.58 M H$_2$O$_2$ solution in HFIP (diluted from 30% in aqueous solution) were directly added by syringe pump over 30 minutes. Then, the solution was stirred for further 15 minutes. At this point, an internal standard (biphenyl) was added and the solution was quickly filtered through a basic alumina plug, which was subsequently rinsed with 2 x 1 mL EtOAc. GC analysis of the solution provided substrate conversions and product yields relative to the internal standard integration. The ratio of isomers was determined by GC (see spectra at the end of this document) or ^{1}H-NMR. Commercially unavailable products were identified by a combination of ^{1}H, ^{13}C{^{1}H}-NMR analysis, and HRMS. The oxidized products were identified by comparison to the GC retention time of authentic products.
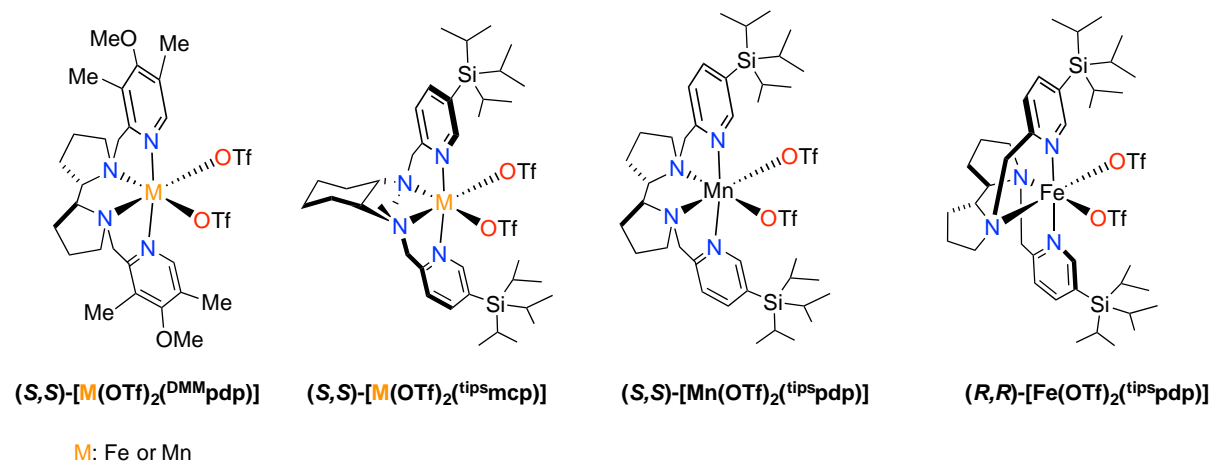
IX.4.3.1. Acetylation

In specific cases, substrates were acetylated according to the following procedure;[5] 0.1 mL methyl imidazole and 1 mL of acetic anhydride were added and the mixture stirred for 15 minutes at room temperature. After 15 minutes, ice (approx. 2 gr) is added to the solution and the mixture was stirred for 15 additional minutes. The organic layer is treated with 2 mL of 1M H_2SO_4. After vigorously shaking the vial, the organic layer is separated and treated first with 2 mL of $NaHCO_3$, and then with 2 mL of water. The resultant organic layer is filtered through a $MgSO_4$ plug and concentrated under vacuum. The crude material was purified by column chromatography using an appropriate solvent system, as described in each individual procedure.

IX.4.3.2. Oxidation with PCC

Alcohol products resulting from the oxidation of *cis*-**S8** and *cis*-**S9** were identified after oxidation to the corresponding carbonyl products according to the following procedure;[13] to a solution of the crude material in CH_2Cl_2 (2 mL) at RT was added Celite® (0.3 mmol) followed by PCC (0.3 mmol). The reaction mixture was stirred at RT for 16 h after which it was filtered through a pad of SiO_2, eluted with EtOAc, and concentrated under vacuum. The crude material was purified by column chromatography using an appropriate solvent system, as described in each individual procedure. Ratio of ketones, determined by GC provided the ratio of the original alcohol regioisomers (spectra showed at the end of the file).

## IX.4.4. Optimization

IX.4.4.1. Different catalysts tested

(S,S)-[M(OTf)₂(ᴰᴹᴹpdp)]   **(S,S)-[M(OTf)₂(ᵗⁱᵖˢmcp)]**   **(S,S)-[Mn(OTf)₂(ᵗⁱᵖˢpdp)]**   **(R,R)-[Fe(OTf)₂(ᵗⁱᵖˢpdp)]**

M: Fe or Mn

Scheme IX.5. Catalysts tested.

Table IX.10. Catalytic oxidation of **S1** in HFIP with a series of related iron and manganese catalysts.

Catalyst	Conv. (%)[a]	Yield P1b (%)[a]	Yield P1c (%)[a]	Yield P1d (%)[a]	Yield P1a (%)[a]
(S,S)-Mn^{DMM}pdp	71	49	17	4	2
***(S,S)*- Mn^{tips}mcp**	**77**	**49**	**10**	**3**	**1**
(S,S)-Mn^{tips}pdp	73	48	11	3	1
(R,R)-Fe^{tips}pdp	67	41	14	4	1
(S,S)-Fe^{DMM}pdp	43	27	9	4	3
(S,S)-Fe^{tips}mcp	60	36	12	2	2

[a] Conversion and yields determined by GC. Reactions were run in duplicate. Values included in the table IX.10 represent average values with typical errors being <5%.

Table IX.11. Catalytic oxidation of **S14** in HFIP with a series of related iron and manganese catalysts.
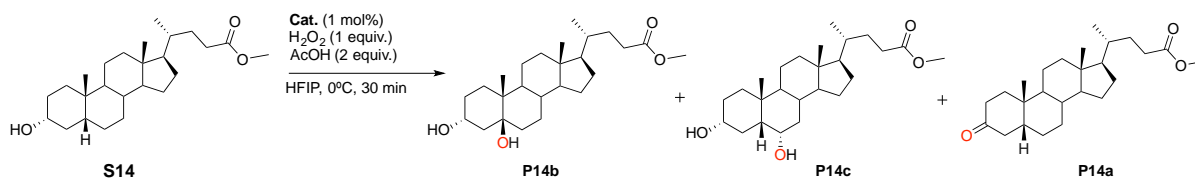
Catalyst[a]	Conv. (%)	Yield P14b (%)	Yield P14c (%)	Yield P14a (%)
(*R,R*)-Fe^{tips}pdp	78	26	14	5
(*S,S*)-Fe^{tips}mcp	70	16	10	4
(*S,S*)-Fe^{DMM}pdp	75	17	10	3
(*S,S*)-Mn^{tips}pdp	76	23	10	6
(*S,S*)-Mn^{tips}mcp	82	20	8	5

[a] Conversion and yields determined by GC. Reactions were run in duplicate. Values included in the table IX.11 represent average values with typical errors being <5%.

IX.4.4.2. Mixture of solvents

Table IX.12. Catalytic oxidation of **S1** in a mixture of solvents.
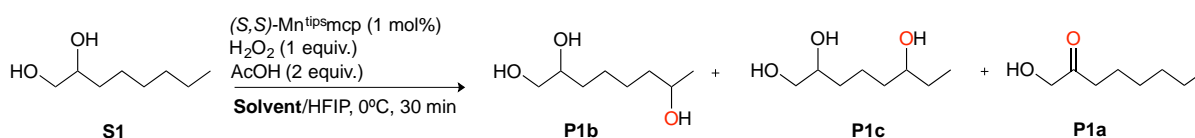
Solvents	Conv. (%)[a]	Yield P1b (%)	Yield P1c (%)	Yield P1a (%)
CH₃CN/HFIP	63	6	3	17
ACOEt/HFIP	47	10	4	11
CH₂Cl₂/HFIP	64	34	9	3

[a] Conversion and yields determined by GC. Reactions were run in duplicate. Values included in the table IX.12 represent average values with typical errors being <5%.

IX.4.4.3. Rate of syringe pump addition of oxidant

Table IX.13. Catalytic oxidation of **S1** at different rate of syringe pump addition of oxidant.
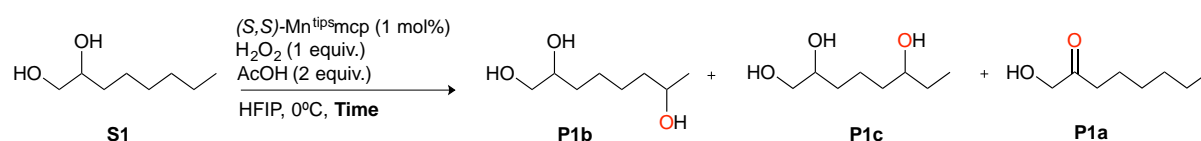
Time	Conv. (%)[a]	Yield P1b (%)	Yield P1c (%)	Yield P1a (%)
15 min	74	52	11[b]	2
30 min	**77**	**49**	**10[b]**	**1**
60 min	88	55	13[b]	2

[a] Conversion and yields determined by GC. [b] 3% of γ octane-triol (tentatively assigned by GC-MS analysis) was also observed. Reactions were run in duplicate. Values included in the table IX.13 represent average values with typical errors being <5%.

IX.4.4.4. Amount of oxidant

Table IX.14. Catalytic oxidation of **S1** with different amounts of H_2O_2.
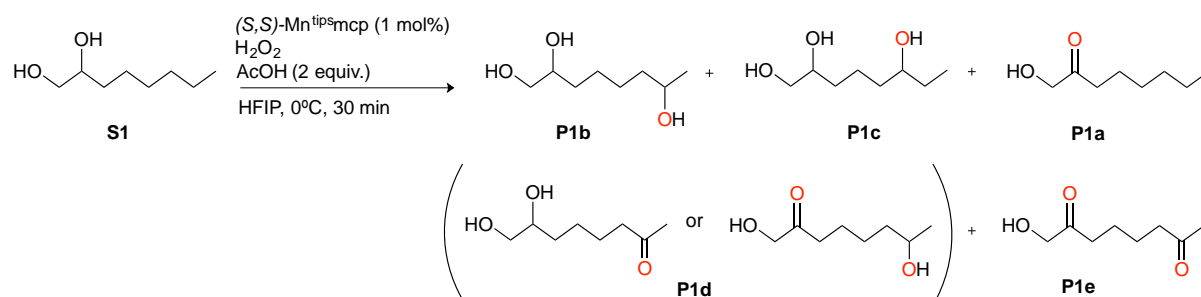
H_2O_2 (equiv.)	Conversion[a] (%)	Yield P1b (%)	Yield P1c (%)	Yield P1a (%)	Yield P1d (%)	Yield P1e (%)
1 equiv.	97	49	10	1	-	-
3 equiv.	97	8	4		23+4	8
5 equiv.	98	2	-		13+2	25

[a] Conversion and yields determined by GC. Reactions were run in triplicate. Values included in the table IX.14 represent average values with typical errors being <5%.

IX.4.4.5. Effect of HFIP on the oxidation of substrates containing other oxygenated functional groups
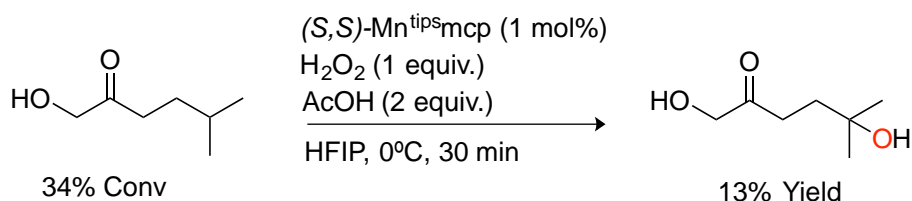
Scheme IX.6. Oxidation of substrate containing other oxygenated functional groups in HFIP.

Table IX.15. Catalytic oxidation of **S0**.
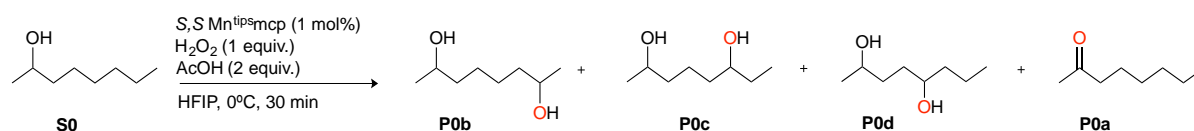
Conversion (%)[a]	Yield P0b (%)	Yield P0c (%)	Yield P0d (%)	Yield P0a (%)
81	45	13	10	5

[a] Conversion and yields determined by GC. Reactions were run in duplicate. Values included in table IX.15 represent average values with typical errors being <5%.

The comparison between the oxidation of 2-octanol and 1,2-octanediol indicates a modest enhanced deactivation by the diol moiety as evidenced by a smaller amount of carbonyl products in the oxidation of the diol.

IX.4.5. Comparison of product distribution between CH₃CN and HFIP

Table IX.16. Catalytic oxidation of **S1** in different solvents.

Solvents	Conv. (%)	Yield P1b (%)	Yield P1c (%)	Yield P1a (%)
CH₃CN[a]	28			21[b]
HFIP[a]	83	49	10	1
HFIP Isolated	-	63[c]	14[c]	-

[a] Conversion and yields determined by GC. Reactions were run in triplicate. Values included in the table IX.16 represent average values with typical errors being <5%. [b] Identification of product by GC-MS analysis. [c] **P1b** and **P1c** isolated together in a 77% combined yield (as an inseparable mixture of isomers) and a ratio of 4.5:1 determined by GC. 3% of γ octane-triol was observed.

Table IX.17. Catalytic oxidation of **S2** in different solvents.

Solvents	Conv. (%)	Yield P2b (%)	Yield P2c (%)	Yield P2a (%)
CH₃CN[a]	53			14
HFIP[a,b]	64	26	2	6
HFIP Isolated	-	39c	-	11

[a] Conversion and yields determined by GC. Reactions were run in triplicate. Values included in the table IX.17 represent average values with typical errors being <5%. [b] additional 5% of 1,2-dihydroxyhexan-5-one was also detected by GC. [c] Isolated with **P2c** (inseparable mixture of isomers), ratio of 10:1 determined by GC. [d] Identified by GC-MS analysis.

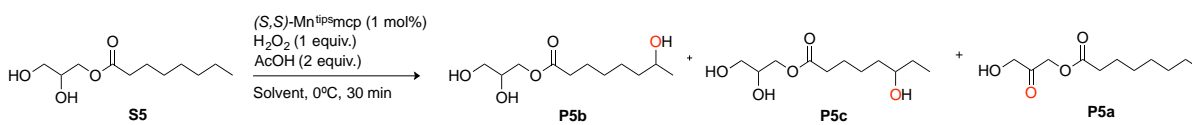**Table IX.18.** Catalytic oxidation of **S3** in different solvents.
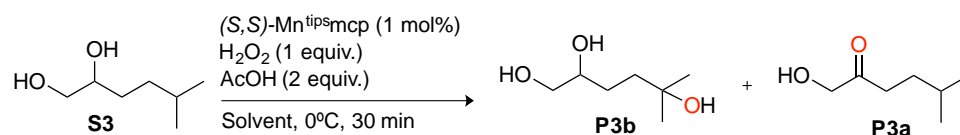
Solvents	Conv. (%)	Yield P3b (%)	Yield P3a (%)
CH$_3$CN[a]	10	-	-
HFIP[a,b]	75	55	5[c]
HFIP Isolated	77	42	

[a] Conversion and yields determined by GC. Reactions were run in triplicate. Values included in the table IX.18 represent average values with typical errors being <5%. [b] In addition, two hydroxyketones are identified by GC-MS analysis (~13% combined yield). [c] Characterization of the product by comparison of the retention time with authentic compound, and by GC-MS.

Table IX.19. Catalytic oxidation of **S4** in different solvents.
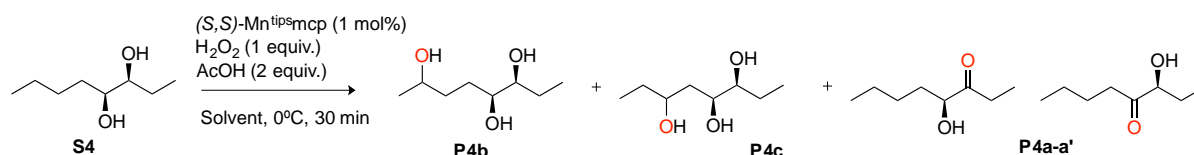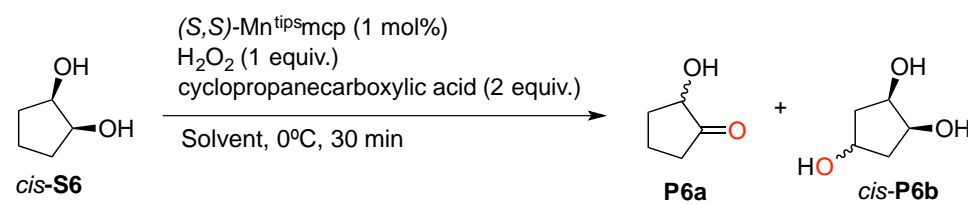
Solvents	Conv. (%)	Yield P4b (%)	Yield P4c (%)	Yield P4a-a' (%)
CH$_3$CN[a]	24			18
HFIP[a]	70	39[b]	3	14[c]
HFIP Isolated	72	35[d]	3[d]	13[c]

[a] Conversion and yields determined by GC. Reactions were run in triplicate. Values included in the table IX.19 represent average values with typical errors being <5%. [b] Mixture of inseparable mixture of diastereoisomers with ratio 1.6:1. [c] Mixture of the two isomers with ratio 1.5:1, products determined by GC-MS analysis. [d] **P4b** and **P4c** isolated together (as an inseparable mixture) in a 38% combined yield and a ratio of 12:1 determined by GC.

**Table IX.20.** Catalytic oxidation of **S5** in different solvents.

Solvents	Conv. (%)	Yield P5b (%)	Yield P5c (%)	Yield P5a (%)
CH$_3$CN[a]	50			7[b]
HFIP[a]	79	50	11	Traces
HFIP Isolated	75	46[c]	10	

[a] Conversion and yields determined by GC. Reactions were run in triplicate. Values included in the table IX.20 represent average values with typical errors being <5%. [b] Identification of product by GC-MS analysis. 4% of C$_5$ hydroxylated isomer (**P5d**) based on GC-MS. [c] Isolated as an inseparable mixture of the 3 regioisomers in C-6 (**P5c**) and C-5 (**P5d**) in 10% and 4% yield respectively (combined yield 60%). [c] Identification of product by GC-MS analysis. 4% of C$_5$ hydroxylated isomer (**P5d**) based on GC-MS.

Table IX.21. Catalytic oxidation of *cis*-**S6** in different solvents.

Solvents	Conv. (%)	Yield P6a (ee)[c] (%)	Yield *cis*-P6b (%)
CH$_3$CN[a]	45	16 (22)	n.d
HFIP[a,b]	72	52 (29)	n.d
HFIP Isolated		54 (29)	n.d

[a] Conversion and yields determined by GC. Reactions were run in duplicate. Values included in the table IX.21 represent average values with typical errors being <5%.). [b] 19 % ee of **P6a** when AcOH is used instead of cyclopropanecarboxylic acid. [c] Enantiomeric excess (ee) determined by GC with a chiral stationary phase. (CYCLOSIL-B column). [c] 19 % ee of **P6a** when AcOH is used instead of cyclopropanecarboxylic acid.

Table IX.22. Catalytic oxidation of *cis*-**S7** in different solvents.
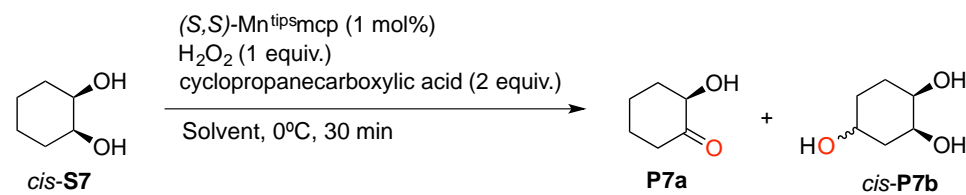
Solvents	Conv. (%)	Yield P7a (ee)[b] (%)	Yield *cis*-P7b (%)
CH₃CN[a]	33	29 (8)	n.d
TFE	82	47 (22)	n.d
HFIP[a,c]	87	75 (63)	n.d
HFIP Isolated	72	64 (63)	n.d

[a] Conversion and yields determined by GC. Reactions were run in triplicate. Values included in the table IX.22 epresent average values with typical errors being <5%. [b] ee determined by GC with a chiral stationary phase. (CYCLOSIL-B column). [c] 49 % ee of **P7a** when AcOH is used instead of cyclopropanecarboxylic acid.

Table IX.23. Catalytic oxidation of *cis*-**S8** in different solvents.
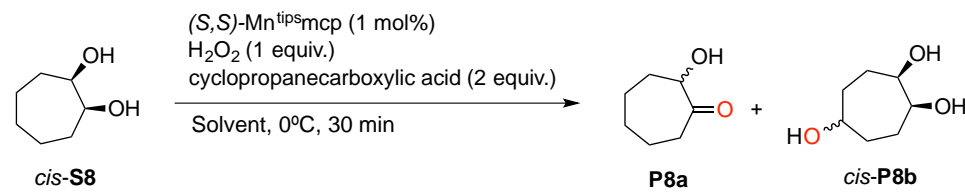
Solvents	Conv. (%)	Yield P8a (ee)[d] (%)	Yield *cis*-P8b (%)
CH₃CN[a]	46	32 (9)[b]	n.d
HFIP[a]	82	48 (42)[b]	8[c]
HFIP Isolated		52 (52)	

[a] Conversion and yields determined by GC. Reactions were run in triplicate. Values included in the table IX.23 represent average values with typical errors being <5%. [b] Using AcOH instead of cyclopropanecarboxylic acid. [c] 13% total yield of inseparable mixture of two regioisomers. [d] ee determined by GC with a chiral stationary phase. (CYCLOSIL-B column)

Table IX.24. Catalytic oxidation of *cis*-**S9** in different solvents.
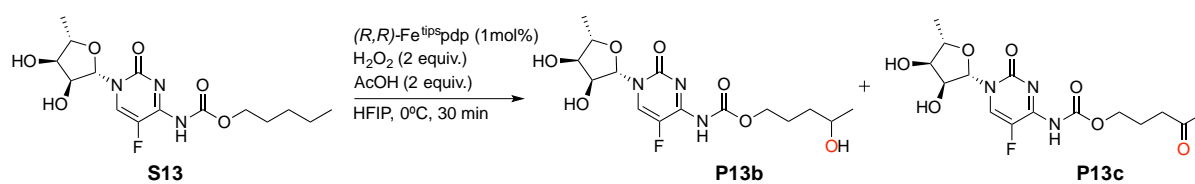

Solvents	Conv. (%)	Yield P5b (ee)[c] (%)	Yield P5c (%)	Yield P5a (%)
CH$_3$CN[a]	36	25	0	
HFIP[a]	78	12(12)	46	19
HFIP Isolated			40[b]	17[b]

[a] Conversion and yields determined by GC. Reactions were run in triplicate. Values included in the table IX.24 represent average values with typical errors being <5%. [b] Isolated together as an inseparable mixture of regioisomers. Identification of C-2 and C-3 alcohols was done by converting the mixture to ketones following PCC oxidation. [c] ee determined by GC with a chiral stationary phase. (CYCLOSIL-B column).

Table IX.25. Catalytic oxidation of **S10** in different solvents.

Solvents	Conv. (%)	Yield P10b (%)
CH$_3$CN[a]	11	0
HFIP[a]	58	35
HFIP[a,b]	76	52
HFIP Isolated[b]	98	74

[a] Conversion and yields determined by GC. Reactions were run in triplicate. Values included in the table IX.25 represent average values with typical errors being <5%. [b] 3 mol% of catalyst and H$_2$O$_2$ followed by and second addition of catalyst (3 mol%) and H$_2$O$_2$. (CYCLOSIL-B column). [c] 49 % ee of **P7a** when AcOH is used instead of cyclopropanecarboxylic acid.

Table IX.26. Catalytic oxidation of **S11** in different solvents.
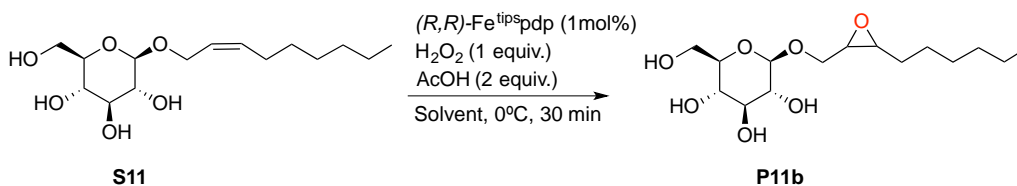
Solvents	Conv. (%)	Yield P11b (%)
CH$_3$CN[a]	100	93
HFIP[a]	97	80
HFIP Isolated[b]	96	61

[a] Conversion and yields determined by GC. Reactions were run in triplicate. Values included in the table IX.26 represent average values with typical errors being <5%.

**Table IX.27.** Catalytic oxidation of **S12** in different solvents.
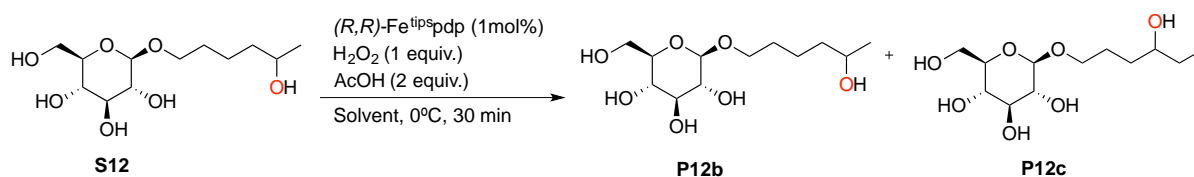
Solvents	Conv. (%)	Yield P12b (%)	Yield P12c (%)
CH$_3$CN[a]	0	0	
HFIP[a]	64	26	6
HFIP[a,b]	78	52	13
HFIP Isolated[b]	76	53[c]	12[c]

[a] Conversion and yields determined by GC. Reactions were run in triplicate. Values included in the table IX.27 represent average values with typical errors being <5%. [b] Isolated using 3 mol% of catalyst. [c] Isolated with **P12c** (inseparable mixture, total yield 65%).

Table IX.28. Catalytic oxidation of **S13** in different solvents.

Solvents	Conv. (%)	Yield P13b (%)	Yield P13c (%)
HFIP Isolated	68	50	12

Table IX.29. Catalytic oxidation of **S14** in different solvents.
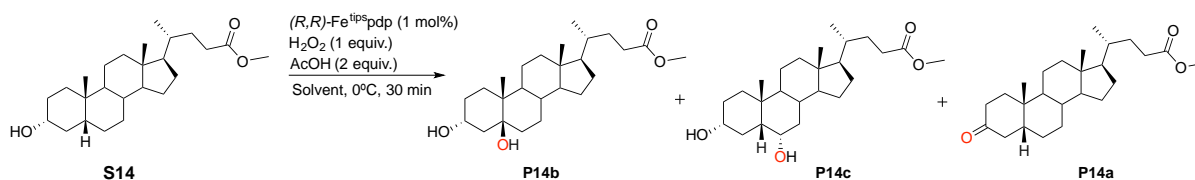
Solvents	Conv. (%)	Yield P14b (ee)[c] (%)	Yield P14c (%)	Yield P14a (%)
CH$_3$CN[a]	67			37
HFIP[a]	78	26	14	5
HFIP Isolated		34	18	

[a] Conversion and yields determined by GC. Reactions were run in triplicate. Values included in the table IX.29 represent average values with typical errors being <5%.

Table IX.30. Catalytic oxidation of **S15** in different solvents and isolated.
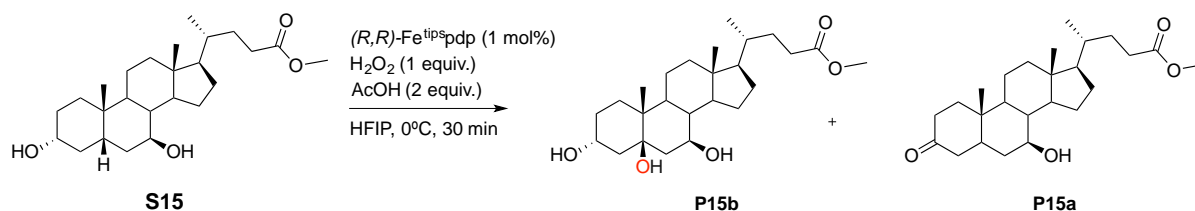
Solvents	Conv. (%)	Yield P13b (%)	Yield P13c (%)
HFIP Isolated	35	17	8

IX.4.5. General procedure for isolation of products

A 25 mL round bottom flask was charged with: catalyst (15.15 or 45.45 µmol, 1.0 or 3 mol%), substrate (1.51 mmol, 1 equiv.), HFIP (12 mL) and a magnetic stir bar. Acetic acid (or cyclopropylcarboxylic acid) was added (2 equiv.) and the mixture was cooled at 0 ºC under magnetic stirring. Then, 2.8 mL of a 0.53 M hydrogen peroxide solution in HFIP (1 equiv.) were added by syringe pump over a period of 30 min. Then, the solution was stirred for further 15 minutes. At this point, the solvent was removed under reduced pressure. This residue was purified by column chromatography in silica gel to obtain the pure products. In several cases, separation between isomers was not possible, and a combined yield is provided.

Modified procedure for the oxidation of glycoside S10. A 25 mL round bottom flask was charged with: catalyst (45.45 µmol, 3 mol%), substrate (1.51 mmol, 1 equiv.), HFIP (12 mL) and a magnetic stir bar. Acetic acid (or cyclopropylcarboxylic acid) was added (2 equiv.) and the mixture was cooled at 0 ºC under magnetic stirring. Then, 2.8 mL of a 0.53 M hydrogen peroxide solution in HFIP (1 equiv.) were added by syringe pump over a period of 30 min. At this point, a second addition of catalyst (45.45 µmol, 3 mol%) dissolved in 100 µL of HFIP was added to the reaction mixture. Then, 2.8 mL of a 0.53 M hydrogen peroxide solution in HFIP (1 equiv.) were added by syringe pump over a period of 30 min. Finally, the solution was stirred for further 15 minutes. At this point, the solvent was removed under reduced pressure. This residue was purified by column chromatography in silica gel to obtain the pure products

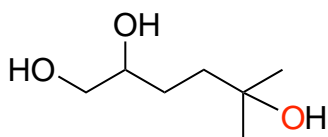### IX.4.5.1. Characterization of isolated products
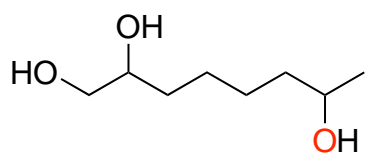
(**P1b**) Purification by flash chromatography on silica gel (SiO$_2$; CH$_2$Cl$_2$/MeOH 9/1) gave the product combined with **P1c**, colorless oil (77% total yield and a ratio of 4.5:1 determined by GC) ^{1}H-NMR (MeOD, 400 MHz) δ, ppm: 3.60-3.49 (m, 1H), 3.51-3.43 (m, 3H), 1.53-1.38 (m, 8H), 1.15 (d, *J* = 6.2 Hz, 3H). ^{13}C{^{1}H-NMR (MeOD, 100 MHz) δ, ppm: 71.8, 67.1, 66.0, 38.8, 33.1, 25.6, 25.6, 22.2. HRMS(ESI+) *m/z* calculated for C$_8$H$_{18}$O$_3$ [M+Na]$^+$ 185.1148, found 185.1152.

*For spectroscopic characterization of the minor product (**P1c**), see digital experimental section.*
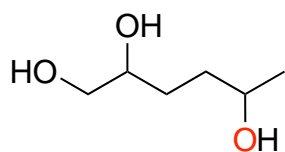
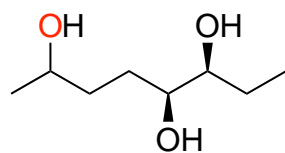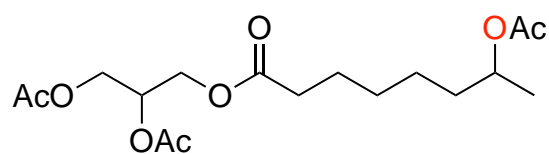(**P2b**) Purification by flash chromatography on silica gel (SiO₂; CH₂Cl₂/MeOH 9/1) gave the product combined with **P2c** (10:1 ratio determined by GC) as a colorless oil (39% yield). ¹H-NMR (MeOD, 400 MHz) δ, ppm: 3.78-3.73 (m, 1H), 3.60-3.43 (m, 4H), 1.70-1.36 (m, 5H). ¹³C{¹H}-NMR (MeOD, 100 MHz) δ, ppm: 72.1, 71.8, 67.4, 67.1, 66.0, 66.0, 34.8, 34.7, 29.4, 29.3, 22.2, 22.2, 22.1. HRMS(ESI+) *m/z* calculated for $C_6H_{14}O_3$ [M+Na]⁺ 157.0835, found 157.0841. The assignment is in agreement with the reported.[14]

*For spectroscopic characterization of the minor product (**P2c**), see digital experimental section.*

(**P3b**) Purification by flash chromatography on silica gel (SiO₂; CH₂Cl₂/MeOH 9/1) gave the product as colorless oil (42% yield) ¹H-NMR (MeOD, 400 MHz) δ, ppm: 3.61-3.41 (m, 3H), 1.74-1.54 (m, 2H), 1.56-1.41 (m, 2H), 1.21 (d, J = 1.6 Hz, 6H).¹³C{¹H}-NMR (MeOD, 100 MHz) δ, ppm: 72.4, 69.9, 65.9, 39.2, 27.9, 27.8, 27.8. HRMS(ESI+) *m/z* calculated for $C_7H_{16}O_3$ [M+Na]⁺ 171.0980, found 171.0987.
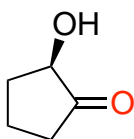
(**P4b**) Purification by flash chromatography on silica gel (SiO₂; CH₂Cl₂/MeOH 9/1) gave the product combined with **P4c** (12:1 ratio determined by GC) as a colorless oil (35% yield) ¹H-NMR (MeOD, 400 MHz) δ, ppm: 3.75 (h, J = 5.5 Hz, 1H), 3.46-3.37 (m, 1H), 3.37-3.28 (m, 1H), 1.72-1.38 (m, 4H), 1.19 (d, J = 6.2 Hz, 3H), 0.99 (t, J = 7.4 Hz, 3H). (MeOD, 100 MHz) δ, ppm:75.5, 73.8, 73.54, 67.4, 67.2, 35.3, 35.1, 29.1, 28.9, 25.4, 22.3, 22.2, 9.4. HRMS(ESI+) m/z calculated for $C_8H_{18}O_3$ [M+Na]⁺ 185.1148, found 185.1149.
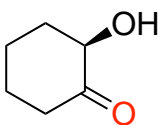
(**P5b**) After esterification, purification by flash chromatography on silica gel (SiO₂; Hexane/EtOAc 1/1) gave the product as a mixture of **P5b** (46%), **P5c** (10%) and **P5d** (4%) as a colorless oil (relative ratios determined by GC, combined yield 60%). ¹H-NMR is reported as a mixture of regioisomers that overlap in the spectrum. ¹H-NMR (MeOD, 400 MHz) δ, ppm: 5.29-5.24 (m, 1H), 4.39-4.32 (m, 3H), 4.22-4.17 (dd, J=12.0,

6.2 Hz, 3H), 2.37 (t, *J*=7.3 Hz, 3H), 2.08 (s, 3H), 2.04 (s, 3H), 1.07-1.47 (m, 6H), 1.35 (s, 5H) 1.22 (d, *J*=6.3 Hz, 3H). $^{13}C\{^1H\}$-NMR (MeOD, 100 MHz) δ, ppm: 173.5, 171.5, 171.1, 170.6, 71.0, 69.4, 62.1, 61.9, 35.4, 33.3, 28.5, 24.7, 24.4, 20.0, 19.6, 19.4, 19.0. HRMS(ESI+) *m/z* calculated for $C_{17}H_{28}O_8$ [M+Na]$^+$ 383.1676, found 383.1685.

**For spectroscopic characterization of the minor product (**P5c**), see digital experimental section.*

(**P6a**) Purification by flash chromatography on silica gel (SiO$_2$; Hexane/EtOAc 6/4) gave the product as a colorless oil (54% yield) ^{1}H-NMR (MeOD, 400 MHz) δ, ppm: 1.62-1.73 (m, 2H), 1.76-1.89 (m, 1H), 1.99-2.09 (m, 1 H), 2.42-2.46 (m, 2H), 4.05 (t, J = 10.0 Hz, 1H). $^{13}C\{^1H\}$-NMR (MeOD, 100 MHz) δ, ppm: 218.4, 75.0, 30.2, 30.8, 16.2. HRMS(ESI+) *m/z* calculated for $C_5H_8O_2$ [M+Na]$^+$ 123.0417, found 123.0426.

(**P7a**) Purification by flash chromatography on silica gel (SiO2; Hexane/EtOAc 6/4) gave the product as a colorless oil (64% yield) 1H-NMR (MeOD, 400 MHz) δ, ppm: 4.20 (ddd, *J* = 12.0, 6.5, 1.1 Hz, 1H), 2.53-2.38 (m, 2H), 2.34 (ddd, *J* = 12.5, 6.3, 2.9 Hz, 1H), 2.09 (ddt, *J* = 13.6, 6.1, 3.1 Hz, 1H), 1.98-1.86 (m, 1H), 1.83-1.73 (m, 1H), 1.64-1.52 (m, 2H). $^{13}C\{^1H\}$-NMR (MeOD, 100 MHz) δ, ppm: 211.3, 75.1, 39.6, 36.5, 27.3, 23.3. HRMS(ESI+) *m/z* calculated for $C_6H_{10}O_2$ [M+Na]$^+$ 137.0573, found 137.0582.
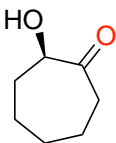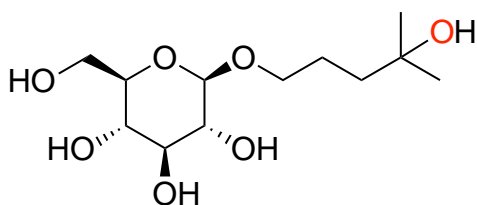

(**P8a**) Purification by flash chromatography on silica gel (SiO$_2$; CH$_2$Cl$_2$/MeOH 9/1) gave the product as a colorless oil (52% yield) ^{1}H-NMR (MeOD, 400 MHz) δ, ppm: 4.35-3.38 (m, 1H), 2.69-2.65 (m, 1H), 2.63-2.40 (m, 1H), 2.02-1.98 (m, 2H), 1.84-1.55 (m,7H). $^{13}C\{^1H\}$-NMR (MeOD, 100 MHz) δ, ppm: 213.7, 76.6, 39.8, 33.5, 29.0, 26.1, 23.2. HRMS(ESI+) *m/z* calculated for $C_7H_{12}O_2$ [M+Na]$^+$ 151.0730, found 151.0735.
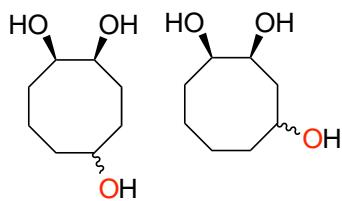
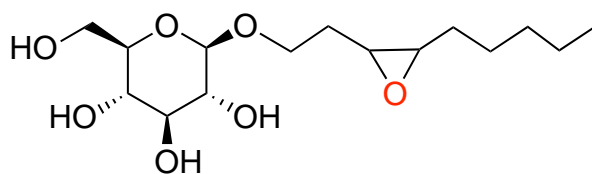(**P9b-c**) Purification by flash chromatography on silica gel (SiO$_2$; CH$_2$Cl$_2$/MeOH 9/1) gave the product as a mixture of **P9b** and **P9c** (2.4:1 ratio determined by GC, 57% combined yield) ^{1}H-NMR (CDCl$_3$, 400 MHz) δ, ppm: 3.89-3.78 (m, 3H), 2.05-1.44 (m, 10H). ^{13}C{^{1}H}-NMR (CDCl$_3$, 100 MHz) δ, ppm:73.2, 72.9, 72.7, 72.2, 72.2, 71.8, 71.3, 70.1, 70.0, 69.6, 68.5, 67.5, 38.9, 37.8, 34.5, 34.2, 33.3, 33.3, 30.3, 30.1, 29.9, 29.5, 29.4, 29.1, 26.6, 26.0, 23.0, 22.1, 21.7, 21.1, 19.2, 19.1. HRMS(ESI+) *m/z* calculated for C$_8$H$_{18}$O$_3$ [M+Na]$^+$ 183.0997, found 183.0989.
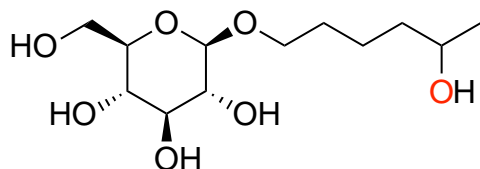

(**P10b**) Purification by flash chromatography on silica gel (SiO$_2$; CH$_2$Cl$_2$/MeOH 6/2) gave the product as a colorless oil (74% yield) ^{1}H-NMR (MeOD, 400 MHz) δ, ppm: 4.26 (s, 1H), 3.94-3.82 (m, 2H), 3.66 (dd, *J* = 11.9, 5.0 Hz, 1H), 3.61-3.48 (m, 1H), 3.39-3.26 (m, 3H), 3.22-3.12 (m, 1H), 1.70 (dq, *J* = 10.9, 6.2 Hz, 2H), 1.53 (dd, *J* = 9.7, 5.7 Hz, 2H), 1.18 (s, 6H). ^{13}C{^{1}H}-NMR (CDCl$_3$, 100 MHz) δ, ppm: 103.0, 76.7, 76.5, 73.7, 70.3, 70.0, 69.9, 61.4, 39.4, 27.9, 27.8, 24.4 HRMS(ESI+) *m/z* calculated for C$_{12}$H$_{24}$O$_7$ [M+Na]$^+$ 303.1414, found 303.1429.
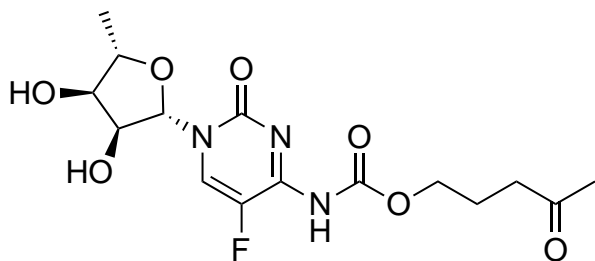

(**P11b**) Purification by flash chromatography on silica gel (SiO$_2$; CH$_2$Cl$_2$/MeOH 6/2) gave the product as a colorless oil (61% yield and 89% yield determined by GC) ^{1}H-NMR (MeOD, 400 MHz) δ, ppm: 4.29 (d, *J* = 9.3 Hz, 1H), 4.11-3.99 (m, 1H), 3.86 (d, *J* = 11.7 Hz, 1H), 3.70 (d, *J* = 37.6 Hz, 2H), 3.32 (dd, *J* = 28.1, 7.6 Hz, 3H), 3.18 (dd, *J* = 18.6, 10.0 Hz, 2H), 3.03-2.89 (m, 1H), 2.02-1.85 (m, 1H), 1.72 (m, 1H), 1.56-1.48 (m, 4H), 1.42-1.25 (m, 4H), 0.85 (t, 3H). ^{13}C{^{1}H}-NMR (MeOD, 100 MHz) δ, ppm: 103.1, 102.9, 76.6, 76.5, 73.7, 73.7, 70.3, 70.2, 66.9, 66.7, 61.4, 61.4, 57.3, 57.1, 54.8, 54.8, 31.4, 28.2, 28.1, 27.5, 25.9, 22.3, 13.0. HRMS(ESI+) *m/z* calculated for C$_{15}$H$_{28}$O$_7$ [M+Na]$^+$ 343.1727, found 343.1737.

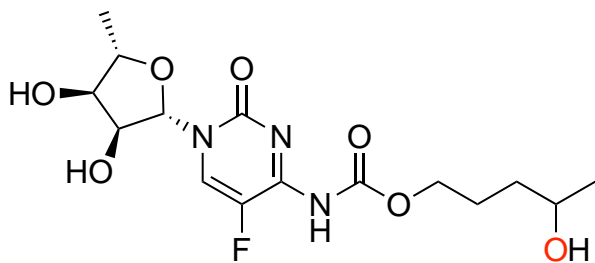(**P12b**) Purification by flash chromatography on silica gel (SiO$_2$; CH$_2$Cl$_2$/MeOH 6/2) gave the product combined with **P12c** as a colorless oil (53% **P12b** and 12% **P12c**, relative ratios determined by GC) ^{1}H-NMR (MeOD, 400 MHz) δ, ppm: 4.27 (d, *J* = 7.8 Hz, 1H), 3.91 (d, *J* = 7.8 Hz, 1H), 3.78-3.65 (m, 2H), 3.57 (q, *J* = 7.4, 6.6 Hz, 1H), 3.40-3.23 (m, 4H), 3.23-3.14 (m, 1H), 1.73-1.59 (m, 2H), 1.58-1.37 (m, 4H), 1.16 (s, 2H). ^{13}C{^{1}H}-NMR (MeOD, 100 MHz) δ, ppm: 103.0, 76.7, 76.5, 73.7, 70.3, 69.4, 67.1, 61.4, 38.5, 29.4, 22.1, 21.9. HRMS(ESI+) *m/z* calculated for C$_{12}$H$_{24}$O$_7$ [M+Na]$^+$ 303.1414, found 303.1418.


(**P13a**) The sample is a mixture of **P13a** and **P13b**. For more details of the spectroscopic characterization see section 9. HRMS(ESI+) *m/z* calculated for C$_{15}$H$_{20}$FN$_3$O$_7$ [M+Na]$^+$ 396.1177, found 396.1178.
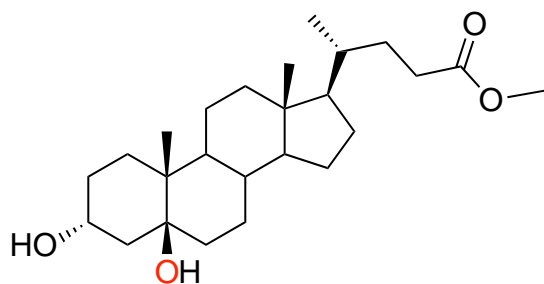

(**P13b**) Purification by flash chromatography on silica gel (SiO$_2$; EtOAc/MeOH 9/1) gave the product as a colorless oil (50% yield) ^{1}H-NMR (D$_2$O, 400 MHz) δ, ppm: 8.00 (d, *J* = 6.0 Hz, 1H), 5.71 (s, 1H), 4.39-3.93 (m, 5H), 3.90-3.69 (m, 2H), 1.79-1.59 (m, 2H), 1.48 (q, *J* = 7.5 Hz, 2H), 1.39 (d, *J* = 6.3 Hz, 3H), 1.11 (d, *J* = 6.2 Hz, 3H). ^{13}C{^{1}H}-NMR (D$_2$O, 100 MHz) δ, ppm: 154.3, 154.2, 128.8, 128.6, 91.8, 79.7, 74.5, 74.0, 67.4, 66.9, 34.0, 24.2, 21.8, 17.2. HRMS(ESI+) *m/z* calculated for C$_{15}$H$_{22}$FN$_3$O$_7$ [M+Na]$^+$ 398.1334, found 398.1332.
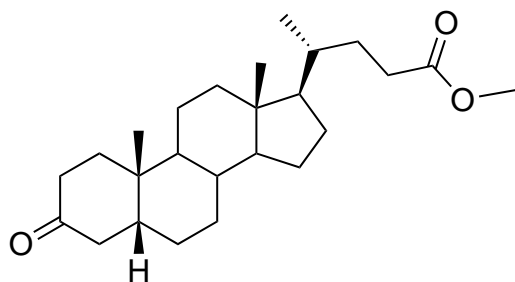
(**P14a**) Purification by flash chromatography on silica gel (SiO$_2$; CH$_2$Cl$_2$/MeOH 9/1) gave the product as a colorless oil (5% yield). ^{1}H-NMR (CDCl$_3$, 400 MHz) δ, ppm: 3.68 (s, 3H), 2.81-2.57 (m, 1H), 2.46-2.28 (m, 2H), 2.30 -2.12 (m, 2H), 2.08-1.99 (m, 3H), 1.96 -1.75 (m, 4H), 1.56 -1.16 (m, 12H), 1.16 -1.05 (m, 4H), 1.03 (s, 3H), 0.93 (d, *J* = 6.5 Hz, 3H), 0.69 (s, 3H). ^{13}C{^{1}H}-NMR (CDCl$_3$, 100 MHz) δ, ppm: 213.2, 174.7, 56.4, 55.9, 51.5, 44.3, 42.8, 42.4, 40.7, 40.1, 37.2, 37.0, 35.5, 35.3, 34.9, 31.0, 31.0, 28.2, 26.6, 25.8, 24.2, 22.7, 21.2, 18.3, 12.1. HRMS(ESI+) *m/z* calculated for C$_{25}$H$_{40}$O$_3$ [M+Na]$^+$ 411.2870, found 411.2877.

(**P14b**) Purification by flash chromatography on silica gel (SiO$_2$; CH$_2$Cl$_2$/MeOH 9/1) gave the product as a colorless oil (34% yield) that crystallizes upon standing. ^{1}H-NMR (CDCl$_3$, 400 MHz) δ, ppm: 4.05-4.00 (m, 1H), 3.68 (s, 3H), 2.41-2.38 (m, 1H), 2-36-2.24 (m, 1H), 2.19-1.69 (m, 5H) 1.65-1.55 (m, 7H), 1.45-1.30 (m, 9H) 1.15-1.09 (m, 4H) 0.92 (d, 6H) 0.66 (s, 3H). ^{13}C{^{1}H}-NMR (CDCl$_3$, 100 MHz) δ, ppm: 174.8, 75.7, 68.1, 56.5, 55.8, 51.5, 43.1, 42.5, 41.9, 39.8, 39.7, 37.0, 35.4, 35.0, 31.1, 31.0, 30.0, 29.7, 28.7, 28.1, 24.2, 21.1, 18.2, 16.3, 12.0. HRMS(ESI+) *m/z* calculated for C$_{25}$H$_{42}$O$_4$ [M+Na]$^+$ 429.2975, found 429.2975. Structure was confirmed by single crystal X-ray diffraction analysis. Crystals were obtained by slow evaporation of a CHCl$_3$ solution of the compound.

Crystal-Structure Determination of P14b

Colorless crystals of **C$_{25}$H$_{42}$O$_4$**, were grown from CHCl$_3$, and used for low temperature (100(2) K) X-ray structure determination. The measurement was carried out on a *Bruker D8 QUEST ECO* diffractometer using graphite-monochromated Mo *K*α radiation (*λ* = 0.71073 Å) from an x-Ray Tube. The measurements were made in the range 2.74 to 23.40° for θ. Full-sphere data collection was carried out with ω and φ scans. A total of 5671 reflections were collected of which 4883 [R(int) = 0.0225] were unique.

Structure solution and refinement was done using SHELXTL[15]. The structure was solved by direct methods and refined by full-matrix least-squares methods on F^2. The non-hydrogen atoms were refined anisotropically. The H-atoms were placed in geometrically optimized positions and forced to ride on the atom to which they are attached.

Final R indices [I>2sigma(I)] **R1 = 0.0597**, wR2 = 0.1292

R indices (all data)   R1 = 0.0951, wR2 = 0.1436
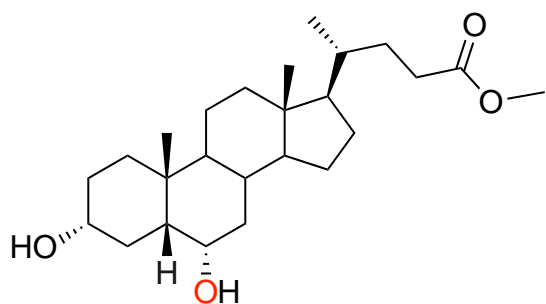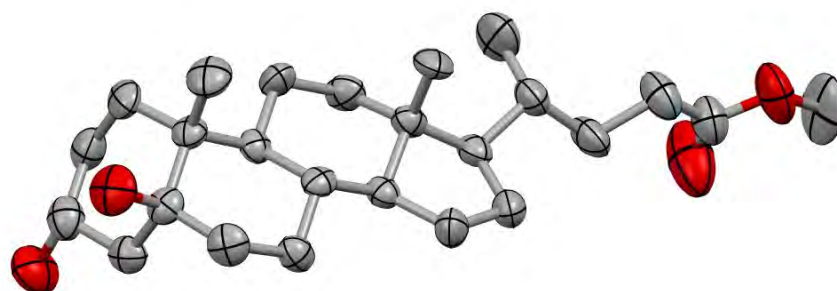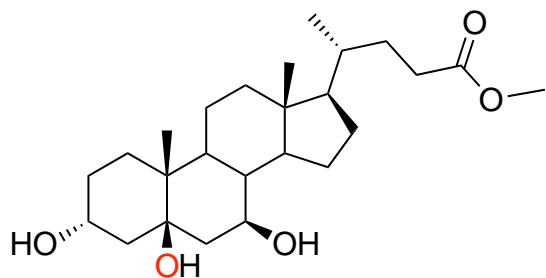

(**P14c**) Purification by flash chromatography on silica gel (SiO$_2$; CH$_2$Cl$_2$/MeOH 9/1) gave the product as a colorless oil (18% yield) ^{1}H-NMR (CDCl$_3$, 400 MHz) δ, ppm: 4.07-4.03 (m, 1H), 3.67 (s, 3H), 2.36-2.22 (m, 4H), 1.99-1.59 (m, 10H), 1.43-1.06 (m, 16H), 0.92 (s, 6H) 0.64 (s, 3H). ^{13}C{^{1}H}-NMR (CDCl$_3$, 100 MHz) δ, ppm: 174.8, 71.5, 68.0, 56.2, 55.4, 51.5, 48.5, 42.8, 40.0, 39.9, 36.0, 35.6, 35.4, 34.9, 34.8, 31.1, 31.0, 30.1, 29.3, 28.1, 24.2, 23.5, 20.8, 18.3, 12.02. HRMS(ESI+) *m/z* calculated for C$_{25}$H$_{42}$O$_4$ [M+Na]$^+$ 429.2975, found 429.2971.
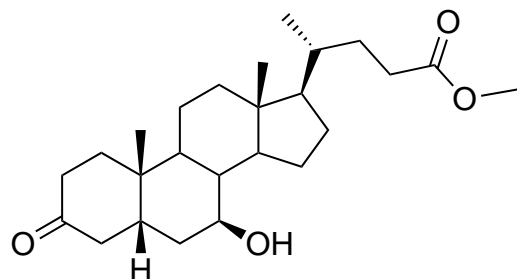
(**P15a**) Purification by flash chromatography on silica gel (SiO$_2$; CH$_2$Cl$_2$/MeOH 9/1) gave the product as a colorless oil (8% yield) the sample is a mixture of **P15a** and **S15.** ^{13}C{^{1}H}-NMR (CDCl$_3$, 100 MHz) δ, ppm: 211.9, 174.7, 70.9, 55.7,

54.9, 51.5, 44.4, 43.8, 43.4, 40.0, 39.4, 37.0, 36.4, 35.2, 34.4, 31.1, 31.0, 28.6, 26.8, 23.4, 21.7, 18.4, 12.1. The two quaternary carbons are not detected due to low amount of sample. HRMS(ESI+) *m/z* calculated for $C_{25}H_{40}O_4$ [M+Na]$^+$ 427.2830, found 427.2819.

(**P15b**) Purification by flash chromatography on silica gel (SiO$_2$; CH$_2$Cl$_2$/MeOH 9/1) gave the product as a colorless oil (17% yield) ^{1}H-NMR (CDCl$_3$, 400 MHz) δ, ppm: 4.06-4.00 (m, 1H), 3.69 (s, 3H), 3.51 (s, 1H), 2.40-2.34 (m, 1H), 2.26-2.21 (m, 1H), 1.95-1.69 (m, 11H), 1.49-1.25 (m, 12H), 0.96-0.93 (m,6H), 0.69 (s, 3H). ^{13}C{^{1}H}-NMR (CDCl$_3$, 100 MHz) δ, ppm: 174.7, 75.0, 72.3, 67.6, 55.8, 54.9, 51.5, 46.1, 43.5, 43.0, 43.0, 41.3, 39.8, 39.2, 35.3, 31.1, 31.0, 29.8, 29.6, 28.7, 26.9, 21.3, 18.4, 16.4, 12.1. HRMS(ESI+) *m/z* calculated for $C_{25}H_{42}O_5$ [M+Na]$^+$ 445.2294, found 445.2927.

IX.4.6 References

(1)   Milan, M.; Bietti, M.; Costas, M., Highly Enantioselective Oxidation of Nonactivated Aliphatic C–H Bonds with Hydrogen Peroxide Catalyzed by Manganese Complexes. *ACS Cent. Sci.* **2017**.

(2)   Font, D.; Canta, M.; Milan, M.; Cusso, O.; Ribas, X.; Gebbink, R. J. M. K.; Costas, M., Readily Accessible Bulky Iron Catalysts exhibiting Site Selectivity in the Oxidation of Steroidal Substrates. *Angew. Chem. Int. Ed.* **2016,** *55* (19), 5776-5779.

(3)   O.Cussó; Garcia-Bosch, I.; Ribas, X.; Lloret-Fillol, J.; Costas, M., Asymmetric Epoxidation with H2O2 by Manipulating the Electronic Properties of Non-heme Iron Catalysts. *J. Am. Chem. Soc.* **2013,** *135* (39), 14871-14878.

(4)   Cussó, O.; Garcia-Bosch, I.; Font, D.; Ribas, X.; Lloret-Fillol, J.; Costas, M., Highly Stereoselective Epoxidation with H2O2 Catalyzed by Electron-Rich Aminopyridine Manganese Catalysts. *Org. Lett.* **2013,** *15* (24), 6158-6161.

(5)   Borrell, M.; Costas, M., Mechanistically Driven Development of an Iron Catalyst for Selective Syn-Dihydroxylation of Alkenes with Aqueous Hydrogen Peroxide. *J. Am. Chem. Soc.* **2017,** *139* (36), 12821-12829.

(6)   Mehltretter, G. M.; Bhor, S.; Klawonn, M.; Döbler, C.; Sundermeier, U.; Eckert, M.; Militzer, H.-C.; Beller, M., A New Practical Method for the Osmium-Catalyzed Dihydroxylation of Olefins- using Bleach as the Terminal Oxidant. *Synthesis* **2003,** *2003* (02), 0295-0301.

(7)   Gouin, S.; Zhu, X. X., Synthesis of 3α- and 3β-dimers from selected bile acids. *Steroids* **1996,** *61* (11), 664-669.

(8)   do Nascimento, P. G. G.; Lemos, T. L. G.; Almeida, M. C. S.; de Souza, J. M. O.; Bizerra, A. M. C.; Santiago, G. M. P.; da Costa, J. G. M.; Coutinho, H. D. M., Lithocholic acid and derivatives: Antibacterial activity. *Steroids* **2015,** *104*, 8-15.

(9)   Miro, P.; Marin, M. L.; Miranda, M. A., Radical-mediated dehydrogenation of bile acids by means of hydrogen atom transfer to triplet carbonyls. *Org. Biomol. Chem.* **2016,** *14* (9), 2679-2683.

(10)   Felici, M.; Contreras-Carballada, P.; Smits, J. M. M.; Nolte, R. J. M.; Williams, R. M.; De Cola, L.; Feiters, M. C., Cationic Heteroleptic Cyclometalated IridiumIII Complexes Containing Phenyl-Triazole and Triazole-Pyridine Clicked Ligands. *Molecules* **2010,** *15* (3), 2039.

(11)   Hodge, P.; Chakiri, A. B., The use of polymer-supported Candida antarctica lipase B to achieve the entropically-driven ring-opening polymerization of macrocyclic bile acid derivatives via transesterification: selectivity of the reactions and the structures of the polymers produced. *RSC Adv.* **2015,** *5* (113), 93057-93066.

(12)   Ogawa, S.; Asakura, K.; Osanai, S., Thermotropic and glass transition behaviors of n-alkyl β-d-glucosides. *RSC Adv.* **2013,** *3* (44), 21439-21446.

(13)   Frost, J. R.; Huber, S. M.; Breitenlechner, S.; Bannwarth, C.; Bach, T., Enantiotopos-Selective C-H Oxygenation Catalyzed by a Supramolecular Ruthenium Complex. *Angew. Chem. Int. Ed.* **2015,** *54* (2), 691-695.

(14)   Yang, Y.; Du, Z.; Ma, J.; Lu, F.; Zhang, J.; Xu, J., Biphasic Catalytic Conversion of Fructose by Continuous Hydrogenation of HMF over a Hydrophobic Ruthenium Catalyst. *ChemSusChem* **2014,** *7* (5), 1352-1356.

(15)   Sheldrick, G. M. *Program for Crystal Structure Refinement, Universität Göttingen, Bruker Advanced X-ray Solutions. SHELXTL Version 6.14, 2000-2003. SHELXL-2013 (Sheldrick, 2013)*,